VOL. 18 NO. 1/2 JULY 1968
PUBLISHED MONTHLY

JOURNAL OF

ELECTROANALYTICAL CHEMISTRY

AND INTERFACIAL ELECTROCHEMISTRY

International Journal devoted to all Aspects of Electroanalytical Chemistry, Double Layer Studies, Electrokinetics, Colloid Stability, and Electrode Kinetics.

ELSEVIER

GENERAL INFORMATION

See also Suggestions and Instructions to Authors which will be sent free, on request to the Publishers.

Types of contributions

(a) Original research work not previously published in other periodicals.
(b) Reviews on recent developments in various fields.
(c) Short communications.
(d) Bibliographical notes and book reviews.

Languages

Papers will be published in English, French or German.

Submission of papers

Papers should be sent to one of the following Editors:
Professor J. O'M. Bockris, John Harrison Laboratory of Chemistry, University of Pennsylvania, Philadelphia 4, Pa. 19104, U.S.A.
Dr. R. H. Ottewill, Department of Chemistry, The University, Bristol 8, England.
Dr. R. Parsons, Department of Chemistry, The University, Bristol 8, England.
Professor C. N. Reilley, Department of Chemistry, University of North Carolina, Chapel Hill, N. C. 27514, U.S.A.

Authors should preferably submit two copies in double-spaced typing on pages of uniform size. Legends for figures should be typed on a separate page. The figures should be in a form suitable for reproduction, drawn in Indian ink on drawing paper or tracing paper, with lettering etc. in thin pencil. The sheets of drawing or tracing paper should preferably be of the same dimensions as those on which the article is typed. Photographs should be submitted as clear black and white prints on glossy paper. Standard symbols should be used in line drawings, the following are available to the printers:

All references should be given at the end of the paper. They should be numbered and the numbers should appear in the text at the appropriate places.
A summary of 50 to 200 words should be included.

Reprints

Fifty reprints will be supplied free of charge. Additional reprints (minimum 100) can be ordered at quoted prices. They must be ordered on order forms which are sent together with the proofs.

Publication

The *Journal of Electroanalytical Chemistry and Interfacial Electrochemistry* appears monthly and four volumes will appear in 1968.
Subscription price: $ 70.00 or Sfr. 304.00 per year; $ 17.50 or Sfr. 76.00 per volume; plus postage. Additional cost for copies by air mail available on request. For advertising rates apply to the publishers.

Subscriptions

Subscriptions should be sent to:

ELSEVIER SEQUOIA S.A., P.O. Box 851, 1001 Lausanne 1, Switzerland

JOURNAL OF ELECTROANALYTICAL CHEMISTRY AND INTERFACIAL ELECTROCHEMISTRY

VOL. 18 (1968)

JOURNAL
of
ELECTROANALYTICAL CHEMISTRY
and
INTERFACIAL ELECTROCHEMISTRY

AN INTERNATIONAL JOURNAL DEVOTED TO ALL ASPECTS OF ELECTROANALYTICAL CHEMISTRY, DOUBLE LAYER STUDIES, ELECTROKINETICS, COLLOID STABILITY AND ELECTRODE KINETICS

Vol. 18 1968

ELSEVIER SEQUOIA S.A.
LAUSANNE

PRINTED IN THE NETHERLANDS

ELECTROANALYTICAL CHEMISTRY AND INTERFACIAL ELECTROCHEMISTRY
Elsevier Sequoia S.A., Lausanne – Printed in The Netherlands

THEORETICAL CALCULATION OF POLAROGRAPHIC SOLUTION-RESISTANCE

D. BRITZ
Department of Chemistry, State University of New York at Buffalo, Buffalo, N.Y. (U.S.A.)
H. H. BAUER
Department of Chemistry, University of Kentucky, Lexington, Ky. (U.S.A.)
(Received October 3rd, 1967)

INTRODUCTION

In experiments using the dropping mercury electrode (DME), the measured cell-impedance always consists of at least three series components: the resistance of the capillary, R_{cap}, the double-layer impedance, Z_{dl} (with or without faradaic effects), and the solution resistance, R_s, between the DME and the large counter-electrode. R_{cap} is a constant for a particular capillary and can be easily and accurately measured; measurement of R_s (or of Z_{dl}), however, requires measurement of the impedance and phase shift, correction for R_{cap}, and resolution into resistive and capacitive components. It would often be convenient to have some initial knowledge of R_s, and attempts have been made to calculate this quantity from knowledge of the specific resistance of the electrolyte and of the characteristics of the capillary.

The first attempt at a theoretical calculation was made by ILKOVIČ[1]. This author ignored the presence of the glass of the capillary and assumed that the DME is a complete sphere, with the counter-electrode a complete spherical shell, concentric with the DME.

This model leads to the equation

$$R_s = (\varrho/4\pi)(1/a - 1/d) \qquad (1)$$

where ϱ is the specific solution-resistance in ohm.cm, a the radius of the DME and d that of the counter-electrode. A number of workers[2-4] have recently made use of this equation. However, the neglect of the presence of the capillary can be expected to lead to low values of R_s, and in fact, as will be seen later, the actual errors are approximately 30%.

DEVAY[5] attempted to allow for the presence of the capillary by assuming that, on the lower half of the mercury drop, currents flow radially, while on the upper half, currents flow in directions normal to the axis of the capillary, *i.e.*, parallel to the plane of the end of the capillary. DEVAY neglected the counter-electrode and derived the equation

$$R_s = 4\varrho/9\pi a \qquad (2)$$

As will be seen later, this model also leads to rather large errors, in this case positive,

and again approximately 30%. The object of this paper is to present a new method of taking into account the presence of the capillary whereby better results than the previous ones are achieved.

THEORY

In the present model, the DME is considered as a sphere of radius a, centre O, lying against an infinite flat plane. The counter-electrode is considered as a spherical section of radius d, concentric with the DME and cut off by the plane, as shown in Fig. 1.

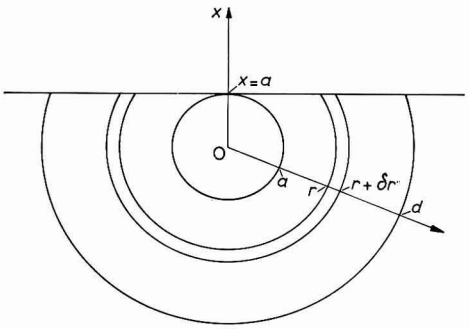

Fig. 1. Representation of the present model: (a), radius of DME; (d), radius of a.c. counter-electrode; (r), arbitrary distance from O; (x), distance coordinate in the direction shown.

Consider any shell, concentric with the DME, at distance r from O, such that $a<r<d$; and a further such shell at distance $r+\delta r$, as shown in Fig. 1. If δr is small, the resistance between the two shells will be given by:

$$\delta R_s = \varrho\, \delta r/A \tag{3}$$

where A is the area of the shell section. Using simple coordinate geometry, one obtains for A,

$$A = 2\pi r^2 + 2\pi \int_0^a (r^2 - x^2)^{\frac{1}{2}} \cdot \mathrm{d}x \tag{4}$$

where x is a distance coordinate as shown in Fig. 1. Integration gives:

$$A = 2\pi r^2 + \pi\{a(r^2 - a^2)^{\frac{1}{2}} + r^2 \sin^{-1}(a/r)\} \tag{4a}$$

The total resistance of all shell elements between $r=a$ and $r=d$ is R_s, given by:

$$R_s = \int_a^d \varrho \frac{1}{A}\, \mathrm{d}r \tag{5}$$

On substituting for A as in eqn. (4a), eqn. (5) becomes

$$R_s = \frac{\varrho}{\pi} \int_a^d \frac{\mathrm{d}r}{2r^2 + a(r^2 - a^2)^{\frac{1}{2}} + r^2 \sin^{-1}(a/r)} \tag{6}$$

No algebraic solution to this integral could be found, and we employed the well-known numerical method of integration by Simpson's Rule. The function as it

stands, however, is not particularly suitable for this process, being somewhat similar to a hyperbolic function—this would require a large number of calculations (*i.e.*, small intervals) for sufficient accuracy. Transformation of the variable r to its inverse, s, *i.e.*

$$s = r^{-1} \tag{7}$$

leads to the equation:

$$R_s = \frac{\varrho}{\pi} \int_{d^{-1}}^{a^{-1}} \frac{\mathrm{d}s}{2 + \sin^{-1}(as) + as(1 - a^2s^2)^{\frac{1}{2}}} \tag{8}$$

This function is more suitable for numerical integration, as it is a rather shallow curve between d^{-1} and a^{-1}, and, consequently, a small number of fairly coarse intervals gives accurate results.

An Algol programme was coded for an English Electric KDF 9 computer to perform the integration and solution of eqn. (8). The programme computes the drop-radius, a, (for the end of drop-life) from input data of m and t, the rate of mercury flow and the drop-time, respectively; other input data are ϱ, d, and N, the number of integration intervals. After some experimenting, it was found that calculated values of R_s do not change significantly with values of N greater than 10, and, subsequently, the value 20 was always used and could have been fixed within the programme. This indicates also that manual integration of eqn. (8) is quite feasible—10–20 intervals would not require a great deal of work.

COMPARISON WITH EXPERIMENTAL RESULTS AND OTHER MODELS

Cell impedances were measured accurately by the technique described elsewhere[6], using neutral solutions of KCl at the concentrations 1.00, 0.10 and 0.01 M. The resistance of the blunt capillary was measured and subtracted from the total series resistance, obtained as the mean of several determinations at different frequencies. The absolute accuracy of the R_s-values thus obtained was better than 1%.

Theoretical values of R_s were calculated for the solutions, using ILKOVIČ's eqn. (1), DEVAY's eqn. (2) and the present eqn. (8). Values of ϱ were taken from ref. 8. Table 1 lists the results of these calculations, together with the experimentally obtained values.

The calculations were made for a drop-radius of 0.5 mm (the experimental value) and a value of d of 20 mm. It is worth mentioning that the distance of the counter-electrode (d) plays a very minor role in the resistance found experimentally,

TABLE 1

COMPARISON OF THEORETICAL CALCULATION WITH EXPERIMENTAL VALUES OF R_s

Electrolyte	R_s *(ohm)*						
	Experimental	*Ilkovic eqn.*	*(% error)*	*Devay eqn.*	*(% error)*	*Present eqn.*	*(% error)*
1.00 *M* KCl	20.5	13.0	−37	23.7	15	18.3	−11
0.10 *M* KCl	155	113	−27	206	33	158	2
0.01 *M* KCl	1380	1028	−26	1870	36	1440	4

and in the values computed according to all of the models. For the Ilkovič model, changing d from 20 mm to infinity, changes R_s by 2.5% (see eqn. (1)). DEVAY recognized the small role played by d, and in fact set d as equal to infinity as an integral part of the model. With our model, changing d from 20 mm to 10 mm decreased the computed value of R_s by 3% (for the 1 M KCl solution). The counter-electrode used in the experiments was a cylinder, 20 mm radius and 40 mm in length. Thus, the discrepancy between experiment and our model in the two more dilute solutions may be due to not considering the small effect of counter-electrode distance and configuration.

There is also long-standing experimental evidence that d has a very minor effect on series resistance[7]: the a.c. wave-height for a reversible reduction decreased by less than 8% as d was increased from 10 mm to 40 mm.

CONCLUSIONS AND DISCUSSION

The results in Table 1 show that the present model is an improvement. It is interesting also to note that the errors with all three models vary in a systematic manner with the concentration of the electrolyte. It appears that the directions of the currents at the DME surface profoundly affect the net resistance of the solution; possibly the current distribution at the drop varies with electrolyte concentration. A further possibility is that the drop geometry, in reality not strictly spherical, varies with electrolyte concentration. More theoretical and experimental work is needed to clarify these points.

REFERENCES

1 D. ILKOVIČ, *Collection Czech. Chem. Commun.*, 4 (1932) 480.
2 J. H. SLUYTERS, *Rec. Trav. Chim.*, 79 (1960) 1092.
3 W. B. SCHAAP AND P. S. MCKINNEY, *Anal. Chem.*, 36 (1964) 1251.
4 G. H. NANCOLLAS AND C. A. VINCENT, *Electrochim. Acta*, 10 (1965) 97.
5 J. DEVAY, *Acta Chim. Acad. Sci. Hung.*, 35 (1963) 255.
6 D. BRITZ AND H. H. BAUER, *J. Sci. Inst.*, 44 (1967) 843.
7 B. BREYER, F. GUTMANN AND S. HACOBIAN, *Australian J. Sci. Res.*, A3 (1950) 567.
8 *Handbook of Chemistry and Physics*, Chemical Rubber Publishing Company, 44th ed.

ELECTROANALYTICAL CHEMISTRY AND INTERFACIAL ELECTROCHEMISTRY
Elsevier Sequoia S.A., Lausanne – Printed in The Netherlands

THEORETICAL CURRENT–TIME CURVES AT CONSTANT POTENTIAL WITH LINEAR ADSORPTION OF THE DEPOLARIZER ON SPHERICAL AND PLANE ELECTRODES

ROLANDO GUIDELLI
Institute of Analytical Chemistry, University of Florence (Italy)
(Received November 28th, 1967)

Since the pioneering work of BRDIČKA on polarographic reversible currents influenced by adsorption of electroactive substances[1,2], a great deal of work has been devoted to the study of the effect of specific adsorption of the depolarizer on electrode processes, in connection with different electrochemical techniques[3,4]. Recently, BARKER AND BOLZAN[5] pointed out that the occurrence of some polarographic maxima is attributable to the adsorption of the depolarizer and they observed the presence of such maxima also with the "normal" pulse polarographic technique, where the mercury electrode maintains an almost constant area during the flow of current. In this work, the authors report the results of an unpublished theoretical treatment, according to which the occurrence of these adsorption maxima is justified on the basis of a simplified model. As a slightly more complex model (to be applied to the electrode with periodical renewal of the diffusion layer (DLPRE)[6]) has been examined independently in this institute, the corresponding theoretical treatment is described here, as well as the conclusions which may be drawn from it in view of the concept of charge separation and recombination, recently emphasized by DELAHAY[7].

FAST ELECTRON TRANSFER

Let us consider a charge transfer process of the type, $A + ne \rightleftharpoons B$, where A and B are soluble in the solution and specifically adsorbed on the electrode surface. The case of one of the two species soluble within the electrode may be immediately reduced to the case under study. Let us assume that an adsorption equilibrium is established and that the fractional surface coverage is sufficiently low to allow the use of adsorption linear isotherms. We will first assume that the electron transfer is so fast as to be polarographically reversible, in order to apply the Nernst equation. It will be further postulated that the electron transfer occurs exclusively with the adsorbed species, although, owing to the linear relation between the surface concentrations, Γ_a and Γ_b, and the volume concentrations, a and b, at the electrode surface, the Nernst equation may be equally well applied to the latter. Under these conditions, the problem of determining the faradaic current which flows at constant potential through a spherical electrode is expressed by the following system of differential equations:

$$\frac{\partial a}{\partial t} = D_a\left(\frac{\partial^2 a}{\partial r^2} + \frac{2}{r}\frac{\partial a}{\partial r}\right) \tag{1}$$

$$\frac{\partial b}{\partial t} = D_b\left(\frac{\partial^2 b}{\partial r^2} + \frac{2}{r}\frac{\partial b}{\partial r}\right) \tag{2}$$

with the initial and boundary conditions:

$$\left.\begin{matrix} a = a^* \\ b = 0 \end{matrix}\right\} \quad \text{for} \quad \begin{cases} r \geqslant r_0, & t = 0 \\ r \to \infty, & t > 0 \end{cases} \tag{3}$$

$$\frac{\Gamma_a}{\Gamma_b} = \exp\left[\frac{nF}{RT}(E - E_0)\right] = \theta \quad \text{or} \quad \frac{a(r_0,t)}{b(r_0,t)} = \frac{\theta K_b}{K_a} = \theta' = \exp\left[\frac{nF}{RT}(E - E_0')\right] \tag{4}$$

$$\frac{\mathrm{d}\Gamma_a}{\mathrm{d}t} + \frac{\mathrm{d}\Gamma_b}{\mathrm{d}t} = K_a\left(\frac{\partial a}{\partial t}\right)_{r=r_0} + K_b\left(\frac{\partial b}{\partial t}\right)_{r=r_0} = D_a\left(\frac{\partial a}{\partial r}\right)_{r=r_0} + D_b\left(\frac{\partial b}{\partial r}\right)_{r=r_0} \tag{5}$$

where a^*, D_a, K_a and b^*, D_b, K_b represent the volume concentrations in the bulk of the solution, the diffusion coefficients, and the adsorption coefficients of A and B, respectively. Equation (5) simply expresses the fact that the sum of the amounts of A and B which are specifically adsorbed on unit area (or which are removed from unit area) of the electrode surface in unit time, equals the sum of the fluxes of A and B towards (or from) the electrode. Passing to the Laplace transforms of eqns. (1), (2), (3), (4) and (5), the transform of b is given by:

$$\bar{b}(r,s) = a^* \frac{r_0}{r} \frac{K_a s + D_a^{\frac{1}{2}} s^{\frac{1}{2}} + D_a/r_0}{s[(\theta' K_a + K_b)s + (\theta' D_a^{\frac{1}{2}} + D_b^{\frac{1}{2}})s^{\frac{1}{2}} + (\theta' D_a + D_b)/r_0]}$$

$$\times \exp\left[-\frac{s^{\frac{1}{2}}}{D_b^{\frac{1}{2}}}(r - r_0)\right] \tag{6}$$

The term on the right can be separated by the use of partial fractions in order to find the inverse transform. Thus, the concentration of B as a function of time, t, and of the distance, r, from the centre of a spherical electrode with radius r_0 is given by:

$$b(r,t) = \frac{a^*}{(\beta - \alpha)(\theta' K_a + K_b)} \frac{r_0}{r} \left\{\left(K_a\beta + \frac{D_a}{r_0\beta} - D_a^{\frac{1}{2}}\right) \exp\left[\frac{r - r_0}{D_b^{\frac{1}{2}}}\beta + \beta^2 t\right]\right.$$

$$\times \operatorname{erfc}\left[\frac{r - r_0}{2D_b^{\frac{1}{2}} t^{\frac{1}{2}}} + \beta t^{\frac{1}{2}}\right] - \left(K_a\alpha + \frac{D_a}{r_0\alpha} - D_a^{\frac{1}{2}}\right) \exp\left[\frac{r - r_0}{D_b^{\frac{1}{2}}}\alpha + \alpha^2 t\right]$$

$$\left. \times \operatorname{erfc}\left[\frac{r - r_0}{2D_b^{\frac{1}{2}} t^{\frac{1}{2}}} + \alpha t^{\frac{1}{2}}\right] + \frac{D_a}{r_0}\frac{\beta - \alpha}{\alpha\beta} \operatorname{erfc}\left[\frac{r - r_0}{2D_b^{\frac{1}{2}} t^{\frac{1}{2}}}\right]\right\} \tag{7}$$

where:

$$\alpha = \tfrac{1}{2}l + \tfrac{1}{2}\sqrt{l^2 - 4m}, \qquad \beta = \tfrac{1}{2}l - \tfrac{1}{2}\sqrt{l^2 - 4m}$$

$$l = (\theta' D_a^{\frac{1}{2}} + D_b^{\frac{1}{2}})/(\theta' K_a + K_b), \quad m = (\theta' D_a + D_b)/r_0(\theta' K_a + K_b)$$

It immediately follows that the faradaic current, expressed by the equation:

$$i = nFA\left\{K_b\left(\frac{\partial b}{\partial t}\right)_{r=r_0} - D_b\left(\frac{\partial b}{\partial r}\right)_{r=r_0}\right\} = -nFA\left\{K_a\left(\frac{\partial a}{\partial t}\right)_{r=r_0} - D_a\left(\frac{\partial a}{\partial r}\right)_{r=r_0}\right\} \tag{8}$$

is given by:

$$\frac{i}{nFA} = \frac{a^*}{(\beta-\alpha)(\theta' K_a + K_b)} \left\{ \frac{K_a K_b(\alpha^2-\beta^2) + (K_a D_b^{\frac{1}{2}} + K_b D_a^{\frac{1}{2}})(\beta-\alpha)}{\pi^{\frac{1}{2}} t^{\frac{1}{2}}} \right.$$

$$+ \left(K_a\beta + \frac{D_a}{r_0\beta} - D_a^{\frac{1}{2}}\right)\left(K_b\beta + \frac{D_b}{r_0\beta} - D_b^{\frac{1}{2}}\right)\beta \exp(\beta^2 t)\,\mathrm{erfc}(\beta t^{\frac{1}{2}})$$

$$\left. - \left(K_a\alpha + \frac{D_a}{r_0\alpha} - D_a^{\frac{1}{2}}\right)\left(K_b\alpha + \frac{D_b}{r_0\alpha} - D_b^{\frac{1}{2}}\right)\alpha \exp(\alpha^2 t)\,\mathrm{erfc}(\alpha t^{\frac{1}{2}}) \right\} + \frac{D_a D_b a^*}{r_0(\theta' D_a + D_b)} \quad (9)$$

In order to simplify eqn. (9) we will limit ourselves to the examination of the case of linear diffusion. Under these conditions, the faradaic current may be derived from eqn. (9) by letting r_0 approach ∞. Thus, if $r_0 \to \infty$:

$\alpha \to l$, $\beta \to 0$, $r_0\beta \to (\theta' D_a + D_b)/(\theta' D_a^{\frac{1}{2}} + D_b^{\frac{1}{2}})$

It immediately follows that:

$$\frac{i}{nFAa^*} = \frac{1}{(\theta' K_a + K_b)^2}$$

$$\times \left\{ \frac{K_a^2 D_b^{\frac{1}{2}}\theta' + K_b^2 D_a^{\frac{1}{2}}}{\pi^{\frac{1}{2}} t^{\frac{1}{2}}} - \frac{\theta'(K_a D_b^{\frac{1}{2}} - K_b D_a^{\frac{1}{2}})^2}{\theta' K_a + K_b} \exp(l^2 t)\,\mathrm{erfc}(l t^{\frac{1}{2}}) \right\} \quad (10)$$

where l has already been defined.

If $K_a = K_b = K$ and $D_a = D_b = D$, eqn. (10) becomes:

$$i/nFAa^* = D^{\frac{1}{2}}/(\theta' + 1)\pi^{\frac{1}{2}} t^{\frac{1}{2}} \quad (11)$$

Equation (11) is identical with the well known equation expressing the current–time curve at constant potential on a plane stationary electrode in the absence of adsorption, in the case that the diffusion coefficients of the two species, oxidized and reduced, are equal. It should be noted that eqn. (11) holds independently of the value of K, *i.e.*, of the amount of adsorbed electroactive material.

If $K_a = K_b = K$ but $D_a \neq D_b$, eqn. (10) becomes:

$$\frac{i}{nFAa^*} = \frac{D_b^{\frac{1}{2}}\theta' + D_a^{\frac{1}{2}}}{(\theta'+1)^2 \pi^{\frac{1}{2}} t^{\frac{1}{2}}} - \frac{\theta'}{(\theta'+1)^3} \cdot \frac{(D_b^{\frac{1}{2}} - D_a^{\frac{1}{2}})^2}{K} \cdot \exp(\gamma^2 t)\,\mathrm{erfc}(\gamma t^{\frac{1}{2}}) \quad (12)$$

where $\gamma = (\theta' D_a^{\frac{1}{2}} + D_b^{\frac{1}{2}})/K(\theta'+1)$.

The second term on the right in eqn. (12) represents the deviation of i from the typical behaviour of reversible polarographic currents at a plane stationary electrode ($i \propto 1/t^{\frac{1}{2}}$), this deviation being due to a difference between the diffusion coefficients of the two species, A and B. However, it should be noted that the second term in eqn. (12) may be neglected with respect to the first in all practical cases. In fact, $\exp(\gamma^2 t)\mathrm{erfc}(\gamma t^{\frac{1}{2}}) \leqslant 1$ for $t \geqslant 0$ and, furthermore, $(D_b^{\frac{1}{2}} - D_a^{\frac{1}{2}})^2$ is very seldom larger than 10^{-5} cm^2/sec. Therefore, if $K > 10^{-5}$ cm, as occurs in the case of an appreciable adsorption of A and B, the second term in eqn. (12) is definitely lower than $\theta'/(\theta'+1)^3$ and decreases with increase in t. As the ratio $\theta'/(\theta'+1)^3$ is always lower than unity and the smaller it becomes the more θ' differs from the value $\frac{1}{2}$, it can be said that:

$$i/nFAa^* \cong (D_b^{\frac{1}{2}}\theta' + D_a^{\frac{1}{2}})/(\theta'+1)^2 \pi^{\frac{1}{2}} t^{\frac{1}{2}} \quad (13)$$

On the other hand, if $(D_b^{\frac{1}{2}} - D_a^{\frac{1}{2}})^2/K$ is > 1, γ is always $\gg 1$ for any value of θ' and,

consequently, in the time-scale of polarographic measurements (approximately 10^{-2} sec $< t < 5$ sec) $\exp(\gamma^2 t)\cdot\operatorname{erfc}(\gamma t^{\frac{1}{2}})$ may be replaced by the first term of its series expansion for large values of the argument, *i.e.*, $1/(\pi^{\frac{1}{2}} t^{\frac{1}{2}}\gamma)$. Under these conditions, eqn. (12) becomes:

$$i/nFAa^* = D_a^{\frac{1}{2}}/\{(D_a^{\frac{1}{2}}/D_b^{\frac{1}{2}})\theta' + 1\}\pi^{\frac{1}{2}} t^{\frac{1}{2}} \tag{14}$$

which represents the well known equation of a reversible polarographic current at a plane stationary electrode in the absence of adsorption, when $D_a \neq D_b$. In both eqns. (13) and (14) the current does not depend on the amount of adsorbed material and, furthermore, appears mainly influenced by the value of the diffusion coefficient of the reduced (oxidized) form in the lower (upper) part of the rising portion of the cathodic wave. While the equality between K_a and K_b renders the deviation from the proportionality relation, $i \propto 1/t^{\frac{1}{2}}$, negligible in all practical cases, a sensible difference between K_a and K_b has a remarkable effect upon the behaviour of the instantaneous faradaic current. Thus, if we assume for simplicity that $D_a = D_b = D$, eqn. (10) becomes:

$$\frac{i}{nFAa^*} = \frac{D^{\frac{1}{2}}}{\pi^{\frac{1}{2}} t^{\frac{1}{2}}} \frac{\theta' + \sigma^2}{(\theta' + \sigma)^2} + D^{\frac{1}{2}}\left[\frac{1}{\theta' + 1} - \frac{\theta' + \sigma^2}{(\theta' + \sigma)^2}\right] \varrho \exp(\varrho^2 t) \operatorname{erfc}(\varrho t^{\frac{1}{2}}) \tag{15}$$

where: $\varrho = D^{\frac{1}{2}}(\theta' + 1)/K_a(\theta' + \sigma)$ and $\sigma = K_b/K_a$.

In order better to understand the extent of the two contributions to the faradaic current represented by the flux of B (of A) and by the rate of change of the surface concentration of B (of A), it has been found convenient to consider these contributions separately, by expressing them in the forms:

$$-D\left(\frac{\partial b}{\partial x}\right)_{x=0} = a^* D^{\frac{1}{2}}\left[\frac{1}{(\theta' + \sigma)\pi^{\frac{1}{2}} t^{\frac{1}{2}}} + \left(\frac{1}{\theta' + 1} - \frac{1}{\theta' + \sigma}\right)\varrho \exp(\varrho^2 t) \operatorname{erfc}(\varrho t^{\frac{1}{2}})\right] \tag{16a}$$

$$D\left(\frac{\partial a}{\partial x}\right)_{x=0} = a^* D^{\frac{1}{2}}\left[\frac{\sigma}{(\theta' + \sigma)\pi^{\frac{1}{2}} t^{\frac{1}{2}}} + \left(\frac{1}{\theta' + 1} - \frac{\sigma}{\theta' + \sigma}\right)\varrho \exp(\varrho^2 t) \operatorname{erfc}(\varrho t^{\frac{1}{2}})\right] \tag{16b}$$

$$K_b\left(\frac{\partial b}{\partial t}\right)_{x=0} = a^* D^{\frac{1}{2}}\sigma \frac{(\theta' + 1)}{(\theta' + \sigma)}\left(\frac{1}{\theta' + 1} - \frac{1}{\theta' + \sigma}\right)\left[\frac{1}{\pi^{\frac{1}{2}} t^{\frac{1}{2}}} - \varrho \exp(\varrho^2 t) \operatorname{erfc}(\varrho t^{\frac{1}{2}})\right] \tag{16c}$$

$$K_a\left(\frac{\partial a}{\partial t}\right)_{x=0} = \frac{\theta'}{\sigma} \cdot K_b\left(\frac{\partial b}{\partial t}\right)_{x=0} \tag{16d}$$

As $\varrho \exp(\varrho^2 t) \operatorname{erfc}(\varrho t^{\frac{1}{2}}) \simeq 1/\pi^{\frac{1}{2}} t^{\frac{1}{2}}$ for $\varrho t^{\frac{1}{2}} > 7$, it immediately appears from eqn. (16) that, when t is sufficiently large, $K_b(\partial b/\partial t)_{x=0}$ and $K_a(\partial a/\partial t)_{x=0}$ tend to 0, while $-D(\partial b/\partial x)_{x=0}$ and $D(\partial a/\partial x)_{x=0}$ tend to the limiting expression, $D^{\frac{1}{2}} a^*/(\theta' + 1)\pi^{\frac{1}{2}} t^{\frac{1}{2}}$, which represents $i/(nFA)$ in the absence of adsorption. Figure 1 shows $(D^{\frac{1}{2}}/a^*)\cdot(\partial a/\partial x)_{x=0}$ (curve a), $-(K_a/D^{\frac{1}{2}}a^*)(\partial a/\partial t)_{x=0}$ (curve b), as well as their sum expressing $i/nFAD^{\frac{1}{2}}a^*$ (curve c) for the following data: $D = 10^{-6}$ cm^2/sec, $K_a = 10^{-3}$ cm, $K_b = 10^{-5}$ cm, $\theta' = 1$. Curve d in the same figure represents $i/nFAD^{\frac{1}{2}}a^*$ for $D = 10^{-6}$ cm^2/sec and $\theta' = 1$, in the absence of adsorption. In order to consider the effect of adsorption upon the mean polarographic currents, eqns. (16a, b, c and d) have been integrated over t from 0 to τ and successively divided by τ taking into account that:

$$\int_0^\tau \exp(\varrho^2 t) \operatorname{erfc}(\varrho t^{\frac{1}{2}})\,\mathrm{d}t = \frac{1}{\varrho^2}\left[\operatorname{erfc}(\varrho\tau^{\frac{1}{2}}) \exp(\varrho^2\tau) + \frac{2}{\pi^{\frac{1}{2}}}\varrho\tau^{\frac{1}{2}} - 1\right]$$

Figure 2 shows

$$\frac{1}{\tau}\int_0^\tau \frac{D^{\frac{1}{2}}}{a^*}\left(\frac{\partial a}{\partial x}\right)_{x=0} \mathrm{d}t, \quad -\frac{1}{\tau}\int_0^\tau \frac{K_a}{D^{\frac{1}{2}}a^*}\left(\frac{\partial a}{\partial t}\right)_{x=0} \mathrm{d}t, \quad -\frac{1}{\tau}\int_0^\tau \frac{D^{\frac{1}{2}}}{a^*}\left(\frac{\partial b}{\partial x}\right)_{x=0} \mathrm{d}t,$$

$$-\frac{1}{\tau}\int_0^\tau \frac{K_b}{D^{\frac{1}{2}}a^*}\left(\frac{\partial b}{\partial t}\right)_{x=0} \mathrm{d}t,$$

as well as $i_{\text{average}}/nFAD^{\frac{1}{2}}a^*$ for $D=10^{-6}$ cm^2/sec, $K_a=10^{-3}$ cm, $K_b=10^{-5}$ cm, $\tau=4$ sec, and $T=25°$ under the simplifying assumption that the adsorption coefficients do not depend on potential in the potential range considered. This assumption will be maintained also in the following part of this paper whenever necessary. The polarographic wave in Fig. 2 shows a maximum, similar to those of the first kind, although the cause of this particular maximum is to be found in the linear adsorption

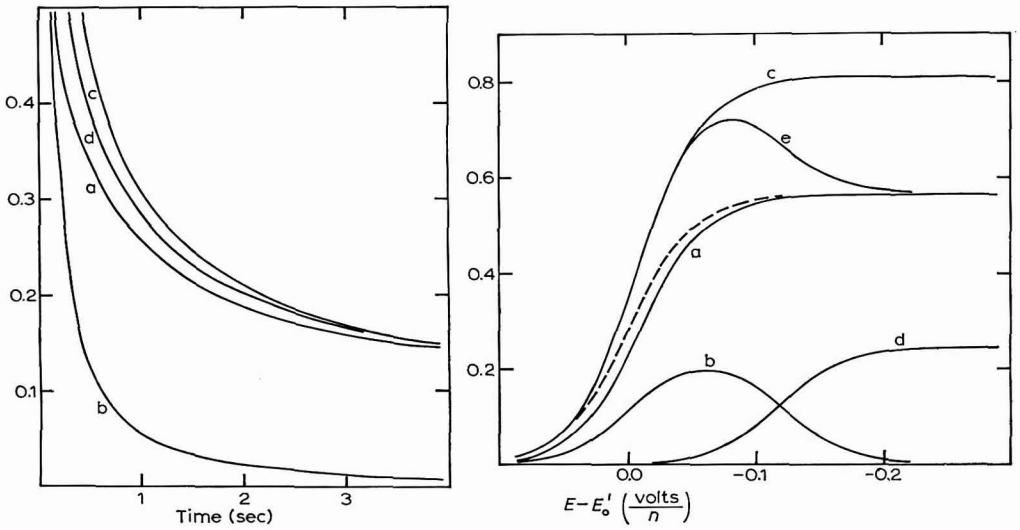

Fig. 1. Calcd. values of

$$\text{(a)}, \frac{D^{\frac{1}{2}}}{a^*}\left(\frac{\partial a}{\partial x}\right)_{x=0}; \quad \text{(b)}, -\frac{K_a}{D^{\frac{1}{2}}a^*}\left(\frac{\partial a}{\partial t}\right)_{x=0}; \quad \text{(c)}, \frac{i}{nFAD^{\frac{1}{2}}a^*}$$

as functions of time. The curves have been obtained from eqns. (15) and (16) for the following data: $D = 10^{-6}$ cm^2/sec, $K_a = 10^{-3}$ cm, $K_b = 10^{-5}$ cm, $\theta' = 1$. Curve d expresses $i/nFAD^{\frac{1}{2}}a^*$ as obtained from eqn. (11) for $D = 10^{-6}$ cm^2/sec and $\theta' = 1$.

Fig. 2. Calcd. values of

$$\text{(a)}, \frac{1}{\tau}\int_0^\tau \frac{D^{\frac{1}{2}}}{a^*}\left(\frac{\partial a}{\partial x}\right)_{x=0} \mathrm{d}t; \quad \text{(b)}, -\frac{1}{\tau}\int_0^\tau \frac{K_a}{D^{\frac{1}{2}}a^*}\left(\frac{\partial a}{\partial t}\right)_{x=0} \mathrm{d}t; \quad \text{(c)}, -\frac{1}{\tau}\int_0^\tau \frac{D^{\frac{1}{2}}}{a^*}\left(\frac{\partial b}{\partial x}\right)_{x=0} \mathrm{d}t;$$

$$\text{(d)}, -\frac{1}{\tau}\int_0^\tau \frac{K_b}{D^{\frac{1}{2}}a^*}\left(\frac{\partial b}{\partial t}\right)_{x=0} \mathrm{d}t; \quad \text{(e)}, \frac{i_{\text{average}}}{nFAD^{\frac{1}{2}}a^*}$$

as functions of potential. The curves have been obtained from eqns. (15) and (16), suitably integrated, for the following data: $D = 10^{-6}$ cm^2/sec, $K_a = 10^{-3}$ cm, $K_b = 10^{-5}$ cm, $\tau = 4$ sec, $T = 25°$. The dashed curve expresses $i_{\text{average}}/nFAD^{\frac{1}{2}}a^*$ obtained by integration of eqn. (11) for $D = 10^{-6}$ cm^2/sec, $\tau = 4$ sec, $T = 25°$.

of A and B, with $K_a > K_b$. The presence of the maximum is due to the sensible contribution of $d\Gamma_a/dt$ to the faradaic current, as is the quantity, $-d\Gamma_a/dt$, at a given time, as well as

$$-\frac{1}{\tau}\int_0^\tau \frac{d\Gamma_a}{dt}\,dt$$

which show a maximum when considered as functions of the applied potential (Fig. 2). In fact, for any value of θ', the instantaneous reduction of a fraction of A adsorbed on the electrode surface with B formation occurs at the beginning of the electrolysis ($t=0$). As the adsorption coefficient of B is lower than that of A, for values of θ' not especially high, this instantaneous transformation produces a high volume concentration of B at the electrode surface ($x=0$). If we consider the equation:

$$b(0,t)=a^*\left[\frac{1}{\theta'+1}+\left(\frac{1}{\theta'+\sigma}-\frac{1}{\theta'+1}\right)\exp(\varrho^2 t)\,\mathrm{erfc}(\varrho t^{\frac{1}{2}})\right]$$

expressing the volume concentration of B at the electrode surface and derived from eqn. (7) by putting $r=r_0$ and letting r_0 tend to ∞, we can see that when t increases, Γ_b passes from the initial value, $K_b a^*/(\theta'+\sigma)$, to the limiting value, $K_b a^*/(\theta'+1)$, corresponding to the stationary conditions with respect to the amount of adsorbed electroactive material. Consequently, as in the case under investigation, $\sigma<1$, Γ_b diminishes because of the diffusion of B from the electrode with increase in time. The relative slowness of this diffusion causes the effect of

$$\frac{d\Gamma_a}{dt}=\theta\frac{d\Gamma_b}{dt}$$

upon the faradaic current to be felt in the time-scale of polarographic measurements. Obviously, when $\theta'\to\infty$, the amount of A adsorbed on the electrode that is instantaneously reduced to B at time $t=0$, approaches 0, while, when $\theta'\to 0$ the surface concentration, Γ_a, tends to become equal to 0 from the very beginning of electrolysis, without any possibility of subsequent changes. The foregoing intuitive considerations justify the fact that

$$-\frac{1}{\tau}\int_0^\tau \frac{d\Gamma_a}{dt}\,dt$$

tends to 0 both for $\theta'\to\infty$ and for $\theta'\to 0$, exhibiting a maximum for intermediate values of potential. When

$$-\frac{1}{\tau}\int_0^\tau \frac{d\Gamma_b}{dt}\,dt$$

is considered, Fig. 2 shows that this quantity grows when the potential decreases, and approaches a limiting value. In fact, intuitively, the larger the amount of B instantaneously produced at time $t=0$ as a consequence of the reduction of A adsorbed on the electrode, the larger the rate of decrease of Γ_b at a given time, t. Simultaneously, when $\theta'\to 0$, the average flux of B,

$$-\frac{1}{\tau}\int_0^\tau D\left(\frac{\partial b}{\partial x}\right)_{x=0}dt,$$

approaches a limiting value larger than the limiting value of the average flux of A'

$$\frac{1}{\tau}\int_0^\tau D\left(\frac{\partial a}{\partial x}\right)_{x=0} \mathrm{d}t,$$

owing to the high volume concentration, $b(0,t)$, produced at time $t=0$, so that the difference between the average flux of B and the average rate of change of Γ_b still gives the usual value, $\bar{\imath}_d = 2nFAD^{\frac{1}{2}}a^*/\pi^{\frac{1}{2}}\tau^{\frac{1}{2}}$, of the mean diffusion limiting current.

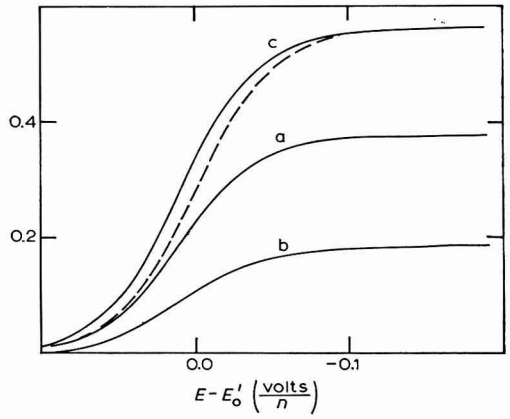

Fig. 3. Calcd. values of

$$\text{(a)}, -\frac{1}{\tau}\int_0^\tau \frac{D^{\frac{1}{2}}}{a^*}\left(\frac{\partial b}{\partial x}\right)_{x=0}\mathrm{d}t;\ \text{(b)}, \frac{1}{\tau}\int_0^\tau \frac{K_b}{D^{\frac{1}{2}}a^*}\left(\frac{\partial b}{\partial t}\right)_{x=0}\mathrm{d}t;\ \text{(c)}, \frac{i_{\text{average}}}{nFAD^{\frac{1}{2}}a^*}$$

as functions of potential. The curves have been obtained from eqns. (15) and (16), suitably integrated, for the following data: $D = 10^{-6}$ cm^2/sec, $K_a = 10^{-5}$ cm, $K_b = 10^{-3}$ cm, $\tau = 4$ sec, $T = 25°$. The dashed curve is identical with that in Fig. 2.

Figure 3 shows the same quantities of Fig. 2 for the following data: $D=10^{-6}$ cm^2/sec, $K_a=10^{-5}$ cm, $K_b=10^{-3}$ cm and $\tau=4$ sec. Under these conditions the average rate of change of Γ_a,

$$\frac{1}{\tau}\int_0^\tau \frac{\mathrm{d}\Gamma_a}{\mathrm{d}t}\,\mathrm{d}t,$$

is practically negligible at all potentials, so that the mean current coincides approximately with

$$\frac{nFA}{\tau}\int_0^\tau D\left(\frac{\partial a}{\partial x}\right)_{x=0}\mathrm{d}t.$$

On the contrary,

$$\frac{1}{\tau}\int_0^\tau \frac{\mathrm{d}\Gamma_b}{\mathrm{d}t}\,\mathrm{d}t$$

grows when potential decreases, and approaches a limiting value. This behaviour is attributable to the fact that the amount of A adsorbed on the electrode before the

electrolysis is not enough to create the amount of B corresponding to stationary conditions through its instantaneous reduction at time $t=0$, as $K_b > K_a$. Consequently, the rate of growth of Γ_b increases (reaching a limiting value) the larger the ratio, $\Gamma_b/\Gamma_a = \theta^{-1}$, which is established on the electrode as a consequence of the applied potential. Obviously, the accumulation of B at the electrode surface causes a decrease in the average flux of B from the electrode with respect to the value it would have in the absence of adsorption, so that, when $\theta' \to 0$ the difference,

$$\frac{nFA}{\tau}\left[\int_0^\tau \frac{d\Gamma_b}{dt}\,dt - \int_0^\tau D\left(\frac{\partial b}{\partial x}\right)_{x=0} dt\right],$$

still yields the usual value of the mean diffusion limiting current. In this connection it is interesting to note that a maximum is present only when the adsorption coefficient, K_a, of the depolarizer is larger than that of the product of the electrode reaction, K_b, although, both for $K_a > K_b$ and $K_b > K_a$ a shift of the half-wave potential towards more positive values of E is to be expected. The effects of the adsorption of A and B

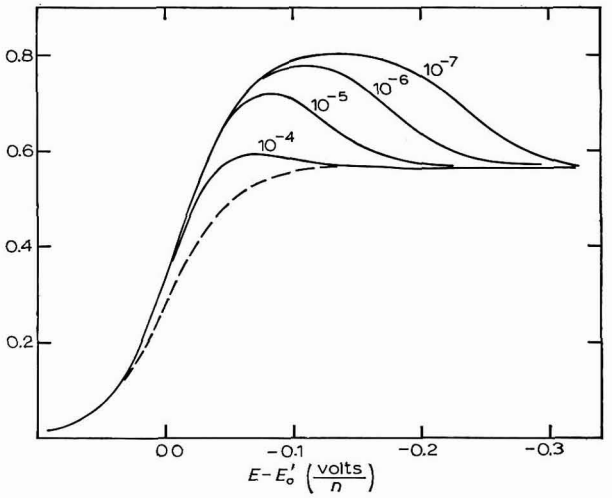

Fig. 4. Calcd. value of $i_{average}/nFAD^{\frac{1}{2}}a^*$ as a function of potential. The curves have been obtained from eqn. (15), suitably integrated, for the following data: $D = 10^{-6}$ cm²/sec, $K_a = 10^{-3}$ cm, $\tau = 4$ sec, $T = 25°$. Numbers on each curve refer to the value of K_b (cm). The dashed curve is identical with that in Fig. 2.

are sensible only if $K_a \neq K_b$. Figure 4 shows the average faradaic currents as functions of potential for $D = 10^{-6}$ cm²/sec, $\tau = 4$ sec, $K_a = 10^{-3}$ cm and $K_b = 10^{-4}$, 10^{-5}, 10^{-6} and 10^{-7} cm, respectively. It may be seen that the maximum due to adsorption grows with an increase in the difference between K_a and K_b, at the same time shifting towards more negative values of potential.

SLOW ELECTRON TRANSFER

The problem of a totally irreversible polarographic wave complicated by linear adsorption of the depolarizer on a stationary spherical electrode may be

expressed by the diffusion equation:

$$\frac{\partial a}{\partial t} = D_a \left(\frac{\partial^2 a}{\partial r^2} + \frac{2}{r}\frac{\partial a}{\partial r}\right) \tag{17}$$

with the initial condition:

$$a = a^* \text{ for } \begin{cases} r \geqslant r_0, & t = 0 \\ r \to \infty, & t > 0 \end{cases} \tag{18}$$

and the boundary condition:

$$\frac{\mathrm{d}\Gamma_a}{\mathrm{d}t} = D_a \left(\frac{\partial a}{\partial r}\right)_{r=r_0} - k_f \Gamma_a \quad \text{for} \quad r = r_0,\ t > 0 \tag{19}$$

where: $\Gamma_a = K_a a(r_0, t)$

The foregoing diffusion problem is similar to that examined by HOLUB AND KORYTA[8,9] in connection with surface reactions of adsorbed substances. Equation (19) expresses the fact that the amount of A adsorbed in unit time on unit area of the electrode surface is given by the difference between the flux of A and the amount of A that is reduced on unit area in the same unit time; k_f is the rate constant for the forward charge transfer process. The expression of the faradaic current is given as usual by:

$$\frac{i}{nFA} = D_a \left(\frac{\partial a}{\partial r}\right)_{r=r_0} - \frac{\mathrm{d}\Gamma_a}{\mathrm{d}t} = k_f K_a a(r_0, t) \tag{20}$$

Passing to the Laplace transforms of eqns. (17), (18) and (19), the transform of $a(r,t)$ is given by:

$$\bar{a}(r, s) = \frac{a^*}{s} - \frac{r_0}{r} \frac{k_f K_a a^*}{s(K_a s + D_a^{\frac{1}{2}} s^{\frac{1}{2}} + k_f K_a + D_a/r_0)} \exp\left[-\frac{s^{\frac{1}{2}}}{D_a^{\frac{1}{2}}}(r - r_0)\right] \tag{21}$$

The term on the right can be separated by the use of partial fractions in order to obtain the inverse transform and, subsequently, taking eqn. (20) into account, the faradaic current is derived:

$$\frac{i}{nFA} = k_f K_a a^* - \frac{k_f^2 K_a a^*}{(k_f + D_a/r_0 K_a)} \left\{1 + \frac{1-\chi}{2\chi} \exp[\lambda^2(1+\chi)^2 t] \operatorname{erfc}[\lambda(1+\chi)t^{\frac{1}{2}}]\right.$$
$$\left. - \frac{1+\chi}{2\chi} \exp[\lambda^2(1-\chi)^2 t] \cdot \operatorname{erfc}[\lambda(1-\chi)t^{\frac{1}{2}}]\right\} \tag{22}$$

where $\lambda = D_a^{\frac{1}{2}}/2K_a$ and $\chi = (1 - (k_f + D_a/r_0 K_a)/\lambda^2)^{\frac{1}{2}}$
Equation (22) holds only for $(k_f + D_a/r_0 K_a) \neq \lambda^2$. If $(k_f + D_a/r_0 K_a) = \lambda^2$, eqn. (21) takes the form:

$$\bar{a}(r, s) = \frac{a^*}{s} - \frac{r_0}{r} \frac{k_f a^*}{s(s^{\frac{1}{2}} + \lambda)^2} \exp\left[-\frac{s^{\frac{1}{2}}}{D_a^{\frac{1}{2}}}(r - r_0)\right] \tag{23}$$

while the faradaic current is given by:

$$\frac{i}{nFA} = k_f K_a a^* - k_f^2 K_a a^* \left[\frac{1}{\lambda^2} + \left(2t - \frac{1}{\lambda^2}\right) e^{\lambda^2 t} \operatorname{erfc}(\lambda t^{\frac{1}{2}}) - \frac{2t^{\frac{1}{2}}}{\pi^{\frac{1}{2}}\lambda}\right] \tag{24}$$

Letting r_0 tend to ∞, the case of spherical diffusion is reduced as usual to that of linear diffusion. Under these conditions, eqn. (22) becomes:

$$\frac{i}{nFA} = k_f K_a a^* \left\{ \frac{1+\xi}{2\xi} \exp[\lambda^2(1-\xi)^2 t] \operatorname{erfc}[\lambda(1-\xi)t^{\frac{1}{2}}] \right.$$
$$\left. - \frac{1-\xi}{2\xi} \exp[\lambda^2(1+\xi)^2 t] \operatorname{erfc}[\lambda(1+\xi)t^{\frac{1}{2}}] \right\} \quad (25)$$

where ξ is given by: $\xi = (1 - k_f/\lambda^2)^{\frac{1}{2}}$, while eqn. (24) is reduced to:

$$\frac{i}{nFA} = k_f K_a a^* \left[(1 - 2k_f t) \exp(k_f t) \operatorname{erfc}(k_f^{\frac{1}{2}} t^{\frac{1}{2}}) + \frac{2k_f^{\frac{1}{2}} t^{\frac{1}{2}}}{\pi^{\frac{1}{2}}} \right] \quad (26)$$

Obviously in the case under investigation, eqn. (26) holds for $\lambda^2 = k_f$. Proceeding along the rising portion of the polarographic wave, k_f increases approaching ∞, so that ξ takes both real ($\lambda^2 > k_f$) and imaginary ($\lambda^2 < k_f$) values. Although in the latter case, eqn. (25) is still valid, it is preferable to give this equation a form more suitable for the numerical calculation of the faradaic current. This may be attained by noting that the expression within the braces in eqn. (25) is given by:

$$\frac{1+\xi}{2\xi} \exp[\lambda^2(1-\xi)^2 t] \operatorname{erfc}[\lambda(1-\xi)t^{\frac{1}{2}}] - \frac{(1-\xi)}{2\xi} \exp[\lambda^2(1+\xi)^2 t] \operatorname{erfc}[\lambda(1+\xi)t^{\frac{1}{2}}]$$
$$= 1 - k_f \mathscr{L}^{-1} \left\{ \frac{1}{s[(s^{\frac{1}{2}} + \lambda)^2 + k_f - \lambda^2]} \right\} \quad (27)$$

In order to obtain the inverse transform of the expression:

$$1/s[(s^{\frac{1}{2}} + \lambda)^2 + k_f - \lambda^2] \quad (28)$$

the well known equation:

$$t^{-\nu} \int_0^\infty \exp\{-u^2/(8t)\} D_{2\nu-1}(2^{-\frac{1}{2}} u t^{-\frac{1}{2}}) f(u)\, du = \mathscr{L}^{-1}\{2^{\nu-\frac{1}{2}} \pi^{\frac{1}{2}} s^{\nu-1} g(s^{\frac{1}{2}})\} \quad (29)$$

may be used, where:

$$g(s) = \mathscr{L}\{f(t)\}$$

and $D_{2\nu-1}(x)$ is a parabolic cylinder function. In the case under investigation, by putting $\nu = 0$, eqn. (29) becomes:

$$\mathscr{L}^{-1}\left\{\frac{g(s^{\frac{1}{2}})}{s}\right\} = \int_0^\infty \exp\{-u^2/(8t)\} \frac{2^{\frac{1}{2}} t^{\frac{1}{4}}}{\pi^{\frac{1}{4}} u^{\frac{1}{2}}} W_{-\frac{1}{4},\frac{1}{4}}\left(\frac{u^2}{4t}\right) f(u)\, du \quad (30)$$

where $W_{-\frac{1}{4},\frac{1}{4}}(x)$ is a Whittaker's function. By noting that:

$$\operatorname{erfc}(x) = \frac{1}{\pi^{\frac{1}{2}} x^{\frac{1}{2}}} \exp(-\tfrac{1}{2}x^2) W_{-\frac{1}{4},\frac{1}{4}}(x^2)$$

the application of eqn. (30) to the expression (28) yields the following equation for the current, in view of eqn. (27):

$$\frac{i}{nFA} = k_f K_a a^* \left[1 - \frac{k_f}{(k_f - \lambda^2)^{\frac{1}{2}}} \int_0^\infty \operatorname{erfc}\left(\frac{u}{2t^{\frac{1}{2}}}\right) e^{-\lambda u} \sin((k_f - \lambda^2)^{\frac{1}{2}} u)\, du \right] \quad (31)$$

An analogous procedure applied to the case for $\lambda^2 > k_f$, yields the equation:

$$\frac{i}{nFA} = k_f K_a a^* \left[1 - \frac{k_f}{(\lambda^2 - k_f)^{\frac{1}{2}}} \int_0^\infty \operatorname{erfc}\left(\frac{u}{2t^{\frac{1}{2}}}\right) e^{-\lambda u} \sinh((\lambda^2 - k_f)^{\frac{1}{2}} u) du\right]$$

When $k_f \to \infty$, eqn. (25) becomes:

$$\lim_{k_f \to \infty} (i/nFA) = D_a^{\frac{1}{2}} a^* / \pi^{\frac{1}{2}} t^{\frac{1}{2}} \tag{32}$$

which represents the well known expression for the diffusion limiting current. Equation (32) may be easily derived from eqn. (25) by expanding the error function complement in the well known series:

$$\operatorname{erfc} x = \frac{\exp(-x^2)}{\pi^{\frac{1}{2}} x}\left[1 - \frac{1}{2x^2} + \frac{1 \cdot 3}{(2x^2)^2} - \frac{1 \cdot 3 \cdot 5}{(2x^2)^3} \cdots\right]$$

and retaining the first term of the expansion. If the adsorption coefficient, K_a, is very low ($K_a \ll \frac{1}{2} D_a^{\frac{1}{2}}$; $K_a^2 \ll D_a/4k_f$) one has:

$$\lambda = (D_a^{\frac{1}{2}}/2K_a) \gg 1$$

$$\xi = (1 - k_f/\lambda^2)^{\frac{1}{2}} \simeq (1 - k_f/2\lambda^2) \simeq 1$$

Under these conditions, the second term within the braces in eqn. (25) may be neglected. In fact, it is the product of two factors one of which (*i.e.*, $(1-\xi)/2\xi$) is very close to 0 while the other (*i.e.*, $\exp[\lambda^2(1+\xi)^2 t] \cdot \operatorname{erfc}[\lambda(1+\xi)t^{\frac{1}{2}}]$) takes unit value for $t=0$, approaching 0 very rapidly on account of the high value of $\lambda(1+\xi)$. The first term within the braces in eqn. (25) consists of the product of a factor very close to 1 (*i.e.*, $1+\xi/(2\xi)$) by the factor:

$$\exp[\lambda^2(1-\xi)^2 t] \operatorname{erfc}[\lambda(1-\xi)t^{\frac{1}{2}}] \simeq \exp(k_f^2 K_a^2 t/D_a) \operatorname{erfc}(k_f K_a t^{\frac{1}{2}}/D_a^{\frac{1}{2}})$$

It immediately follows that the faradaic current is given by:

$$i/nFA \simeq k_f K_a a^* \exp(k_f^2 K_a^2 t/D_a) \operatorname{erfc}(k_f K_a t^{\frac{1}{2}}/D_a^{\frac{1}{2}}) \tag{33}$$

Equation (33) represents the well known expression of the instantaneous polarographic current at a plane stationary electrode for the case of a slow electron transfer in the absence of adsorption, once it is noted that $k_f K_a$ expresses the rate constant for the forward charge transfer process with the concentration of A at $x=0$ expressed by $a(0,t)$ instead of Γ_a. Consequently, eqn. (33), which constitutes a limiting case of eqn. (25) for low values of K_a, represents the exact solution of a problem analogous to that considered in this paragraph, where the possibility of removal of the depolarizer A from the electrode surface is excluded ($d\Gamma_a/dt=0$), *i.e.*, where the equality between the rate of charge transfer and the flux of the depolarizer is assumed

$$\left(k_f K_a a(0,t) = D_a \left(\frac{\partial a}{\partial x}\right)_{x=0}\right).$$

Figure 5 shows the current–time curves in the case of linear adsorption of the depolarizer as obtained from eqn. (25) for $D = 10^{-6}$ cm^2/sec, $K_a = 10^{-3}$ cm and $k_f = 0.1$, 0.5 and 1.0 sec^{-1}, respectively. The dashed curves in the same figure express the *i–t* curves derived from eqn. (33) for the same data mentioned previously. From Fig. 5 it appears that the differences between the two equations may be appreciable.

In order to separate the two contributions, $D_a(\partial a/\partial x)_{x=0}$ and $-K_a(\partial a/\partial t)_{x=0}$, to the faradaic current also for the case of a slow electron transfer, it will be noted that, obtaining $(\partial \bar{a}(r,s)/\partial r)_{r=r_0}$ from eqn. (21) and letting r_0 approach ∞

$$D_a\left(\frac{\partial \bar{a}}{\partial x}\right)_{x=0} = \frac{D_a{}^{\frac{1}{2}} k_f a^*}{s^{\frac{1}{2}}\{s+(D_a{}^{\frac{1}{2}}/K_a)s^{\frac{1}{2}}+k_f\}} = \frac{D_a{}^{\frac{1}{2}} k_f a^*}{s^{\frac{1}{2}}[(s^{\frac{1}{2}}+\lambda)^2+k_f-\lambda^2]} \tag{34}$$

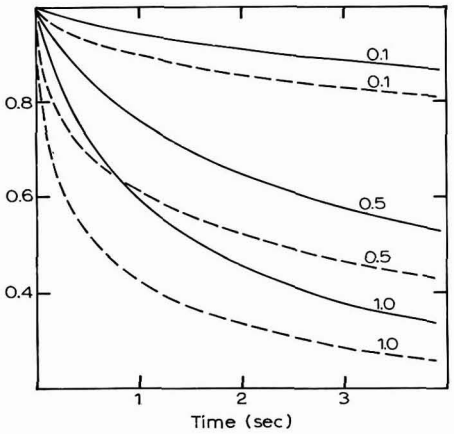

Fig. 5. Calcd. value of $i/nFAk_fK_aa^*$ as a function of time. The solid curves have been obtained from eqn. (25) or eqn. (31) and the dashed curves from eqn. (33), for $D_a = 10^{-6}$ cm²/sec and $K_a = 10^{-3}$ cm. Numbers on each curve refer to the value of k_f (sec^{-1}).

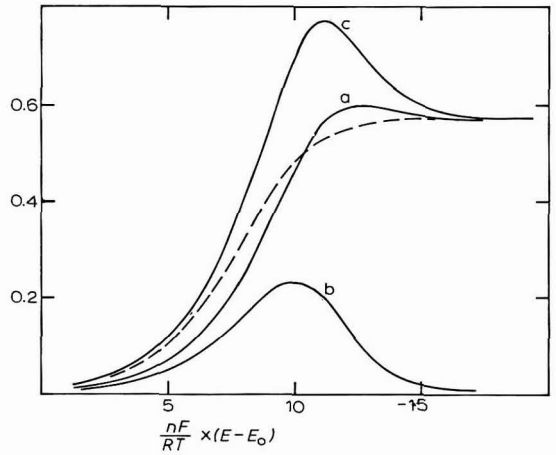

Fig. 6. Calcd. values of

$$\text{(a)}, \frac{D_a}{K_a a^*}\left(\frac{\partial a}{\partial x}\right)_{x=0}; \text{ (b)}, -\frac{1}{a^*}\left(\frac{\partial a}{\partial t}\right)_{x=0}; \text{ (c)}, \frac{i}{nFAK_a a^*}$$

as functions of potential. The curves have been obtained from eqns. (35), (38), (25) for $k_f < \lambda^2$ and from eqns. (36), (39), (31) for $k_f > \lambda^2$. It is assumed that $D_a = 10^{-6}$ cm²/sec, $K_a = 10^{-3}$ cm, $t = 1$ sec, $T = 25°$. The values of $E - E_0$ have been derived from the equation: $E - E_0 = -(RT/\alpha nF)\ln(k_f/k_s)$ for $\alpha = 0.5$ and $k_s = 10^{-2}$ sec^{-1}. The dashed curve expresses $i/nFAK_aa^*$ as obtained from eqn. (33) for the same data.

By separating the second term in eqn. (34), the inveres transform is given by:

$$D_a\left(\frac{\partial a}{\partial x}\right)_{x=0} = \frac{k_f K_a a^*}{\xi}\{\exp[\lambda^2(1-\xi)^2 t]\,\mathrm{erfc}[\lambda(1-\xi)t^{\frac{1}{2}}] - \exp[\lambda^2(1+\xi)^2 t]\,\mathrm{erfc}[\lambda(1+\xi)t^{\frac{1}{2}}]\} \quad (35)$$

If $k_f > \lambda$, it is more convenient to represent the flux of A in the form:

$$D_a\left(\frac{\partial a}{\partial x}\right)_{x=0} = \frac{D_a^{\frac{1}{2}} k_f a^*}{\pi^{\frac{1}{2}} t^{\frac{1}{2}} (k_f-\lambda^2)^{\frac{1}{2}}} \int_0^\infty \exp\left[-\left(\frac{u^2}{4t} + \lambda u\right)\right] \sin((k_f-\lambda^2)^{\frac{1}{2}} u)\,\mathrm{d}u \quad (36)$$

which has been obtained from eqn. (34) by means of the well known equation:

$$\mathscr{L}^{-1}\left\{\frac{g(s^{\frac{1}{2}})}{s^{\frac{1}{2}}}\right\} = \frac{1}{\pi^{\frac{1}{2}} t^{\frac{1}{2}}} \int_0^\infty \exp\{-u^2/(4t)\} f(u)\,\mathrm{d}u$$

With regard to the rate of change of Γ_a, obtaining

$$\overline{\left(\frac{\partial a(r,t)}{\partial t}\right)}_{r=r_0}$$

from eqn. (21) and letting r_0 approach ∞, gives

$$-K_a\overline{\left(\frac{\partial a}{\partial t}\right)}_{x=0} = \frac{k_f K_a a^*}{\{s+(D_a^{\frac{1}{2}}/K_a)s^{\frac{1}{2}}+k_f\}} = \frac{k_f K_a a^*}{[(s^{\frac{1}{2}}+\lambda)^2+k_f-\lambda^2]} \quad (37)$$

By separating the second term in eqn. (37) in the usual way, it follows that:

$$-K_a\left(\frac{\partial a}{\partial t}\right)_{x=0} = k_f K_a a^* \left\{\frac{1+\xi}{2\xi}\exp[\lambda^2(1+\xi)^2 t]\,\mathrm{erfc}[\lambda(1+\xi)t^{\frac{1}{2}} - \frac{1-\xi}{2\xi}\exp[\lambda^2(1-\xi)^2 t]\,\mathrm{erfc}[\lambda(1-\xi)t^{\frac{1}{2}}]\right\} \quad (38)$$

When $k_f > \lambda$, $-K_a(\partial a/\partial t)_{x=0}$ may be given the following form:

$$-K_a\left(\frac{\partial a}{\partial t}\right)_{x=0} = \frac{k_f K_a a^*}{2\pi^{\frac{1}{2}} t^{\frac{3}{2}} (k_f-\lambda^2)^{\frac{1}{2}}} \int_0^\infty u\cdot\exp\left[-\left(\frac{u^2}{4t} + \lambda u\right)\right]\cdot\sin((k_f-\lambda^2)^{\frac{1}{2}} u)\,\mathrm{d}u \quad (39)$$

Equation (39) has been derived from eqn. (37) by making use of the general equation:

$$\mathscr{L}^{-1}\{g(s^{\frac{1}{2}})s^{(\frac{1}{2}n-\frac{1}{2})}\} = \frac{t^{-(\frac{1}{2}n+\frac{1}{2})}}{2^{\frac{1}{2}n}\pi^{\frac{1}{2}}} \int_0^\infty \exp\{-u^2/(4t)\}\, He_n(2^{-\frac{1}{2}} u t^{-\frac{1}{2}})\, f(u)\,\mathrm{d}u$$

for $n=1$, where $He_n(x)$ is a Hermite polynomial.

Figure 6 shows

$$\frac{i}{nFAK_a a^*},\ \frac{D_a}{K_a a^*}\left(\frac{\partial a}{\partial x}\right)_{x=0},\ \text{and}\ -\frac{1}{a^*}\left(\frac{\partial a}{\partial t}\right)_{x=0}$$

as functions of potential for $t=1$ sec, $D_a = 10^{-6}$ cm^2/sec, $K_a = 10^{-3}$ cm and for the transfer coefficient, $\alpha = 0.5$. The above quantities have been obtained from eqns. (25), (35) and (38) for $k_f < \lambda^2$ and from eqns. (31), (36) and (39), for $k_f > \lambda^2$. In the latter case, the integrations have been performed numerically with an IBM 7090. Figure 6 shows that the presence of a maximum due to adsorption is to be expected also in the case of a slow electron transfer, if K_a is sufficiently high, and, furthermore,

that the cause of the maximum is still mainly represented by the contribution of $d\Gamma_a/dt$ to the faradaic current. The intuitive explanation of the maximum in the curve, $-d\Gamma_a/dt$ *vs.* E, is analogous to that already given for the case of a fast electron transfer, the only difference being that in the present case the surface concentration, Γ_a, as well as its rate of change, do not depend on the adsorption of the product of the electrode reaction. It follows that $d\Gamma_a/dt$ is always negative, approaching 0 for sufficiently large values of time at any given potential and for $E \to \infty$ or $E \to -\infty$ at any given time.

CONCLUSIONS

According to the simplified model previously considered, the presence of polarographic maxima due to linear adsorption of the depolarizer is to be expected in the case of both fast and slow charge transfer processes, provided the adsorption coefficients of the electroactive substances are sufficiently high. This is in partial disagreement with BARKER AND BOLZAN[5], who claim that irreversibility suppresses any tendency for maximum formation. They observed the presence of maxima due to adsorption with the "normal" pulse-polarographic technique, making use, for the interpretation of their experimental results, of an equation derivable from eqn. (15) by neglecting K_b with respect to $\theta' K_a$, *i.e.*, by neglecting the adsorption of the product of the electrode reaction. Such an equation is not very accurate, as even if the tendency of B to be adsorbed is much lower than that of A ($K_b \ll K_a$) the maxima due to adsorption extend to potentials where $\theta' \ll 1$. Thus Fig. 4 shows that maxima of different heights and shapes are to be expected for values of K_b that are very low but differ one from another. According to the concept of charge separation and recombination introduced by DELAHAY[7], the measurable current differs from the faradaic current, being expressed, for the case under investigation, by the equation:

$$\frac{i}{AF} = nD_a \left(\frac{\partial a}{\partial x}\right)_{x=0} + \sum_{i \neq a} Z_i \frac{d\Gamma_i}{dt} \qquad (40)$$

where the summation includes all ionic species except A. The examples of polarographic maxima reported by BARKER[5,10] refer to the reduction of some metal ions to the metallic state on mercury in complexing solutions of halides. Under these conditions (if we exclude the possibility of interaction of the depolarizer adsorbed within the double layer with the electro-inactive species specifically and not specifically adsorbed) it seems reasonable to suppose that the contribution of the second term on the right in eqn. (40) to the measurable current becomes negligible in the time-scale of polarographic measurements and also, although to a less degree, of pulse polarographic measurements. Consequently, the polarographic current should be proportional to the flux of the depolarizer and therefore, in accordance with the treatment previously outlined, it should not exhibit maxima. The very existence of the maxima reported by BARKER AND BOLZAN[5] seems to indicate that in the time-scale of the pulse-polarographic measurements carried out by these authors the measurable current does not differ excessively from the faradaic current, as expressed by eqn. (8). This may be attributed to the fact that under these experimental conditions the non-faradaic charge relative to the adsorption of one mole of A (or of a species containing A) is probably lower than the faradaic charge relative to the reduc-

tion of one mole of A. Obviously, the best agreement between experimental and faradaic currents is to be expected when the specifically adsorbed species containing A is electrically neutral. In fact, the measurements of K_a as a function of the concentration of bromide, carried out by BARKER AND BOLZAN[5] in connection with the reduction of Pb^{2+} on mercury in bromide solutions seem to show (although from a completely different point of view) that the oxidized species preferentially adsorbed under these conditions is the neutral species, $PbBr_2$. Another reason for the agreement between experimental and faradaic currents may be that a change in the surface concentration of Γ_a, expressed by $d\Gamma_a/dt$, may induce a simultaneous change in the surface concentrations of some electroinactive ionic species. Such an interaction among electroinactive species and depolarizer within the double layer would make the contribution of the second term on the right in eqn. (40) significant also in the time-scale of polarographic measurements, causing the application of eqn. (40) to be problematic. However, when the reduction of Pb^{2+} in bromide solutions is considered, one should assume that the effects of this possible interaction are analogous to those to be expected under the hypothesis of adsorption of the neutral species $PbBr_2$, so that this latter hypothesis seems more plausible.

SUMMARY

The theoretical current–time curves at constant potential on spherical and plane electrodes have been derived in the case that the depolarizer and the product of the electrode reaction are adsorbed on the electrode surface according to linear isotherms. Under the assumption that the adsorption coefficients are independent of potential, the theoretical treatment shows that a maximum in the voltammetric curves is to be expected both for slow and fast charge transfer processes, if the adsorption coefficient of the depolarizer is sufficiently high and greater than that of the product of the electrode reaction, the latter condition being required only for a Nernstian charge transfer. Possible differences between faradaic and directly measurable currents have been examined, in view of the concept of charge separation or recombination.

REFERENCES

1 R. BRDIČKA AND E. KNOBLOCH, *Z. Elektrochem.*, 47 (1941) 721.
2 R. BRDIČKA, *Z. Elektrochem.*, 48 (1942) 278.
3 M. SENDA AND P. DELAHAY, *J. Phys. Chem.*, 65 (1961) 1580.
4 M. SLUYTERS-REHBACH, B. TIMMER AND J. H. SLUYTERS, *J. Electroanal. Chem.*, 15 (1967) 151.
5 G. C. BARKER AND J. A. BOLZAN, *Z. Anal. Chem.*, 216 (1966) 215.
6 D. COZZI, G. RASPI AND L. NUCCI, *J. Electroanal. Chem.*, 12 (1966) 36.
7 P. DELAHAY, *J. Phys. Chem.*, 70 (1966) 2373.
8 K. HOLUB AND J. KORYTA, *Collection Czech. Chem. Commun.*, 30 (1965) 3785.
9 K. HOLUB, *Collection Czech. Chem. Commun.*, 31 (1966) 1655.
10 G. C. BARKER, *Transactions of the Symposium on Electrode Processes*, edited by E. YEAGER, John Wiley and Sons, New York, 1961.

ELECTROANALYTICAL CHEMISTRY AND INTERFACIAL ELECTROCHEMISTRY 21
Elsevier Sequoia S.A., Lausanne – Printed in The Netherlands

THE RELAXATION AND SURFACE CONDUCTIVITY CORRECTIONS IN THE THEORY OF ELECTROPHORESIS OF NON-CONDUCTING SOLID SPHERICAL PARTICLES*

M. SENGUPTA AND AMAL K. BOSE
Department of Chemistry, Science College, Calcutta-9 (India)
(Received November 9th, 1967)

The Henry[1] equation for the electrophoretic velocity, U, of a solid spherical particle of radius, a, under an applied field, E, through a solution of viscosity coefficient, η_1, and dielectric constant, ε_1, is:

$$U = (E\varepsilon_1\zeta/6\pi\eta_1)(1+\lambda F_1(\varkappa a)) \quad (1)$$

where $F_1(\varkappa a)$ is the Henry function of the ratio of the particle radius to the thickness $(1/\varkappa)$ of the electrical double layer in the outer solution ($\varkappa$ is the Debye–Huckel parameter given by: $\varkappa^2 = 4\pi e^2 \Sigma n_i z_i^2/\varepsilon_1 kT$), λ is a function of the specific conductivities, σ_1 and σ_2, of the solution and the solid, respectively, *viz.*, $\lambda = (\sigma_1 - \sigma_2)/(2\sigma_1 + \sigma_2)$, ζ is the electrical potential difference between the moving solid surface (at the plane of shear) and the solution, and the other symbols have their usual meaning. Two different corrections have been applied to this equation in order to take into account the effects of the relaxational polarisation of the ion-atmosphere surrounding the charged particle, and of surface conductivity.

THE RELAXATION EFFECT

The relaxation effect, *i.e.*, the retardation of particle motion due to the deformation of the ion-atmosphere surrounding the charged particle by the applied field, has been treated mathematically by BOOTH[2] and OVERBEEK[3]. They find that additional terms involving higher powers of ζ should be included in eqn. (1). For symmetrical electrolytes, the term containing the second power of ζ vanishes, so that the electrophoretic velocity is given up to the third power of ζ by an equation of the type:

$$U = C_1\zeta + C_3\zeta^3 \quad (2)$$

where $C_1\zeta$ is identical with the Henry expression (right-hand side of eqn. (1)) for non-conducting particles, and C_3 is given by:

$$C_3 = -E(\varepsilon_1 kT/6\pi\eta_1 e)(e/kT)^3 M \quad (3)$$

* An abstract of this paper has been published in the Proceedings of the 54th Session of the Indian Science Congress, Hyderabad, 1967.

M, according to BOOTH, has the value

$$M = q_3 X_3^* + q_3 Y_3^* + q_3^* Z_3 \tag{4}$$

where q_3 and q_3^* are functions of the ionic mobilities and X_3^*, Y_3^* and Z_3 are complicated but known functions of $\varkappa a$; while according to OVERBEEK, for 1–1 electrolytes,

$$M = f_3 + [(\varrho_+ + \varrho_-)/2e](\varepsilon_1 kT/6\pi\eta_1 e) f_4 \tag{5}$$

where again f_3 and f_4 are known functions of $\varkappa a$, and the ϱ_+, ϱ_- are the ionic frictional coefficients*. Despite the independent derivations and the different forms, the two results have been reported[4,5] to be in close agreement, within a computational error of about 3%.

From the relaxation correction eqn. (2), the electrophoretic velocity, U, can be calculated as a function of $\varkappa a$ for some assumed value of ζ. If the particle radius be unknown, then ζ and a can be taken to be two different adjustable parameters. This has been done by PAINE[5] and the calculated mobility *vs.* concentration curve has been shown to be in close agreement with the results observed for copper oxide sols, except at higher concentrations particularly for the largest particles. The method is rather laborious, particularly considering the complexity of the Booth expression (eqns. (3) and (4)) that has been used. STACKELBERG *et al.*[6], who have investigated the electrophoretic mobility of paraffin oil emulsions with 1% oleic acid, have used the Overbeek expression (eqns. (3) and (5)) for the calculation of U. They report that a ζ-potential value of -100 mV gives the best fit of the calculated ($a \sim 10^{-4}$ cm) curves and experimental, when NaCl is present as the indifferent electrolyte.

The application of the relaxation correction for the theoretical interpretation of the mobility *vs.* concentration curve by the above authors involves, however, the assumption that ζ remains constant while the electrolyte concentration is varied; but ζ is known to depend in a complex manner on the ionic state of the solution, and its magnitude varies with the electrolyte concentration and the nature of the ions present in the solution, either because of purely electrostatic effects (double-layer interactions) or because of the specific nature of the ions present. Hence, the assumption that this dependence is absent, or weak, in some particular concentration regions, *e.g.*, at low concentrations, is, although plausible, arbitrary. More or less the same criticism has been made by OVERBEEK[3] in respect to the application of Debye–Huckel relaxation equation by PAINE to electrophoretic data for very small particles ($\varkappa a < 1/10$) of inorganic sols.

SURFACE CONDUCTIVITY EFFECT

A somewhat different modification of the Henry equation has been made in order to take into account the effect of surface conductivity. The presence of an increased conductivity at the interface between two phases has been known for some time from conductivity measurements in capillaries (MCBAIN[7]) and in diaphragms (BRIGGS[8]), and has been shown to affect the ζ-potential measurements in

* The authors are indebted to Prof. B. N. GHOSH for drawing their attention to the recent extension of the Overbeek equation by WIERSEMA (*J. Colloid Sci.*, 22 (1966) 78). However, it has not been possible to incorporate these results into the present analysis.

such systems by electroosmosis (MANEGOLD AND SOLF[9]) or streaming potential (RUTGERS[10]). The importance of a surface conductivity correction in electrophoresis was pointed out by BIKERMAN[11] who gave a treatment for the electrophoresis of cylindrical particles moving with the axis along the direction of field. For spherical particles, the treatment has been given independently by BOOTH[12] and HENRY[13]. The analysis of both these authors concerns, however, only the Henry term of eqn. (2). They showed that the surface conductivity manifests itself in its effect simply as an increased conductivity of the material of the particle, so that an equation of the form of eqn. (1) is again obtained, *viz.*,

$$U = (E\varepsilon_1\zeta/6\pi\eta_1)(1 + \lambda_s F_1(\varkappa a)) \tag{6}$$

where

$$\lambda_s = [\sigma_1 - (\sigma_2 + 2\sigma_s/a)]/2\sigma_1 + (\sigma_2 + 2\sigma_s/a)],$$

σ_s being the specific surface conductivity. For non-conducting particles,

$$\lambda_s = (\sigma_1 - 2\sigma_s/a)/(2(\sigma_1 + \sigma_s/a).$$

The difficulty in verifying the applicability of formula (6) in the absence of a knowledge of the magnitude of the specific surface conductivity, σ_s, has been mentioned by various authors[6,13,14]. As is well known, the accurate experimental measurement of this quantity is difficult and data are generally meagre except for the glass–water interface. Even for this system the earlier values were uncertain even as to the order of magnitude; recent more accurate measurements have given values of the order of $10^{-9}\ \Omega^{-1}$ in $10^{-4}\ N$ electrolyte solutions; theoretical estimates based on the BIKERMAN[15] or the URBAN–WHITE–STRASSNER[16] formulae give quantities of the same order. Using a value of this order of magnitude, TAYLOR AND WOOD[14] have concluded that for decalin droplets of radius 25 μ in distilled water of conductivity, $3.7 \cdot 10^{-6}\ \Omega^{-1}\ \mathrm{cm}^{-1}$, the surface conductivity correction is negligible. A similar conclusion was reached by PAINE[5] who concluded that even the assumption of an infinitely large surface conductivity would produce only an insignificant effect on the calculated value of the electrophoretic mobility of the CuO sol particles investigated.

SCOPE OF APPLICABILITY OF THE TWO CORRECTIONS, AND THE COMPARATIVE EVALUATION OF EQUATIONS (2) AND (6)

Apart from these considerations, there is some uncertainty as to the relative scope of applicability of the two corrections to the electrophoresis equation. Thus, according to BOOTH[12,17], the two corrections are quite distinct and the higher terms of eqn. (2) should likewise be corrected for the surface conductivity effect, although no derivation has so far been given. BIKERMAN[18] and OVERBEEK[3] maintain, however, that the relaxation correction includes the surface conductivity correction and that both methods attack fundamentally the same problem. It is, however, clear on careful consideration, that OVERBEEK refers to that part of surface conductivity due to the excess ions of the double layer and their electroosmotic movement in the applied field, *i.e.*, the "normal" surface conductivity, the theoretical treatment for which has been given by BIKERMAN[15] and URBAN–WHITE–STRASSNER[16]. There may be present, however, a significant contribution to surface conductivity from the

migration of ions along the surface phase itself; the measured surface conductivity in such cases may far exceed the value calculated theoretically from the ζ-potential. Experimental measurements on mineral oxide–water systems (BUCHANAN *et al.*[19]) have shown that the measured surface conductivity exceeds by some orders of magnitude the theoretical value calculated from the ζ-potential; the excess conductivity has been attributed to the semi-conducting properties of the materials. A similar conclusion was reached for the glass–water system, the excess conductivity being attributed to conduction through the swollen glass surface (OVERBEEK[3]). There would doubtless have been many more instances of such "abnormal" surface conductivity, but for the paucity of accurate experimental measurements.

Considering now the Henry–Booth equation for the surface conductivity effect in electrophoresis (eqn. (6)), we find that the specific surface conductivity, σ_s, has been taken into consideration simply as an excess conductivity of the surface layer, or more specifically, has been taken to be given by: $\sigma_s = \lim_{a_2 \to a_1 = a} + \sigma_3(a_2 - a_1)$, where σ_3 is the specific conductivity of a spherical shell of thickness $(a_2 - a_1)$ surrounding the spherical particle of radius, a. It is obvious that since no detailed picture of the mechanism by which this conductivity arises has been invoked, the electrophoresis equation so deduced should be applicable irrespective of whether it is a case of "normal" or "abnormal" surface conductivity. It may, in fact, be more successful empirically than the relaxation eqn. (2), in so far as it is more comprehensive than the latter in taking into account any "abnormal" surface conductivity present.

The results of a comparative estimation of the two corrections, in the few cases where this has been carried out, are uncertain and inconclusive. The conclusions of PAINE[5] and TAYLOR AND WOOD[14] have already been mentioned. Considering the surface conductivity eqn. (6), we find, however, that the surface conductivity factor, λ_s, appears multiplied with the Henry-function term, $F_1(\varkappa a)$. Now, the latter tends to zero as $\varkappa a \to 0$, so that for small values of $\varkappa a$, the surface conductivity correction would be small anyway, as in the case of the CuO sol particles mentioned. On the other hand, for large $\varkappa a$ ($\geqslant 25$), the magnitude of the correction depends on the magnitude of the λ_s-factor (BOOTH[12]), and despite the small order of magnitude of σ_s (usually $\sim 10^{-9}\ \Omega^{-1}$) may not always be as insignificant as in the case investigated by TAYLOR AND WOOD. Finally, the conclusion of STACKELBERG *et al.* that the results of their measurements can best be accounted for on the basis of relaxation correction only, cannot also be considered to be conclusive. They have compared the observed mobility values of paraffin oil droplets with those calculated by the equations of Henry and Overbeek (our eqns. (1) and (2 with 3,5), respectively); it is obvious, however, that in order to decide between the applicability of surface conductivity and relaxation corrections, the comparison should rather be between eqns. (6) and (2 with 3 and 5). The results of this comparison, assuming a reasonable value for σ_s, show that, for values of ζ within the limits wherein the relaxation eqn. (2) is valid, the choice between the two corrections becomes much more difficult.

In one special case, however, it appears that a more or less correct appraisal of the applicability of eqns. (2) and (6) can be made notwithstanding the uncertainty with regard to the exact value of the specific surface conductivity, σ_s. For electrophoretic measurements with particles of different known sizes at the same electrolyte concentration, the true ζ-potential (ζ) and the specific surface conductivity (σ_s)

should remain constant. The ζ-potential calculated by the Smoluchowski equation, $\zeta_{\text{Smol.}}$, should, however, vary with the particle size, and from this variation the values of the constants, ζ and σ_s, can be found. BOOTH[12] suggested a comparison of these values with those obtained from streaming potential measurement in capillaries of the same material, of different radii. However, an easier verification of formula (6) from electrophoresis measurements alone has been indicated by GHOSH[20]. For the largest particles ($\varkappa a \geqslant 100$), the Henry function factor, $F_1(\varkappa a)$, can be taken to be unity, so that eqn. (6) reduces to $U = E\varepsilon_1\zeta/4\pi\eta_1 \cdot \sigma_1/(\sigma_1 + \sigma_s/a)$. This may be transformed into the linear form:

$$1/\zeta_{\text{Smol.}} = 1/\zeta + \sigma_s/\zeta\sigma_1 a \tag{7}$$

by introducing the apparent ζ-potential, $\zeta_{\text{Smol.}}$, calculated by the Smoluchowski equation: $\zeta_{\text{Smol.}} = 4\pi\eta_1 U/E\varepsilon_1$. The reciprocal of the apparent ζ-potential should thus be a linear function of the reciprocal of the particle size*. This has actually been verified[20] for the data of MOONEY[21] on the variation of the electrophoretic mobility of hydrocarbon droplets with their radius. The value of the constants, ζ and σ_s, having been determined from the above linear plot, these can then be used in the complete eqn. (6) and the mobility–radius curve calculated over the whole range of values of $\varkappa a$. The theoretical curve thus calculated can then be compared with the experimental curve, for when $\varkappa a$ is large or small.

The relaxation eqn. (2) can also be applied as usual to the same data. Since, however, U is the experimentally determined quantity and ζ the calculated one, the application of the relaxation correction in the form of eqn. (2) is awkward as it involves the solution of a third-degree equation. This may be simplified by inverting series (2) (*cf.* however ref. 22), when for the case of symmetrical electrolytes we obtain

$$\zeta = (U/C_1) - (C_3/C_1)(U/C_1)^3 \tag{9}$$

where, using the Overbeek expression for 1–1 electrolytes,

$$C_1 = (E\varepsilon_1/6\pi\eta_1)f_1, \quad (f_1 = 1 + \tfrac{1}{2}F_1) \tag{10}$$

$$C_3 = -\frac{E\varepsilon_1}{6\pi\eta_1}\left(\frac{e}{kT}\right)^2\left[f_3 + \frac{\varrho_+ + \varrho_-}{2e}\,\frac{\varepsilon_1 kT}{6\pi\eta_1 e}\,f_4\right] \tag{11}$$

A calculation by means of series (9) should then lead to a constant value of the true *zeta*-potential, ζ, for varying $\varkappa a$.

THE EXPERIMENTAL DATA OF MOONEY AND STACKELBERG, AND THE CALCULATIONS

The experimental determination of the mobility of particles of varying sizes at the same electrolyte concentration has not been carried out extensively. However, the data of MOONEY AND STACKELBERG mentioned are pertinent for our purpose, and are used to illustrate the method of verification of the theoretical equations. The mobility values for different radii were obtained from the figures given by these authors by suitable photo-magnification and then transference on to graph paper.

* The linear plot can also be made in the form:

$$1/U = (1/U_{\text{Smol.}})(1 + \sigma_s/\sigma_1 a) \tag{8}$$

from which: $\zeta = 4\pi\eta_1/E\varepsilon_1$ intercept, and σ_s/σ_1 = slope/intercept.

MOONEY's results are for mobility measurements in emulsions of "Stanolind" in distilled water and some electrolyte solutions, and of three other oils: iodobenzene, tribromohydrin (*sym*-1,2,3-tribromopropane) and dimethylaniline, all in distilled water. Particle diameters and velocities were recorded in terms of divisions in the eye-piece micrometer scale (1 div. = 0.001092 cm). The potential gradient was 9.875 V/cm, the distilled water used had an impurity content of $2 \cdot 10^{-5}$ N ($\varkappa = 1.47 \cdot 10^5$ cm^{-1}) and the temperature (unrecorded) was carefully maintained constant. STACKELBERG's data (mobilities in μ/sec in distilled water, 10^{-4} N and 10^{-3} N KCl solutions) are for droplets of paraffin oil with 1% oleic acid, to which the requisite quantity of tetrachloroethane or tetrachloroethylene was added in order to reduce creaming. The results were converted to a field strength of exactly 1 V/cm and a temperature of 25°. The distilled water used had an impurity content of 10^{-5} N ($\varkappa = 10^5$ cm^{-1}).

Calculations for relaxation correction have not been carried out exhaustively, but only with suitably chosen data, because only the general nature of results was of interest*. The Overbeek equation (eqns. (10) and (11)) has been used. A temperature of 25° was assumed for MOONEY's data; the values of η_1 and ε_1 were taken to be 8.95 mP and 78.54, respectively, and, assuming the electrolytic impurity to have been KCl (which is not critical), the ion-conductance values (Ω^{-1} cm^2) were taken to be 73.52 and 76.34. The log $\varkappa a$-values were calculated from these figures. The values of the functions, f_1, f_3, f_4, for each $\varkappa a$ were obtained from a plot (on a suitably large scale) of these functions from their tables of values as given by OVERBEEK[3]. The values of the coefficients, C_1 and C_3, were then calculated from the values of f_1, f_3, f_4. The values of ζ-potential were calculated by using: (i) only the Henry term (*i.e.*, U/C_1) and (ii) the complete Overbeek expression of eqn. (9), of which only the latter is shown graphically.

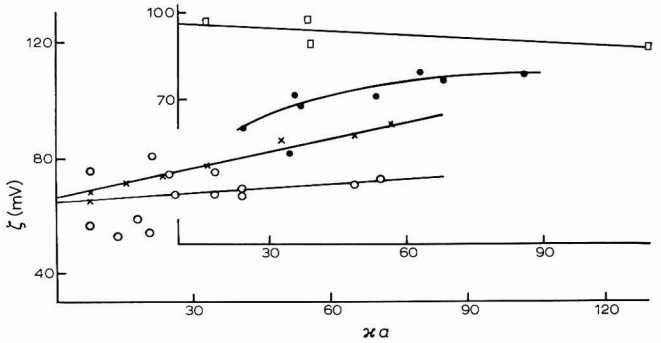

Fig. 1. Relaxation correction (eqns. (9)–(11)) applied to electrophoretic mobility data of MOONEY (distilled water, tribromohydrin) (×), and VON STACKELBERG (paraffin oil) ((○) distilled water, $C_2H_2Cl_4$; (●) 10^{-4} N KCl, $C_2H_2Cl_4$; (□) 10^{-4} N KCl, C_2Cl_4).

Relaxation correction calculations with STACKELBERG's data are similar. Results of relaxation correction calculations are shown in Fig. 1.

The surface conductance correction calculations are more exhaustive. For STACKELBERG's data, the $1/U$-values in (μcm sec^{-1} V^{-1})$^{-1}$ were first plotted against

* Results of some further relaxation correction calculations with data for Stanolind, are given in ref. 23.

$1/a$ in $(\mu)^{-1}$. For MOONEY's data, $1/U$ in (scale div./sec)$^{-1}$ and $1/a$ in (scale div.)$^{-1}$ were plotted directly, so that the ordinates are in units of 1.1058 (μcm sec^{-1} V^{-1})$^{-1}$ and the abscissae in units of 5.46 $(\mu)^{-1}$. From the intercept and slope of the linear curve best fitting in the region of large $\varkappa a$, the values of the constants, ζ and σ_s, were obtained for each solution. For some suitably chosen a-values, the values of log $\varkappa a$ and the ratio $\sigma_s/\sigma_1 a$ were then calculated. The corresponding values of the quantities, λ_s, for the particles (assumed to be non-conducting), of the Henry function, $F_1(\varkappa a)$ $(=2(f_1(\varkappa a)-1))$, and of $(1+\lambda_s F_1)$ were calculated successively; finally, the values of reciprocal mobility $(1/U)$ were obtained. In the case of MOONEY's results,

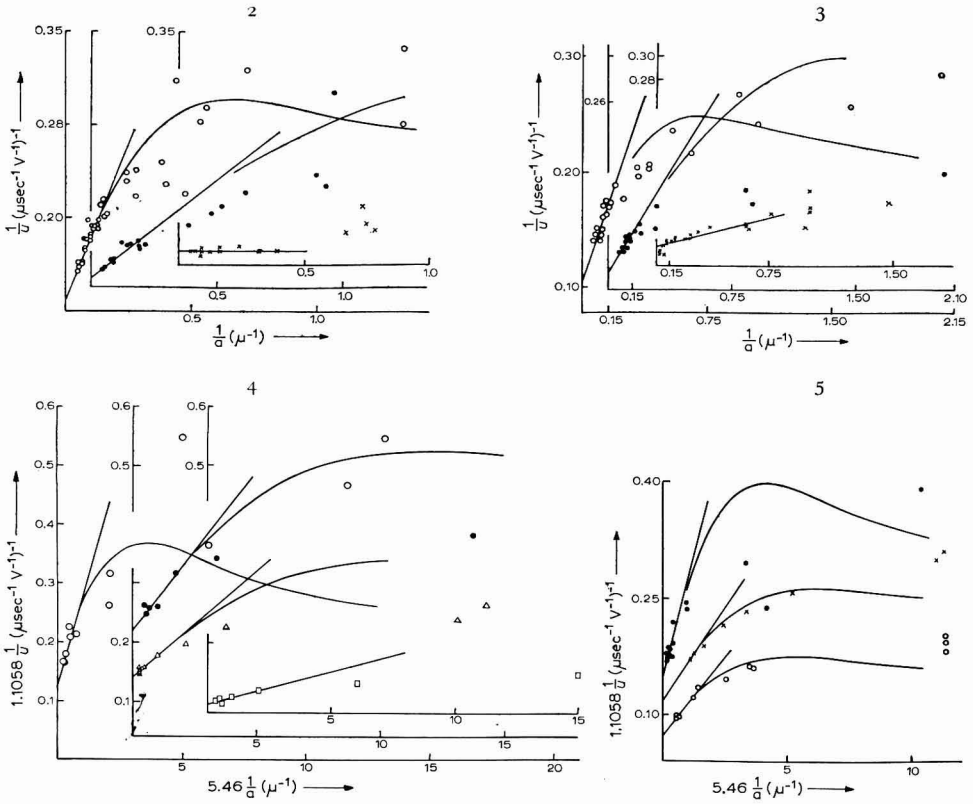

Figs. 2–5. Surface conductivity correction (eqn. (6)) applied to electrophoretic mobility data of VON STACKELBERG (Figs. 2–3) and MOONEY (Figs. 4–5).

Fig. 2. $C_2H_2Cl_4$-weighted paraffin oil droplets. (○) Distilled water (ζ = 111.3 mV); (●) 10^{-4} N KCl (ζ = 95.9 mV, $\sigma_s/\sigma_1 = 0.111 \times 10^{-3}$); (×) 10^{-3} N KCl.

Fig. 3. C_2Cl_4-weighted paraffin oil droplets. (○) Distilled water (ζ = 132.6 mV); (●) 10^{-4} N KCl (ζ = 126.7 mV; $\sigma_s/\sigma_1 = 0.209 \times 10^{-3}$); (×) 10^{-3} N KCl.

Fig. 4. Stanolind droplets in aq. solns. (○) Distilled water (ζ = 134.1 mV, $\sigma_s/\sigma_1 = 0.719 \times 10^{-3}$); (●) 10^{-4} N HCl (ζ = 11.8 mV, $\sigma_s/\sigma_1 = 0.134 \times 10^{-3}$); (△) 10^{-4} N NaOH (ζ = 112.1 mV, $\sigma_s/\sigma_1 = 0.140 \times 10^{-3}$); (□) 10^{-3} N NaOH.

Fig. 5. Organic oil droplets in distilled water. (●) dimethylaniline (ζ = 100.1 mV); (×) tribromohydrin (ζ = 132.6 mV); (○) iodobenzene (ζ = 214.3 mV).

the $1/U$-values in $(cm/sec)^{-1}$ are further converted into $(scale\ div./sec)^{-1}$ for comparison with the experimental values.

The results of the surface-conductance correction calculations are shown in Figs. 2–5.

DISCUSSION

A fairly systematic variation of the calculated ζ-potential values can be seen from Fig. 1, in spite of the scatter of the points due to experimental error (which in some cases is quite large for the smaller particles). As already mentioned, a constant value of the ζ-potential would be warranted from the experimental conditions.

It should be noted that some error has been introduced in the calculations because of the use of the Overbeek series expression (eqns. (2), (3), (5)) in the inverted form (eqn. (9)), because only an infinite series can be identical with its inverted form. This error has been estimated by MYSELS[4] to be about 10% in the case of BOOTH'S series for his results with lauryl sulphate micelles. Also, the error introduced by omission of higher terms in the inverted Booth series, which was estimated for this fairly regularly convergent series to be of the order of the last term accounted for, *i.e.*, of the order of $(\zeta_{Booth} - \zeta_{Overbeek})$*, was shown to be small, so that the inverted series was found to give quite reliable results (see, however, ref. 23).

In surface conductance correction calculations, the initial linear plots have in all cases been made exclusively with regard to the experimental values for large droplets (*i.e.*, for experimental points lying close to the $1/U$-axis) because the linear relationship holds strictly only for large values of $\varkappa a$. The agreement of the calculated curve with the experimental points (which could have been improved by some slight alteration in the value of the constants, ζ and σ_s, obtained by slightly changing the initial linear plot) is consequently not always good over the smaller range of values of the particle radii. This, however, is not of any great consequence, since not only do experimental results for small particles tend to be more inaccurate due to Brownian motion, but also because the reciprocal plot greatly magnifies the percentage experimental error.

The calculated curves show in all cases a maximum, which shifts towards smaller radii with increase in concentration (for 10^{-4} N solution, the maximum lies beyond the range of the smallest radius values in our calculations; for 10^{-3} N solutions, the complete curve does not differ at all from the linear extrapolation). This is quite distinct from the maxima often found in mobility–concentration curves[6], which are usually explained as due to an increase of the relaxation effect on the low concentration side, and a real decrease of ζ on the high concentration side, owing to compression of double layer or specific interaction of the surface charge with the ions in solution. Similarly, different maxima have been observed in electroosmotic mobility *vs.* concentration, and streaming potential *vs.* concentration curves, which have been explained by BIKERMAN as due to the opposing influences, with increasing dilution, of a real increase of ζ and decrease of field strength owing to surface conductance.

Also, the theoretical $1/U$-curves tend in all cases to a limiting value for large

* ζ_{Booth} and $\zeta_{Overbeek}$ are the ζ-potential values calculated by the relaxation correction equations of BOOTH and OVERBEEK, which take into account terms up to the order of ζ^4 and ζ^3, respectively.

$1/a$. For small particles, $\varkappa a \ll 1$ and $F_1(\varkappa a) \sim 0$, so that eqn. (6) becomes $U = E\varepsilon_1\zeta/6\pi\eta_1$. On introducing $\zeta_{\text{Smol.}}$ it is seen that $1/\zeta_{\text{Smol.}}$ should tend to the value $3/2\zeta$ after passing through the aforesaid maximum.

The values of the specific surface conductivity, σ_s, calculated from STACKELBERG's results in distilled water (specific conductivity $= 2 \cdot 10^{-6}\ \Omega^{-1}\ \text{cm}^{-1}$) are found to be $0.83 \cdot 10^{-9}$ and $0.79 \cdot 10^{-9}\ \Omega^{-1}$, for $C_2H_2Cl_4$- and C_2Cl_4-weighted paraffin oil droplets. Taking the specific conductivity of the distilled water in MOONEY's results as $3.42 \cdot 10^{-6}\ \Omega^{-1}\ \text{cm}^{-1}$, the specific surface conductivity of Stanolind, dimethylaniline, tribromohydrin and iodobenzene droplets in distilled water are found to be 2.45, 1.67, 0.75 and $1.02 \times 10^{-9}\ \Omega^{-1}$, respectively. These figures are of the correct order of magnitude.

The value of ζ for Stanolind drops in distilled water is found to be 134.1 mV compared with the value 90.9 mV found earlier by GHOSH[20]. The difference is ascribed entirely to the restricted range of $1/a$-values of our linear extrapolation. In $10^{-4}\ N$ NaOH solution, the complete curve begins to deviate from the linear extrapolation only in the region of larger $1/a$-values: naturally, the ζ-potential found (112.1 mV) does not differ much from that reported earlier (111.7 mV).

The application of the relaxation correction eqn. (2) and also the surface conductivity correction eqn. (6) to the experimental results obtained with hydrocarbons and other organic liquid droplets, involves the assumption that the latter can adequately be considered as solid. In fact, the different conditions of motion obtaining at the liquid–liquid interface as compared to the liquid–solid interface, and also the dissolution of the electrolyte in the fluid of the drop (giving rise to a charge and potential distribution inside the drop which in turn modify the body forces acting therein) would complicate and modify the solutions of the relaxation and surface conduction correction equations. As the droplets formed are mostly of the non-polar type of hydrocarbon and other organic liquids, electrolytes would be virtually insoluble in them, and the second effect mentioned can be neglected. Further, it is known (LEVICH[24]) that even minute traces of impurities retard, or completely stop, the tangential motion at the interface of two liquids. Thus, as a first approximation, the droplets can be adequately considered as solid, and the application of eqns. (2) and (6) justified[25].

CONCLUSION

In conclusion, it may be said that the question of whether the relaxation correction or the surface conductivity correction is more successful for the interpretation of electrophoretic mobility data, cannot be decided only on the basis of the mobility data considered above. It is seen that the measurement of the variation of mobility with particle size offers a very promising method in this direction. However, the question as to how far either of the above refinements to the theory is individually successful, or which is the more successful, must be left open until more precise mobility data has been accumulated, particularly over the range of small particle dimensions in solutions of very low electrolyte concentrations, and on well defined solid surfaces.

As is clear from our earlier discussion, the relaxation and (normal) surface conductivity treatments are fundamentally the same, being essentially the correc-

tions to include the effect of polarisation of the electrical double layer near the charged particle surface. The relaxation correction has, moreover, the advantage of being more comprehensive and rigorous mathematically. But in the case when an abnormally high conductance is present at the interface between the two phases, owing to any mechanism whatsoever (which appears, from available evidence and from plausible considerations, to be the general rule rather than the exception), only the surface conductivity method appears to be sufficiently comprehensive to take this into account. In addition, it possesses greater mathematical simplicity and is easier to apply, which has recently led to the successful application of this model for incorporating an essentially important correction to some other related fields[26].

ACKNOWLEDGEMENTS

The authors would like to express their thanks to Professors B. N. GHOSH and S. K. MUKHERJEE, and Dr. T. C. ROY for their kind encouragement. The award of a senior fellowship of the C.S.I.R., Govt. of India, during the tenure of which this work was completed, is also gratefully acknowledged.

SUMMARY

A comparative evaluation has been made of the two corrections to the Henry electrophoresis equation for non-conducting solid spherical particles, namely, the correction due to the polarisation of the ion-atmosphere surrounding the moving charged particle, and that due to a possibly high conductivity at its surface. It has been shown that such a comparison can be carried out correctly in the case of mobility data for particles of varying sizes in a solution of constant electrolyte concentration, such as the mobility data of MOONEY and VON STACKELBERG for various organic oil droplets. It has been shown that in the case of the relaxation correction calculation, a constant characteristic value of the *zeta*-potential for each system, as warranted by the theoretical equation under the experimental conditions, is not obtained. Strictly, some allowance must be made for the approximations introduced owing to the method of calculation used. In the case of surface conductivity correction calculations, the theoretical equation is in good agreement with the experimental values for particles of large size. The more interesting conclusions from the theoretical equation in the region of small particle size cannot be verified because of experimental difficulties and the consequent errors in the existing experimental results in this region.

REFERENCES

1 D. C. HENRY, *Proc. Roy. Soc. London*, A 133 (1931) 106.
2 F. BOOTH, *Proc. Roy. Soc. London*, A 203 (1950) 514.
3 J. TH. G. OVERBEEK, *Koll. Beih.*, 54 (1943) 316; *Advances in Colloid Science*, Interscience Publishers, New York, 1950, Volume III, p. 97; *Colloid Science*, Elsevier Publishing Co., Amsterdam, 1952, Vol. I, p. 194.
4 D. STIGTER AND K. J. MYSELS, *J. Phys. Chem.*, 59 (1955) 45.
5 H. H. PAINE, *Trans. Faraday Soc.*, 51 (1955) 995.
6 M. VON STACKELBERG, H. HEINDZE, F. WILKE AND R. DOPPELFELD, *Z. Elektrochem.*, 61 (1957) 781.
7 J. W. MCBAIN, C. R. PEAKER AND A. M. KING, *J. Am. Chem. Soc.*, 51 (1929) 3294.
8 D. R. BRIGGS, *J. Phys. Chem.*, 32 (1928) 641.

9 E. MANEGOLD AND K. SOLF, *Kolloid-Z.*, 55 (1931) 273.
10 A. J. RUTGERS, *Trans. Faraday Soc.*, 36 (1940) 69.
11 J. J. BIKERMAN, *Trans. Faraday Soc.*, 36 (1940) 154.
12 F. BOOTH, *Trans. Faraday Soc.*, 44 (1948) 955.
13 D. C. HENRY, *Trans. Faraday Soc.*, 44 (1948) 1021.
14 A. J. TAYLOR AND F. W. WOOD, *Trans. Faraday Soc.*, 53 (1957) 523.
15 J. J. BIKERMAN, *Z. Phys. Chem.*, A 163 (1933) 378.
16 F. URBAN, H. L. WHITE AND E. A. STRASSNER, *J. Phys. Chem.*, 39 (1935) 311.
17 F. BOOTH, *Progress in Biophysics and Biophysical Chemistry*, Pergamon Press, Oxford, 1953, Vol. III, p. 97.
18 J. J. BIKERMAN, *Z. Phys. Chem.*, A 171 (1934) 209.
19 D. J. O'CONNER, N. STREET AND A. S. BUCHANAN, *Australian J. Chem.*, 7 (1954) 245.
20 B. N. GHOSH, K. C. ROY AND P. B. ROYCHOWDHURY, *J. Indian Chem. Soc.*, 32 (1955) 29.
21 M. MOONEY, *Phys. Rev.*, 23 (1924) 396.
22 R. J. HUNTER, *J. Phys. Chem.*, 66 (1962) 1367.
23 D.-N. BISWAS AND M. SENGUPTA, to be published.
24 V. G. LEVICH, *Physico-chemical Hydrodynamics*, Academy of Sciences of the USSR, Moscow, 1952.
25 M. SENGUPTA, to be published.
26 C. T. O'KONSKI, *J. Phys. Chem.*, 64 (1960) 605.

ELECTROANALYTICAL CHEMISTRY AND INTERFACIAL ELECTROCHEMISTRY
Elsevier Sequoia S.A., Lausanne – Printed in The Netherlands

BEITRÄGE ZUR HOCHFREQUENZTITRATION*

TEIL VI. ZUR THEORIE DER KENNKURVEN

L. PAZSITKA UND R. BERTRAM
Institut für Physikalische Chemie und Elektrochemie, Abt. Elektrochemie, TH Braunschweig (Deutschland)

(Eingegangen am 13. Oktober, 1967)

EINLEITUNG

Heute fasst man alle elektrodenlosen Messmethoden, besser gesagt, Messverfahren mit indirektem Kontakt unter dem Namen *Hochfrequenztitration* zusammen. Die erste kontaktlose Messung hat HÖBER[1] 1912 durchgeführt; obwohl seitdem zahlreiche Arbeiten, sogar Monographien[2-8] auf diesem Gebiet erschienen sind, ist die Entwicklung der theoretischen Grundlagen jedoch noch keineswegs abgeschlossen.

Mit dem Begriff der "elektrodenlosen" Verfahren zur Bestimmung elektrischer Kenngrössen eines Messgutes pflegt man im allgemeinen zu Recht die Vorstellung von mehr oder weniger komplizierten elektronischen Schaltungen zu verknüpfen, deren sinnvolle Handhabung ein gewisses Mass an hochfrequenztechnischen Kenntnissen erfordert; insbesondere dann, wenn ein nicht alltägliches Messproblem in befriedigender Weise gelöst werden soll. Bei Verwendung von Hochfrequenz treten nicht nur Schwierigkeiten hinsichtlich der Anpassung der das Messgut enthaltenden Zelle an die Schaltung auf, sondern auch Schwierigkeiten bezüglich der Interpretation des Anzeigewertes. Solange Eichsubstanzen zur Verfügung stehen oder nur eine Relativanzeige interessiert, werden Bedenken dieser Art gegenstandslos.

Eine eindeutige Relation zwischen Messwert und elektrischer Kenngrösse des Messwertes ist nur möglich, wenn die elektrische Funktion einer Messzelle bekannt ist, und wenn jedes einzelne Element der aus dieser Funktion resultierenden Ersatzschaltung der tatsächlichen Bauform der Zelle und der Art des Messgutes zuzuordnen ist.

Für die historisch ältere "Spulenzelle"[2,9] ist es bislang nicht gelungen, ein funktionierendes Ersatzschaltbild aufzustellen, weshalb solche Zellen nur für Relativmessungen verwendbar sind. Für "Kondensatorzellen"[2,10-13] ist das Ersatzschaltbild eindeutig bekannt. Trotzdem ist auch hier der Anzeigewert prinzipiell mehrdeutig, solange nicht Wirk- und Blindanteil der gesamten Zellimpedanz getrennt gemessen werden.

THEORIE

Das Ersatzschaltbild einer elektrodenlosen kapazitiven Zelle lässt sich durch entsprechende Bauweise auf die in Abb. 1 dargestellte Form zurückführen, wobei wir

*Für I–V Teil, siehe die Literaturliste[9-13].

unter C die nur durch die Isolierschicht bedingte Einkopplungskapazität, unter K die durch Zellform und Dielektrizitätskonstante (DK) des Messmediums gegebene Zellinnenraumkapazität, und unter R den durch Zellform und Leitfähigkeit der Füllung festgelegten Zellinnenraumwiderstand verstehen wollen. Hierbei ist

$$C = (F/2d_{\text{Wand}})\,\varepsilon_{\text{Wand}}\varepsilon_0;$$

C hängt nur von der Bauweise der Zelle ab, während sich die Zellinnenraumkapazität K auch mit der DK der zu messenden Probe ändert.

$$K = (F/d_{\text{Probe}})\,\varepsilon_{\text{Probe}}\,\varepsilon_0 \quad \text{oder}$$

$K = \varepsilon_{\text{Probe}} K_0$, wobei K_0 die Kapazität der Zelle bei $\varepsilon = 1$ (Vakuum) bedeutet. $F/d_{\text{Probe}} = z$ ist die sog. Zellkonstante. Der Zellinnenraumwiderstand wird dann $R = 1\varkappa/z$[13].

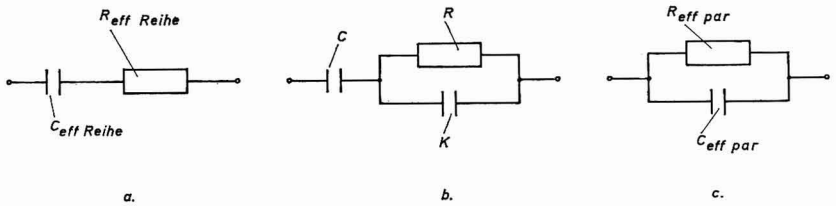

Abb. 1. (a), Reihensubstitution; (b), Ersatzschaltbild; (c), Parallelsubstitution einer kapazitiven Zelle.

Das Ersatzschaltbild einer elektrodenlosen kapazitiven Zelle kann man sowohl durch eine Reihenschaltung wie auch durch eine Parallelschaltung, bestehend aus einem variablen Kondensator C_{eff} und einem regelbaren Widerstand R_{eff} substituieren. Der Zusammenhang zwischen den Grössen C_{eff}, R_{eff}, C, R und K ist bei Reihenschaltung gegeben durch

$$R_{\text{eff Reihe}} = \frac{R}{1+(\omega RK)^2} \quad \text{und} \quad C_{\text{eff Reihe}} = C\,\frac{1+(\omega RK)^2}{1+\omega^2R^2K(C+K)} \;.$$

Die Impedanz ergibt sich damit zu

$$z = R_w + jR_b = \frac{R}{1+(\omega RK)^2} - j\,\frac{\omega R^2K(K/C+1)+1/\omega C}{1+(\omega RK)^2} \;.$$

Bei der Parallelschaltung ergeben sich die Relationen

$$R_{\text{eff par}} = \frac{1+(\omega R(C+K))^2}{\omega^2RC^2} \quad \text{und} \quad C_{\text{eff par}} = C\,\frac{1+\omega^2R^2K(C+K)}{1+(\omega R(C+K))^2} \;.$$

Als Admittanz erhalten wir

$$G = G_w + jG_b = \frac{\omega^2RC^2}{1+(\omega R(C+K))^2} + j\omega C\,\frac{1+\omega^2R^2K(C+K)}{1+(\omega R(C+K))^2} \;.$$

Unter den *Kennkurven* der Hochfrequenztitration versteht man die Funktionen der Wirk- bzw. Blindkomponente der Zellimpedanz oder -admittanz in Abhängigkeit von einer elektrischen Kenngrösse der Messprobe. Für kapazitive Zellen trägt man den Wirkwiderstand bzw. die effektive Kapazität in Abhängigkeit von der

TABELLE 1

KENNKURVEN DER HOCHFREQUENZTITRATION

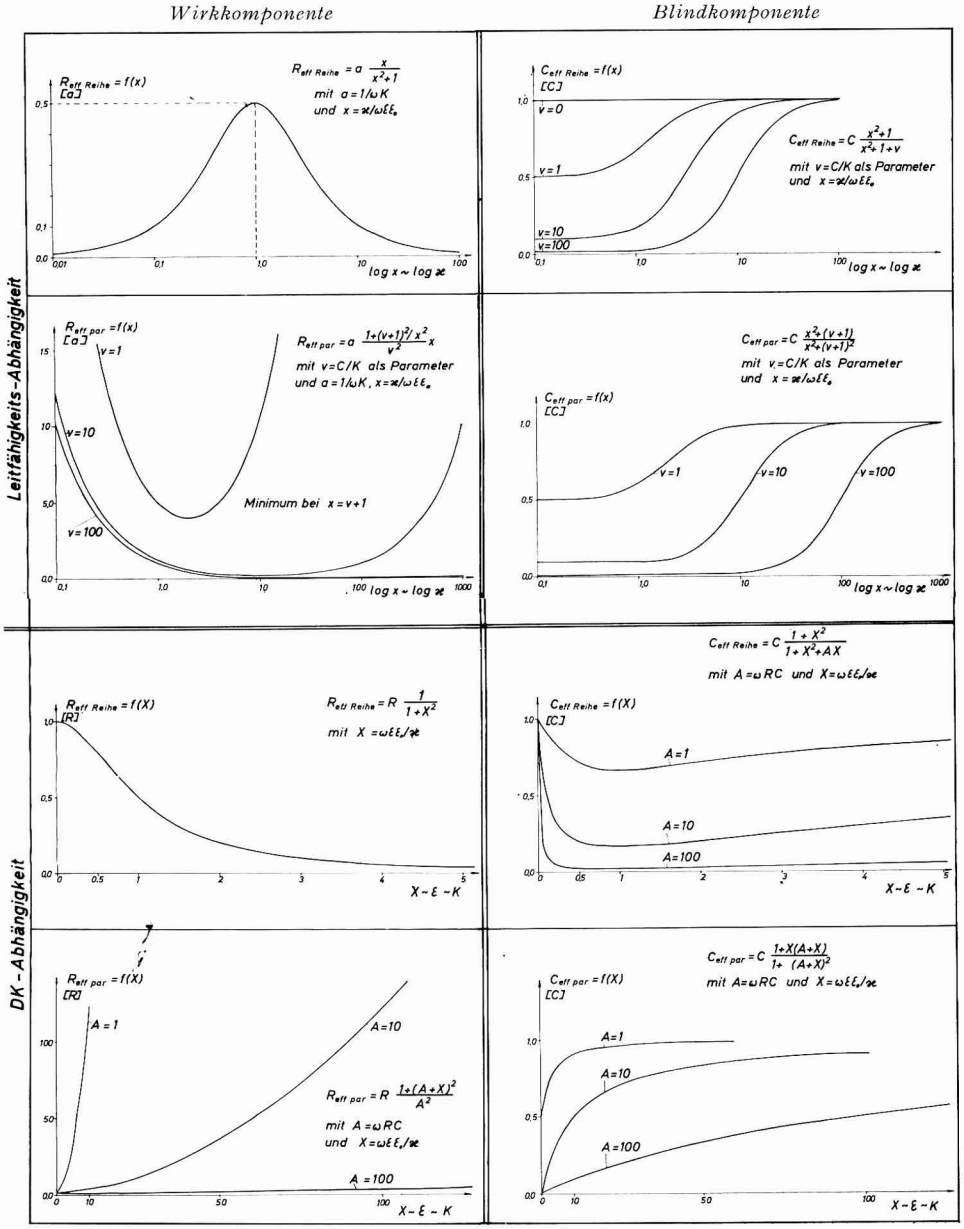

Leitfähigkeit $\varkappa$ bzw. von der Dielektrizitätskonstante ε auf. Durch Einführung einer neuen Variablen x als Funktion der Leitfähigkeit $\varkappa$ bzw. X als Funktion der Dielektrizitätskonstante ε ist es gelungen, die Zahl der unabhängigen Variablen um eins zu

reduzieren und dadurch die *verallgemeinerten* Kennkurven (Tabelle 1) sowohl für die Reihen-, als auch für die Parallelsubstitution zu erhalten.

Bei der Betrachtung der Leitfähigkeitsabhängigkeit erhält man für die Wirkkomponente in der Reihenschaltung den gleichen Zusammenhang für alle Zellenarten bei jeder Messfrequenz und DK der Substanz. Für die effektive Kapazität der Impedanz und Admittanz, und für die Wirkkomponente der Admittanz in Abhängigkeit der Leitfähigkeit ergibt sich eine Schaar von Kurven, deren Verlauf von den Kenngrössen der Zelle und von der DK der Messprobe bestimmt wird, von der Frequenz jedoch unabhängig ist. Die Steigungen dieser Kurven ergeben die Empfindlichkeit bei Leitfähigkeitsänderungen für die betreffende Komponente. An den Wendepunkten ist maximale Empfindlichkeit vorhanden. Gegenüber der Reihensubstitution fällt in der Parallelschaltung das Minimum der Wirkkomponente mit dem Wende-

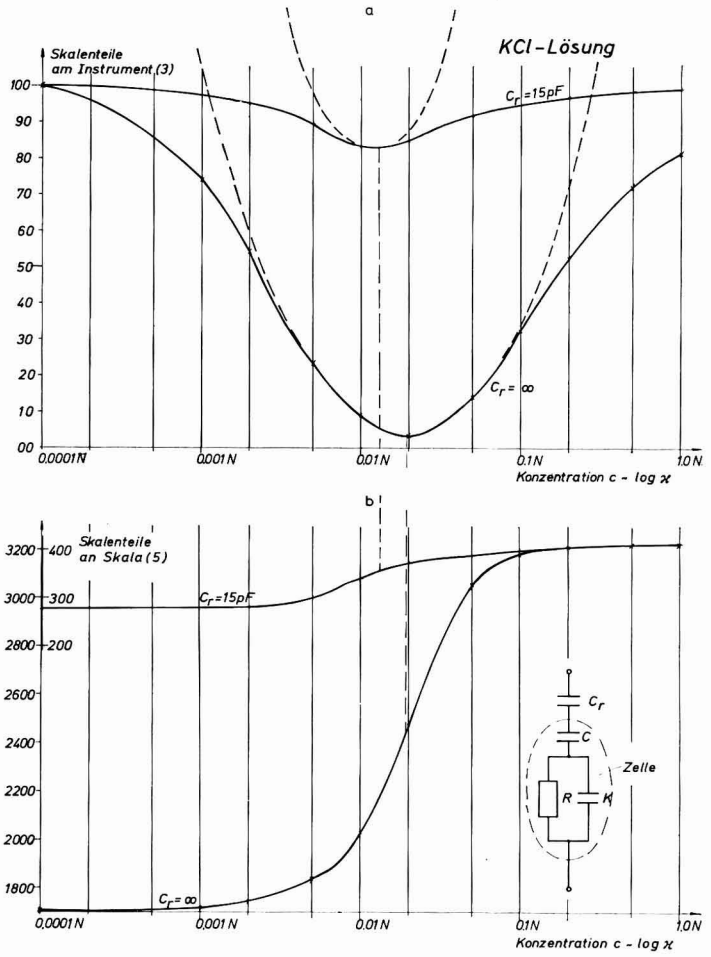

Abb. 2. Leitfähigkeitskennkurven eines Hochfrequenztitrimeters (aufgenommen mit dem HFT 30 C der Firma WTW). (a) Kennkurve der Wirkkomponenten-Methode; (b) Kennkurve der Blindkomponenten-Methode.

punkt der Blindkomponentenkurve zusammen; das Minimum verschiebt sich zu höheren Leitfähigkeiten mit zunehmendem C/K-Verhältnis. Der Messbereich wird ebenso durch Änderung von C/K verändert.

Für die DK-Abhängigkeit erhält man ähnliche Zusammenhänge. Der Verlauf dieser Kennkurven war bisher nicht bekannt. Die Wirkkomponente in der Reihenschaltung ist unabhängig von der Wandkapazität C, es ergibt sich der gleiche Zusammenhang für alle Zellenarten, Leitfähigkeiten und Frequenzen. Für die effektive Kapazität der Impedanz und der Admittanz, und für die Wirkkomponente der Admittanz erhält man mit der Variablen X eine Schaar von Kurven, deren Verlauf von den Kenngrössen der Zelle, von der Leitfähigkeit der Messprobe und von der Frequenz bestimmt wird. Die Steigung der Kennkurven ergibt die DK-Empfindlichkeit, bei Impedanzmessung die DK-Messempfindlichkeit. An dem Wendepunkt ist maximale, an den Minima minimale Empfindlichkeit vorhanden.

MESSERGEBNISSE

Zum Beweis der Richtigkeit dieser Darstellung der Kennkurven wurden folgende Messungen durchgeführt. Zuerst wurden mit dem bekannten Hochfrequenztitrimeter HFT 30 C der Firma WTW Leitfähigkeitskennkurven aufgenommen. Bei diesem Gerät wird ein die Zelle enthaltender Parallelschwingkreis, der aus einem 30 MHz-Oszillator gespeist wird, mit einer zur Zelle parallelgeschalteten Kapazität auf Resonanz abgestimmt. Die Änderung dieser Kapazität in Abhängigkeit von der Leitfähigkeit stellt die Blindkomponenten-Methode; die Änderung des Anodenstromes die Wirkkomponenten-Methode dar. In Abb. 2 ist der von der Firma angegebene Kennkurven-Verlauf ($C_r = \infty$) wiedergegeben. Um allein das Verhältnis

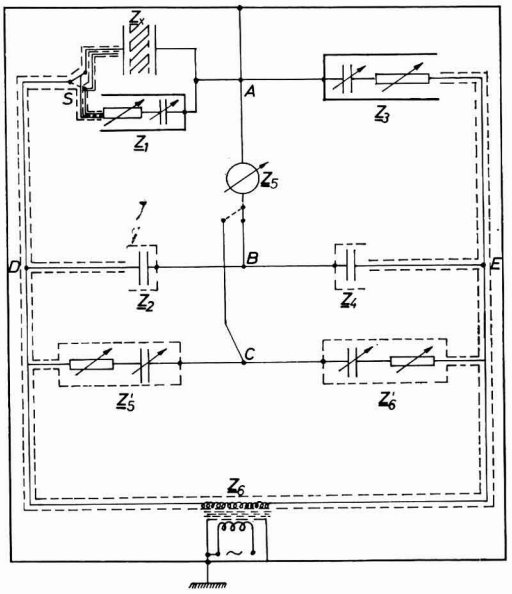

Abb. 3. Abgeschirmte symmetrische Wheatstone-Brücke.

C/K zu verändern, wurde zur Zelle eine Kapazität C_r in Reihe geschaltet. Daraus ergibt sich ein anderer Verlauf ($C_r = 15$ pF) für die Wirk- und Blindkomponentenanzeige. Gestrichelt eingezeichnet ist jeweils der theoretische Verlauf; das Abbiegen der Kennkurve der Wirkkomponenten-Methode ist auf die Eigenbedämpfung des Schwingkreises mit Zelle zurückzuführen. Für die Blindkomponente fällt die theoretische Kurve sehr gut mit dem gemessenen Verlauf zusammen, sodass sie nicht eingezeichnet wurde. Man erkennt, dass das Minimum der Wirkkomponente mit dem Wendepunkt der Blindkomponenten-Methode zusammenfällt, dass das Minimum zur kleineren Leitfähigkeit hin verschoben wird, und dass mit wachsendem C/K-Verhältnis der Messbereich zunimmt.

Den Beweis bezüglich der Frequenzabhängigkeit erbrachten wir mit einer selbstgebauten, im Frequenzbereich von 100 Hz–20 kHz arbeitender Wheatstone-

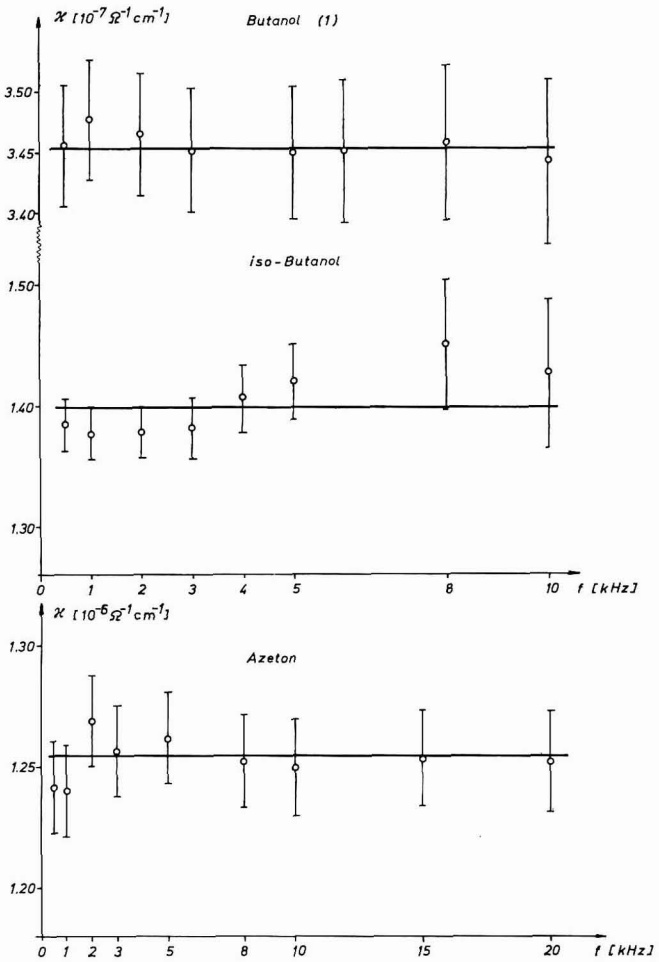

Abb. 4. Die Frequenzabhängigkeit der spezifischen Leitfähigkeit für verschiedene organische Lösungsmittel (p.a.) bei 20°.

Brücke mit Wagnerschem Hilfszweig (Abb. 3). In diesem Frequenzbereich wurde nach dem Substitutionsverfahren gearbeitet. Wirk- und Blindanteil der Zellimpedanz konnten hinreichend genau abgeglichen werden, wodurch die Bestimmung der Leitfähigkeit bzw. der DK ermöglicht wurde.

Die Gültigkeit der Kennkurven wird im Niederfrequenzbereich durch Leitfähigkeitsmessungen (Abb. 4) belegt. Die spezifische Leitfähigkeit in Abhängigkeit von der Frequenz wurde mit Hilfe der Wirkkomponente in der Reihenschaltung bestimmt. Im Rahmen der durch die Messgenauigkeit gegebenen Fehlergrenze ergibt sich ein von der Frequenz unabhängiger Wert. Um eine ausreichende Empfindlichkeit bei der Messung zu erhalten, wurden für diesen Zweck Zellen mit extrem hohen Wandkapazitäten[9] verwendet.

Die Aufnahme von DK-Kennkurven bei verschiedenen Leitfähigkeiten stösst deshalb auf Schwierigkeiten, weil entsprechende Eichsubstanzen fehlen. Für den Fall sehr kleiner Leitfähigkeit ist die DK-Kennkurve der Blindkomponenten-Methode allgemein bekannt[2]. Für Substanzen mit höheren Leitfähigkeiten sind die zugehörigen DK-Werte im Hochfrequenzbereich weitgehend unbekannt. Einer Darstellung von mit Eichsubstanzen erstellter DK-Kennkurven für beliebige Leitfähigkeiten müssen daher umfangreiche paarweise Messungen von Leitfähigkeit und DK vorangehen. Diese Messungen werden z.Zt. von uns weitergeführt.

Der Deutschen Forschungsgemeinschaft und dem Verband der Chemischen Industrie danken wir für die Bereitstellung von Sach- und Personalmitteln.

ZUSAMMENFASSUNG

In dem Referat werden Kennkurven einer kapazitiven Zelle behandelt. Durch Einführung einer neuen Variablen x als Funktion der Leitfähigkeit $\varkappa$ bzw. X als Funktion der Dielektrizitätskonstante ε ist es gelungen, die verallgemeinerten Kennkurven zu erhalten. Es werden erstmalig DK-Kennkurven für beliebige Leitfähigkeit des Messgutes angegeben. Als Anwendung werden Messungen bei Hoch- und Niederfrequenz gezeigt.

SUMMARY

This report deals with characteristic curves of capacitive measuring cells. By introducing a new variable, x, as a function of the conductance, $\varkappa$, and X as a function of the dielectric constant, ε, it has been possible to obtain the generalized characteristic curves. For the first time, characteristic curves of the dielectric constant for any conductivity of the substance investigated, are specified. As an example of application, measurements are shown at high and low frequencies.

LITERATUR

1 R. HÖBER, *Pfluegers Arch. Ges. Physiol.*, 148 (1912) 189.
2 K. CRUSE UND R. HUBER, *Die Hochfrequenztitration*, Verlag Chemie, Weinheim/Bergstr., 1957.
3 F. OEHME, *Angewandte Konduktometrie*, Dr. A. Hüthing Verlag, Heidelberg, 1961.
4 F. OEHME, *Dielektrische Messmethoden*, Verlag Chemie, Weinheim/Bergstr., 1962.
5 E. PUNGOR, *Oszillometria és Konduktometria*, Akadémiai kiadó, Budapest, 1963.

6 G. G. BLAKE, *Conductimetric Analysis at Radio-Frequency*, Chapman and Hall Ltd., London, 1950.
7 K. CRUSE UND R. BERTRAM, *Hochfrequenztitration*, in: *Analyse der Metalle*, II. Band: *Betriebsanalysen*, Springer Verlag, Berlin, 1961.
8 C. N. REILLEY, *High-Frequency Methods*, in: P. DELAHAY, *New Instrumental Methods in Electrochemistry*, Interscience Publishers, New-York–London, 1954.
9 K. THIES UND K. CRUSE, Beiträge zur HFT., Teil V, *Z. Instrumentenk.*, 73 (1965) 121.
10 H. B. RICKE UND K. CRUSE, Beiträge zur HFT., Teil I, *Z. Instrumentenk.*, 68 (1960) 293; 69 (1961) 10.
11 H. B. RICKE UND K. CRUSE, Beiträge zur HFT., Teil II, *Z. Instrumentenk.*, 69 (1961) 39.
12 R. BERTRAM UND K. CRUSE, Beiträge zur HFT., Teil III, *Z. Instrumentenk.*, 71 (1963) 221.
13 R. BERTRAM UND K. CRUSE, Beiträge zur HFT., Teil IV, *Ber. Bunsenges. Phys. Chem.*, 69 (1965) 215.

ELECTROANALYTICAL CHEMISTRY AND INTERFACIAL ELECTROCHEMISTRY
Elsevier Sequoia S.A., Lausanne – Printed in The Netherlands

REDOX EQUILIBRIA

V. THE LOCATIONS OF INFLECTION POINTS ON TITRATION CURVES FOR HOMOGENEOUS REACTIONS

JAMES A. GOLDMAN
Department of Chemistry, Polytechnic Institute of Brooklyn, New York (U.S.A.)
(Received November 21st, 1967)

INTRODUCTION

In a recent investigation[1] of the locations of inflection points on *idealized* titration curves for *symmetrical* ($n_1=n_2=p$) redox reactions, it was demonstrated that there always exists two inflection points whenever $p\Delta E^{0\prime}>85.6$ mV at 25°. Furthermore, the point of minimum slope is always located subsequent to the half-way point, and the location of the point of maximum slope always occurs prior to the equivalence point.

Titration curves for homogeneous redox reactions were investigated by MURGULESCU AND DRAGULESCU[2] who demonstrated rigorously that, the inflection point, corresponding to the point of maximum slope, can never—even when the redox titration reaction is symmetrical—coincide with the equivalence point. However, in order to solve explicitly for the difference in location between the equivalence point and the inflection point, it was necessary to introduce approximations such that the resultant equation explicitly predicted that the two points do coincide for symmetrical reactions although their declaration[2] is more moderate: "... only in symmetrical reactions do the equivalence and inflection point approximately coincide."

For "asymmetrical" *i.e.*, homogeneous, redox reactions the deviation of the location of the inflection from the equivalence point was demonstrated to be dependent upon the magnitude of the equilibrium constant for the redox titration reaction and the relative values of the stoichiometric coefficients—which in this case are the n-values, the number of electrons transferred in each redox half-reaction. Their conclusions were that for all redox reactions that were not symmetrical, the locations of the inflection and equivalence point could *never* coincide and that the inflection preceded the equivalence point whenever the n-value for the couple being titrated was greater than the n-value for the titrant redox couple. When the two n-values were equal, the equivalence and inflection points coincided, but when the n-value for the titrant was greater than that for the couple being titrated, the inflection point followed the equivalence point.

It will now be demonstrated that their conclusions are not rigorously correct. Previously[1] it was demonstrated by this author that for *symmetrical* reactions the equivalence point and the inflection point—when it exists—*never* coincide. Now it is to be further demonstrated that for *homogeneous i.e.*, "asymmetrical," reactions,

the locations of the equivalence and inflection point *can* coincide for a particular value of $\Delta E^{0\prime}$, and that this situation can occur only if the n-value for the couple being titrated is *greater* than the n-value for the titrant couple.

THE EXISTENCE AND LOCATIONS OF THE INFLECTION POINT

For homogeneous reactions of the type:

$$n_2\mathrm{Ox}_1 + n_1\mathrm{Red}_2 = n_2\mathrm{Red}_1 + n_1\mathrm{Ox}_2 \tag{1}$$

where a solution containing *only* Red_2 is being titrated *with* a solution containing *only* Ox_1 (all other ions in the solutions, not involved in the redox couples, are assumed to be non-oxidizable or non-reducible), the fraction titrated at any potential, E, may be calculated from[3]

$$f = \{1 + k \exp(n_1\psi)\}/\{1 + k \exp(-n_2\psi)\} \tag{2}$$

where $\psi = (F/RT)(E - E^*)$, $k = \exp(-n\delta)$, $\delta = (F/RT)\Delta E^{0\prime}$, $n = n_1n_2/(n_1 + n_2)$, $E^* = (n_1E_1{}^{0\prime} + n_2E_2{}^{0\prime})/(n_1 + n_2)$, and $\Delta E^{0\prime} = (RT/n_1n_2F) \ln K$, where K represents the equilibrium constant for the reaction defined by eqn. (1); R, T, and F have their customary significance.

Using eqn. (2) one readily obtains

$$\frac{\mathrm{d}E}{\mathrm{d}f} = \frac{RT}{F} \frac{[1 + k \exp(-n_2\psi)]^2}{k^2[n_1 + n_2][\exp\{(n_1 - n_2)\psi\}] + k[n_1 \exp(n_1\psi) + n_2 \exp(-n_2\psi)]} \tag{3}$$

which upon setting $n_1 = n_2 = p$ reduces to eqn. (4) of ref. 1.

From eqn. (3) it is concluded that the slope of the titration curve is always finite, positive, and never equal to zero.

Differentation of eqn. (3) to obtain $(\mathrm{d}E^2/\mathrm{d}f^2)$ yields

$$\frac{\mathrm{d}^2E}{\mathrm{d}f^2} = -\frac{[1 + k \exp(-n_2\psi)]}{k} G \frac{\mathrm{d}E}{\mathrm{d}f} \tag{4}$$

where

$$G = (NL + NR)/D^2$$

and

$$NL = [2n_2k \exp(-n_2\psi)][k(n_1 + n_2) \exp\{(n_1 - n_2)\psi\} + n_1 \exp(n_1\psi) + n_2 \exp(-n_2\psi)]$$

$$NR = [1 + k \exp(-n_2\psi)][k(n_1{}^2 - n_2{}^2) \exp\{(n_1 - n_2)\psi\} + n_1{}^2 \exp(n_1\psi) - n_2{}^2 \exp(-n_2\psi)]$$

$$D = k(n_1 + n_2) \exp\{(n_1 - n_2)\psi\} + n_1 \exp(n_1\psi) + n_2 \exp(-n_2\psi)$$

Equation (4) is analogous to eqn. (7) of ref. 1.

At the equivalence point, $\psi = 0$, so that eqn. (4) becomes

$$\left(\frac{\mathrm{d}^2E}{\mathrm{d}f^2}\right)_{f=1} = -\frac{(1 + k)}{k} G^* \left(\frac{\mathrm{d}E}{\mathrm{d}f}\right)_{f=1} \tag{5}$$

where

$$\left(\frac{\mathrm{d}^2E}{\mathrm{d}f^2}\right)_{f=1} = \frac{RT}{F} \frac{1 + k}{k(n_1 + n_2)} \tag{6}$$

and $G^*(=G$ at $f=1, \psi=0)$ is

$$G^* = \{2n_2k + (n_1 - n_2)(1+k)\}/(1+k)(n_1+n_2) \quad (7)$$

If $n_1 = n_2 = p$, then eqns. (5), (6) and (7) immediately reduce to eqns. (10), (6), and (11) of ref. 1.

From eqns. (4) and (7) it is evident that the second derivative of E with respect to f can be equal to zero only if the value of G^* is equal to zero. This condition can only be satisfied when

$$k = (n_2 - n_1)/(n_2 + n_1) \quad (8)$$

Therefore, the reason why the inflection point can never coincide with the equivalence point in symmetrical reactions is now immediately evident. The coincidence could not occur for non-zero values of k, *i.e.*, finite values of $\Delta E^{0\prime}$, because $k=0$ only if $\Delta E^{0\prime}$ would be infinitely large. Thus, as was previously demonstrated[3], for symmetrical reactions, the difference between the locations of the inflection and equivalence points approaches zero as the difference between the values of the formal potentials of the two couples become larger and larger.

Furthermore, it is now seen that for homogeneous reactions, the inflection point *can* coincide with the equivalence point—it is only necessary that the value of n_2 be greater than that of n_1, that is, the n-value corresponding to the couple being titrated must exceed the value that corresponds to the titrant couple.

This situation resembles that which arises in heterovalent precipitation titration curves[4] where, for a particular concentration of titrant, the inflection point (corresponding to the point of maximum slope) coincides with the equivalence point when a solution of the ion of *higher* valence is titrated *with* a solution of the ion of *lower* valence. It should be recognized that *in* the titration reaction equation, the *higher* valence appears as the stoichiometric coefficient of the *titrant*. Similarly, in the redox titration equation, the higher n-value, corresponding to the couple *being titrated*, appears as the stoichiometric coefficient of the *titrant*.

The conclusion previously demonstrated[1], and presently again proved, that the inflection and equivalence points can never coincide for symmetrical redox reactions, also resembles that demonstrated for isovalent precipitation reactions[5] wherein the inflection point (corresponding to the maximum slope) can never coincide with, but must always precede, the equivalence point.

From eqn. (8), for any pair of n-values, the values of k are readily calculated, and in turn, the values of $\Delta E^{0\prime}$ and K, for which the inflection point coincides with the equivalence point in *homogeneous* redox reactions (Table 1).

It is convenient to introduce the "asymmetry coefficient"[6,7]

$$u = n_1/n_2 \quad (9)$$

so that eqn. (8) may be rewritten as

$$k = (1-u)/(1+u) \quad (10)$$

For symmetrical reactions, $u=1$, whereas the greater the difference between the values of n_1 and n_2, the smaller is the value of u. From eqn. (10) it is then obvious that the larger the value of u, the smaller will be the magnitude of k. However, for a particular value of u—and thus, k—there may correspond more than one value

TABLE 1

PARAMETERS OF HOMOGENEOUS REACTIONS FOR WHICH THE INFLECTION AND EQUIVALENCE POINTS COINCIDE AT 25°

n_2	n_1	u	k	$\Delta E^{0\prime}$ (mV)	K
2	1	0.5000	0.3333	42.28	27.0
3	1	0.3333	0.5000	23.70	16.0
3	2	0.6667	0.2000	34.40	$3.12 \cdot 10^3$
4	1	0.2500	0.6000	16.37	12.4
4	2	0.5000	0.3333	21.14	$7.30 \cdot 10^2$
4	3	0.7500	0.1429	29.11	$8.22 \cdot 10^5$
5	1	0.2000	0.6667	12.47	11.4
5	2	0.4000	0.4286	15.21	$3.77 \cdot 10^2$
5	3	0.6000	0.2500	18.96	$6.55 \cdot 10^4$
5	4	0.8000	0.1111	25.36	$3.88 \cdot 10^8$

of $\Delta E^{0\prime}$ (and K) because of the manner in which $\Delta E^{0\prime}$ (and K) depend upon k (see in Table 1 the values of $\Delta E^{0\prime}$ for $n_2=2$, $n_1=1$ and for $n_2=4$, $n_1=2$).

Because for a given pair of n-values, the inflection and equivalence points can coincide for a particular value of $\Delta E^{0\prime}$, it is evidently more meaningful to designate reactions where $u \neq 1$ as "homogeneous" instead of "asymmetrical".

As the value of u increases—approaching unity—for a given value of n_2, the larger must be the value of $\Delta E^{0\prime}$ in order for the inflection and equivalence points to coincide. When $u=1$, only an infinitely large value of $\Delta E^{0\prime}$ is sufficient to cause coincidence. It is interesting to observe that the rate of increase of $\Delta E^{0\prime}$-values for successive pairs of n-values (for a given value of n_2) is relatively slow compared to the corresponding rate of increase in the values of K. This occurs because of the manner in which K depends upon $\Delta E^{0\prime}$, that is, the essential factor is the *product* of the two n-values composing the pair. This influence is moderated in the dependence of k upon $\Delta E^{0\prime}$ because there the essential factor is the product divided by the sum of the two n-values.

Returning to eqn. (5), it is seen that $(d^2E/df^2)_{f=1}$ is negative when G^* is positive, and when G^* is negative then the second derivative is positive. Therefore, a positive value of G^* corresponds to the equivalence point following the inflection point (corresponding to the point of maximum slope) whereas a negative value of G^* corresponds to the equivalence point being located before the inflection point. From eqn. (7), G^* will be positive when for a given pair of n-values, the magnitude of k exceeds that listed in Table 1 for that pair, and the equivalence point then occurs *after* the inflection point. When for this pair of n-values, the magnitude k just equals that listed in Table 1, the equivalence and inflection points *coincide*. Then, for this pair of n-values, when the value of k is less than the corresponding value listed in Table 1, the equivalence point comes *before* the inflection point.

In other words, for a given pair of n-values, there is a particular value of $\Delta E^{0\prime}$ for which the equivalence and inflection points coincide and it is that value which is listed in Table 1. When the value of $\Delta E^{0\prime}$ is less than that listed there, the equivalence point occurs *after* the inflection point; whereas when the value of $\Delta E^{0\prime}$ is greater than that listed in Table 1, then the equivalence point occurs *before* the inflection point. This behavior may be compared to that for *symmetrical* reactions where the equivalence point always comes *after* the inflection point[1].

SUMMARY

For titration curves of homogeneous redox reactions, it has been demonstrated that the inflection point corresponding to the maximum slope can coincide with the equivalence point. For any given pair of n-values, this can occur only at a particular value of $\Delta E^{0\prime}$. For commonly encountered pairs of n-values, the appropriate values of $\Delta E^{0\prime}$ have been evaluated at 25°. If, for a given pair of n-values, a value of $\Delta E^{0\prime}$ is less than that presented, then the inflection point occurs *before* the equivalence point; if a value of $\Delta E^{0\prime}$ is greater than that listed, then the inflection point occurs *after* the equivalence point. In general, the smaller the value of the asymmetry coefficient, the smaller is the value of $\Delta E^{0\prime}$ required for the inflection point to coincide with the equivalence point.

REFERENCES

1 J. A. GOLDMAN, *J. Electroanal. Chem.*, 14 (1967) 373.
2 I. G. MURGULESCU AND C. DRAGULESCU, *Z. Physik. Chem.*, 185A (1940) 375.
3 J. A. GOLDMAN, *J. Electroanal. Chem.*, 11 (1966) 255.
4 L. MEITES AND J. A. GOLDMAN, *Anal. Chim. Acta*, 30 (1964) 18.
5 L. MEITES AND J. A. GOLDMAN, *Anal. Chim. Acta*, 29 (1963) 472.
6 F. L. HAHN AND M. FROMMER, *Z. Physik. Chem.*, 127 (1927) 1.
7 C. LITEANU AND D. CORMÖS, *Talanta*, 7 (1960) 25.

ELECTROANALYTICAL CHEMISTRY AND INTERFACIAL ELECTROCHEMISTRY
Elsevier Sequoia S.A., Lausanne – Printed in The Netherlands

EQUATIONS OF THE POLAROGRAPHIC WAVES OF SIMPLE OR COMPLEXED METAL IONS

II. THE METAL ION IS REDUCED WITH AMALGAM FORMATION IN THE PRESENCE OF A HYDROLYSABLE LIGAND IN BUFFERED MEDIUM

MIHAIL E. MACOVSCHI
Institute of Physical Chemistry, Roumanian Academy of Sciences, Bucharest (Roumania)
(Received November 1st, 1967)

In a previous paper[1] we presented the case of a non-hydrolysable ligand; if, however, the ligand is subjected to a hydrolytic equilibrium:

$$X + H \rightleftharpoons HX \quad (1)$$

or:

$$Y + OH \rightleftharpoons YOH \quad (2)$$

the phenomena are obviously more complicated.

In the present work, only the case of a weak acid ligand (equilibrium (1)) is considered; for the case of a weak base it is sufficient to replace X by Y and pH by pOH in the results, and to make the proper substitutions in the notations.

For both equilibria (1) and (2) we assume that the metal ion is reduced with amalgam formation and that the medium is buffered.

We also keep to the condition: "there is a single complex, MX_q, in the solution", a condition which simplifies the calculations without interfering with explanations of the phenomena; for the same reason the calculations are made for monobasic acids.

The following notations are used in which, for the sake of simplicity, the charge of the ions is neglected:

C_M^0 – free metal ion concentration at the electrode surface,
C_X^0 – free ligand concentration at the electrode surface,
$C_{MX_q}^0$ – complex concentration at the electrode surface,
C_{HX}^0 – non-dissociated acid concentration at the electrode surface,
C_H^0 – H ion concentration at the electrode surface,
C_{am}^0 – amalgam concentration at the mercury drop surface,
C_M – free metal ion concentration in the bulk solution,
C_X – free ligand concentration in the bulk solution,
C_{MX_q} – complex concentration in the bulk solution,
C_{HX} – non-dissociated acid concentration in the bulk solution,
C_H – H ion concentration in the bulk solution,
C_M^{tot} – total (analytical) concentration of the metal ion in the bulk solution,
C_X^{tot} – total concentration of the ligand in the bulk solution,
$f\ldots$ – the respective activity coefficients.

The dissociation constants, β_q and α, of the complex and the acid HX, respectively, which are the same in the bulk solution and at the electrode surface are:

$$\beta_q = (C_X f_X)^q C_M f_M / C_{MX_q} f_{MX_q} = (C_X{}^0 f_X)^q C_M{}^0 f_M / C_{MX_q}{}^0 f_{MX_q} \quad (3)$$

$$\alpha = C_X f_X C_H f_H / C_{HX} f_{HX} = C_X{}^0 f_X C_H{}^0 f_H / C_{HX}{}^0 f_{HX} \quad (4)$$

1. DEDUCTION OF THE EQUATION OF THE POLAROGRAPHIC WAVE; THE CONCEPT OF "MASS CURRENT"

The concentrations at the electrode surface and in the bulk solution are the same if there is no current passing through the solution, but if the current exists, some transport phenomena appear, as illustrated in Fig. 1.

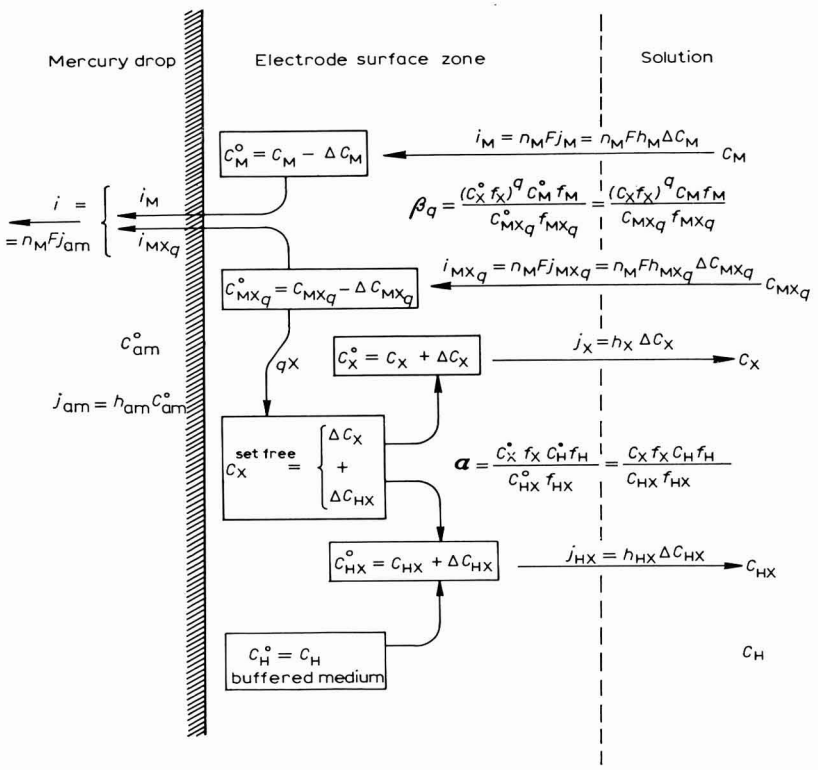

Fig. 1. Distribution of concns., diffusion and ionic equilibrium near the dropping electrode and in bulk soln.

Discharge of M ions leads to concentration variation, ΔC_M, at the electrode surface; similarly, for MX_q ions a variation, ΔC_{MX_q} appears. Therefore:

$$C_M{}^0 = C_M - \Delta C_M \quad (5)$$

$$C_{MX_q}{}^0 = C_{MX_q} - \Delta C_{MX_q} \quad (6)$$

The concentrations, $C_M{}^0$ and $C_{MX_q}{}^0$, become lower than C_M and C_{MX_q}; consequently,

M and MX_q ions diffuse from the bulk solution towards the dropping electrode surface.

Of the total current, i, passing through the solution, a fraction, i_M, is carried by M ions and another, i_{MX_q}, by the complex MX_q, *i.e.*:

$$i = i_M + i_{MX_q} \tag{7}$$

The concentration gradient being assumed constant, we can express the current, i_M, by:

$$i_M = k_M \Delta C_M = k_M (C_M - C_M^0) \tag{8}$$

The current carried by the MX_q ions (fraction i_{MX_q}) is also usually expressed by an Ilkovič relation:

$$i_{MX_q} = k_{MX_q} \Delta C_{MX_q} \tag{9}$$

where the constant k_{MX_q} is in fact the constant k_M but with the diffusion coefficient of the simple metal ions, D_M, replaced by the diffusion coefficient of the complexed metal ions, D_{MX_q}. Therefore, k_{MX_q} is not an Ilkovič constant because it does not contain, as is usual, the charge of the ionic species to which it refers (the complex MX_q) but the charge of the metal ion, M*; if k_{MX_q} is considered just as an Ilkovič constant, relation (9) is erroneous.

In the polarographic literature, the expression of the current inside the mercury drop:

$$i = k_{am} C_{am}^0 \tag{10}$$

is also accepted as an Ilkovič relation, where C_{am}^0 is the concentration of the amalgam formed at the mercury drop surface by discharge of the metal ions (simple or complexed); k_{am} as well as k_{MX_q} is inferred from k_M by replacing the diffusion coefficient of the metal ions into the solution, D_M, by that of the metal atoms into the mercury. It must be emphasized that this expression is also erroneous because the Ilkovič relation implies an ionic conductivity, the ions charge being n_M, while inside the amalgam the electric conductivity is realized by the electrons, and the diffusing particles are not ions but atoms.

We can see that the adaptation of the Ilkovič equation to a different situation leads to purely formal equations without real physical significance.

The phenomena that appear during the polarography of a solution may be correctly represented by means of a new concept: "mass current".

Writing the Ilkovič constant as:

$$k = nFh \tag{11}$$

where h is a constant containing all the parameters of the Ilkovič constant (in the same form) except n and F, we have for the current:

$$i = nFh\Delta C \tag{12}$$

* The complex MX_q may have a positive, zero, or negative charge; this charge is generally different from that of the ion M. If k_{MX_q} were an Ilkovič constant, then for a complex with zero charge, the relation:

$$i_{MX_q} = k_{MX_q} \Delta C_{MX_q} = 0 \ (!)$$

would be valid, although M ions of the complex are implied in the transport of the current through the solution.

The "mass current" is defined as:

$$j = h\Delta C \tag{13}$$

It represents the moles (gram ions) of the species considered that reach (or leave) by diffusion the dropping electrode surface in unit time. In contrast with the "diffusion rate" which refers to the unit surface, the "mass current" implies the *whole* dropping electrode surface (of the drop).

As the drop surface varies with time, the mass current (as well as the electrical polarographical current) will depend on the capillary constants (h being the intermediate).

The relation between the electric current carried by a ionic species and the mass current of the same species is:

$$i = nFj \tag{14}$$

where n is the charge involved in the current transport. It must be emphasized that n may be different from the external charge of the species considered*.

Using the concept of the mass current which we have introduced, the relations (7), (8) and (9) can be written as:

$$i_M = n_M F j_M = n_M F h_M (C_M - C_M^0) = k_M (C_M - C_M^0) \tag{15}$$

$$i_{MX_q} = n_M F j_{MX_q} = n_M F h_{MX_q} (C_{MX_q} - C_{MX_q}^0) \tag{16}$$

$$i = i_M + i_{MX_q} = n_M F (j_M + j_{MX_q}) \tag{17}$$

Inside the mercury drop the diffusion of M atoms is described by the relation:

$$j_{am} = h_{am} C_{am}^0 \tag{18}$$

In quasi-stationary conditions, all the metal ions reduced on the mercury surface are diffusing toward the centre of the drop, *i.e.*,

$$j_{am} = j_M + j_{MX_q} \tag{19}$$

Equations (17), (18) and (19) give:

$$i = n_M F j_{am} = n_M F h_{am} C_{am}^0 \tag{20}$$

If we make the formal notation:

$$n_M F h_{am} = k_{am} \tag{21}$$

then eqn. (20) will take the form of relation (10); this is the explanation for obtaining correct results although it involves starting from a formal equation.

Discharge of the metal ions of MX_q complex leads to breaking of the complex; at the dropping electrode surface a supplementary quantity of ligand appears, part of which remains as it is, and part of which produces by equilibrium (1) the undissociated acid, HX. In this way the concentration variations, ΔC_X and ΔC_{HX}, appear. Therefore:

$$C_X^0 = C_X + \Delta C_X \tag{22}$$

$$C_{HX}^0 = C_{HX} + \Delta C_{HX} \tag{23}$$

* For example, in the complex MX_q, the charge of the complex is different (generally) from the charge of the metal ion, depending upon q and the charges of M and X ions; in the current transport, only the charge of the M ions is involved.

Concentrations C_X^0 and C_{HX}^0 are higher than C_X and C_{HX} and the X ions and HX molecules will diffuse inward towards the solution:

$$j_X = h_X \Delta C_X \tag{24}$$

$$j_{HX} = h_{HX} \Delta C_{HX} \tag{25}$$

During the formation of the undissociated acid, a part of the H ions to the electrode surface are used in the HX molecules, but as we have emphasized, the medium is buffered; in other words, the condition:

$$C_H^0 = C_H \tag{26}$$

is always fulfilled*.

From Fig. 1 it can be seen that each of the given ionic species, M, X and H, is characterised by a mass circuit:

(a) M ions, single or complexed, diffuse from the bulk solution towards the dropping electrode, where they are reduced.

The metal formed is dissolved in the mercury and then diffuses into the mercury drop. Obviously, the mass circuit of species M is open. The current carried by the metal ions (M or MX_q) is measured by the galvanometer of the polarograph, the electrical circuit being closed externally;

(b) X ions are carried to the dropping electrode surface as MX_q and back into the bulk solution as X and HX;

(c) H ions are carried from the electrode surface into the solution as HX; the mass circuit of H ions is also open because of the solution buffering.

For the mass current, in quasi-stationary conditions, the following relations are valid:

$$\begin{cases} j_{am} = j_M + j_{MX_q} \\ q j_{MX_q} = j_X + j_{HX} \end{cases} \tag{27}$$

The thermodynamic expression for the dropping electrode potential is:

$$E = \varepsilon - (RT/n_M F) \ln (C_{am}^0 f_{am} / C_M^0 f_M) \tag{28}$$

To find the equation of the polarographic wave, $E = E(i)$, the concentrations must be expressed in terms of current. Taking account of eqn. (20):

$$E = \varepsilon - (RT/n_M F) \ln (i f_{am} / n_M F h_{am} C_M^0 f_M) \tag{29}$$

From (17), (15), (16), (3) and (22) it follows that:

$$i_d - i = n_M F \left[h_M C_M^0 + h_{MX} C_M^0 \frac{(C_X + \Delta C_X)^q f_M f_X^q}{\beta_q f_{MX_q}} \right] \tag{30}$$

where i_d is the diffusion limiting current (when $C_M^0 = 0$ and $C_{MX_q}^0 = 0$):

$$i_d = n_M F (h_M C_M + h_{MX_q} C_{MX_q}) \tag{31}$$

Expressing ΔC_X in terms of current and of C_M^0, and introducing the value obtained into eqn. (30), one finds a relation which makes possible the expression of C_M^0 in terms of current. Combining the expression obtained with (29) gives the equation of the polarographic wave.

* It is assumed that the buffer system forms practically no complex with the given metal ion.

Based on eqns. (4), (26), (22) and (23):

$$\alpha = \Delta C_X C_H f_X f_H / \Delta C_{HX} f_{HX} \tag{32}$$

But from (27), (24), (25), (16), (7) and (15):

$$h_{HX} \Delta C_{HX} = q j_{MX_q} - h_X \Delta C_X \tag{33}$$

$$j_{MX_q} = \frac{i_{MX_q}}{n_M F} = \frac{i - i_M}{n_M F} = \frac{i - k_M(C_M - C_M{}^0)}{n_M F} \tag{34}$$

Replacing (33) and (34) in (32) gives:

$$\Delta C_X = \frac{q[i - k_M(C_M - C_M{}^0)]}{h_X n_M F} \cdot \frac{\alpha f_{HX}}{\alpha f_{HX} + \frac{h_{HX}}{h_X} C_H f_H f_X} \tag{35}$$

Introducing (35) into (30) and making the notations:

$$k_M C_M{}^0 = y \tag{36}$$

$$(h_{MX_q} f_M / h_M f_{MX_q})(q f_X / h_X)^q = Q \tag{37}$$

produces the function:

$$\Phi_{(y)} = y \frac{Q}{\beta_q} \left[\frac{h_X}{q} C_X + \frac{i + y - k_M C_M}{n_M F} \cdot \frac{\alpha f_{HX}}{\alpha f_{HX} + (h_{HX}/h_X) C_H f_H f_X}\right]^q$$
$$+ y + i - i_d = 0 \tag{38}$$

Solution φ of the function $\Phi_{(y)} = 0$* is related to the $C_M{}^0$ value as follows:

$$C_M{}^0 = \varphi(C_M, C_X, C_H, \beta_q, \alpha, q, i, n_M, f \ldots, h \ldots)/k_M \tag{39}$$

The concentrations, C_M, C_X and C_H, from $\Phi_{(y)}$ are obtained from the following system:

$$\begin{cases} C_X{}^{tot} = C_X + q C_{MX_q} + C_{HX} \\ C_M{}^{tot} = C_M + C_{MX_q} \\ \beta_q = C_M f_M (C_X f_X)^q / C_{MX_q} f_{MX_q} \\ \alpha = C_H f_H C_X f_X / C_{HX} f_{HX} \\ C_H = 10^{-pH} \end{cases} \tag{40}$$

Taking into account system (40)**, relation (38) may be written in the form:

$$\Phi_{(y)} = y \frac{Q}{\beta_q} \left[\frac{h_X}{q} (C_X{}^{tot} - q C_{MX_q}) \cdot \frac{\alpha f_{HX}}{\alpha f_{HX} + C_H f_H f_X} + \right.$$
$$\left. + \frac{i + y - k_M C_M}{n_M F} \cdot \frac{\alpha f_{HX}}{\alpha f_{HX} + (h_{HX}/h_X) C_H f_H f_X}\right]^q + y + i - i_d = 0 \tag{41}$$

* For the demonstration that solution φ is unique, see the Appendix.

** $C_X{}^{tot} - q C_{MX_q} = C_X + C_{HX} = C_X \left(1 + \frac{C_H f_H f_X}{\alpha f_{HX}}\right) = C_X \frac{\alpha f_{HX} + C_H f_H f_X}{\alpha f_{HX}}$

Introducing C_M^0 from (39) into (29) and using the expression of the half-wave potential of the simple metal ion*:

$$E_{\frac{1}{2}}^M = \varepsilon - (RT/n_M F) \ln (f_{am} h_M / f_M h_{am}) \quad (42)$$

the equation of the polarographic wave will be:

$$E = E_{\frac{1}{2}}^M - (RT/n_M F) \ln (i/\varphi) \quad (43)$$

2. S AND S' VARIATIONS FROM EQUATIONS (38)–(41)

In eqns. (38)–(41), the parameters α and C_H are related to each other as follows:

$$S = \frac{\alpha f_{HX}}{\alpha f_{HX} + (h_{HX}/h_X) C_H f_H f_X} = \frac{1}{1 + C_H h_{HX} f_H f_X / \alpha h_X f_{HX}} \quad (44)$$

$$S' = \frac{\alpha f_{HX}}{\alpha f_{HX} + C_H f_H f_X} = \frac{1}{1 + C_H f_H f_X / \alpha f_{HX}} \quad (45)$$

As C_H, h, f and α cannot be negative, S and S' obviously vary from 0 to 1. Figure 2 gives the plot of the functions:

$$S = S(\mathrm{pH} - \mathrm{p}\alpha + \mathrm{p}\, h_{HX} f_H f_X / h_X f_{HX}) \quad (46)$$

$$S' = S'(\mathrm{pH} - \mathrm{p}\alpha + \mathrm{p}\, f_H f_X / f_{HX}) \quad (47)$$

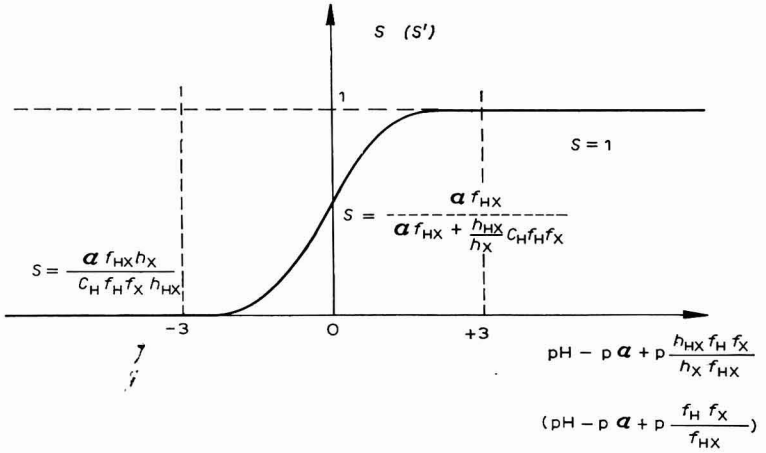

Fig. 2. Dependence of S and S' functions on $\mathrm{pH} - \mathrm{p}\alpha + \mathrm{p}\ldots$.

It is seen that for:

(i) $\mathrm{pH} - \mathrm{p}\alpha + \mathrm{p}\ldots \geqslant 3$**, $S(S') = 1$; in other words for a sufficiently alkaline pH, the weak acid is practically totally dissociated and the pH of the solution has no effect on complex formation (*i.e.*, the case when "the ligand is a non-hydrolysable substance");

* Taking into account the above discussion on the validity of relations (9) and (10), the half-wave potential of the simple metal ion was expressed in terms of h instead of k.

** C_H/α from $S(S')$ – relations (44)–(45) – is considered a negligible quantity compared with 1 if it represents at the most 0.1%, *i.e.*, $C_H/\alpha \leqslant 10^{-3}$. In the same way, 1 is negligible in comparison to C_H/α if $C_H/\alpha \geqslant 10^3$. For less precise estimations, the omission may be made even at a rate of 1%.

(ii) $pH - p\alpha + p\ldots \leqslant -3$: S and S' have a very low value which depends directly upon the ratio α/C_H;

(iii) $-3 < pH - p\alpha + p\ldots < 3$: the dependence of S and S' upon the pH is given by a non-linear function.

3. DISCUSSION OF EQUATION $\Phi_{(y)}=0$—EQUATIONS (38)–(41)

For the case of a non-hydrolysable ligand[1] it was demonstrated that equation $\Phi_{(y)}=0$ may be solved in the following cases:

β_q high — $C_X^{tot} \gg qC_M^{tot}$

β_q low — $C_X^{tot} \gg qC_M^{tot}$

β_q low — $C_X^{tot} = qC_M^{tot}$

β_q low — $qC_M^{tot} < C_X^{tot} < (C_X^{tot} \gg qC_M^{tot})$

As equations (38)–(41) differ from that of the non-hydrolysable ligand (see relation (27), ref. 1) only by

$$\frac{\alpha f_{HX}}{\alpha f_{HX} + (h_{HX}/h_X) C_H f_H f_X}$$

in the parenthesis, the same cases will be taken into account for parameters C_X^{tot} (respectively, C_X) and β_q; the effect of the parameters α and C_H will also be observed. The deduction of the equation of the polarographic wave for simple metal ion will also be shown.

A. No complexes are formed

The condition for which the metal ion forms no complex may be expressed in two ways:

$$\text{(a)} \quad \beta_q = \infty \tag{48}$$

or:

$$\text{(b)} \quad C_X^{tot} = 0 \tag{49}$$

which implies:

$$\begin{cases} C_X = 0 \\ C_{MX_q} = 0 \\ C_{HX} = 0 \\ i - k_M C_M + y = 0 \end{cases} \tag{50}$$

In both cases, (a) or (b), the result* is:

$$\varphi = i_d - i \tag{51}$$

$$E = E_{\frac{1}{2}}^M - (RT/nF) \ln \{i/(i_d - i)\} \tag{52}$$

which is the equation of the polarographic wave for the simple metal ion[2].

B. The ligand is in great excess and the complex is stable (approximation of Lingane type)

If $C_X^{tot} \gg qC_M^{tot}$ and β_q is low, it follows from relation (41) that:

* In the following, the charge of the metal ion, M, will be written as n instead of n_M.

$$\Phi_{(y)} = y\ \frac{Q}{\beta_q}\left(\frac{h_X}{q} C_X{}^{tot} S'\right)^q + i - i_d = 0 \tag{53}$$

$$\varphi = \frac{(i_d - i)\beta_q}{Q\{(h_X/q) C_X{}^{tot} S'\}^q} \tag{54}$$

$$E = E_{\frac{1}{2}}{}^M + \frac{RT}{nF} \ln \frac{\beta_q f_{MX_q} h_M}{f_M h_{MX_q}} - q\,\frac{RT}{nF} \ln (C_X{}^{tot} f_X) -$$

$$- q\,\frac{RT}{nF} \ln \frac{\alpha f_{HX}}{\alpha f_{HX} + C_H f_H f_X} - \frac{RT}{nF} \ln \frac{i}{i_d - i} \tag{55}$$

(i) $pH - p\alpha + p\ldots \gg 3$: $S' = 1$; the pH of the solution has no effect and eqn. (55) is transformed into the Lingane equation[3]:

$$E = E_{\frac{1}{2}}{}^M + \frac{RT}{nF} \ln \frac{\beta_q f_{MX_q} h_M}{f_M h_{MX_q}} - q\,\frac{RT}{nF} \ln (C_X{}^{tot} f_X) - \frac{RT}{nF} \ln \frac{i}{i_d - i} \tag{56}$$

(ii) $pH - p\alpha + p\ldots \ll -3$: $S' = f_{HX}/C_H f_H f_X$; the weak acid, besides that of the complex exists practically only in the associate form, HX, and then $f_X = 1$. Consequently, eqn. (55) becomes the equation of Laitinen *et al.*[4]*:

$$E = E_{\frac{1}{2}}{}^M + \frac{RT}{nF} \ln \frac{\beta_q f_{MX_q} h_M}{f_M h_{MX_q}} - q\,\frac{RT}{nF} \ln C_X{}^{tot}$$

$$- q\,\frac{2.303\,RT}{nF} \ln \left(pH - p\alpha + p\,\frac{f_H}{f_{HX}}\right) - \frac{RT}{nF} \ln \frac{i}{i_d - i} \tag{57}$$

As Laitinen *et al.*[4] showed, eqn. (57) indicates a linear plot between $E_{\frac{1}{2}}{}^{MX_q}$ and pH, with a slope: $-q\ 2.303RT/nF$.

(iii) $-3 < pH - p\alpha + p\ldots < 3$: S and S' have the expressions (44) and (45); the relation between $E_{\frac{1}{2}}{}^{MX_q}$ and pH is more complicated; it results from eqn. (55) and is intermediate between the linear plot of (ii), and the non-dependence of (i).

The above discussion is illustrated in Fig. 3, which theoretically represents the dependence of $E_{\frac{1}{2}}{}^{MX_q}$ on the $pH - p\alpha + p\,(f_H f_X/f_{HX})$. It must be emphasized that the intersection of the extrapolated lines corresponding to (i) and (ii), occurs just on the $E_{\frac{1}{2}}{}^{MX_q}$ axis, *i.e.*, at $pH - p\alpha + p\,(f_H f_X/f_{HX}) = 0$. As $p\,(f_H f_X/f_{HX}) \approx 0$ and as in the solution the pH may be varied within 0–14, it is, theoretically, possible to determine the dissociation constant, α, of the acid, if the latter lies between 10^{-3} and 10^{-11} mole l^{-1}.

C. The ligand is in great excess and the complex is less stable (approximation of Buck)

If $C_X{}^{tot} \gg qC_M{}^{tot}$ and β_q is high, it follows from (41) that:

$$\Phi_{(y)} = y\ (Q/\beta_q)\ \{(h_X/q) C_X{}^{tot} S'\}^q + y + i - i_d = 0 \tag{58}$$

$$\varphi = (i_d - i) \Big/ \left\{1 + \frac{Q}{\beta_q}\left(\frac{h_X}{q} C_X{}^{tot} S'\right)^q\right\} \tag{59}$$

* In the original paper[4] the equation appears as:

$$E_{\frac{1}{2}}{}^{MX_q} - E_{\frac{1}{2}}{}^M = 0.0296 \log \beta_q - q\ 0.0296(pH - p\alpha) - q\ 0.0296 \log C_{HX}$$

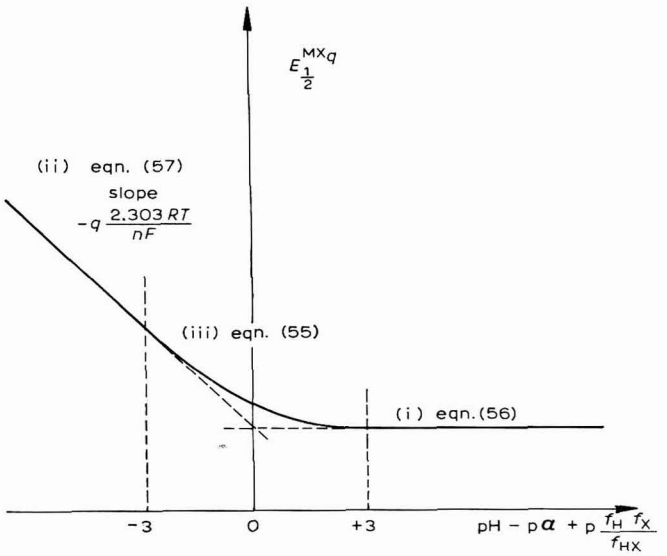

Fig. 3. Dependence (theoretical) of $E_{\frac{1}{2}}^{MX_q}$ on pH − pα + p ($f_H f_X/f_{HX}$). The three regions are (i) linear, corresponding to eqn. (56); (ii) linear, corresponding to eqn. (57) and (iii) non-linear, corresponding to eqn. (55).

$$E = E_{\frac{1}{2}}^{M} - \frac{RT}{nF}\ln\left[\frac{h_{MX_q}f_M}{f_{MX_q}h_M}\cdot\frac{(C_X^{tot}f_X)^q}{\beta_q}\left(\frac{\alpha f_{HX}}{\alpha f_{HX}+C_H f_H f_X}\right)^q + 1\right] - \frac{RT}{nF}\ln\frac{i}{i_d - i} \tag{60}$$

(i) $S' = 1$; eqn. (60) becomes the Buck[5] equation:

$$E = E_{\frac{1}{2}}^{M} - \frac{RT}{nF}\ln\left[\frac{h_{MX_q}f_M}{f_{MX_q}h_M}\cdot\frac{(C_X^{tot}f_X)^q}{\beta_q} + 1\right] - \frac{RT}{nF}\ln\frac{i}{i_d - i} \tag{61}$$

(ii) $S' = \alpha f_{HX}/C_H f_H f_X$; eqn. (60) becomes:

$$E = E_{\frac{1}{2}}^{M} - \frac{RT}{nF}\ln\left[\frac{h_{MX_q}f_M}{f_{MX_q}h_M}\cdot\frac{(C_X^{tot}f_X)^q}{\beta_q}\left(\frac{\alpha f_{HX}}{C_H f_H f_X}\right)^q + 1\right] - \frac{RT}{nF}\ln\frac{i}{i_d - i} \tag{62}$$

If α is very small, eqn. (62) becomes the simple metal ion equation (a complexing of the H appears to the detriment of the metal ion);

(iii) $-3 < pH - p\alpha + p\ldots < 3$: eqn. (60) cannot be simplified.

D. The amount of ligand is just sufficient for stable complex MX_q formation (approximation of Butler and Kaye)

If $C_X^{tot} = qC_M^{tot}$ and β_q is small, it follows from (41) that:

$$\Phi_{(y)} = y(Q/\beta_q)(iS/nF)^q + i - i_d = 0 \tag{63}$$

$$\varphi = (i_d - i)\beta_q/Q(i/nF)^q S^q \tag{64}$$

$$E = E_{\frac{1}{2}}^{M} + \frac{RT}{nF} \ln \frac{\beta_q f_{MX_q} h_M}{f_M h_{MX_q}} - q \frac{RT}{nF} \ln \frac{q}{nF h_X} -$$
$$- q \frac{RT}{nF} \ln \frac{\alpha f_{HX} f_X}{\alpha f_{HX} + (h_{HX}/h_X) C_H f_H f_X} - \frac{RT}{nF} \ln \frac{i^{q+1}}{i_d - i} \quad (65)$$

Compared with the Butler and Kaye relation[6], eqn. (65) is more precise; it takes into account the fact that species X and HX have different diffusion coefficients. (Butler and Kaye used an average value for the diffusion coefficient included in the average "Ilkovič constant $\bar{k}_X$").

If $S = 1$, relation (65) transforms into the corresponding relation for the case of the non-hydrolysable ligand.

E. The ligand is in slight excess and the complex is stable

If $qC_M^{tot} < C_X^{tot} < (C_X^{tot} \gg qC_M^{tot})$ and β_q is low, C_{MX_q} is practically equal to C_M^{tot}; therefore:

$$\Phi_{(y)} = y \frac{Q}{\beta_q} \left[\frac{h_X}{q} (C_X^{tot} - qC_M^{tot}) S' + \frac{iS}{nF} \right]^q + i - i_d = 0 \quad (66)$$

$$\varphi = (i_d - i) \beta_q / Q \left[\frac{h_X}{q} (C_X^{tot} - qC_M^{tot}) S' + \frac{iS}{nF} \right]^q \quad (67)$$

$$E = E_{\frac{1}{2}}^{M} + \frac{RT}{nF} \ln \frac{\beta_q f_{MX_q} h_M}{f_M h_{MX_q}} - q \frac{RT}{nF} \ln \frac{q f_X}{nF h_X} -$$
$$- q \frac{RT}{nF} \ln S - \frac{RT}{nF} \ln \left\{ i \left[\frac{nF h_X}{q} (C_X^{tot} - qC_M^{tot}) \frac{S'}{S} + i \right]^q / (i_d - i) \right\} \quad (68)$$

Equations (55) or (65) may be obtained from eqn. (68) by developing the expression and keeping only the first or the last term.

For $S = S' = 1$, we have the case of the non-hydrolysable ligand.

4. CONCLUSIONS

For deducing the equations of the polarographic wave, it is necessary to express the current–concentration relation in the mathematical form that will take into account the diffusion coefficient of the given substance and the fact that the dropping electrode has a variable surface in time. For the case of simple metal ions, these requirements are satisfied by the Ilkovič relation, but in the case of amalgam diffusion into the mercury or of complex ions, the Ilkovič relation is no longer valid, as has been demonstrated in the first paragraph. However, in the calculations used in the polarographic literature, the use of some relation of Ilkovič type, defining an "Ilkovič constant" in each case, was accepted. To avoid the formality of these relations without physical significance, as well as the confusion occurring because of the specific definitions of each "Ilkovič constant", a new concept "mass current", was introduced. This new concept is not imposed but arises from the necessity to clarify some polarographic problems.

As for the equations of the polarographic waves, (38)–(41), it must be stressed that the α and C_H parameters appear in relation to each other in the S and S' expres-

sions. It can be seen, also, that the variation of these expressions (S and S') usually results in displacement of the wave without modification of its form—relations (55), (60), (65)—if the other parameters are kept constant. A slight wave modification may be observed in relation (68) but as $S/S' \approx 1$, it is very small. This also confirms the possibility of the determination of the dissociation constant, α, of a weak acid by following the polarographic wave displacement as a function of pH.

APPENDIX

To obtain results with physical meaning, function $\Phi_{(y)}$ must have a single real solution and only one.

Demonstration

(a) $\Phi_{(y)}$ has at the most one real solution. $\Phi_{(y)}$ is defined with the limits $y=0$ and $y=k_M C_M$. The derivative of $\Phi_{(y)}$ is:

$$\frac{d\Phi_{(y)}}{dy} = \frac{Q}{\beta_q}\left(\frac{h_X}{q}C_X + \frac{i+y-k_M C_M}{nF}\cdot\frac{\alpha f_{HX}}{\alpha f_{HX}+(h_{HX}/h_X)C_H f_H f_X}\right)^{q-1}\cdot$$
$$\left[\frac{h_X}{q}C_X + \frac{i+(q+1)y-k_M C_M}{nF}\cdot\frac{\alpha f_{HX}}{\alpha f_{HX}+(h_{HX}/h_X)C_H f_H f_X}\right]+1 \qquad \text{(i)}$$

As $i+y \geqslant |k_M C_M|$ $(i \geqslant i_M)$ and C_X, C_H, Q and β_q and α cannot be negative, the derivative has no more real roots, *i.e.*, $\Phi_{(y)}$ may have at the most one real solution.

(b) The real root, φ, does exist. The value of $\Phi_{(y)}$ at the ends of the interval are:

$$\Phi_{(0)} = i - i_d \leqslant 0 \qquad \text{(ii)}$$

$$\Phi_{(k_M C_M)} = k_M C_M \frac{Q}{\beta_q}\left(\frac{h_X}{q}C_X + \frac{i}{nF}\cdot\frac{\alpha f_{HX}}{\alpha f_{HX}+(h_{HX}/h_X)C_H f_H f_X}\right)^q + k_M C_M + i - i_d \qquad \text{(iii)}$$

Introducing in (iii) the expressions of β_q and Q from (3) and (37) and writing the parentheses in the form: $\left(\frac{h_X}{q}C_X\right)^q + iP_{q-1}$ gives:

$$\begin{aligned}\Phi_{(k_M C_M)} &= nF h_{MX_q} C_{MX_q} \\ &+ k_M C_M \frac{Q}{\beta_q}\cdot\frac{i}{nF}\cdot\frac{\alpha f_{HX}}{\alpha f_{HX}+(h_{HX}/h_X)C_H f_H f_X} P_{q-1} + k_M C_M + i - i_d \\ &= k_M C_M \frac{Q}{\beta_q}\cdot\frac{i}{nF}\cdot\frac{\alpha f_{HX}}{\alpha f_{HX}+(h_{HX}/h_X)C_H f_X f_H} P_{q-1} + i \geqslant 0\end{aligned} \qquad \text{(iv)}$$

Depending on the i parameter, the sign of $\Phi_{(y)}$ varies thus:

$$\begin{cases} i=0 & \Phi_{(0)}<0 & \Phi_{(k_M C_M)}=0 \\ 0<i<i_d & \Phi_{(0)}<0 & \Phi_{(k_M C_M)}>0 \\ i=i_d & \Phi_{(0)}=0 & \Phi_{(k_M C_M)}>0 \end{cases} \qquad \text{(v)}$$

As $\Phi_{(y)}$ changes its sign within the definition domain, the real root, φ, does exist.

SUMMARY

During polarography of a solution in which the complex MX_q is formed with

dissociation constant, β_q (X being the anion of a weak acid with dissociation constant, α) the current is carried to the dropping electrode by all metal ions simple or complexed; therefore the total current, i, is a sum of two currents: i_M and i_{MX_q}. When the complex metal ion is reduced, the complex is broken and the concentrations of species X and HX at the dropping electrode surface are modified; as the solution is buffered, the concentration of H ions remains constant. These hypotheses lead to the following polarographic wave equation:

$$E = E_{\frac{1}{2}}^{M} - (RT/nF) \ln (i/\varphi)$$

where φ is the solution of the equation:

$$\Phi_{(y)} = \frac{y}{\beta_q} \cdot \frac{h_{MX_q} f_M}{f_{MX_q} h_M} \left(\frac{q f_X}{h_X}\right)^q$$

$$\left[\frac{h_X}{q} C_X + \frac{i + y - k_M C_M}{nF} \cdot \frac{\alpha f_{HX}}{\alpha f_{HX} + (h_{HX}/h_X) C_H f_H f_X}\right]^q + y + i - i_d = 0$$

C_X is the free ligand concentration in the bulk solution, C_M is the metal ion concentration in the bulk solution, f are the activity coefficients and h new constants introduced for the constants of Ilkovič type, consequent to the introduction of the new concept "mass current". h constants are related to Ilkovič constants by the relation: $h = nFk$.

The validity of some relations of the Ilkovič type and the effect of pH on the polarographic waves in a buffered medium are discussed. The possibility of determining the dissociation constant, α, of the weak acid by displacement of the polarographic waves as a function of pH is confirmed.

REFERENCES

1 M. MACOVSCHI, *J. Electroanal. Chem.*, 16 (1968) 457.
2 J. HEYROVSKÝ AND J. KŮTA, *Tratat de Polarografie*, Ed. Acad. R.P.R., Bucharest, 1959, p. 118.
3 J. J. LINGANE, *Chem. Rev.*, 29 (1941) 1.
4 H. A. LAITINEN, E. I. ONSTOTT, J. C. BAILAR, JR. AND S. SWANN, JR., *J. Am. Chem. Soc.*, 71 (1949) 1550.
5 R. P. BUCK, *J. Electroanal. Chem.*, 5 (1963) 295.
6 C. G. BUTLER AND R. C. KAYE, *J. Electroanal. Chem.*, 8 (1964) 463.

ELECTROANALYTICAL CHEMISTRY AND INTERFACIAL ELECTROCHEMISTRY
Elsevier Sequoia S.A., Lausanne – Printed in The Netherlands

AUSSAGEMÖGLICHKEITEN UND GRENZEN INSTATIONÄRER ELEKTROCHEMISCHER VERFAHREN FÜR DIE UNTERSUCHUNG DER ADSORPTION UND ADSORPTIONSKINETIK VON REAKTANDEN UND REAKTIONSPRODUKTEN

F. MÖLLERS UND W. JAENICKE
Institut für Physikalische Chemie der Universität Erlangen-Nürnberg (Deutschland)
(Eingegangen am 20 Oktober 1967)

1. EINLEITUNG UND PROBLEMSTELLUNG

An einer Elektrode adsorbierte elektrochemisch umsetzbare Stoffe lassen sich mit instationären Verfahren elektrisch bestimmen, wenn es gelingt, die gemessene Ladungsmenge in adsorbierten und herandiffundierten Anteil zu trennen. Als erster verwandte LORENZ[1,2] die Variation der Stromdichte bei galvanostatischen Einschaltvorgängen zu diesem Zweck. WILL UND KNORR[3] arbeiteten mit einer potentiostatischen Dreieckspannungsmethode, bei der sie die Geschwindigkeit der Spannungszunahme änderten. CHRISTIE, LAUER UND OSTERYOUNG[4] benutzten potentiostatische Spannungssprünge variabler Grösse.

Mit den gleichen Methoden lässt sich auch die Adsorption von Zwischen- oder End-produkten elektrochemischer Reaktionen untersuchen. Hier wird z.B. mit einer bestimmten Ladungsmenge ein Stoff erzeugt und dessen Verbleib an der Elektrodenoberfläche mit einem zweiten galvanostatischen Impuls umgekehrter Richtung bestimmt[5]. Neben Diffusion und Adsorption sind hier auch noch chemische Reaktionen bei der Aufteilung der gemessenen Ladungsmenge zu berücksichtigen. Hier liegen einige qualitative Angaben über intermediär adsorbierte Zwischenprodukte vor[6], ferner eine Arbeit von HERMAN, TATWADI UND BARD[7], deren Methode allerdings voraussetzt, dass am Ende des ersten Impulses die Sättigungskonzentration des adsorbierten Reaktionsproduktes erreicht ist. ANSON[8] verwendete eine potentiostatische Methode, bei der nach einem ersten Potentialsprung durch einen zweiten das Ausgangspotential wiederhergestellt wird. Bisher wurde dies Verfahren jedoch nur benutzt, um die Adsorption von Ausgangsprodukten zu untersuchen, wobei die beim zweiten Impuls gemessene Ladungsmenge nur zur Bestimmung der Elektrodenkapazität diente.

Ganz gleich, ob die Adsorption von Ausgangs- oder Reaktions-produkten untersucht wird—stets entsteht bei der Messung die umgeladene Form des verwendeten Stoffes, die ihrerseits adsorbierbar sein kann. Es muss also Adsorptionsverdrängung berücksichtigt werden. Ausserdem beruht die Trennung von adsorbierter und diffundierender Substanz stets darauf, dass die Geschwindigkeit des Umsatzes variiert wird. Daher kann auch die Kinetik der Adsorption die Messresultate beeinflussen.

Ziel der vorliegenden Arbeit ist es, an einem einfach zu handhabenden System festzustellen, wie weit die vorliegenden Auswertungsmethoden eindeutige Aussagen

über die Grösse der Adsorption von Ausgangs- und Reaktions-produkt gestatten und ob die Resultate darüber hinaus ausreichen, um auch Adsorptionsverdrängung und Adsorptionskinetik zu erfassen. Als System diente Chinon–Hydrochinon, als Elektrode ein ruhender Quecksilbertropfen.

2. ZUR BESTIMMUNG DER ADSORPTION MIT GALVANOSTATISCHEN IMPULSEN

(a) *Adsorption von Ausgangsstoffen*

Wird ein Reaktand der Konzentration c, der an einer ebenen Elektrode mit der Oberflächenkonzentration Γ^* adsorbiert ist, durch die Stromdichte i entladen, so gilt in dem Zeitintervall von 0 bis zur Transitionszeit τ für die Diffusionsgleichung folgende Randbedingung auf der Elektrode:

$$D\left(\frac{\partial c}{\partial x}\right)_{x=0} = j = \frac{i}{zF} + \frac{\mathrm{d}\Gamma^*}{\mathrm{d}t} - \frac{C}{zF}\cdot\frac{\mathrm{d}U}{\mathrm{d}t} = \frac{i}{zF} + \frac{\mathrm{d}}{\mathrm{d}t}\left(\Gamma^* - \frac{C}{zF}U\right) \qquad (1)$$

z ist die Ladungszahl je Formelumsatz.

Für anodischen Strom ist i und z positiv. Durch geeignete Wahl der Zeitpunkte $t=0$ und $t=\tau$ auf der experimentell bestimmten Spannungs–Zeitkurve lässt sich das Zeitintervall so definieren, dass der Ladestrom $C\mathrm{d}U/\mathrm{d}t$ minimal wird (siehe S. 70). In diesem Bereich kann Γ^* unabhängig von U gesetzt werden. Der verbleibende Anteil wird zweckmässig in das Adsorptionsglied hineingenommen und $\mathrm{d}\Gamma^* - (C/zF)\mathrm{d}U = \mathrm{d}\Gamma$ gesetzt. Das Diffusionsproblem ist auch mit diesen Vereinfachungen nur definiert, wenn $\Gamma\,(c(x=0),\, t)$ gegeben, also die Adsorptionskinetik bekannt ist. LORENZ[1] hat statt dessen vier verschiedene Möglichkeiten des Verlaufs von $\Gamma(t)$ oder $\Gamma(c)$ während eines Stromimpulses mit $i=\text{const.}$ vorgegeben und die Differentialgleichung für diese Modelle gelöst. Sie sind Ausdruck jeweils bestimmter vereinfachter Vorstellungen über die Adsorptionskinetik.

Jedes Modell liefert einen Wert für $\Gamma(t=0)$, nämlich $\Gamma_1 \ldots \Gamma_4$, aus einer Messung von i,τ und der Lösungskonzentration $c^0=c(t=0)$. Für die vorliegende Arbeit ist es zweckmässig, Γ als Funktion von

$$G = i\tau/zF \quad \text{sowie von} \quad y = zF(\pi D)^{\frac{1}{2}}c^0/2i(\tau)^{\frac{1}{2}} \qquad (2)$$

darzustellen (Abb. 1); y nimmt im Falle reiner Diffusion den Wert 1 an.

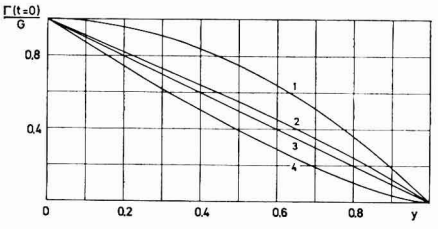

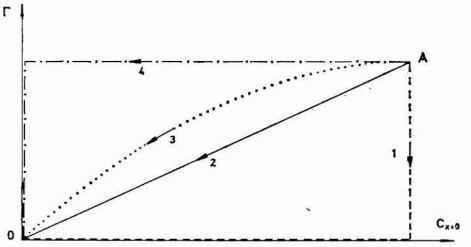

Abb. 1. Diagramm zur Auswertung chronopotentiometrischer Messungen mit einfachen Impulsen gemäss Modell 1–4. Ordinate: $\Gamma(t=0)/G = zF\Gamma(t=0)/i\tau$; Abzisse: $y = zF\sqrt{\pi D}c^0/2\; i(\tau^{\frac{1}{2}})$.

Abb. 2. Verlauf der Oberflächenkonzentration Γ als Funktion der Lösungskonzentration c an der Stelle $x = 0$, wenn der Ausgangszustand A ($t = 0$; $c = c^0$) nach Modell 1–4 durch konstanten Strom in den Zustand 0 ($t = \tau$; $\Gamma = 0$; $c = 0$) überführt wird.

Modell 1. Zu Beginn des Impulses wird mit der gesamten Stromstärke die Adsorptionsschicht abgebaut und danach wird der herandiffundierte Reaktand entladen. Dies Modell führt auf

$$\Gamma_1(t=0) = G(1-y^2) \tag{3}$$

(vgl. Abb. 1, Kurve 1).

Modell 2. Adsorptionsschicht und Diffusionsschicht werden so abgebaut, dass stets

$$\Gamma_2 = Kc(x=0) \tag{4}$$

Dann ist

$$\Gamma_2(t=0) = G\frac{(2/\pi^{\frac{1}{2}})u - 1 + \exp(u^2)\operatorname{erfc}(u)}{u^2} \tag{5}$$

wobei $u=(D\tau)^{\frac{1}{2}}/K$. Da wegen Gleichung (4)

$$y = \frac{(2/\pi^{\frac{1}{2}})u - 1 + \exp(u^2)\operatorname{erfc}(u)}{(2/\pi^{\frac{1}{2}})u}$$

lässt sich auch für diesen Ansatz $\Gamma_2(t=0)$ als $\Gamma_2(G,y)$ darstellen (Abb. 1, Kurve 2).

Modell 3. Die Adsorptionsschicht wird mit einer konstanten Stromstärke abgebaut, die so bemessen ist, dass Γ und $c(x=0)$ zur Transitionszeit gleichzeitig verschwinden. Hierfür gilt:

$$\Gamma_3(t=0) = G(1-y) \tag{6}$$

(Abb. 1, Kurve 3).

Modell 4. Die Diffusionsschicht wird zunächst abgebaut, ohne dass die Adsorptionsschicht angegriffen wird. Ist die Konzentration des Reaktanden vor der Elektrode auf 0 gesunken, beginnt die Entladung der Adsorptionsschicht, wobei ein Teil des Stroms benötigt wird, um den nachdiffundierenden Reaktanden umzusetzen. Die strenge Lösung dieses Modells[9] liefert:

$$\Gamma_4(t=0) = G\{(1/\pi^{\frac{1}{2}})\arccos(2y^2-1) - (2/\pi)y(1-y)^{\frac{1}{2}}\} \tag{7}$$

(Abb. 1, Kurve 4).

Das Diagramm Abb. 1 eignet sich zur Auswertung von Messungen nach den vier Modellen. Die Übereinstimmung der Modelle und damit die Brauchbarkeit der gewonnenen Resultate für die Adsorption steigt mit abnehmendem y. Experimentell entspricht dies zunehmender Stromdichte, da hierbei ein relativ kleinerer Teil des gesamten Umsatzes aus der Diffusionsschicht stammt.

Die bisher betrachteten Modelle liefern einen Wert für die im Gleichgewicht bei $t=0$ adsorbierte Menge. Zur Diskussion des Adsorptionsverhaltens *während* des Stromimpulses ist es zweckmässig, wie im Ansatz zu Modell 2 Γ als Funktion von c zu betrachten. Dies ist für die vier Modelle in Abb. 2 geschehen. Zur Zeit $t=0$ befindet sich das System jeweils bei A, bei $t=\tau$ im Nullpunkt bei 0. Kurve 3 entspricht einer Parabel mit dem Scheitelpunkt bei A.

Der wahre Verlauf von Γ während des Stromimpulses muss in jedem Fall zwischen den durch 1 und 4 gegebenen Kurven liegen. Er hängt von der Adsorptionskinetik des Reaktanden und des Reaktionsproduktes ab. Solange das Adsorptionsgleichgewicht eingestellt bleibt, d.h. bei kleinen Stromdichten, wird die Ad-

sorptionsisotherme durchlaufen und $\Gamma(c)$ bleibt unabhängig von i. Mit wachsender Stromdichte sinkt $\Gamma(c)$ dagegen immer weiter unter den Gleichgewichtsverlauf.

Wie im Abschnitt 5(a) gezeigt wird, ermöglicht daher eine Auswertung der Messresultate als Funktion der Stromdichte Aussagen über die Adsorptionskinetik.

(*b*) *Adsorption von Reaktionsprodukten*

Produkte elektrochemischer Umsetzungen lassen sich durch galvanostatische Impulse mit Stromumkehr untersuchen. Dabei bildet ein erster Impuls der Stromdichte i_1 während der (unter der Transitionszeit liegenden) Zeit t_1 den interessierenden Stoff. Dieser wird durch einen zweiten entgegengesetzt gerichteten Impuls der Stromdichte i_2 wieder in das Ausgangsprodukt zurückverwandelt. Für die Transitionszeit τ, des zweiten Impulses gilt, falls das Reaktionsprodukt lediglich wegdiffundiert[5]:

$$1 + |i_2/i_1| = (t_1 + \tau)^{\frac{1}{2}}/\tau^{\frac{1}{2}} \tag{8}$$

Wird das Reaktionsprodukt an der Elektrodenoberfläche durch Adsorption festgehalten, liegt τ über dem so definierten Wert, reagiert es zu einem Folgeprodukt weiter, wird ein kleineres τ gefunden.

Zur Lösung der (eindimensionalen) Diffusionsgleichung müssen bei Adsorption des Reaktionsproduktes entsprechend den Überlegungen im Fall einfacher Impulse folgende Randbedingungen gewählt werden:

$$D\left(\frac{\partial c}{\partial x}\right)_{x=0} = -\frac{i_1}{z_1 F} + \frac{\mathrm{d}\Gamma}{\mathrm{d}t} \quad \text{für } 0 < t < t_1$$

$$D\left(\frac{\partial c}{\partial x}\right)_{x=0} = +\frac{i_2}{z_2 F} + \frac{\mathrm{d}\Gamma}{\mathrm{d}t} \quad \text{für } t_1 < t < (t_1 + \tau)$$

c bedeutet hier die Konzentration des Reaktionsproduktes während des ersten Impulses und damit die des Reaktanden während des zweiten Impulses. Es ist $z_1 = -z_2$.

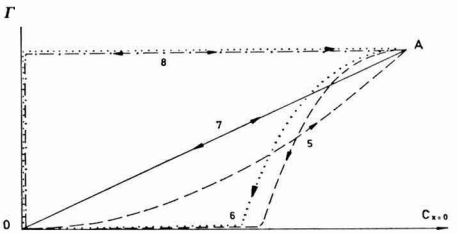

Abb. 3. Verlauf der Oberflächenkonzentration Γ eines Reaktionsprodukts als Funktion seiner Lösungskonzentration c an der Stelle $x = 0$ bei doppelten Impulsen. (0), Ausgangs- und Endzustand ($t = 0$ und $t = t_1 + \tau$; $\Gamma = 0$, $c = 0$); (A), Zustand bei Stromumkehr ($t = t_1$).

Ohne Kenntnis der Adsorptionskinetik $\Gamma(c,t)$ sind wieder spezielle Annahmen zur Lösung nötig. Es lassen sich zum Beispiel die vier für den einfachen Impuls diskutierten Fälle beliebig für beide Impulse kombinieren. Im folgenden werden aus mathematischen und physikalischen Gründen nur vier dieser Möglichkeiten (Modelle 5–8) behandelt. Die vier diskutierten Modelle sind in Abb. 4 veranschaulicht, die den Diffusionsstrom j als Funktion der Zeit wiedergibt.

Der Verlauf $\Gamma(c)$ während der beiden Impulse ist in Abb. 3 gezeichnet. Zum Unterschied von den in Abb. 2 dargestellten Zuständen handelt es sich hier um die Adsorption eines Reaktionsproduktes. Abgesehen vom Grenzfall stets eingestellten Gleichgewichts sind daher hier nur solche Fälle physikalisch sinnvoll, bei denen die adsorbierte Menge während des ersten Impulses oberhalb, während des zweiten Impulses unterhalb des Gleichgewichtswertes liegt.

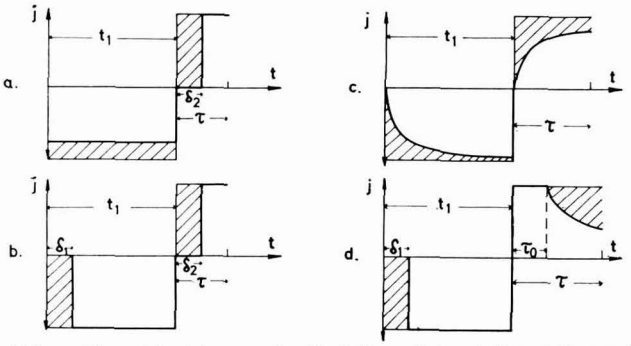

Abb. 4. Charakterisierung der Modelle 5–8 durch Darstellung des Stofftransports $j = D(\partial c/\partial x)_{x=0}$ als Funktion der Zeit t. Die schraffierte Fläche bedeutet die Oberflächenkonzentration Γ, die während der Dauer t_1 des ersten Impulses auf-, während der Dauer τ des zweiten Impulses wieder abgebaut wird (a, b, c, d = Modelle 5, 6, 7, 8).

Modell 5. Während des ersten Impulses wird die Adsorptionsschicht mit einem konstanten Bruchteil der Stromdichte i_1 aufgebaut, zu Beginn des zweiten Impulses mit der gesamten Stromdichte i_2 abgebaut (Kombination der Modelle 3 und 1, Abb. 3, Kurve 5; Abb. 4a):

$$0 < t < t_1 : j = -i_1/z_1F + \Gamma/t_1$$

$$t_1 < t < (t_1+\delta) : j = 0$$

$$(t_1+\delta) < t < (t_1+\tau) : j = i_2/z_2F$$

werden die Messgrössen durch

$$a = (t_1+\tau)^{\frac{1}{2}}/\tau^{\frac{1}{2}}, \quad b = |i_2/i_1|, \quad \text{und } G' = -i_2\tau/z_2F$$

dargestellt, erhält man*

$$\Gamma_5(t=t_1) = G'\left[\frac{a^2-1}{b} - (a+1)\left\{\frac{a+1}{2} - \left\{1 - \frac{a^2-1}{b} + \left(\frac{a+1}{2}\right)^2\right\}^{\frac{1}{2}}\right\}\right] \tag{9}$$

Modell 6. Zu Beginn des ersten Impulses wird die gesamte Adsorptionsschicht aufgebaut, zu Beginn des zweiten Impulses wieder abgebaut (Kombination von Modell 1 mit 1; Abb. 3, Kurve 6; Abb. 4b):

$$0 < t < \delta_1 : \quad j = 0$$

$$\delta_1 < t < t_1 : \quad j = -i_1/z_1F$$

$$t_1 < t < (t_1+\delta_2) : \quad j = 0$$

$$(t_1+\delta_2) < t < (t_1+\tau) : \quad j = +i_2/z_2F$$

* vgl. Anhang 1.

Für diesen Fall resultiert, wenn $b \neq 1$*:

$$\Gamma_6(t=t_1) = G'\left[1 - \left\{\frac{1-[1+(b-1)\{(a^2-1)/b-1\}]^{\frac{1}{2}}}{b-1}\right\}^2\right] \quad (10a)$$

und (nach Entwicklung des Wurzelausdrucks) für $b=1$:

$$\Gamma_6(t=t_1) = G'[1-(a^2-1-b)^2/4b^2] \quad (10b)$$

Modell 7. Adsorptionsschicht und Diffusionsschicht werden so auf- und abgebaut, dass während der gesamten Versuchszeit $0 < t < (t_1+\tau)$

$$\Gamma_7 = Kc(x=0) \quad (11)$$

(Kombination von Modell 2 mit 2; Abb. 3, Kurve 7; Abb. 4c). Dies liefert die Lösung*:

$$f(a\cdot(D\tau)^{\frac{1}{2}}/K) = (1+b)f(D\tau)^{\frac{1}{2}}/K \quad (12)$$

wobei $f(x) = (2x/\pi^{\frac{1}{2}}) - 1 + \exp(x^2)\mathrm{erfc}(x)$

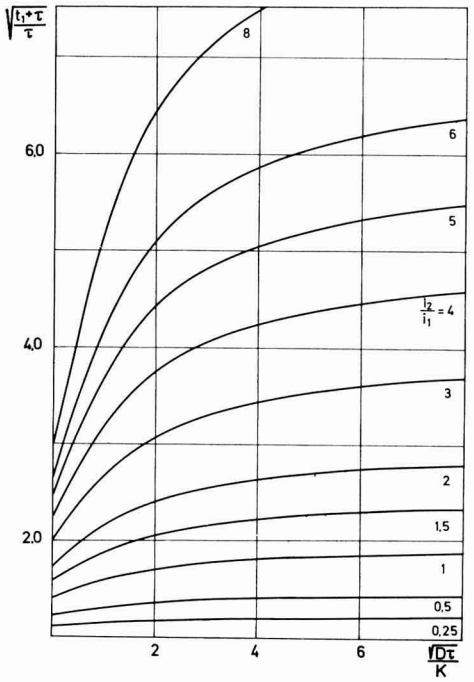

Abb. 5. Graphische Darstellung der Grösse $((t_1+\tau)/\tau)^{\frac{1}{2}} = a$ als Funktion von $\sqrt{D\tau}/K$ mit dem Parameter $|i_2/i_1| = b$ zur Auswertung nach K gemäss Gleichung (12).

Um die Messergebnisse auswerten zu können, wurde aus Gleichung (12) die Grösse $(D\tau)^{\frac{1}{2}}/K$ für diskrete Werte von b als Funktion von a mit einer Rechenmaschine berechnet[10]. Die graphische Darstellung (Abb. 5) erlaubt, K aus dem gemessenen Wert von a zu ermitteln. Setzt man dies und den für $c(x=0, t=t_1)$ gefundenen Wert:

* Siehe Anhang 1.

$$c(x=0,t=t_1) = \frac{i_1 K}{z_1 F D}\left[\frac{2}{\pi^{\frac{1}{2}}}\cdot\frac{(Dt_1)^{\frac{1}{2}}}{K} - 1 + \exp\left(\frac{Dt_1}{K^2}\right)\operatorname{erfc}\left\{\frac{(Dt_1)^{\frac{1}{2}}}{K}\right\}\right]$$

in Gleichung (11) ein, erhält man mit der Abkürzung $u_1=(Dt_1)^{\frac{1}{2}}/K$:

$$\Gamma_7(t=t_1) = \frac{i_1 t_1}{z_1 F}\,\frac{\left[\frac{2}{\pi^{\frac{1}{2}}}u_1 - 1 + \exp(u_1^2)\operatorname{erfc}(u_1)\right]}{u_1^2} \qquad (13)$$

Modell 8. Die Adsorptionsschicht wird zu Beginn des ersten Impulses aufgebaut, jedoch beim 2. Impuls erst wieder abgebaut, nachdem $c(x=0)$ Null geworden ist (Kombination von Modell 1 und 4, Abb. 3, Kurve 8; Abb. 4d). Es ist also:

$0<t<\delta_1$: $j=0$

$\delta_1<t<(t_1+\tau_0)$: $j=-i_1/z_1F$

$t_1<t<(t_1+\tau_0)$: $j=i_2/z_2F$

$(t_1+\tau_0)<t<(t_1+\tau)$: $c(x=0)=0$

Für den Spezialfall $b=1$ haben HERMAN, TATWADI UND BARD[7] eine Lösung angegeben. In ihr heben sich jedoch zwei Glieder weg, wenn man berücksichtigt (Abb. 4d), dass für das Zeitintervall $\delta_1<t<(t_1+\tau_0-\delta_1)$ die Bedingung reiner Diffusion, Gleichung (7) gilt.

Für den allgemeinen Fall $b\neq 1$ ergeben sich eine Reihe von Beziehungen für Γ_8, in denen τ_0 und δ_1 auftreten:

Die Bedingung, dass für $t>t_1+\tau_0$, $c(x=0)=0$ sein soll, liefert analog einem Ansatz von BERZINS UND DELAHAY[5] $\partial c/\partial x(x=0)$ für den Zeitraum $\tau_0<t<\tau$. Durch Integration erhält man das schraffierte Gebiet auf der rechten Seite von Abb. 4d:

$$\Gamma_8(t=t_1)=G'\left[\frac{(1+b)(1-r)}{\pi}\arccos\frac{1-r}{1+r} - \frac{(1+b)^2(1+s)}{\tau}\arccos\frac{1-s}{1+s}\right] \qquad (14)$$

mit $r=(\tau/\tau_0)-1$ und $s=r/(1+b)^2$.

Die Bedingung, dass im Zeitintervall $\delta_1<t<(t_1-\delta_1+\tau_0)$ der Fall reiner Diffusion vorliegt, erlaubt eine weitere Bestimmung der adsorbierten Menge über die Zwischengrösse δ_1, da die Integration der Stromstärke bis zum Zeitintervall δ_1 die Grösse Γ_8 als schraffiertes Gebiet auf der linken Seite von Abb. 4d ergibt:

$$\Gamma_8(t=t_1)=i_1\delta_1/zF=G'\{(a^2-1)/b+(2+b)/(1+s)\} \qquad (15)$$

Aus (14) und (15) lässt sich aus den Messwerten i_1, i_2, t_1, τ nach einen Iterationsverfahren Γ_8 berechnen.

Wie im Anhang 2 gezeigt ist, erhält man einen Minimalwert für Γ, wenn man annimmt, dass die Adsorptionsschicht zu Beginn des ersten Impulses auf- und am Ende des zweiten Impulses abgebaut wird (vgl. Modell 8).

Der Maximalwert ergibt sich nach Anhang 2, wenn die Schicht am Ende des ersten Impulses plötzlich auf- und am Anfang des zweiten Impulses abgebaut wird. Dies ist aber physikalisch sinnlos. Modell 5 liefert nur wenig unter dem Maximum liegende Werte für Γ. Bei ihm schneiden sich aber die Kurven für Auf- und Abbau der Adsorptionsschicht (Abb. 4, Kurve 5). Physikalisch sinnvoll ist dies Modell höchstens für grosse $|i_2/i_1|$, da hier der Schnittpunkt nach rechts rückt[10].

Um den Bereich einzugrenzen, innerhalb dessen Γ liegen kann, wurde daher

vorgezogen, für den Maximalwert Modell 6 zu benutzen und es mit Modell 8 als Minimalwert zu vergleichen. Die Resultate für Modell 7 liegen etwa in der Mitte zwischen diesen beiden Grenzen.

In Abb. 6 ist Γ/G' nach diesen beiden Modellen als Funktion von $a/(1+b)$ wiedergegeben. Diese Darstellung liefert für den Fall reiner Diffusion die Ordinate $=0$ und die Abzisse $=1$. Abbildung 6 veranschaulicht unmittelbar, dass die Wahl des Modells das Resultat bei der Messung von Reaktionsprodukten in viel grösserem Mass beeinflusst als bei Reaktanden und daher die Interpretation der Ergebnisse weit unsicherer ist.

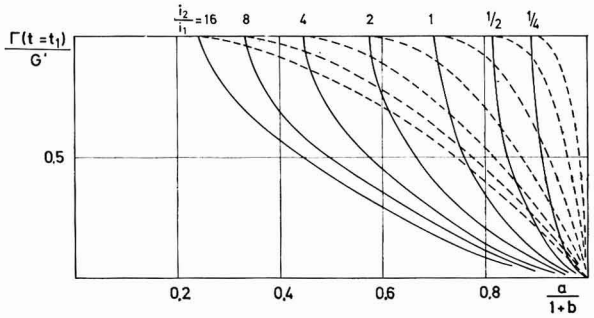

Abb. 6. Diagramm zur Auswertung chronopotentiometrischer Messungen mit Stromumkehr gemäss Modell 6 und 8. Ordinate: $\Gamma(t=t_1)/G' = zF\Gamma(t=t_1)/i_2\tau$; Abzisse: $a/(1+b) = \{(t_1+\tau)/\tau\}^{\frac{1}{2}} \times \{(i_1+i_2)/i_1\}^{-1}$.

3. EXPERIMENTELLES

(a) *Versuchsanordnung*

Die Anordnung für galvanostatische Messungen ist in Abb. 7 wiedergegeben. Ihre Leistungsfähigkeit ist durch die Eigenschaften der operativen Verstärker begrenzt (± 50 V Maximalspannung, 5 mA Ausgangsstrom, Grenzfrequenz 15 MHz). Sie arbeitet mit 1% Messgenauigkeit bei Zellwiderständen unter 20 kΩ. Zur Einstellung der Stromstärke wurde die Zelle durch ein Ampèremeter ersetzt und dem Generator ein Dauerimpuls entnommen.

Für die chronocoulometrischen Messungen[4] diente die Anordnung der Abb. 8. Sie erlaubt, die Ladungsmenge als Funktion der Zeit unmittelbar als Spannung abzulesen.

Die elektrolytische Zelle bestand aus einer gesättigten Kalomelvergleichselektrode mit Lugginkapillare, die mit dem Leitelektrolyt gefüllt war, einem Platinnetz als Gegenelektrode und in ihrer Achse einem ruhenden Hg-Tropfen als Arbeitselektrode. Die Tropfenoberfläche konnte durch ein elektronisch gesteuertes Magnetventil auf 2% reproduzierbar eingestellt werden. Sie wurde mit einem Kathetometer und durch Eichung in $CdSO_4$-Lösung zu 5.00 mm² bestimmt. Die Reproduzierbarkeit der Grösse $i\sqrt{\tau}$ lag bei der gesamten Messapparatur je nach der Grösse von τ zwischen 2 und 4%. Um den Einfluss der Oberflächenkrümmung unter 4% zu halten, mussten bei der gegebenen Tropfengrösse daher Transitionszeiten unter 0.85 sec gewählt werden[10].

Als Leitelektrolyt diente 0.1 *M* KNO_3 + Phosphatpuffer aus je 0.05 *M*

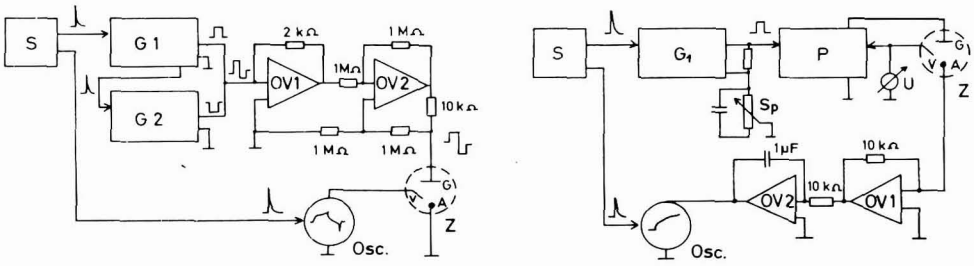

Abb. 7. Versuchsanordnung für Chronopotentiometrie mit Stromumkehr (bistabiler Multivibrator) zur Einschaltung des Generators G_1 und der Zeitablenkung des Oszillographen (Speicheroszillograph Tektronix, Type 564 mit Differenzverstärker 2 A 63, Zeitbasis 3 B 3). (S), Startschalter; (G_1), Stromimpulsgenerator für Impulse zwischen $2 \cdot 10^{-5}$ und 20 sec und Ströme bis 20 mA; (G_2), durch G_1 gestarteter Stromimpulsgenerator gleicher Eigenschaften wie G_1, jedoch umgekehrter Stromrichtung; (OV1), operativer Verstärker (Tektronix Operational Amplifier Type O), der den Stromimpuls aus G_1 und G_2 in einen Spannungsimpuls verwandelt; (OV2), operativer Verstärker, der den Strom in der Zelle Z unabhängig von ihrem Polarisationszustand proportional dem Spannungsimpuls von OV1 regelt; Zelle Z mit Arbeitselektrode A, Gegenelektrode G und Vergleichselektrode V.

Abb. 8. Versuchsanordnung für Chronocoulometrie mit doppeltem Potentialsprung. (Sp), Spannungsteiler zur Vorgabe des Ruhepotentials an der Vergleichselektrode V gegen die Arbeitselektrode A in der Zelle Z; (S), Startschalter; (G_1), Impulsgenerator (vgl. Abb. 7), der über einen Festwiderstand einen Spannungsimpuls zur Ruhespannung addiert; (P), Potentiostat (nach Wenking) zur Regelung des Potentials der Vergleichselektrode auf den durch G_1 und Sp gegebenen Sollwert (gemessen durch U (Röhrenvoltmeter der Fa. KNICK)); (OV1), operativer Verstärker, der den Stromimpuls in einen Spannungsimpuls verwandelt; (OV2), operativer Verstärker, der den Spannungsimpuls über die Zeit integriert und die Ordinatenablenkung für den Oszillographen (Tektronix, vgl. Abb. 7) liefert.

KH_2PO_4 und Na_2HPO_4. Die Lösungen wurden in einer besonderen Apparatur unter Luftabschluss mit frisch entgastem doppelt destilliertem Wasser hergestellt und mit über BTS-Katalysator gereinigtem Stickstoff in die Zelle gedrückt. Die Versuchstemperatur betrug 25.0°. Jede Messung wurde an einem neuen Tropfen, etwa 5 sec nach seiner Herstellung, vorgenommen. Ein Einfluss des Tropfenalters wurde zwischen 1 und 30 sec untersucht, jedoch wurden keine Unterschiede gefunden.

(*b*) *Auswertung der Messungen*

Die Bestimmung der Transitionszeit aus der oszillographischen Potential–Zeitkurve ist nicht ohne eine gewisse Willkür möglich[11]. Es wurde die Methode von

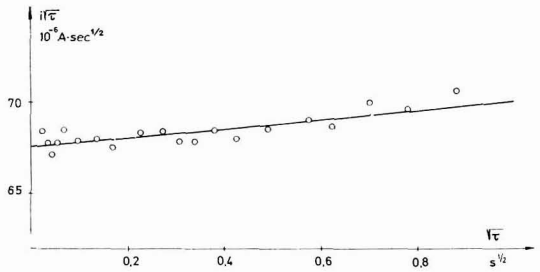

Abb. 9. Chronopotentiometrische Eichmessung in $3.0 \cdot 10^{-3}$ *M* $CdSO_4$-Lösung. Grundelektrolyt: wässrige Lösung von 0.1 *M* KNO_3 und 0.01 *M* HNO_3. Ausgezogen: theoretischer Verlauf unter Berücksichtigung der Krümmung der Elektrodenoberfläche.

REINMUTH[12] gewählt, bei der Tangenten an die Stellen maximaler Steigung der Potential–Zeitkurve bei $t=0$ und bei $t>\tau$ gelegt werden und als Transitionszeit der Abstand der Schnittpunkte einer Tangente minimaler Steigung mit diesen beiden Geraden definiert wird. Zur Kontrolle wurde die Steigung der Tangente bei $t=0$ mit der für die Leerlösung gemessenen verglichen. Bei doppelten Impulsen erwies sich die Methode von BERZINS UND DELAHAY[5] als zweckmässiger.

In Abb. 9 ist für $CdSO_4$ das so bestimmte $i\sqrt{\tau}$ als Funktion von $\sqrt{\tau}$ aufgetragen und mit der berechneten Korrektur für den Einfluss der Tropfenkrümmung (ausgezogene Kurve) verglichen. Da für Cadmium Adsorption chronopotentiometrisch nicht feststellbar ist[13], zeigt das Zusammenfallen von Messpunkten und berechneter Kurve, dass die gewählte Bestimmungsmethode für τ genau genug ist, um aus den Abweichungen von ihr auf Adsorption zu schliessen.

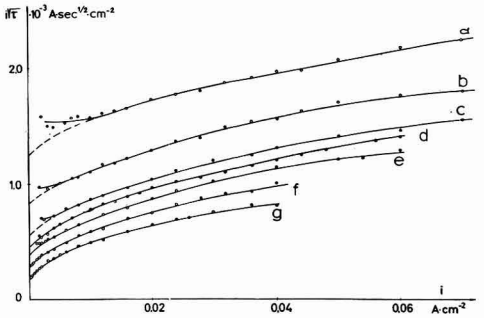

Abb. 10. Chronopotentiometrische Messungen mit einfachen Impulsen in Hydrochinonlösungen. Parameter: Hydrochinonkonzentration; Grundelektrolyt: wässrige Lösung von 0.1 M KNO_3, 0.05 M KH_2PO_4 und 0.05 M Na_2HPO_4 (pH = 6.7). Konzentration ($M\cdot10^3$): (a) 3.03; (b) 2.02; (c) 1.35; (d) 1.11; (e) 0.93; (f) 0.68, (g) 0.40.

4. MESSERGEBNISSE

Es wurde die Adsorption von Hydrochinon galvanostatisch nach zwei Methoden bestimmt: in Hydrochinonlösung mit einfachen Impulsen, in Chinonlösung als Reaktionsprodukt mit einer Folge von kathodischen und anodischen Impuls. Auf entsprechende Weise wurde die Adsorption des Chinons untersucht.

Zur Kontrolle dienten potentiostatische Messungen an Hydrochinonlösungen. Die Adsorption des Chinons liess sich potentiostatisch nicht messen, da sich das Ruhepotential infolge einer Korrosionsreaktion mit der Elektrode nicht stabil einstellte.

Die Messergebnisse mit einfachen Impulsen sind in den Abb. 10 und 11 dargestellt. Die Zunahme von $i\sqrt{\tau}$ mit i deutet auf Adsorption hin. Die Extrapolation für $i\rightarrow0$ liefert den Grenzfall reiner Diffusion (Gleichung (2) mit $y=1$) und gestattet, den Diffusionskoeffizienten zu bestimmen. Es ergibt sich für den benutzten Elektrolyten und $c<7\cdot10^{-3}$ M, D(Hydrochinon) $=0.59\cdot10^{-5}$ cm^2/sec, D(Chinon) $=0.68\cdot10^{-5}$ cm^2/sec.

In den konzentrierteren Hydrochinonlösungen steigt $i(\tau^{\frac{1}{2}})$ bei sinkenden Stromdichten wieder an. Dies kann nur auf einer langsamen Folgereaktion des

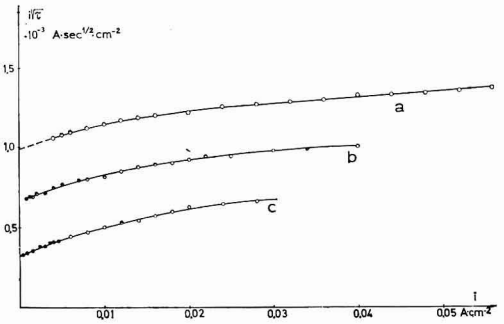

Abb. 11. Chronopotentiometrische Messungen mit einfachen Impulsen in Chinonlösungen. Parameter: Chinonkonzentration; Grundelektrolyt: siehe Abb. 10. Konzentration ($M \cdot 10^3$): (a) 2.11; (b) 1.41; (c) 0.685.

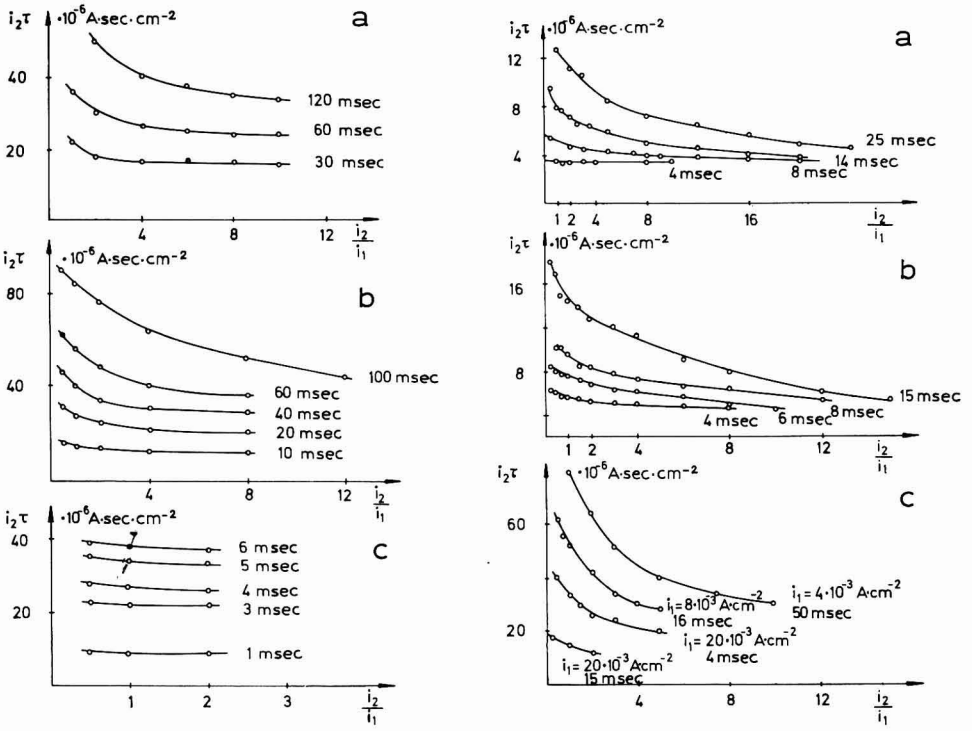

Abb. 12. Chronopotentiometrische Messungen mit Stromumkehr in Chinonlösung verschiedener Konzentration c^0 zur Untersuchung der Adsorption von Hydrochinon bei verschiedenen Stromdichten i_1 und Zeiten t_1. Grundelektrolyt: siehe Abb. 10. (a) $i_1 = 10^{-3}$ A cm^{-2}, $c_0 = 0.7 \cdot 10^{-3}$ M; (b) $i_1 = 2 \cdot 10^{-3}$ R cm^{-2}, $c_0 = 1.4 \cdot 10^{-3}$ M; (c) $i_1 = 10^{-2}$ A cm^{-2}, $c_0 = 1.4 \cdot 10^{-3}$ M. Parameter: t_1.

Abb. 13. Chronopotentiometrische Messungen mit Stromumkehr in Hydrochinonlösungen verschiedener Konzentration c^0 zur Untersuchung der Adsorption von Chinon bei verschiedenen Stromdichten i_1 und Zeiten t_1. Grundelektrolyt: siehe Abb. 10. (a), $i_1 = 10^{-3}$ A cm^{-2}, $c_0 = 2.6 \cdot 10^{-3}$ M; (b) $i_1 = 2 \cdot 10^{-3}$ A cm^{-2}, $c_0 = 3 \cdot 10^{-3}$ M; (c) $c_0 = 2 \cdot 10^{-3}$ M. Parameter: t_1; bei (c) t_1 und i_1.

Primärprodukts beruhen, die oxydierbare Substanzen nachliefert. Da die Grenzwerte von $i(\tau^{\frac{1}{2}})$ für $i=0$ nach Gleichung (2) zu berechnen sind, lassen sich die Messwerte leicht korrigieren (gestrichelte Kurven in Abb. 10).

Die Messergebnisse mit Stromumkehr sind in den Abb. 12 und 13 wiedergegeben. Es wurde die Darstellung $i_2\tau$ gegen $b=|i_2/i_1|$ mit i_1 und t_1 als Parameter gewählt. Bei gegebener Konzentration des Ausgangsstoffes bedeutet Konstantes i_1t_1 für jede Kurve einen festen Wert für die Adsorption des Reaktionsproduktes.

Zu jedem Messpunkt der Abb. 10–13 gehört ein bestimmtes Γ. Die Interpretation der Messungen gemäss Abschnitt 2 liefert aber nicht Γ, sondern nur Grenzen, innerhalb deren es liegen muss. Der so gefundene Bereich von Γ hängt von der zur Messung verwendeten Stromdichte ab. Er lässt sich daher noch etwas schärfer durch den Maximalwert der Näherung, die kleine Γ liefert, und den Minimalwert der Näherung, die grosse Γ liefert, einschränken.

Die so gewonnenen Bereiche sind als Striche in den Adsorptionsisothermen der Abb. 14 und 15 eingezeichnet. Dabei gelten die senkrechten Striche für die Adsorption der Substanz als Ausgangsstoff, die schrägen für die Adsorption als Reaktionsprodukt. Die Striche liegen im letzteren Fall schräg, weil die durch i_1t_1 gegebene Strommenge des ersten Impulses je nach der Methode zu jedem Γ auch ein $c(x=0, t=t_1)$ liefert, wobei zu einem grösseren Γ ein kleineres c gehört und umgekehrt.

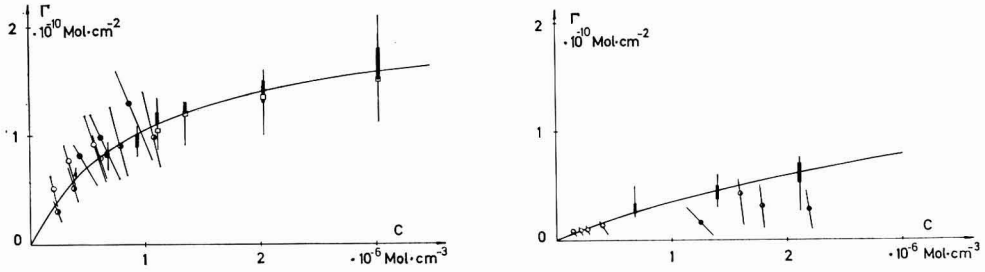

Abb. 14–15. Adsorptionsisothermen von Hydrochinon (14) und Chinon (15) an Hg bei 25° in einer Lösung von 0.1 M KNO_3, 0.05 M KH_2PO_4 und 0.05 M Na_2HPO_4 (pH 6.7). Senkrechte Striche: Messung mit einfachen Impulsen; stark ausgezogen: Berücksichtigung der kinetischen Korrektur; schräge Striche: Messung mit Stromumkehr. Kreise: Messwerte nach Modell 7: Abb. 14. (○), $i_1 = 1$; (◑), $i_1 = 2$; (●), $i_1 = 10$ mA cm^{-2}; (□), chronocoulometrische Messung. Abb. 15. (○), $i_1 = 2$; (⊙), $i_1 = 4$; (◑), $i_1 = 8$; (●), $i_1 = 20$ mA cm^{-2}. Ausgezogen: nach Langmuir berechnete, den Messwerten angepasste Kurve.

In Abb. 14 sind gleichzeitig als Quadrate die Resultate der potentiostatischen Messungen eingetragen. Diese Versuche liessen sich nicht auf kleine Konzentrationen ausdehnen, da sich hier keine zur Ausschaltung der Durchtrittsüberspannung ausreichenden Potentialsprünge herstellen lassen, ohne dass Korrosion der Elektrode einsetzt.

5. DISKUSSION

(a) *Genauere Bestimmung der Adsorptionsisotherme mit einer kinetischen Korrektur*

Geht man vom Adsorptionsgleichgewicht des Ausgangsstoffes aus, wie bei den Messungen mit einfachen Impulsen, so braucht keine Adsorptionsverdrängung

berücksichtigt zu werden und man kann die Isotherme mit einer kinetischen Korrektur recht genau gewinnen.

Wie bereits in Abschnitt 2 diskutiert, hängt das jeweils geeignete Modell für den Konzentrationsverlauf von Γ während des Impulses von der Adsorptionskinetik ab. Solange die Adsorptionsgeschwindigkeit gross gegenüber der Geschwindigkeit der Elektrodenreaktion ist, bleibt das Adsorptionsgleichgewicht eingestellt.

In diesem Fall ist $\Gamma(c)$ unabhängig von der Stromdichte. Da mit wachsender Stromdichte der aus der Diffusionsschicht entladene Anteil der Substanz gegenüber dem aus der Adsorptionsschicht stammenden zurücktritt, müssen sich alle $\Gamma(i)$-Kurven einander nähern und dem wahren Wert $\Gamma(t=0)$ anschmiegen.

Wenn jedoch die Entladungsgeschwindigkeit mit der Adsorptionsgeschwindigkeit vergleichbar wird, sinkt $\Gamma(c)$ um $\Delta\Gamma$ unter den Gleichgewichtswert. Ein übersichtlicher Ansatz für das Verhalten von $\Delta\Gamma(c)$ während des Impulses lässt sich unter der Annahme gewinnen, dass während eines Zeitintervalls τ' unmittelbar nach dem Einschalten des Stroms ein der Stromdichte proportionaler Teil $i\tau'$ der Adsorptionsschicht entsprechend Modell 1 (Abschnitt 2a) abgebaut wird und der Rest dann genähert nach einem der Modelle 1–4 (vgl. Abb. 4) verschwindet, als ob keine kinetische Hemmung vorläge.

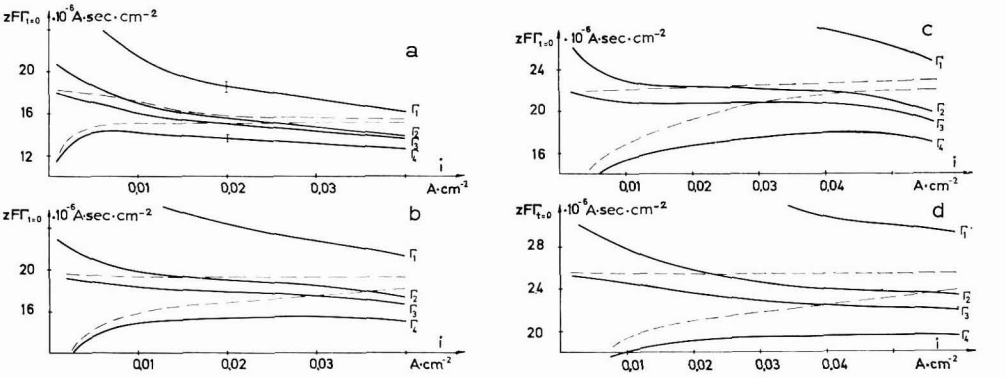

Abb. 16. Ausgezogen: nach Modell 1–4 berechnete Werte von $zF\Gamma$ für Hydrochinon als Funktion der Stromdichte i für vier der in Abb. 10 wiedergegebenen Messkurven bei verschiedenen Konzentrationen c_0 (mit Fehlerbreite). c_0 ($\cdot 10^3$ M): (a) 0.40; (b) 0.68; (c) 0.93; (d) 1.11. Gestrichelt: mit kinetischer Korrektur $\tau'=0.3$ ms aus den Werten Γ_3 und Γ_4 berechnetes Γ_3' und Γ_4'.

Bei grösserer Stromdichte wird also Modell 1 eine immer bessere, Modell 4 eine immer schlechtere Näherung. Daraus folgt, dass bei wachsender Stromdichte der wahre Wert von $\Gamma(t=0)$ früher durch Γ_1 dargestellt werden muss, als ohne Einfluss der Kinetik, während sich Γ_4 ihm langsamer nähern oder wieder von ihm entfernen sollte. Wie Abb. 16 am Beispiel des Hydrochinons zeigt, trifft dies tatsächlich zu. Der wahre Wert von $\Gamma(t=0)$ muss unabhängig von der Stromdichte sein und zwischen Γ_1 und Γ_4 liegen. Da Γ_4 ein Maximum besitzt, entfernt sich der nach diesem Modell berechnete Wert bei hohen Stromdichten vom richtigen.

Um den Einfluss der Adsorptionskinetik auf die Auswertung wenigstens näherungsweise auch quantitativ zu berücksichtigen, kann man die Verfahren 2–4 gemäss der zuvor geschilderten Annahme über den Zeitverlauf von Γ abändern. Dazu verkleinert man die Transitionszeit von τ um τ' und berechnet die verbleibende

Adsorptionsschicht mit der neuen Transitionszeit τ–τ' nach Verfahren 2–4. τ' wird solange variiert, bis die korrigierte Grösse Γ_4' gerade monoton ansteigt und gleichzeitig Γ_2' und Γ_3' noch kein Minimum aufweisen. Die Γ'-Werte sind für jede Stromdichte die Summe aus $zFi\tau'$ und dem für τ–τ' nach Methode 2–4 berechneten Adsorptionswert. Die Resultate für Γ_3' und Γ_4' sind in Abb. 16 gestrichelt wiedergegeben, und sie erlauben eine wesentlich genauere Eingrenzung von $\Gamma(t=0)$ als mit den unkorrigierten Modellen 1–4.

Der so erhaltene Bereich ist in Abb. 14 und 15 mir breiten senkrechten Strichen eingetragen*. Die ausgezogenen Kurven sind den so erhaltenen Werten angepasste Langmuir-Isothermen der Form:

$$\Gamma=\Gamma_\infty c/(k_D/k_A+c) \tag{16}$$

mit den in Tab. 1 wiedergegebenen Konstanten Γ_∞ und k_D/k_A. Die Werte für Γ_∞ stimmen innerhalb der Fehlergrenze mit Werten überein, die LORENZ UND GAUNITZ[14] aus Impedanzmessungen erhalten haben.

TABELLE 1

KONSTANTEN DER ADSORPTIONSISOTHERMEN FÜR HYDROCHINON UND CHINON AN QUECKSILBER BEI 25°

	Hydrochinon	*Chinon*
Γ_∞ galvanostatisch, ohne kinet. Korrektur (Mole/cm²)	$1.7\ldots2.7\cdot10^{-10}$	$>0.8\cdot10^{-10}$
Γ_∞ galvanostatisch, mit kinet. Korrektur (Mole/cm²)	$2.1\cdot10^{-10}$	$2.4\cdot10^{-10}$
Γ_∞ aus Impedanzmessung[15] (Mole/cm²)	$2.8\pm0.4\cdot10^{-10}$	
k_D/k_A galvanostatisch, mit kinet. Korrektur (Mole/cm³)	$1.0\cdot10^{-6}$	$4.7\cdot10^{-6}$

(*b*) *Bestimmung der kinetischen Konstanten aus der Relaxationszeit* τ'

Die mit einfachen Stromimpulsen für Hydrochinon (H) und Chinon (Q) gefundenen Relaxationszeiten τ'_H und τ'_Q können dazu dienen, Geschwindigkeitskonstanten der Adsorption und Desorption abzuschätzen.

Dazu wird angenommen, dass unter Stromfluss folgende Gleichungen für die Adsorptionsgeschwindigkeit gelten:

$$d\Gamma_H/dt=k_{AH}c_H(\Gamma_\infty-\Gamma_H-\Gamma_Q)-k_{DH}\Gamma_H-i/zF \tag{17}$$

$$d\Gamma_Q/dt=k_{AQ}c_Q(\Gamma_\infty-\Gamma_H-\Gamma_Q)-k_{DQ}\Gamma_Q+i/zF \tag{18}$$

Hier und im folgenden bedeutet c die Konzentration vor der Adsorptionsschicht ($c(x=0)$).

Der Flächenbedarf $1/\Gamma_\infty$ für oxydierte und reduzierte Form ist als gleich angenommen. Im folgenden wird nur der Fall des Hydrochinons diskutiert, da die Resultate sich auf Chinon unmittelbar übertragen lassen.

* Dabei ist der in der Adsorption enthaltene Anteil an Doppelschichtaufladung CU/zF (vgl. Gleichung (1)) abgezogen; er wurde aus der Doppelschichtkapazität der depolarisatorfreien Lösung und dem Potentialanstieg von *ca.* 0.1 V zwischen den zur Bestimmung von τ dienenden Punkten der $U(t)$-Kurve zu $0.11\cdot10^{-10}$ Mole/cm² bestimmt. Abbildungen 14 und 15 geben also Γ^* (Gleichung (1)) wieder.

Gemäss dem in Abschnitt 2a beschriebenen Modell liegt bei Versuchsbeginn Adsorptionsgleichgewicht mit $i=0$, $\Gamma_H=\Gamma^0_H$ und $c_Q=0$, $c_H=c^0_H$ $\Gamma_Q=0$ vor:

$$0=k_{AH}c_H\,(\Gamma_\infty-\Gamma_H{}^0)-k_{DH}\Gamma_H{}^0 \tag{19}$$

Nach Einschalten des Stroms stellt sich innerhalb von τ' ein quasistationärer Zustand ein, bei dem Γ^0_H um $\Delta\Gamma=i\tau'_H/zF$ auf Γ'_H vermindert wird, während c_H und c_Q noch ihre Anfangswerte beibehalten. Dann wird aus (17) und (18) zum Zeitpunkt τ'

$$0=k_{AH}c^0_H(\Gamma_\infty-\Gamma'_H-\Gamma_Q)-k_{DH}\Gamma'_H-i/zF \tag{20}$$

$$0=-k_{DQ}\Gamma_Q+i/zF \tag{21}$$

Aus (19) bis (21) lassen sich Γ_∞ und Γ_Q eliminieren und man erhält:

$$\tau'_H=\frac{zF\Delta\Gamma}{i}=\frac{zF(\Gamma^0_H-\Gamma'_H)}{i}=\frac{1}{k_{DH}}\cdot\frac{k_{DQ}{}^{-1}+(k_{AH}c^0_H)^{-1}}{k_{DH}{}^{-1}+(k_Ac^0_H)^{-1}} \tag{22}$$

Eine entsprechende Gleichung gilt für τ'_Q.

Es sollte also möglich sein, aus der Konzentrationsabhängigkeit von τ'_H und τ'_Q die vier Geschwindigkeitskonstanten zu berechnen. Abbildung 16 zeigt jedoch unmittelbar, dass mit wachsender Konzentration die Genauigkeit, mit der τ'_H bestimmt werden kann, stark abnimmt. Die gestrichelten Kurven Γ'_3 und Γ'_4 konnten alle mit dem gleichen $\tau'_H=3\cdot10^{-4}$ sec gewonnen werden. Die Konzentrationsabhängigkeit von τ'_H geht also in der Fehlerbreite unter. Dies ist bei τ'_Q noch stärker der Fall. Zur Abschätzung der Geschwindigkeitskonstanten wurden daher nur die Relaxationszeiten für die kleinsten Konzentrationen benutzt und das aus der Isotherme genauer zugängliche Verhältnis k_D/k_A hinzugezogen. Die Resultate sind in Tab. 2 wiedergegeben. Die Adsorptionsgeschwindigkeiten beider Substanzen sind innerhalb der Fehlergrenzen der Methode gleich, dagegen ist die Desorptionsgeschwindigkeit des Chinons grösser.

TABELLE 2

KINETISCHE KONSTANTEN FÜR DIE ADSORPTION VON HYDROCHINON UND CHINON AN QUECKSILBER BEI 25°

Substanz	*Relax. Zeit* τ' *(sec)*	*Bestimmt bei c = (Mole/cm³)*	k_D *(sec⁻¹)*	k_Ac *(sec⁻¹)*
Hydrochinon	$3\pm0.3\cdot10^{-4}$	$0.4\cdot10^{-6}$	$2.8\cdot10^3$	$1.1\cdot10^3$
Chinon	$2\pm0.5\cdot10^{-4}$	$0.68\cdot10^{-6}$	$6.7\cdot10^3$	$1.0\cdot10^3$

Die Ergebnisse können nur die Grössenordnung der Geschwindigkeitskonstanten wiedergeben. Bereits die Bestimmung von Γ beruht nur auf einer Korrektur mit Hilfe der für reine Diffusion gültigen Transitionszeiten. Um τ' zu gewinnen, müssen die Messungen bis zu möglichst hohen Stromdichten und kurzen Transitionszeiten ausgedehnt werden. Es gelang zwar, Zeiten von 10^{-4} sec bei Versuchen in gleicher Lösung innerhalb von 10% zu reproduzieren, doch beeinflusst in diesem Bereich die gewählte graphische Bestimmungsmethode der Transitionszeit das Ergebnis bereits stärker als ihre Messungenauigkeit.

Eine weit grössere Unsicherheit liegt jedoch in dem für die Berechnung der

Adsorptionskinetik benutzten Ansatz, nach dem die kinetisch bedingte Abweichung von der Gleichgewichtskonzentration sich durch einen konstanten Zeitparameter τ' ausdrücken lässt. In Wirklichkeit sollte jedoch zumindest bei hohen Stromdichten die Relaxationszeit absinken, also τ' auch von i abhängen.

Der kinetische Ansatz verlangt ferner, dass die Adsorptionsschicht im Grenzfall nach Modell 1 (Abschnitt 2a) abgebaut wird. Dies setzt voraus, dass der Depolarisator zwar bevorzugt im adsorbierten Zustand entladen wird, aber auch aus der Diffusionsschicht heraus noch einen genügenden Austauschstrom besitzt. Wenn nämlich jedes Molekül nur in einem besonderen Adsorptionszustand entladen werden kann, würde ein Potentialsprung stets bei $\Gamma'=0$ auftreten, und es hinge von der kinetischen Hemmung ab, wie gross die Konzentration vor der Oberfläche zu diesem Zeitpunkt noch ist. Mit wachsender Stromdichte würde die bei $t=\tau$ verbleibende Konzentration wachsen und die kinetische Korrektur müsste nicht durch $\Delta\Gamma(i)$ sondern durch ein $\Delta c(i)$ vorgenommen werden*.

Die Form der Potential–Zeitkurven am System Hydrochinon/Chinon ist mit der genannten Vorstellung zu vereinbaren. Dagegen ist beim Durochinon (2,3,5,6-Methylchinon) der Unterschied der Austauschströme aus Adsorptionsschicht und Diffusionsschicht so gross, dass zwei Transitionszeiten messbar werden (Abb. 17). Für die erste Transitionszeit gilt $i\tau_1=$const.; beim Durochinon muss also die Adsorptionsgeschwindigkeit noch geringer sein, als beim Chinon**.

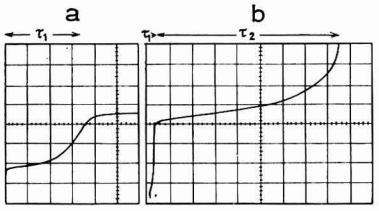

Abb. 17. Potential–Zeitverlauf galvanostatischer Einzelimpulse in $3\cdot10^{-3}$ *M* Durochinonlösung (Grundelektrolyt: je 50 Vol.% Wasser und Aceton, 0.1 *M* KNO_3, 0.05 *M* KH_2PO_4, 0.05 *M* Na_2HPO_4). (a), Impulsbeginn: Abzisse $2\cdot10^{-3}$ sec/cm; Ordinate 0.1 V/cm; i = 40 mA/cm². (b), gesamter Impuls: Abzisse $100\cdot10^{-3}$ sec/cm; Ordinate 0.1 V/cm; i = 32 mA/cm².

Bisher wurden Adsorptionsgeschwindigkeiten nur durch Impedanzmessungen an polarisierbaren Elektroden bestimmt[15]. So untersuchten LORENZ UND GAUNITZ[14] auch die Adsorption des Hydrochinons an der Hg-Elektrode bei Potentialen von 1.6–0.4 V unterhalb des Normalpotentials und gaben die Desorptionsfrequenz mit *ca.* 10^5 sec^{-1} an.

Die grosse Diskrepanz zwischen diesem und dem hier gefundenen Wert lässt sich kaum durch die Unsicherheit der Methoden erklären. Es ist daher anzunehmen, dass die beiden Verfahren einen verschiedenen Zustand als Adsorption erfassen: bei der chronopotentiometrischen Methode werden die Moleküle als adsorbiert bezeichnet,

* Eine solche Korrektur führt auf die gleiche Grössenordnung von k_A (vgl. ref. 10).

** Eine Korrosion des Quecksilbers durch Durochinon zu einer monomolekularen Oxydschicht ist auszuschliessen, da das Normalpotential des Durochinons um 0.46 V unter dem der HgO-Elektrode liegt. Es muss also der Depolarisator an der Oberflächensubstanz beteiligt sein, was von einer Adsorption nicht zu unterscheiden ist.

die bevorzugt entladen werden; Impedanzmessungen erfassen Ladungsverschiebungen in der Doppelschicht, wobei ein besonderer Ordnungszustand nicht notwendig mit erfasst wird. Jedenfalls zeigen die Messungen an Durochinon, dass langsame Adsorption durchaus vorkommt*.

(c) *Adsorption von Reaktionsprodukten und Adsorptionsverdrängung*

Benutzt man für die Adsorption eines Stoffes als Reaktionsprodukt die gleichen Methoden zur Eingrenzung der Resultate nach Modell 5–8 wie bei seiner Adsorption als Ausgangsstoff gemäss Modell 1–4, so überdecken die erhaltenen Werte den gleichen Bereich (vgl. Abb. 14 und 15). Da im Fall der Adsorption von Reaktionsprodukten ausser kinetischer Hemmung auch Adsorptionsverdrängung eine Rolle spielen muss, lässt sich die Interpretation der Messungen nicht wie vorher durch eine kinetische Korrektur weiter einengen.

Im Gleichgewichtsfall gilt für die Adsorption von Hydrochinon in Gegenwart von Chinon (wenn Γ_∞ für beide Stoffe gleich gesetzt wird):

$$\frac{\Gamma_H}{\Gamma_\infty} = \frac{c_H}{c_H + k_{DH}/k_{AH} + c_Q \cdot (k_{DH}/k_{AH}) \cdot (k_{AQ}/k_{DQ})} \tag{23}$$

In Gegenwart von Chinon muss also Γ_H stets unterhalb der Adsorptionsisotherme des reinen Hydrochinons liegen.

Da die Diffusionskoeffizienten beider Stoffe ähnlich sind, gilt genähert $c_H + c_Q = c^0$ und man erhält bei gleicher Adsorbierbarkeit, also $k_{DH}/k_{AH} = k_{DQ}/k_{AQ}$ eine lineare Isotherme. Auf jeden Fall weicht die Gleichgewichtsisotherme bei Adsorptionsverdrängung weniger von einer Geraden ab, als wenn nur ein Stoff vorhanden ist. Dann gewinnt Modell 7, das unter den diskutierten Modellen bereits einen mittleren Wert ergab, an Gewicht. Die nach ihm berechneten $\Gamma_7(t=t_1)$ sind daher in Abb. 14 und 15 (als teilweise oder vollständig ausgefüllte Kreise) besonders gekennzeichnet. Ihre Lage gegenüber der wahren Isotherme (ausgezogene Kurve) lässt sich adsorptionskinetisch verstehen. Jede kinetische Hemmung muss die Adsorption des Reaktionsproduktes während des ersten Impulses zu höheren Werten, während des 2. Impulses zu niedrigeren Werten verschieben. Diese Effekte heben sich jedoch nicht auf, denn bei der Auswertung in den Abb. 14 und 15 war der Einfluss der Stromdichte des zweiten Impulses bereits durch Extrapolation auf hohe Stromdichten korrigiert. Daher resultiert ein zu hoher Wert für Γ. Die Abweichung wird an der Kurve für Hydrochinon (Abb. 14) bei hohen Stromdichten i_1 gerade merklich (ausgefüllte Kreise in Abb. 14).

Bei der Adsorption des Chinons (Abb. 15) ist zunächst die Adsorptionsverdrängung durch das stärker adsorbierbare Hydrochinon zu berücksichtigen, die bei Doppelimpulsen zu Werten unterhalb der ausgezogenen Kurve führt. Es kommt ausserdem noch eine chemische Folgereaktion mit dem Elektrodenmaterial hinzu, bei der ein Reaktionsprodukt entsteht, das bei Stromumkehr nicht mehr vollständig reduziert wird. Die Geschwindigkeit der Folgereaktion steigt mit der Konzentration so stark an, dass die Adsorption mit wachsender Konzentration wieder absinkt (Abb. 15).

Wir danken Herrn Dipl.-Ing. E. SCHMITT (Institut für Nachrichtentechnik

* Es ist bemerkenswert, dass die Messung der Impedanz auch für die Geschwindigkeitskonstante der elektrochemischen Chinonoxydation um Grössenordnungen höhere Werte liefert als die Polarographie[17].

der TH Karlsruhe) für den Entwurf des Impulsgenerators und Herrn G. SCHMEISSER für das Programmieren der Rechnung für Gleichung (12).

ANHANG 1

Zur Berechnung von Γ nach den Modellen 5–8

Wenn $-j=D\left(\frac{\partial c}{\partial x}\right)_{x=0}$ eine beliebige Funktion der Zeit ist, erhält man durch Laplace-Transformation für die Konzentration des Reaktionsprodukts zur Zeit t an der Elektrodenoberfläche[16]

$$c(t) = \frac{1}{(\pi D)^{\frac{1}{2}}} \int_0^t \frac{j(\vartheta)\mathrm{d}\vartheta}{(t-\vartheta)^{\frac{1}{2}}} \tag{24}$$

Bei einer Folge galvanostatischer Rechteckimpulse, von denen der i-te zur Zeit t_i beginnt und sich vom vorhergehenden in der Amplitude um Δj_i unterscheidet, ist demnach $c=0$, wenn für die Gesamtzeit t_n gilt:

$$0 = \sum_{i=0}^{n} \int_{t_i}^{t_n} \frac{\Delta j_i \mathrm{d}\vartheta}{(t_n-\vartheta)^{\frac{1}{2}}} \tag{25}$$

So lässt sich bei Modell 5, 6 und 8 das Integral in mehrere durch die Randbedingungen gegebene Zeitabschnitte zerlegen (Abb. 4). Als zusätzliche Nebenbedingungen treten auf: in Modell 5: $zF\Gamma=i_2\delta_2$, in Modell 6: $zF\Gamma=i_1\delta_1=i_2\delta_2$, in Modell 8: $zF\Gamma=i_1\delta_1$. Für das vierte Intervall der Randbedingung in Modell 8 vgl. ref. 7.

Bei Modell 7 wird ebenfalls das Prinzip der Addition zweier Teilintegrale für $0\ldots t_1+\tau$ und für $t_1\ldots(t_1+\tau)$ verwendet und auf beide die für die Einzelimpulse angegebene Lösung[1] angewendet.

ANHANG 2

Bestimmung des Modells mit grösstem und kleinstem Wert für Γ

Hierzu denkt man sich die Zeitintervalle $z_1F\Gamma/i_1$ und $z_2F\Gamma/i_2$, in denen die Adsorptionsschicht wie in Modell 6 auf- und abgebaut wird, innerhalb der Impulszeiten t_1 bzw. τ beliebig verschoben, z.B. um ϑ_1 und ϑ_2 (in Abb. 4b ist speziell $\vartheta_1=\vartheta_2=0$).

Dann erhält man aus (25):

$$0 = i_1\{(t_1+\tau)^{\frac{1}{2}} - (t_1+\tau-\vartheta_1)^{\frac{1}{2}} + (t_1+\tau-\vartheta_1-z_1F\Gamma/i_1)^{\frac{1}{2}} - \tau^{\frac{1}{2}}\}$$
$$- i_2\{\tau^{\frac{1}{2}} - (\tau-\vartheta_2)^{\frac{1}{2}} + (\tau-\vartheta_2-z_2F\Gamma/i_2)^{\frac{1}{2}}\}$$

Wenn $z_1F\Gamma/i_1=\delta_1 \ll \tau$ und $z_2F\Gamma/i_2=\delta_2 \ll \tau-\vartheta_2$
lassen sich die Wurzeln entwickeln, und man erhält für Γ:

$$zF\Gamma = \frac{2i_1(\tau^{\frac{1}{2}})(1+b-a)}{(\tau-\vartheta_2)^{-\frac{1}{2}} - (t_1+\tau-\vartheta_1)^{-\frac{1}{2}}}$$

Dieser Ausdruck hat seinen Maximalwert für $\vartheta_1 \sim t_1$, $\vartheta_2 \sim 0$, er wird am kleinsten für $\vartheta_1 \sim 0$ und $\vartheta_2 \to \tau_1$.

ZUSAMMENFASSUNG

An der ruhenden Quecksilberelektrode wird die Adsorption von Hydrochinon und von Chinon jeweils als Ausgangsprodukt und als Produkt einer elektrochemischen Umsetzung untersucht. Dies geschieht galvanostatisch durch einzelne Stromimpulse und durch doppelte Impulse mit Stromumkehr, ferner potentiostatisch durch einfache Spannungssprünge.

Zur Auswertung der Messungen mit einfachen Impulsen dienen z.T. bereits von LORENZ aufgestellte Modelle für den Zusammenhang zwischen adsorbierter Menge und Konzentration während des Impulses. Für die Messungen mit doppelten Impulsen werden vier weitere Modelle diskutiert.

Die nach den verschiedenen Modellen für einfache Impulse berechnete Adsorption hängt von der Stromdichte des Impulses ab. Diese Abhängigkeit lässt sich durch eine kinetische Hemmung der Adsorption deuten. Es wird versucht, die Hemmung quantitativ durch eine Relaxationszeit zu erfassen. Diese ermöglicht die Adsorptionsisothermen recht genau zu bestimmen. Ein kinetischer Ansatz, der die Adsorptionsverdrängung berücksichtigt, erlaubt, aus den für Chinon und Hydrochinon ermittelten Relaxationszeiten die Geschwindigkeitskonstanten von Adsorption und Desorption abzuschätzen. Die benutzten Methoden sind auch geeignet, die Adsorption von Zwischen- oder Reaktions-produkten an Elektroden zu untersuchen, jedoch beeinflusst die Wahl des Modells hier die Resultate erheblich.

SUMMARY

The adsorption of hydroquinone and of quinone, both as reactant and as product in an electrochemical process, was investigated at a stationary mercury electrode. This was done galvanostatically, with a single current pulse and with a double pulse with current reversal, as well as potentiostatically with a single potential jump.

In order to evaluate the measurements with single pulses, the model set up by LORENZ for the relation between adsorbed amount and concentration during the pulse, was used in part. For the double pulse measurements, four further models were discussed.

The adsorption calculated from the different models for the single pulse depends on the current density in the pulse. This dependence indicates a kinetic hindrance to the adsorption. An attempt was made to explain this hindrance quantitatively in terms of a relaxation time. This made it possible to determine the adsorption isotherm quite accurately. A kinetic law considering the adsorption displacement allowed the derivation of rate constants for adsorption and desorption from the relaxation times for quinone and hydroquinone. The methods used are also suitable for the investigation of the adsorption of intermediates or reaction products at the electrode, although here the choice of the model considerably affects the results.

LITERATUR

1 W. LORENZ, *Z. Elektrochem.*, 59 (1955) 730.
W. LORENZ UND H. MÜHLBERG, *Z. Elektrochem.*, 59 (1955) 735.

2 W. LORENZ UND F. MÖCKEL, *Z. Elektrochem.*, 60 (1956) 507.
W. LORENZ UND F. MÖCKEL, *Z. Elektrochem.*, 60 (1956) 939.
3 F. G. WILL UND C. A. KNORR, *Z. Elektrochem.*, 64 (1960) 258.
4 J. H. CHRISTIE, G. LAUER UND R. A. OSTERYOUNG, *J. Electroanal. Chem.*, 7 (1964) 60.
5 T. BERZINS UND P. DELAHAY, *J. Am. Chem. Soc.*, 75 (1953) 4205.
6 H. HOFFMANN, *Diplomarbeit*, 1960; W. JAENICKE UND H. HOFFMANN, *Z. Elektrochem.*, 66 (1962) 803.
7 H. B. HERMAN, S. V. TATWADI UND A. J. BARD, *Anal. Chem.*, 35 (1963) 2210.
8 F. C. ANSON, *Anal. Chem.*, 38 (1966) 54.
9 F. C. ANSON, *Anal. Chem.*, 33 (1961) 1123.
10 F. MÖLLERS, Dissertation Erlangen, 1967.
11 C. D. RUSSELL UND I. M. PETERSON, *J. Electroanal. Chem.*, 5 (1963) 467.
12 W. H. REINMUTH, *Anal. Chem.*, 33 (1961) 485.
13 G. SALIÉ UND W. LORENZ, *Z. Elektrochem.*, 68 (1964) 197.
14 W. LORENZ UND U. GAUNITZ, *Collection Czech. Chem. Commun.*, 31 (1966) 1389.
15 W. LORENZ, *Z. Physik. Chem. Leipzig*, 224 (1963) 145.
16 O. DRAČKA, *Collection Czech. Chem. Commun.*, 25 (1960) 338; H. HOFFMANN UND W. JAENICKE, *Z. Elektrochem.*, 66 (1962) 9.
17 J. M. HALE UND R. PARSONS, *Trans. Faraday Soc.*, 59 (1963) 1429; J. R. GALLI UND R. PARSONS, *J. Electroanal. Chem.*, 10 (1965) 245.

ELECTROANALYTICAL CHEMISTRY AND INTERFACIAL ELECTROCHEMISTRY
Elsevier Sequoia S.A., Lausanne – Printed in The Netherlands

A NEW ANALYSIS OF DATA OBTAINED WITH GALVANOSTATIC AND COULOSTATIC SINGLE PULSES

D. J. KOOIJMAN*

Analytical Chemistry Laboratory, State University of Utrecht (The Netherlands)
and
Department of Chemistry, New York University, New York, N. Y. 10003 (U.S.A.)

(Received November 13th, 1967)

INTRODUCTION

A number of relaxation methods have been developed for the study of fast electrode reactions. The most important are the faradaic impedance method, the faradaic rectification method, the potential step, the galvanostatic single step and the coulostatic pulse method. The last three methods are at a disadvantage compared with the faradaic impedance method, in that the explicit functions of $i(t)$ and $\eta(t)$, respectively, are of a cumbersome form because they contain exponential error functions of which the argument is, in many cases, complex. This has two consequences. Firstly, in order to analyze experimental data, one has to simplify the overvoltage–time and the current–time expressions, respectively, by expansion for very short or long electrolysis times. This is definitely not an ideal approach to the problem, as for very short times the reaction is controlled predominantly by the charging process of the double layer, and at very long times the reaction becomes increasingly controlled by diffusion. Secondly, if the kinetic parameters of very fast electrode reactions are to be determined, one should know the double-layer capacitance, C_d, and the diffusion coefficients. The former datum is especially difficult to obtain from experimental data and often is determined by measurements in the absence of the redox couple. Measurements of the double-layer capacitance in the presence of the redox couple should be limited to electrolysis times in the nanosecond range[1], which is nearly impossible, especially if the ohmic resistance is high.

The first objection to the three transient methods can be overcome by using numerical tables, as has been shown by KOOIJMAN AND SLUYTERS[2]. Both C_d and the faradaic impedance can be determined, particularly by the use of the methodology applied by SLUYTERS and coworkers[3,4], the so-called complex plane method. An analogous procedure is proposed here for the potential step, the galvanostatic single step and the coulostatic pulse method by which the three parameters governing the electrode process, *i.e.*, the double-layer capacity, the exchange current and the diffusional parameters, can be calculated from experimental data.

* On leave from the State University of Utrecht.

THEORY

A. The coulostatic pulse method

The explicit voltage–time relation, as derived by DELAHAY[5] and REINMUTH[6] is:

$$\eta(t) = \{\eta_0/(\gamma-\beta)\}[\gamma \exp \beta^2 t \operatorname{erfc} \beta\sqrt{t} - \beta \exp \gamma^2 t \operatorname{erfc} \gamma\sqrt{t}] \quad (1)$$

where η_0 is the overvoltage resulting from the coulostatic charging of the double layer in a very short time; β and γ are given by the relations:

$$\beta+\gamma = \frac{i_0}{nF}\left(\frac{1}{C_O^*\sqrt{D_O}} + \frac{1}{C_R^*\sqrt{D_R}}\right) \quad \text{and} \quad \beta\gamma = \frac{nFi_0}{RTC_d} \quad (2)$$

There i_0 is the apparent exchange current density; C_O^* and C_R^* are the bulk concentrations of the Ox and Red species, respectively; D_O and D_R are the diffusion coefficients; C_d is the double-layer capacitance. The other symbols, n, F, R and T, have their usual meaning.

In an earlier paper[2] we have demonstrated that eqn. (1) can be written in the following implicit form:

$$\eta(t)/\eta_0 = f((\beta+\gamma)^2/\beta\gamma,\ a\sqrt{t}) \quad \text{or} \quad f((\beta+\gamma)^2/\beta\gamma,\ \beta\gamma t) \quad (3)$$

in which

$$a = \beta\gamma/(\beta+\gamma) \quad (4)$$

As a has a dimension of $[\sec^{-\frac{1}{2}}]$ and $(\beta+\gamma)^2/\beta\gamma$ is dimensionless, the function in eqn. (3) depends on dimensionless quantities. The advantage of (3) over (1) is that (3) depends on two variables instead of three in (1).

If at a certain time, t_1, the quantity $\eta(t)/\eta_0$ is known, there is a relation between $(\beta+\gamma)^2/\beta\gamma$ and $a\sqrt{t_1}$ or $\beta\gamma t_1$. Therefore, in principle, these quantities can be determined from the two values of $\eta(t)/\eta_0$ ($\eta_0=\eta$ at $t=0$) at two different electrolysis times. This could be done, for example, by a computer, analyzing a whole series of $\eta(t)/\eta_0$-values at different times by means of (1). This would be a difficult task as three variables, β, γ and t, are involved while β and γ, moreover, are often complex quantities. A much simpler approach to the problem is to use (3) and another independent relationship between $(\beta+\gamma)^2/\beta\gamma$ and $a\sqrt{t}$. For the latter one can use the derivative of $\eta(t)$ with respect to time. One obtains in dimensionless form:

$$(t/\eta_0)(\mathrm{d}\eta/\mathrm{d}t) = g\{(\beta+\gamma)^2/\beta\gamma,\ a\sqrt{t}\} \quad \text{or} \quad g\{(\beta+\gamma)^2/\beta\gamma,\ \beta\gamma t\} \quad (5)$$

The values of $(\beta+\gamma)^2/\beta\gamma$ and $a\sqrt{t}$ or $\beta\gamma t$ can be obtained from both (3) and (5) at one electrolysis time, provided that the functions f and g are tabulated beforehand. This has been done, and Fig. 1 shows the corresponding nomogram. The procedure for obtaining the values of $(\beta+\gamma)^2/\beta\gamma$ and $\beta\gamma t$ from this nomogram is as follows. At a certain time, t_1, one calculates the values of

$$\eta(t_1)/\eta_0 \text{ and } \frac{t_1}{\eta_0}\left(\frac{\mathrm{d}\eta}{\mathrm{d}t}\right)_{t=t_1};$$

the corresponding point in the nomogram yields the values of both $(\beta+\gamma)^2/\beta\gamma$ and $\beta\gamma t$. Logarithmic interpolation between the drawn lines is feasible without appreciable error.

As the electrode process depends on three parameters, *i.e.*, C_d, i_0 and $[1/(C_O^*\sqrt{D_O}) + 1/(C_R^*\sqrt{D_R})]$, one has to find another relationship to solve these three quantities. In fact, the most reasonable choice is to determine separately the diffusional parameter from either polarographic data or from experiments with the

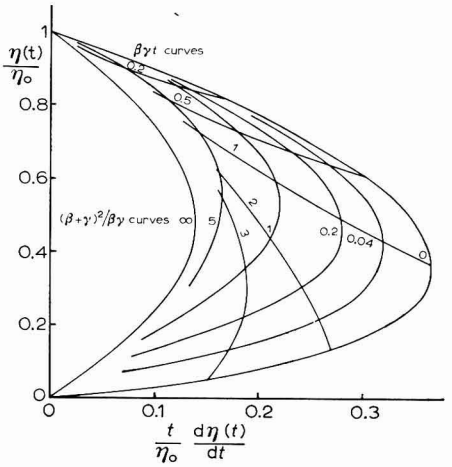

Fig. 1. Plots of $\eta(t)/\eta_0$ *vs.* $t/\eta_0 \times \mathrm{d}\eta(t)/\mathrm{d}t$ for different $(\beta + \gamma)^2/\beta\gamma$-values of an electrode reaction at several values of $\beta\gamma t$ in the coulostatic pulse method. More detailed nomograms can be constructed from available data* (computed on the basis of eqn. (1) by means of tables of probability integrals[12]).

galvanostatic single step method at sufficiently long time. If slow reactions at not too high concentrations are studied, one could also determine C_d from the relation:

$$C_d = q/\eta_0 \tag{6}$$

in which q is the increment in charge density injected to the electrode, being studied at $t = 0$. Note that the above procedure remains valid, even if (6) is not valid, provided experimental data are used at electrolysis times much greater than the finite time during charge injection.

There is much resemblance between this procedure of analyzing coulostatic step measurements and the procedure of analyzing faradaic impedance measurements by the complex plane method. In this method Z', the real component of the cell impedance, is plotted against Z'', the imaginary one. This can be conceptualized in our notation as $Z'/|\vec{Z}|$ against $(1/\omega|\vec{Z}|)(\mathrm{d}Z'/\mathrm{d}t)$, also two dimensionless quantities.

B. The galvanostatic single step method

The voltage–time relation, as derived by BERZINS AND DELAHAY[7] is:

$$\eta(t) = \frac{i}{C_d(\beta-\gamma)}\left[\begin{matrix}(\gamma/\beta^2)(\exp\beta^2 t\ \mathrm{erfc}\ \beta\sqrt{t} + 2\beta\sqrt{t/\pi} - 1) \\ -(\beta/\gamma^2)(\exp\gamma^2 t\ \mathrm{erfc}\ \gamma\sqrt{t} + 2\gamma\sqrt{t/\pi} - 1)\end{matrix}\right] \tag{7}$$

* Deposited as Document 9733 with the ADJ Auxiliary Publications Project, Photoduplication Service, Library of Congress, Washington, D.C. 20540. A copy may be secured by writing the Document number and remitting $3.75 for photoprints or $2.00 for 35 mm microfilm. Advance payment is required. Make check or money order payable to: Chief, Photoduplication Service, Library of Congress.

in which β and γ are defined by (2).

Again, it is possible to write (7) in a dimensionless form:

$$aC_d\eta/i\sqrt{t}=f((\beta+\gamma)^2/\beta\gamma,\ a\sqrt{t}) \tag{8}$$

The left-hand side of this equation depends only on the measurable quantities, η and i, and the diffusional parameter which can be easily determined with this method by measurement at sufficiently long electrolysis times. As was the case with the procedure for the coulostatic pulse method, outlined above, one needs another independent relationship between $a\sqrt{t}$ and $(\beta+\gamma)^2/\beta\gamma$. One can use for this relationship:

$$(t/\eta(t))(\mathrm{d}\eta(t)/\mathrm{d}t)=g\{(\beta+\gamma)^2/\beta\gamma,\ a\sqrt{t}\} \tag{9}$$

The values of $(\beta+\gamma)^2/\beta\gamma$ and $a\sqrt{t}$ can be obtained from (8) and (9) and therefore also the values of i_0 and C_d, since the diffusion parameter can be easily obtained from experiments at long times. Nomograms showing the plot of $^{10}\log(10aC_d\eta/i\sqrt{t})$ against $t/\eta(t)\times \mathrm{d}\eta(t)/\mathrm{d}t$ are given in Fig. 2. Logarithmic interpolation between the lines in Fig. 2 is feasible without appreciable error (a logarithmic scale was used in Fig. 2 solely because of the extended range covered).

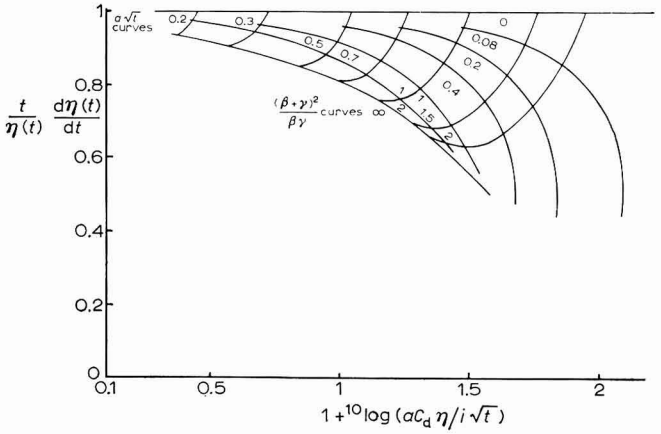

Fig. 2. Plots of $[1+{}^{10}\log(aC_d\eta/i\sqrt{t})]$ *vs.* $t/\eta\times \mathrm{d}\eta/\mathrm{d}t$ for different $(\beta+\gamma)^2/\beta\gamma$-values of an electrode reaction at several values of $a\sqrt{t}$ for the galvanostatic pulse method. More detailed nomograms can be constructed from available data*.

C. Combination of coulostatic pulse method and galvanostatic single step method

In the procedures outlined above, one needs to determine the derivatives of the voltage–time curve. This could be done electronically but such a method is perhaps difficult at very short times. Moreover, the allowed signal ($\eta<5$ mV) is weak. We have obtained satisfactory results by simply drawing the tangent to a point on experimental curves, but the error in this procedure can easily exceed 5%. Therefore we prefer to combine the coulostatic pulse and the galvanostatic single pulse method, that is by combining eqns. (3) and (8). The resulting nomograms are given in Fig. 3.

D. A convenient relation between the galvanostatic single step and the coulostatic pulse method

Equation (7) is in abbreviated form:

$$\eta(t) = iZ_g(t) \tag{10}$$

where Z_g is detèrmined by eqn. (7). The coulostatic pulse method can be conceived as a galvanostatic double pulse method for which the second pulse has zero amplitude while the length of the first pulse is infinitely short:

$$\eta_c(t) = \lim_{\substack{i \to \infty \\ t_1 \to 0}} i(Z_g(t) - Z_g(t-t_1)) \tag{11}$$

By expanding $Z_g(t-t_1)$ in a Taylor series and by noting that $\lim_{\substack{i \to \infty \\ t_1 \to 0}} it_1/C_d = \eta_0$ one obtains:

$$\eta_c(t)/\eta_0 = (C_d/i)(d\eta_g(t)/dt) \tag{12}$$

Equation (12) holds if $Z(t)$ is independent of i, which is the case for an electrode process without complications. This equation provides a convenient way for measuring double-layer capacitance in the presence of electroactive species without knowledge about the other parameters involved in the electrode process.

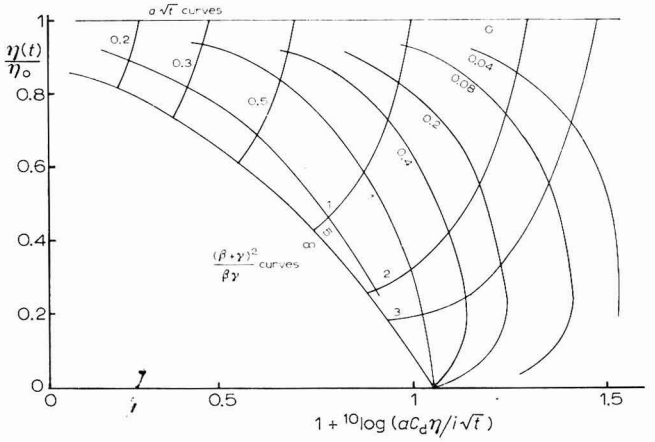

Fig. 3. Plots of $\eta(t)/\eta_0$ obtained with the coulostatic pulse method *vs.* $[1 + {}^{10}\log(aC_d\eta/i\sqrt{t})]$ for the galvanostatic pulse method for different $(\beta + \gamma)^2/\beta\gamma$-values of an electrode reaction at several values of $a\sqrt{t}$. More detailed nomograms can be constructed from available data*.

E. Potential-step method

The current–time equation for this method, as derived by GERISCHER AND VIELSTICH[8] is:

$$i(t) = K \exp \lambda^2 t \operatorname{erfc} \lambda\sqrt{t} \tag{13}$$

in which

$$K = i_0\{\exp[\alpha(nF/RT)\eta] - \exp[-(1-\alpha)(nF/RT)\eta]\} \tag{14a}$$

* See footnote on p. 83.

and

$$\lambda = \frac{i_0}{nF}\left\{\frac{\exp[\alpha(nF/RT)\eta]}{C_R^*\sqrt{D_R}} + \frac{\exp[-(1-\alpha)(nF/RT)\eta]}{C_O^*\sqrt{D_O}}\right\} \quad (14b)$$

As double-layer charging is ignored in the potential-step method, on the assumption of an ideal potentiostat, eqn. (13) is less intricate than (1) or (7). In condensed form:

$$i(t) = f(K,\lambda\sqrt{t}) \quad (15)$$

Again one can write

$$t(\mathrm{d}i/\mathrm{d}t) = g(K,\lambda\sqrt{t}) \quad (16)$$

From (15) and (16), both the kinetic parameter, $i_0 \exp[(\alpha nF/RT)\eta]$, and the diffusional parameter, $[1/(C_R^*\sqrt{D_R}) + \exp\{-(nF/RT)\eta\}/(C_O^*\sqrt{D_O})]$, can be obtained. This is nearly the same method as that proposed by OLDHAM AND OSTERYOUNG[9] to which we refer for nomograms, if only the exchange current density must be obtained. Nomograms based on (15) and (16) should be used if the values of both the kinetic and the diffusional parameters must be calculated.

DISCUSSION

The advantages of the above procedures for analyzing experimental data of the three transient methods, coulostatic pulse, galvanostatic single step and the potential-step method are as follows. Firstly, more reliable values of the exchange current can be obtained and faster electrode reactions can be studied as the whole region of the η–t curve, including the most kinetically useful region, can be analyzed. Secondly, the other parameters, especially the double-layer capacitance, can be obtained from experiments in the presence of the redox couple, so that occurrence of abnormal behavior of the double layer can be observed (see, for example, the $Tl^+/Tl(Hg)$[10] and the Hg^{2+}/Hg[11] electrode reactions). Thirdly, the conditions for charging the double-layer capacitance in the coulostatic pulse method are no longer so severe.

These methods can be compared with the complex plane method of SLUYTERS and coworkers. Faradaic impedance measurements are more accurate than the galvanostatic single pulse and the coulostatic pulse measurements, because the first method needs the oscilloscope only as a zero detector, and because of the use of tuned amplifiers. This advantage, however, will probably be offset by the easy way of compensation of the ohmic drop with the single pulse method and the resulting enhancement of the sensitivity in voltage measurement. We believe that the typical feature of the coulostatic pulse method, *i.e.*, much less interference of the ohmic resistance, enables the study of reactions even faster than can be studied with the faradaic impedance or galvanostatic single pulse methods. We do not see much application of the potential-step methods because of instrumental reasons unless there are special reasons to hold the overvoltage constant.

ACKNOWLEDGEMENT

The author is much indebted to the Office of Naval Research and the Netherland Organization for Scientific Research (Z.W.O.) for the support of this investiga-

tion. The author wishes to thank Professor P. DELAHAY and Dr. J. H. SLUYTERS for their kind interest in this work.

SUMMARY

Methods of analyzing experimental data from coulostatic and galvanostatic pulse measurements are given, by which it is possible to determine the three parameters involved in the electrode process, *i.e.*, double-layer capacity, kinetic and diffusional parameters, in the presence of the electroactive species. This method does not require such a stringent condition for the charging of the double layer in the coulostatic pulse method, as previous methods of analysis of data.

REFERENCES

1 A. D. GRAVES, C. J. HILLS AND D. INMAN, *Adv. Electrochem. Electrochem. Eng.*, Vol. 4, edited by P. DELAHAY, Interscience–Wiley, New York, 1966, p. 166.
2 D. J. KOOIJMAN AND J. H. SLUYTERS, *Electrochim. Acta*, in press.
3 M. SLUYTERS-REHBACH AND J. H. SLUYTERS, *Rec. Trav. Chim.*, 82 (1965) 525.
4 M. SLUYTERS-REHBACH, D. J. KOOIJMAN AND J. H. SLUYTERS, *Polarography 1964*, edited by G. J. HILLS, McMillan, London, 1966, p. 135.
5 P. DELAHAY, *J. Phys. Chem.*, 66 (1962) 2208.
6 W. H. REINMUTH, *Anal. Chem.*, 34 (1962) 1272.
7 T. BERZINS AND P. DELAHAY, *J. Am. Chem. Soc.*, 77 (1955) 6448.
8 H. GERISCHER AND W. VIELSTICH, *Z. Physik. Chem., N.F.*, 3 (1954) 16.
9 K. B. OLDHAM AND R. A. OSTERYOUNG, *J. Electroanal. Chem.*, 11 (1966) 397.
10 M. SLUYTERS-REHBACH, B. TIMMER AND J. H. SLUYTERS, *Rec. Trav. Chim.*, 82 (1963) 553.
11 M. SLUYTERS-REHBACH AND J. H. SLUYTERS, *Rec. Trav. Chim.*, 83 (1964) 985.
12 V. N. FADDEYEVA AND N. M. TERENT'EV, *Tables of the Probability Integral for Complex Argument*, Eng. ed., Pergamon Press, Oxford, 1961.

ELECTROANALYTICAL CHEMISTRY AND INTERFACIAL ELECTROCHEMISTRY
Elsevier Sequoia S.A., Lausanne – Printed in The Netherlands

A RECALCULATION OF THE IODINE FARADAY*

A. J. ZIELEN
Chemistry Division, Argonne National Laboratory, Argonne, Ill., 60439 (U.S.A.)
(Received November 16th, 1967; in revised form, January 22nd, 1968)

Precision determinations of the faraday were made early in the century with both the silver[1] and iodine[2] coulometers. Unfortunately, the results were found to differ by about 0.02%; many years passed before the consensus of atomic constant data finally established, in 1955, that the iodine faraday was the more reliable value[3]. In 1960, a redetermination of the faraday, made with remarkable care with an improved silver coulometer, was completed at the National Bureau of Standards (NBS)[4]. The major systematic error in the old determination was apparently eliminated in the new result by changing from silver deposition to dissolution. The new silver faraday has eclipsed the older work to the point where the iodine faraday was dropped by COHEN AND DUMOND[5] as an input datum in the latest (1963) adjustment of the atomic constants. The rejection was perhaps also based on the fact that the two faraday values still differ by a disturbing 40 p.p.m.

This neglect of the only independent, high-precision verification of the faraday seems a great waste. Moreover, an examination of the old data has indicated that perhaps the best use has not been made of the available information. The initial determination and subsequent recalculations of the iodine faraday have always been indirect, depending on the old and erroneous silver deposition coulometer for measurement of the total coulombs passed. BATES AND VINAL[2] also determined the total coulombs, in six of their ten runs, by maintaining constant cell current and measuring the voltage drop across a standard resistance. If the results of these so-called "absolute" experiments are used exclusively to calculate the iodine faraday, the mean value is found to be in excellent agreement (3 p.p.m.) with the new silver faraday.

The new value of the iodine faraday so obtained is presented below along with an up-to-date revision of all other precision determinations of the faraday. Recalculations of the oxalate[6] and electromagnetic[7] values are included. Also, the last published value of the iodine faraday, which was used in the 1952 and 1955 adjustments of the fundamental constants, is not related in any obvious fashion to the value given in the original paper. DUMOND AND COHEN[8] list it as a private communication with no details other than to credit the result to a 1949 recalculation of the old data by VINAL and a 1951 revision by HIPPLE. The probable sequence of the Vinal–Hipple calculation is presented and revised anew with the latest atomic weight of iodine. The results are summarized in Table 1.

* Based on work performed under the auspices of the U.S. Atomic Energy Commission.

TABLE 1

VALUES OF THE FARADAY

Method	*F (C g equiv.$^{-1}$)*	*Weight*
Silver (dissolution)	96,486.82±0.66	100
Iodine (new)	96,486.5±2.3	8.2
Iodine (old)	96,490.7±1.9	0
Oxalate	96,481.6±3	0
Electromagnetic	96,487.6±1.3	25.8
Weighted mean	96,486.95±0.57	134.0
Best 1963 value[5]	96,487.0±0.5	

SUMMARY OF CALCULATIONS

Silver (dissolution) faraday

COHEN AND DUMOND[5] obtained this result after a complete reworking of the original data. Their faraday value differs very little from the 96487.2 C given in the latest NBS revision[9], but the uncertainty estimate is almost 4-fold less than the 2.4 C listed in the first report[4].

Iodine (new) faraday

Runs 3, 4, 6, 8, 10, and 11 of the original paper[2] are the experiments that include the total coulombs passed as determined by a standard cell and resistor. Seventeen iodine coulometer measurements were made in these six runs, but the two belonging to run 3 were dropped because of the admitted experimental difficulties. The mean electrochemical equivalent of iodine was then calculated to be 1.315255±0.000031 mg/absolute C, where the ± is the external consistency estimate of σ divided by $\sqrt{15}$. The international units of the original data were converted on the basis of one U.S. international = 0.999835 absolute C[10]. The quotient of the latest (1961) atomic weight of iodine, 126.9044 ± 0.0005, and the electrochemical equivalent gives the faraday value listed in Table 1.

The above calculation abandons the weights assigned by BATES AND VINAL[2] to the individual runs. To be valid for the present use, the original weights would have to be corrected by removing the error contribution of the silver coulometer and adding another one corresponding to the unsteadiness of the cell current. This information is not available, and the unweighted average remains as the best alternative. Actually, the use of the mean value can be further justified. The only run of exceptionally low weight, 3, was rejected, and the relatively high weights assigned to runs 10 and 11 should be decreased somewhat, because they were the only runs where difficulty was encountered in maintaining constant cell current. Thus, even if a more sophisticated calculation were possible, the final result would probably not differ significantly from the simple mean of the five runs. However, for the sake of completeness, retention of doubtful run 3 would lower the iodine faraday by 1.0 C, and the use of the original weights for all six runs would raise the listed value by 2.2 C.

Iodine (old) faraday

ROSA, VINAL AND MCDANIEL[11] present a good discussion of the ambiguity that

resulted from the initial international system definitions of the ampere and ohm and the value assigned eventually to the volt. BATES AND VINAL[2] originally used the defined or silver ampere, but subsequent recalculations of their data have been based on the volt and ohm units maintained by the NBS. Thus, the Vinal–Hipple value[8] of the iodine faraday (physical scale) can be obtained as follows:

$$F = \frac{(126.91)(1.000275)(0.8501759)(0.999835)}{(0.001118)(1.0182684/1.0183)} = 96521.5 \qquad (1)$$

The numerator terms in order are: the 1951 atomic weight of iodine; conversion factor to physical scale; weighted mean of silver/iodine ratio, runs 2–11 with weights as assigned; absolute C conversion factor. The denominator terms are: the 1908 defined ampere as grams of deposited silver/second, and a correction ratio consisting of the observed and 1910 assigned value of the 20° e.m.f. of the Weston normal cell. The mean observed e.m.f. value can be computed readily from the 211 silver coulometer runs in the third and final NBS series[11].

The faraday result listed in Table 1 is obtained from (1) after substitution of the 1961 atomic weight of iodine. The uncertainty value is the one obtained by VINAL; it is probably based on an internal consistency estimate, since the Ag/I ratio alone would contribute 2.7 C to the external consistency value.

Oxalate faraday

The 1953 value[6] has been revised on the basis of 133.9995 for the ^{12}C scale molecular weight of $Na_2C_2O_4$ as compared to the previous value of 134.014. The faraday so obtained appears to be too low by about twice the estimated error and probably should be rejected. Previous comment on this work has held the results suspect because of the sequential trend of the data[10]. The NBS has apparently abandoned this project.

Electromagnetic faraday

An elegant means of obtaining the faraday is by the relation[7]:

$$F = m_p \gamma (\mu_p/\mu_N)^{-1} \qquad (2)$$

where m_p is the proton rest mass, γ the gyromagnetic ratio of the proton, and μ_p/μ_N the proton magnetic moment in nuclear magnetons. The symbols are taken from COHEN AND DUMOND[5].

HUGGINS AND SANDERS[12] have presented a convenient listing of the six precision determinations of γ made to date, and, of more importance, they have normalized the results on the basis of the most recent international comparison of electrical standards and the latest evaluation of the absolute ampere. However, it was necessary to correct the listed γ-values for sample diamagnetism. The corrections of 28.1 and 28.4 p.p.m. used by THOMAS[13] and CAPPTULLER[14], respectively, for their mineral oil samples were retained. The remaining four determinations were all made with water samples, and a correction of 26.2 p.p.m. was used[13]. Weighting as the inverse square of the listed uncertainties[12], the weighted mean result was $\gamma = 26752.05 \pm 0.13$ rad sec^{-1} gauss^{-1}. The $\pm$ value is the combined result obtained from 3.1 p.p.m. external consistency and an estimated 4 p.p.m. for the absolute ampere evaluation[12].

A larger uncertainty is involved in the proton magnetic moment where a total

of five accurate determinations is available. The results fall into two distinct groups, unfortunately indicating a systematic error. The low values are: 2.79276 ± 0.00006[15], 2.79275 ± 0.00010[16], and 2.79277 ± 0.00005[17] with a weighted mean of 2.792764 ± 0.000036 nuclear magnetons. And the two high values are: 2.79290 ± 0.00006[18] and 2.792863 ± 0.00002[19] with a weighted mean of 2.792867 ± 0.000019 nuclear magnetons. It was necessary to apply a diamagnetic correction only to the last determination[19], and again the 26.2 p.p.m. water value was used. The $\pm$ values for each mean were obtained by internal consistency, since this gave the larger error estimate.

Selection of the "best" or more probable of the two proton moments can only be on the basis of external evidence. In this case, the low group must be the choice, since it computes to better agreement with all electrochemical determinations of the faraday except the suspect oxalate value. Similar reasoning led COHEN AND DUMOND[5] to reject the high proton moment but without the added support of the new iodine faraday value.

For the proton rest mass, the 0.08 p.p.m. accurate value of 1.00727663 atomic mass units[5] was used. Substituting the selected results in (2) gives the values of Table 1. If the high proton magnetic moment had been the choice, the electromagnetic faraday would be decreased by 3.5 C.

Final best values

The weights assigned in Table 1 are, after rejection of the doubtful values, in proportion to the inverse square of the listed uncertainties. The final, weighted mean differs very little from the 1963 best value mainly because of the overpowering weight assigned to the silver faraday in both computations. However, the important point is that for the first time the silver and iodine determinations of the faraday are in accord; together they supply the only evidence for selecting the final best value of the proton magnetic moment.

REFERENCES

1 E. B. ROSA AND G. W. VINAL, *Bull. Bur. Std.*, 13 (1916-17) 479.
2 S. J. BATES AND G. W. VINAL, *J. Am. Chem. Soc.*, 36 (1914) 916.
3 E. R. COHEN, J. W. M. DUMOND, T. W. LAYTON AND J. S. ROLLETT, *Rev. Mod. Phys.*, 27 (1955) 363.
4 D. N. CRAIG, J. I. HOFFMAN, C. A. LAW AND W. J. HAMER, *J. Res. Nat. Bur. Std., A.*, 64 (1960) 381.
5 E. R. COHEN AND J. W. M. DUMOND, *Rev. Mod. Phys.*, 37 (1965) 537.
6 D. N. CRAIG AND J. I. HOFFMAN, *Nat. Bur. Std. (U.S.), Circ.*, 524 (1953) 13.
7 J. A. HIPPLE, H. SOMMER AND H. A. THOMAS, *Phys. Rev.*, 76 (1949) 1877.
8 J. W. M. DUMOND AND E. R. COHEN, *Rev. Mod. Phys.*, 25 (1953) 691.
9 W. J. HAMER AND D. N. CRAIG, *J. Electrochem. Soc.*, 111 (1964) 1434.
10 E. R. COHEN, K. M. CROWE AND J. W. M. DUMOND, *The Fundamental Constants of Physics*, Interscience Publishers, Inc., New York, 1957, pp. 9–11, 26–27.
11 E. B. ROSA, G. W. VINAL AND A. S. MCDANIEL, *Bull. Bur. Std.*, 10 (1914) 475.
12 R. W. HUGGINS AND J. H. SANDERS, *Proc. Phys. Soc. London*, 86 (1965) 53.
13 H. A. THOMAS, *Phys. Rev.*, 80 (1950) 901.
14 H. CAPPTULLER, *Z. Instrumentenk.*, 69 (1961) 191.
15 H. SOMMERS, H. A. THOMAS AND J. A. HIPPLE, *Phys. Rev.*, 82 (1951) 697.
16 K. R. TRIGGER, *Bull. Am. Phys. Soc.*, 1 (1956) 220
17 J. H. SANDERS AND K. C. TURBERFIELD, *Proc. Roy. Soc. London, Ser. A*, 272 (1963) 79.
18 H. S. BOYNE AND P. A. FRANKEN, *Phys. Rev.*, 123 (1961) 242.
19 B. A. MAMYRIN AND A. A. FRANTSUZOV, *Zh. Eksperim.i Teor. Fiz.*, 48 (1965) 416; *Soviet Phys. JETP (English Transl.)*, 21 (1965) 274.

ELECTROANALYTICAL CHEMISTRY AND INTERFACIAL ELECTROCHEMISTRY
Elsevier Sequoia S.A., Lausanne – Printed in The Netherlands

ON THE IMPEDANCE OF GALVANIC CELLS

XXIII. ELECTRODE REACTIONS WITH SPECIFIC ADSORPTION OF THE ELECTROACTIVE SPECIES; THE Pb^{2+}/Pb(Hg) ELECTRODE IN M KNO_3–KCl MIXTURES*

B. TIMMER, M. SLUYTERS-REHBACH AND J. H. SLUYTERS
Laboratory for Analytical Chemistry, State University of Utrecht (The Netherlands)
(Received October 19th, 1967)

INTRODUCTION

The investigation of cell impedances is suitable for the study of adsorption of electroactive species at the electrode–solution interface. The concentrations of the electroactive species, and thus their adsorption, vary strongly in the potential region where a peak is observed in an a.c. polarogram. Consequently, the impedance in the peak region contains much information about the adsorption of reactants.

In recent papers[1,2] we have shown that the electrode impedance can be analysed, even in the case where adsorption of reactants has complicated the impedance so that the classical circuit[4] is invalid. For the systems Pb^{2+}/Pb(Hg) in 1 M KCl, and In^{3+}/In(Hg) in 1 M KCNS, it was found that the cell impedances are rather complex, owing to the specific adsorption of lead and indium. It appeared that the measured impedances could be analysed according to several equations, obtained from different theories. In our opinion, the equations derived by REINMUTH[2,19] have the soundest theoretical foundation for reversible electrode systems. His equations are based on the idea of coupling between charging and faradaic processes, as introduced by DELAHAY[3]. In this paper a critical discussion of the different theoretical equations will be presented.

From the equations derived by REINMUTH[2,19] it can be deduced that the classical Randles circuit[4] follows if the electroactive species are not too strongly adsorbed at the interface. This is the case, for example, for the quinhydrone[5] and the thallium couple[2,6] (see also ref. 7 and our comment on that paper[8]).

Further experimental data are presented here for the lead system. The Pb^{2+}/Pb(Hg) reaction has been measured in M KNO_3–KCl mixtures. It is known that lead is specifically adsorbed at the electrode–solution interface from KCl solutions[1,9], whereas no adsorption can be detected from M KNO_3 solutions. It must be expected, therefore, that the specific adsorption of lead increases with KCl concentration. Simultaneously, the measured impedances should change from the classical Randles circuit[4] (with an increasing enhancement of the double-layer capacitance) to the circuit based on REINMUTH's equations. The indium system will be treated more extensively in a following paper.

* Abstracted from B. TIMMER, Thesis, State University of Utrecht, 1968.

THEORY

In recent years a number of theories has been presented for electrode systems with adsorption of reactants. Usually some assumptions about the reaction mechanism are made in order to simplify the equations. SENDA AND DELAHAY[10] assumed that charge transfer can take place only between adsorbed species, and not between species in solution. BATICLE AND PERDU[7] have presented a method for analysing impedance data according to the theory given by SENDA AND DELAHAY. However, the first step of the proposed method is the determination of the double-layer capacitance by extrapolation of Y_{el}''/ω to infinite frequency (Y_{el}'' is the imaginary component of the electrode admittance, Y_{el}). This procedure will not be feasible in many cases because the contribution of the adsorption impedance to Y_{el}'' will still be too large at the highest frequencies that are attainable experimentally[8] and the analysis procedures proposed by BATICLE AND PERDU are thus only of limited importance.

A main objection against the theory of SENDA AND DELAHAY is the fact, that the essential concept of the coupling between faradaic and double-layer charging processes[3] has not been considered in their theory, so that the resulting expressions for the impedance should be used only as an approximation. DELAHAY[11] has published the first theoretical expressions for the cell impedance using his new concept. We have given analysis procedures according to these new expressions[1] and it has been shown that both the lead system[1] in 1 *M* KCl and the indium system[2] in 1 *M* KCNS can be analysed according to them. However, objections have been raised against these expressions[2,12] and they should not be used for analysing impedance data. Subsequently, HOLUB *et al.*[13] presented more refined expressions for the cell impedance of a non-ideal reversible system. Unfortunately, the resulting equations are so complicated that it seems impossible to use them for analysing impedance data and it seems worthwhile therefore to introduce some simplifications.

REINMUTH[19] assumed that the electrode reaction is reversible and derived expressions for the electrode admittance, Y_{el}, for the metal ion–amalgam electrode reactions or reactions with both electroactive species soluble in solution, using Laplace transformations. The results can be represented as follows[2] (*cf.* Appendix):

$$Y_{el}' = 1/2\sigma\omega^{-\frac{1}{2}} + \omega(C_{LF} - C_{HF}) \cdot u/(u^2 + 2u + 2) \tag{1a}$$

$$Y_{el}'' = 1/2\sigma\omega^{-\frac{1}{2}} + \omega(C_{LF} - C_{HF}) \cdot (u + 2)/(u^2 + 2u + 2) + \omega C_{HF} \tag{1b}$$

where Y_{el}' and Y_{el}'' are the real and imaginary components of Y_{el}, σ is the Warburg coefficient, ω the angular a.c. frequency and

$$C_{HF} = (\partial q^*/\partial E)_{\Gamma^*};\ u = u'\sqrt{\omega} = (2\omega)^{\frac{1}{2}}(\partial \Gamma^*/\partial \psi)_E \text{ and}$$

$$C_{LF} = \left(\frac{\partial q^*}{\partial E}\right)_{\psi} - nF\frac{\sigma_R}{\sigma}\left(\frac{\partial \Gamma^*}{\partial E}\right)_{\psi} \tag{1c}$$

with $q^* = q + nF\Gamma_O$; $\Gamma^* = \Gamma_O + \Gamma_R$; $\psi = C_O\sqrt{D_O} + C_R\sqrt{D_R}$ and $\sigma_R/\sigma = [1 + \exp(-\varphi)]^{-1}$, where C_O and C_R are the surface concentrations, $\varphi = nF(E - E_{\frac{1}{2}})/RT$ and σ_R is the Warburg coefficient pertaining to the R-component. In our opinion, eqns. (1) are the best expressions for the electrode admittance so far available for electrode systems with adsorption of reactants, and only they will be used in this paper for analysing

experimental impedance data. The restriction of reversibility is of minor importance, because so far all systems with reactant adsorption have been found to be reversible.

For reversible metal ion–metal electrodes with reactant adsorption, one has[2]

$$Y_{el}' = 1/2\sigma\omega^{-\frac{1}{2}} \tag{2a}$$

$$Y_{el}'' = 1/2\sigma\omega^{-\frac{1}{2}} + \omega(dq^*/dE) \tag{2b}$$

It can be seen from eqns. (1) and (2) that only the thermodynamic[2] quantities q^* and Γ^* may be obtained from Y_{el}-values, whereas derivatives of Γ_O, Γ_R and q cannot be obtained separately. The equivalent circuit for electrode systems with reactant adsorption, based on eqn. (1), is given in Fig. 1. At high and low frequencies, capacitances C_{HF} and C_{LF} will be found parallel to a Warburg-like impedance.

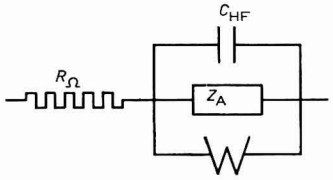

Fig. 1. Equivalent circuit, based on eqns. (1).

$C_{HF} = (\partial q^*/\partial E)_{\Gamma^*}$; $W = \sigma\omega^{-\frac{1}{2}}(1-j)$ and

$$Z_A = \left(\frac{\partial\Gamma^*}{\partial\psi}\right)_E \cdot \frac{1-j}{\sqrt{2\omega}(C_{LF}-C_{HF})} - \frac{j}{\omega(C_{LF}-C_{HF})}$$

In principle, equations for Y_{el} based on the concept of the coupling between faradaic and double-layer charging processes, should always be used instead of the classical equations. However, in practice the new equations are of importance only if there is strong potential-dependent specific adsorption of reactants. For only in that case are the three expressions given by DELAHAY[3] for electrode processes without *a priori* separation of charging and faradaic currents, significantly different from the classical flux equations, because the $d\Gamma/dt$ terms are then not negligible with respect to the diffusion flux terms of the reactants. This may also be seen if, for example, eqns. (1) are considered for electrode systems with no, or weak, adsorption of reactants. Then the $d\Gamma^*/dE$- and $d\Gamma^*/d\psi$-terms, and thus $C_{LF}-C_{HF}$ and u, are small, so that for no reactant adsorption, ($\Gamma^* \approx 0$), eqns. (1) become equal to the classical Y_{el} expressions. The classical expressions result also for weak adsorption with, however, C_{LF} instead of the double-layer capacitance, $dq/dE = C_d$, parallel with the faradaic impedance. Thus, the more convenient classical equations and Randles' circuit are limiting cases for electrode systems with no, or weak, reactant adsorption and they may be used for such systems without introducing large errors.

Some controversy might arise about the definition of the Randles' circuit. Usually, the double-layer capacitance, $dq/dE = C_d$, for the supporting electrolyte is introduced in the circuit. However, for weak reactant adsorption formally the same circuit is valid with a capacitance value, C_{LF}, different from the double-layer capacitance, C_d, for the supporting electrolyte. For such cases also the name, *Randles' circuit*, will be used, because experimentally no distinction can be made between

the two if the data are analysed with the complex plane method[1,14]. It should be noted that after analysis of the impedance data, one should be cautious with the interpretation. If at certain electrode potentials a capacitance value is found larger than the C_d-value for the supporting electrolyte, it can be interpreted in two ways; it may be either an increased genuine $C_d = dq/dE$, or the additional capacitive component introduced in the faradaic impedance by adsorption of the reactants is significant (*cf.* eqn. (1c)). The latter is the case for the thallium system at potentials near $E_{\frac{1}{2}}$, which we have interpreted erroneously earlier[6].

PROCEDURES FOR ANALYSING IMPEDANCE DATA

From the series resistance, R_S, and capacitance, C_S, as measured with the a.c. bridge, the components of the cell impedance are calculated with $Z' \triangleq AR_S$ and $Z'' = A/\omega C_S$ where A is the surface area of the electrode. Then, the ohmic resistance, R_Ω of the cell is determined, either by extrapolation of Z' to infinite frequency or from the value of Z' at potentials where the faradaic impedance is infinite. Y_{el}' and Y_{el}'' are computed from $Y_{el}' = (Z' - R_\Omega)/[(Z' - R_\Omega)^2 + (Z'')^2]$ and $Y_{el}'' = Z''/[(Z' - R_\Omega)^2 + (Z'')^2]$. The basic idea of the complex plane method is that Y_{el}' is first investigated. The following cases may be envisaged[16].

(P1) No reactant adsorption

This case has been dealt with extensively[14,15]. The frequency-dependence of $Y_{el}'/\sqrt{\omega}$ is investigated. If $Y_{el}'/\sqrt{\omega}$ is found constant, the system behaves reversibly with $Y_{el}'/\sqrt{\omega} = 1/2\sigma$. If $Y_{el}'/\sqrt{\omega}$ *decreases* with frequency, σ and the charge transfer resistance, θ, can be evaluated from this frequency-dependence[15]. The θ and σ evaluated as a function of potential should be in accordance with classical theory. Once θ and σ are known, C_d can be computed from Y_{el}'' with $\omega C_d = Y_{el}'' - Y_{el}'/(p+1)$ with $p = \theta/\sigma\omega^{-\frac{1}{2}}$. If C_d is found frequency-independent and equal to the C_d-value for the supporting electrolyte alone at all potentials, it can be concluded that no adsorption of reactants is present and that the classical theory and the Randles' circuit for the cell impedance are applicable.

(P2) Weak reactant adsorption

If the capacitance value evaluated from Y_{el}'' as outlined under (P1) is found frequency-independent, but at some potentials different from the C_d-value for the supporting electrolyte, it can be inferred that weak reactant adsorption is present. In that case C_{LF} has been found. Note that the reaction should be reversible or $Y_{el}'/\sqrt{\omega} = 1/2\sigma$, because otherwise eqns. (1) are not applicable. Thus $Y_{el}'/\sqrt{\omega}$ should be found constant with frequency, and the evaluated σ-values as a function of potential should obey[15]:

$$\sigma = \sigma_m \cosh^2 \tfrac{1}{2}\varphi \tag{3a}$$

with

$$\sigma_m = 4RT/n^2F^2\sqrt{2}(C_O^*\sqrt{D_O} + C_R^*\sqrt{D_R}) \tag{3b}$$

where $\varphi = nF(E - E_{\frac{1}{2}})/RT$ and C^* is the bulk concentration. If, also, frequency-independent capacitances, C_{LF}, are evaluated, it can be concluded that weak reactant

adsorption is present. The adsorption has altered only the capacitance value and not the Randles circuit. The value of C_{HF} and u' cannot be evaluated in this case.

(P3) Strong reactant adsorption

An *increase* of $Y_{el}'/\sqrt{\omega}$ with frequency is found for systems with probable strong reactant adsorption[1,2]. This increase cannot be analysed with the Randles' circuit, because that circuit can explain only constant or decreasing $Y_{el}'/\sqrt{\omega}$-values. It can be tried out to analyse the impedance data according to eqns. (1).

In principle, the four parameters, σ, u', C_{LF} and C_{HF}, can be calculated from the admittance, measured at two frequencies. In practice, the calculation is rather involved and inaccurate results will be obtained. More reliable results may be expected if a whole series of experimental data at different frequencies is analysed at the same time. First of all, σ should be evaluated as a function of potential because the σ-terms in eqns. (1) usually predominate. Values of σ may be obtained by calculation from known diffusion coefficients with eqn. (3), where $E_{\frac{1}{4}}$ is found from d.c. polarograms or from experimental σ-values at potentials away from $E_{\frac{1}{4}}$. Another possibility is to make plots of $Y_{el}'/\sqrt{\omega}$ *vs.* ω. For small u-values, eqn. (1a) reduces to:

$$Y_{el}'/\sqrt{\omega} \approx 1/2\sigma + (C_{LF} - C_{HF})u'\omega \tag{4}$$

The intercept of the plot at $\omega = 0$ yields, therefore, the value of $1/2\sigma$. The latter procedure is feasible only for systems with not too strong adsorption. An estimated value of $(C_{LF} - C_{HF})u'$ may also be obtained from the plot. Further, for small u-values (*cf.* eqn. (1b))

$$C_{rev} \equiv (Y_{el}'' - Y_{el}')/\omega \approx C_{LF} - (C_{LF} - C_{HF})u'\sqrt{\omega} \tag{5}$$

The plot of C_{rev} *vs.* $\sqrt{\omega}$ will yield C_{LF} and also $(C_{LF} - C_{HF})$ u'-values. If it is assumed that $C_{HF} = C_d$ for the supporting electrolyte, u' can be found. It should be noted that the plots according to eqns. (4) and (5), give accurate results for potentials near $E_{\frac{1}{4}}$ only if u is small, *i.e.*, for systems with not too strong adsorption of reactants.

Once σ is known, the general procedure is as follows. Equation (1a) can be rewritten as:

$$(Y_{el}'/\omega - 1/2\sigma\sqrt{\omega}) \cdot (u^2 + 2u + 2)/u = C_{LF} - C_{HF}$$

For several u'-values, $C_{LF} - C_{HF}$ is calculated from the Y_{el}'-values obtained from the measured impedance data at different frequencies. The best u'-value is chosen, such that the least spread is found in $C_{LF} - C_{HF}$ over the whole frequency range. With the u'- and $C_{LF} - C_{HF}$-values thus found, C_{HF}-values are computed from Y_{el}'' with eqn. (1b). The results should be frequency-independent within experimental error. It can be concluded that eqns. (1) and the circuit of Fig. 1 are applicable if one set of frequency-independent σ-, u'-, C_{LF}- and C_{HF}-values yields theoretical Y_{el}'- and Y_{el}''-values, calculated from eqns. (1), that agree within experimental error with the experimental values over the whole frequency range. The whole procedure can be repeated for all electrode potentials in the peak region, so that u', C_{LF} and C_{HF} are found as a function of potential.

It should be remembered that only *reversible* electrode systems with specific adsorption of reactants have been considered with the adsorption in equilibrium with the concentrations just outside the diffuse double layer. So far, no systems with specific adsorption have been studied that did not obey these conditions. However,

it could be possible that a system is measured the impedance data of which cannot be analysed according to the procedures described in this section. In that case a more refined theoretical derivation should be developed.

For a reversible metal ion–metal electrode with strong adsorption of reactants, eqns. (2) are applicable. These expressions fit with a Randles' circuit with a capacitance different from C_d for the supporting electrolyte alone. Experimental data for such systems can be analysed therefore as outlined in (P2) and the more involved procedures of (P3) need not be followed.

If diffusion polarization predominates, eqns. (1) reduce to the classical equations, $Y_{el}'/\sqrt{\omega} = 1/2\sigma$ and $Y_{el}'' - Y_{el}' = \omega C_{LF}$. Therefore, impedance data for potentials not too close to $E_{\frac{1}{4}}$, directly yield σ and C_{LF}; for these potentials, u' and C_{HF} cannot be determined. The σ-values obtained at these potentials may be used for obtaining $E_{\frac{1}{4}}$- and σ_m-values with eqns. (3), thus providing another way for calculating theoretical σ-values over the whole peak potential range, besides the possibilities already given in section (P3).

EXPERIMENTS AND RESULTS

All impedance measurements were performed in the usual way[1,2,15] with a DME (knock-off time, 3.6 sec). Solutions were prepared from reagent-grade chemicals and acidified to pH 2 with 0.1 N HNO_3. All potentials are referred to the SCE. The measurements were performed at 25°. Cell impedances for 0.5 mM Pb^{2+} in $(1-x)M$ $KNO_3 + xM$ KCl mixtures ($x = 0$, 0.2, 0.4, 0.6, 0.8 and 1.0) were measured as a function of electrode potential and of frequency (320–2000 Hz). Much higher frequencies cannot be used because of the inaccuracy of Y_{el}' at these frequencies ($Z' \approx R_\Omega$); at low frequencies the balancing of the bridge becomes difficult. The ohmic resistance of the cell was evaluated by extrapolation of Z' to infinite frequency and the components of the electrode admittance, Y_{el}' and Y_{el}'', were computed as indicated.

First Y_{el}' is examined[1,16]. It appears that up to $x = 0.4$, the frequency-dependence of Y_{el}' in the peak potential region, $|E - E_{\frac{1}{4}}| < 50$ mV, is in accordance with the classical faradaic impedance theory[14,15], $Y_{el}'/\sqrt{\omega}$ being constant. The potential-dependence of the Warburg coefficient, σ, calculated from $Y_{el}'/\sqrt{\omega} = 1/2\sigma$, obeys eqns. (3). Therefore, no influence on Y_{el}' by reactant adsorption, if at all present, is found (*cf.* sections (P1) and (P2)) and the systems behave completely reversibly. In Table 1, the peak potential, $E_{\frac{1}{4}}$- and σ_m-values are given. The values of the capacitance parallel with Z_F, calculated with $C_{rev} = (Y_{el}'' - Y_{el}')/\omega$ were found to be independent

TABLE 1

DATA OF THE LEAD SYSTEM IN $(1-x)$ M KNO_3 + x M KCl MIXTURES

x	$-E_{\frac{1}{4}}$ (mV)	σ_m ($\Omega cm^2\ sec^{-\frac{1}{2}}$)	u' ($sec^{\frac{1}{2}}$)	$\Gamma_o^* \cdot 10^{12}$ (mole/cm²)
0	402	125±3		0
0.2	410	125±2		2.7±0.6
0.4	417	121±3		6.3±0.8
0.6	422	120±4	$\sim 4 \cdot 10^{-3}$	12±2
0.8	428	119±5	$\sim 6 \cdot 10^{-3}$	24±5
1.0	433	113±10	0.01–0.02	45±10

of frequency, so that it can be concluded that the cell impedance is described fully by the classical Randles' circuit for solutions with $x \leqslant 0.4$.

For $x=0$ (1 M KNO_3) the double-layer capacitance values obtained in the presence of 0.5 mM Pb^{2+} are equal to the C_d-values for the supporting electrolyte alone (*cf.* (P1)). For increasing KCl concentrations, however, the capacitance increases for solutions with 0.5 mM Pb^{2+} at potentials near $E_{\frac{1}{2}}$, see Fig. 2a. This indicates that lead is not specifically adsorbed at the interface from 1 M KNO_3 solutions and that adsorption becomes increasingly significant for solutions with increasing KCl concentrations (*cf.* section (P2)).

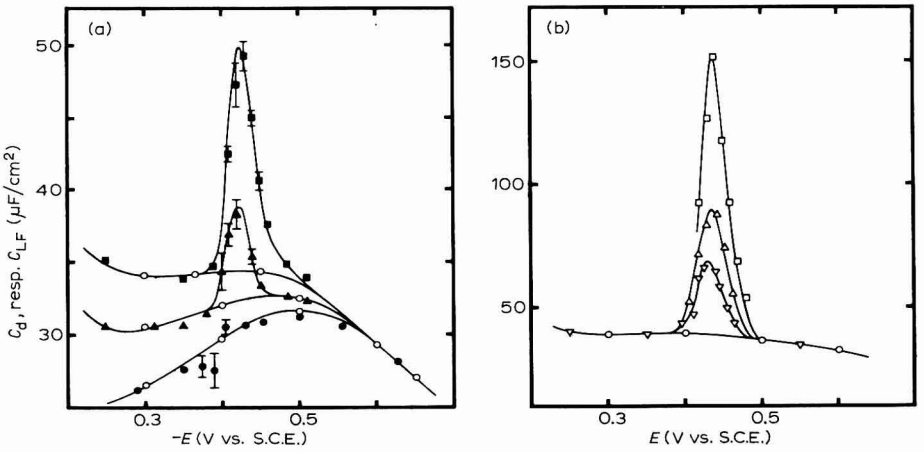

Fig. 2. The double-layer capacitance as a function of potential for $(1-x)$ M KNO_3 + x M KCl mixtures with and without 0.5 mM Pb^{2+}. (○), C_d-values for supporting electrolyte; C_{LF}-values for solns. + 0.5 mM Pb^{2+} with $C_{LF} = (Y_{el}'' - Y_{el}')/\omega$ for x-values: (●), 0; (▲), 0.2; (■), 0.4; and C_{LF}-values, evaluated as indicated in the text for x-values: (▽), 0.6; (△), 0.8; (□), 1.0.

For solutions with $x \geqslant 0.6$, the reactant adsorption is so extensive that it exerts an increasing influence not only on the enhancement of the C_{LF}-values but also on the contribution of the reactant adsorption to Y_{el}' (*cf.* (P3)). Therefore the frequency-dependence of Y_{el}' will deviate more and more from the classical theory for solutions with $x \geqslant 0.6$. This was found experimentally: for $x=0.6$ there is a slight *increase* of $Y_{el}'/\sqrt{\omega}$ with frequency at certain potentials; for $x=1.0$ (1 M KCl) this increase is substantial (note that some irreversibility of the electrode reaction would cause a *decrease* of $Y_{el}'/\sqrt{\omega}$ with frequency). Simultaneously, the calculated capacitance values from $C_{rev}=(Y_{el}''-Y_{el}')/\omega$ are no longer frequency-independent.

The impedance data for solutions with $x \geqslant 0.6$ have been analysed according to eqns. (1) and (P3). The procedures (P3) are valid only for reversible systems. We have found that the lead system in M KNO_3–KCl mixtures with $C_{KCl} < 0.5$ M is reversible. BARKER[9] has shown with the faradaic rectification method that the lead system behaves reversibly in 1 M KCl. Therefore, there is no indication that the lead electrode reaction would not behave reversibly for M KNO_3–KCl mixtures with $C_{KCl} > 0.5$ M. Moreover, it is likely that a decrease of $Y_{el}'/\sqrt{\omega}$ with frequency would have been found in that case.

For $x=0.6$ and 0.8, the effect of reactant adsorption is still small enough, so

that plots according to eqns. (4) and (5) yield accurate results. The σ-values obtained from the $Y_{el}'/\sqrt{\omega}$ *vs.* ω plots for various electrode potentials obeyed eqn. (3a) for both $x=0.6$ and $x=0.8$. The C_{LF}-values obtained from plots according to eqn. (5) are shown in Fig. 2b. It is not possible to obtain accurate C_{HF}- or u'-values for $x=0.6$ and 0.8, because of the rather small deviation from classical theory. An estimate of u' may be obtained as follows. If it is assumed that $C_{HF}=C_d$ for the supporting electrolyte alone (reasonable for not too strong adsorption) one can calculate u' from the $(C_{LF}-C_{HF})$ u'-values obtained from the slopes of the plot according to eqns. (4) and (5). The value, $3\cdot10^{-3}<u'<5\cdot10^{-3}$ sec$^{\frac{1}{2}}$ was found for $x=0.6$ and $4\cdot10^{-3}<u'<7\cdot10^{-3}$ sec$^{\frac{1}{2}}$ for $x=0.8$.

Finally, for $x=1.0$ (1 *M* KCl) the adsorption of lead is so strong that plots according to eqns. (4) and (5) for potentials near $E_{\frac{1}{2}}$ are no longer feasible. Therefore, the general procedure (P3) has been followed for 0.5 m*M* Pb^{2+} in 1 *M* KCl. For potentials further away from $E_{\frac{1}{2}}$, 20 mV$<|E-E_{\frac{1}{2}}|<$50 mV, σ could be evaluated with sufficient accuracy from plots according to eqn. (4). From these σ-values, $E_{\frac{1}{2}}$ and σ_m were calculated with eqn. (3), *cf.* Table 1. The analysis was then performed for the whole peak potential region as described in (P3) with theoretical σ-values calculated with $\sigma_m=120$ Ωcm^2 sec$^{-\frac{1}{2}}$ and $E_{\frac{1}{2}}=-433$ mV. It appeared that the procedures could be followed for all potentials and a good agreement was found between experimental data and eqns. (1). The results are presented in Fig. 2b and Table 2. As can be seen, the increase of the capacitance is substantial for 0.5 m*M* Pb^{2+} in *M* KCl, indicating strong specific adsorption of lead at the interface.

TABLE 2

ADMITTANCE PARAMETERS FOR 0.5 m*M* Pb^{2+} IN 1 *M* KCl

$-E$ (*mV*)	σ_{exp} ($\Omega cm^2\ sec^{-\frac{1}{2}}$)	σ_{calc} ($\Omega cm^2\ sec^{-\frac{1}{2}}$)	C_{LF} ($\mu F/cm^2$)	C_{HF} ($\mu F/cm^2$)	u' ($sec^{\frac{1}{2}}$)
390	830±50	890	40±2		
400	405±20	440	42±2		
410	220±15	235	55±5		
420	135±20	152	90±10	40±10	0.02—0.03
430	105±20	121	125±15	45±10	0.02—0.03
440	110±20	129	150±15	40±20	0.01—0.02
450	175±15	185	115±10	60±20	0.01—0.02
460	300±10	330	90±10	50±15	0.01—0.02
470	575±50	625	65±10		
480	1150±100	1290	49±1		

σ_{calc} is calculated from eqn. (3) with $E_{\frac{1}{2}}=-433$ mV and $\sigma_m=120$ Ω cm^2 sec$^{-\frac{1}{2}}$.

DISCUSSION

From the experimental results it can be concluded that the specific adsorption of lead increases continuously with KCl concentration. Simultaneously, the measured cell impedances were found to change from the classical Randles' circuit (with increasing capacitance values) to the circuit of Fig. 1. This indicates that the Randles' circuit is indeed a limiting case of the more general circuit of Fig. 1, when the reactants are not too strongly adsorbed at the interface, as was argued in the theoretical part. The different procedures proposed in this paper, were shown to be applicable, according as the adsorption increased.

The increase of the capacitance, C_{LF}, for 0.5 mM Pb^{2+} solutions may not be interpreted as an increase of dq/dE alone, as eqn. (1c) shows. The potential-dependence of C_{LF} may be explained as follows[2]. If it is assumed that a linear isotherm holds for the adsorption of O (reasonable for low concentrations), *i.e.*, $\Gamma_O = kC_O$, and that $\Gamma_R = 0$, it follows from eqn. (1c) that

$$C_{LF} - \left(\frac{\partial q}{\partial E}\right)_\psi = nF\frac{\sigma_O}{\sigma}\left(\frac{\partial \Gamma_O}{\partial E}\right)_\psi \qquad (6)$$

If the potential-dependence of the adsorption is mainly determined by the potential dependence of C_O, *i.e.*,

$$1/k \cdot dk/dE \ll 1/C_O \cdot dC_O/dE$$

it follows from eqn. (6) together with $\sigma_O/\sigma = [1+\exp\varphi]^{-1}$ and $C_O^*/C_O = 1+\exp(-\varphi)$,

$$C_{LF} - \left(\frac{\partial q}{\partial E}\right)_\psi = \frac{n^2F^2}{RT}\frac{\exp\varphi}{(1+\exp\varphi)^3}\Gamma_O^* \qquad (7)$$

where $\Gamma_O^* = kC_O^*$. As $(dq/dE)_\psi$ is not known, it is assumed that $(dq/dE)_\psi$ is not significantly different from C_d for the supporting electrolyte at that potential. This will not introduce large errors, because in general dq/dE does not vary much with reactant concentration if the adsorption is not too strong. Note that C_{HF} in Table 2 is equal to C_d for the supporting electrolyte, within experimental error. In Fig. 3, plots according to eqn. (7) are presented for $x = 0.6$ and $x = 1.0$, as examples. For all solutions the plots show that eqn. (7) is obeyed and therefore the experimentally-found increase of C_{LF} as a function of potential can be explained with a relatively simple model. In Table 1 the resulting Γ_O^*-values are given.

The dependence of the lead adsorption on KCl concentration can be interpreted in different ways. One possibility is that $\Gamma = kC_{total}$ with k dependent of

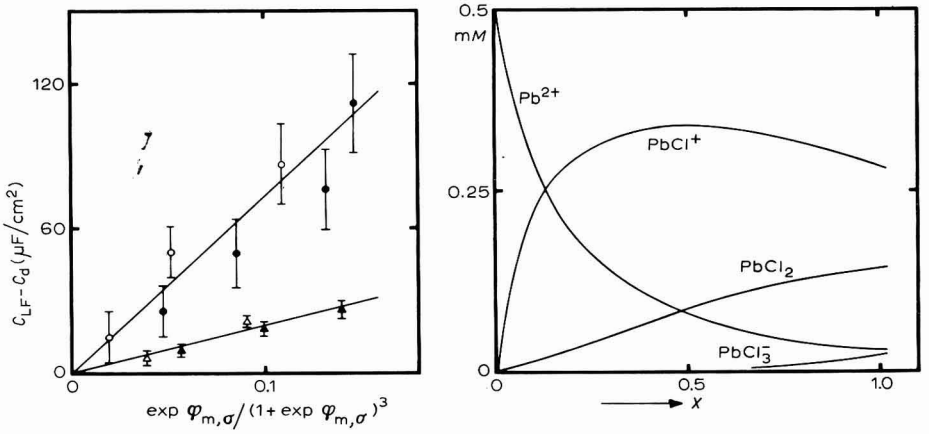

Fig. 3. Plots according to eqn. (7); (△,▲), x = 0.6; (○, ●), x = 1.0. Light spots refer to potentials anodic to E_i and dark spots to potentials cathodic to E_i.

Fig. 4. Concns. of lead chloride complexes in $(1-x)$ M KNO_3 + x M KCl mixtures, calcd. with[17] $K_1 = 8$, $K_2 = 4$, $K_3 = 0.4$ and $K_4 = 0.7$ and total lead concn. 0.5 mM.

KCl concentration (C_{total} is the sum of the concentrations of all lead ion complexes present in solution). The dependence can be explained also by supposing that one specific lead–chloride complex is adsorbed, $\Gamma = kC_{PbCl_x^{2-x}}$ with k and x independent of KCl concentration. The concentrations of the different complexes may be calculated from literature data[17]. However, the reported stability-constant values show a rather large scatter, so that the calculated concentrations are not very accurate. Moreover, there may be some lead–nitrate complexes in mixtures of high KNO_3 and low KCl concentrations. If a comparison is made between the calculated concentrations of the different lead–chloride complexes (Fig. 4) with Γ_O^* of Table 1, it appears that $\Gamma_O^* = kC_{PbCl_2}$ fits best. It seems, therefore, that the neutral species, $PbCl_2$, is adsorbed at the interface. Note that the variation of $E_{\frac{1}{2}}$ with KCl concentration is in accordance with Fig. 4, except for $x=0$ ($E_{\frac{1}{2}} = E_O + (RT/nF) \ln C_{Pb^{2+}}$ yields -396, -411, -417, -422, -428 and -433 mV for $x=0$ to $x=1.0$, respectively).

We have shown[1] that impedance data for 0.5 mM Pb^{2+} in 1 M KCl can also be explained and analysed according to the theory of SENDA AND DELAHAY[10] in which the coupling of faradaic and double-layer charging processes was not considered, or to the erroneous equations of DELAHAY[11]. This is the case because of the relatively large number of parameters that must be evaluated. Therefore it is necessary to be cautious in concluding from the fact that the cell impedances can be analysed according to a certain theory, that the theory is correct and generally applicable.

Finally, we wish to comment on a recent paper by DELAHAY AND HOLUB[18], the manuscript of which was kindly supplied by Professor DELAHAY. In their paper a derivation of the electrode admittance at the equilibrium potential is given for reversible systems. The resulting expressions are very intricate and unfortunately no comparison has been made by the authors with eqns. (1), derived earlier by REINMUTH[2,19] for the same case and valid for the whole peak-potential range, although a manuscript of ref. 2 was communicated to Professor DELAHAY. We have tried to compare both sets of expressions for Y_{el}, but dit not find agreement. Moreover, the equations given by DELAHAY AND HOLUB do *not* reduce to the classical equations for Y_{el}, as they should do when the terms involving Γ's and q-derivatives are set equal to zero (valid for no, or weak, reactant adsorption). Also their[18] Fig. 1 must be incorrect and was certainly not used by us, because their $R\omega^{\frac{1}{2}} (= \omega^{\frac{1}{2}}/Y_{el}')$ should *decrease* with frequency (*cf.* Fig. 1 of ref. 1). Thus, it must be concluded that DELAHAY AND HOLUB have made some mistakes in the derivation (note that one of the boundary conditions (eqn. (4) of ref. 18) is incorrect). Although DELAHAY AND HOLUB do not present procedures for analysing impedance data, they concluded that six double-layer parameters are required in such an analysis. As can be seen from eqns. (1), only three quantities, *i.e.*, C_{LF}, C_{HF} and u', may be obtained, which favours the possibilities of the analysis.

We thought it worthwhile to present our derivation of Y_{el} for reversible systems (eqns. (1)) because so far no reliable derivation has been given. A derivation analogous to that by DELAHAY AND HOLUB[18] is presented in the Appendix. E and $\psi = C_O/D_O + C_R/D_R$ were chosen as independent variables, as was done by REINMUTH[2,19], because in this case more surveyable equations result than when E and one of the concentrations of O or R are chosen, as was done by DELAHAY AND HOLUB[18].

APPENDIX

Derivation of eqns. (1)

A reversible electrode system is considered for the usual conditions: mass transfer controlled by semi-infinite linear diffusion in the presence of a large excess of supporting electrolyte and low a.c. overvoltage allowing the use of the linearized Nernst equation.

DELAHAY[3] has presented three general equations that should be solved. For reversible systems one can write these equations as follows (*cf.* refs. 11 and 18)

$$D_O(\partial C_O/\partial x)_{x=0} - D_R(\partial C_R/\partial x)_{x=0} = \mathrm{d}\Gamma^*/\mathrm{d}t \tag{A1}$$

where x is the distance from the electrode with $x \geqslant 0$ in solution and $x \leqslant 0$ in the amalgam. Further, one has for reversible systems the Nernst equation which reads in linearized form[20]

$$(nF/RT)\eta = C_O(0,t)/\bar{C}_O - C_R(0,t)/\bar{C}_R \tag{A2}$$

in which $\bar{C}_O$ and $\bar{C}_R$ are the surface concentrations due to the d.c. potential (*cf.* ref. 21).

Note that the equivalent for eqn. (A2) given by DELAHAY (eqn. (4) of ref. 18) is incorrect. The a.c. overvoltage, η, is given by

$$\eta = \eta_a \exp(j\omega t) \tag{A3}$$

where η_a is the amplitude of the a.c. signal.

The last general equation as given by DELAHAY[3] reads

$$i = -nFD_O(\partial C_O/\partial x)_{x=0} + \mathrm{d}q^*/\mathrm{d}t \tag{A4}$$

The time derivatives of Γ^* and q^* in eqns. (A1) and (A4) are written as the partial derivatives of the two independent variables, $\psi = C_O/D_O + C_R/D_R$ and E.

$$\frac{\mathrm{d}\Gamma^*}{\mathrm{d}t} = \left(\frac{\partial\Gamma^*}{\partial\psi}\right)_E \frac{\mathrm{d}\psi}{\mathrm{d}t} + \left(\frac{\partial\Gamma^*}{\partial E}\right)_\psi \frac{\mathrm{d}E}{\mathrm{d}t} = \gamma_\psi \frac{\mathrm{d}\psi}{\mathrm{d}t} + \gamma_E \frac{\mathrm{d}E}{\mathrm{d}t} \tag{A5}$$

$$\frac{\mathrm{d}q^*}{\mathrm{d}t} = \left(\frac{\partial q^*}{\partial\psi}\right)_E \frac{\mathrm{d}\psi}{\mathrm{d}t} + \left(\frac{\partial q^*}{\partial E}\right)_\psi \frac{\mathrm{d}E}{\mathrm{d}t} = q_\psi \frac{\mathrm{d}\psi}{\mathrm{d}t} + q_E \frac{\mathrm{d}E}{\mathrm{d}t} \tag{A6}$$

The concentrations, $C_O(x,t)$ and $C_R(x,t)$, obeying Fick's equations for O and R are for the steady state[18]

$$C_O(x,t) = \bar{C}_O\{1 - P\eta_a \exp[-(\omega/2D_O)^{\frac{1}{2}}(1+j)x + j\omega t]\} \tag{A7}$$

$$C_R(x,t) = \bar{C}_R\{1 + N\eta_a \exp[(\omega/2D_R)^{\frac{1}{2}}(1+j)x + j\omega t]\} \tag{A8}$$

The factors P and N are determined by introducing eqns. (A7) and (A8) into eqns. (A1) and (A2). Once N and P are known, eqn. (A4) yields expressions for the electrode admittance, Y_{el}, with

$$i/\eta_a \exp(j\omega t) = Y_{el}' + jY_{el}'' \tag{A9}$$

Introduction of eqns. (A7) and (A8) into eqns. (A1) and (A2), together with eqns. (A3) and (A5) yields

$$N + P + nF/RT = 0 \tag{A10}$$

$$N\lambda_R(1-j) = P\lambda_O(1-j) + \gamma_\psi(2\omega)^{\frac{1}{2}}(P\lambda_O - N\lambda_R) - \gamma_E\omega \tag{A11}$$

with $\lambda_O = \bar{C}_O(\omega D_O/2)^{\frac{1}{2}}$ and $\lambda_R = \bar{C}_R(\omega D_R/2)^{\frac{1}{2}}$. After elimination of N and separation of the real and imaginary parts, one obtains

$$P = \frac{\omega\gamma_E(1+u) - (nF/RT)\lambda_R(2+2u+u^2) + j\omega\gamma_E}{(\lambda_O+\lambda_R)(2+2u+u^2)} \tag{A12}$$

where $u = \gamma_\psi(2\omega)^{\frac{1}{2}}$.
Introduction of eqn. (A4) with eqns. (A3), (A6), (A7) and (A8) into eqn. (A9) yields:

$$Y_{el}' + jY_{el}'' = -nFP\lambda_O(1+j) + j\omega q_E + jq_\psi(2\omega)^{\frac{1}{2}}(N\lambda_R - P\lambda_O) \tag{A13}$$

Thus Y_{el}' and Y_{el}'' are, respectively, the real and imaginary part of the right-hand side of eqn. (A13). One has after introduction of P and N, eqns. (A10) and (A12).

$$Y_{el}' = \frac{n^2F^2}{RT}\cdot\frac{\lambda_O\lambda_R}{\lambda_O+\lambda_R} - nF\,\frac{\lambda_O}{\lambda_O+\lambda_R}\,\omega\gamma_E\,\frac{u}{(2+2u+u^2)} + \frac{q_\psi(2\omega)^{\frac{1}{2}}\omega\gamma_E}{2+2u+u^2}$$

$$Y_{el}'' = \frac{n^2F^2}{RT}\cdot\frac{\lambda_O\lambda_R}{\lambda_O+\lambda_R} - nF\,\frac{\lambda_O}{\lambda_O+\lambda_R}\,\omega\gamma_E\,\frac{2+u}{(2+2u+u^2)} - \frac{q_\psi(2\omega)^{\frac{1}{2}}\omega\gamma_E\,(1+u)}{2+2u+u^2} + \omega q_E$$

It is shown easily that (*cf.* ref. 1) $(n^2F^2/RT)\cdot\lambda_O\lambda_R/(\lambda_O+\lambda_R) = 1/2\sigma\omega^{-\frac{1}{2}}$ and $\lambda_O/(\lambda_O+\lambda_R) = \sigma_R/\sigma$, so that

$$Y_{el}' = \frac{1}{2\sigma\omega^{-\frac{1}{2}}} - nF\,\frac{\sigma_R}{\sigma}\,\omega\gamma_E\,\frac{u}{2+2u+u^2} + \frac{q_\psi(2\omega)^{\frac{1}{2}}\omega\gamma_E}{2+2u+u^2} \tag{A14}$$

$$Y_{el}'' = \frac{1}{2\sigma\omega^{-\frac{1}{2}}} - nF\,\frac{\sigma_R}{\sigma}\,\omega\gamma_E\,\frac{2+u}{2+2u+u^2} - \frac{q_\psi(2\omega)^{\frac{1}{2}}\omega\gamma_E\,(1+u)}{2+2u+u^2} + \omega q_E \tag{A15}$$

First an attempt is made to write eqn. (A14) in the same form as eqn. (1a). We have

$$\frac{q_\psi(2\omega)^{\frac{1}{2}}\gamma_E}{2+2u+u^2} = \left(\frac{\partial q^*}{\partial\psi}\right)_E\left(\frac{\partial\Gamma^*}{\partial E}\right)_\psi\left(\frac{\partial\Gamma^*}{\partial\psi}\right)_E^{-1}\frac{u}{2+2u+u^2} = \left(\frac{\partial q^*}{\partial\Gamma^*}\right)_E\left(\frac{\partial\Gamma^*}{\partial E}\right)_\psi\frac{u}{2+2u+u^2} \tag{A16}$$

In order to simplify eqn. (A16), we write (note that Γ^* and E are two independent variables, so that two partial derivatives suffice)

$$\mathrm{d}q^* = \left(\frac{\partial q^*}{\partial\Gamma^*}\right)_E\mathrm{d}\Gamma^* + \left(\frac{\partial q^*}{\partial E}\right)_{\Gamma^*}\mathrm{d}E$$

or, by differentiation to Γ^* at constant ψ

$$\left(\frac{\partial q^*}{\partial\Gamma^*}\right)_\psi = \left(\frac{\partial q^*}{\partial\Gamma^*}\right)_E + \left(\frac{\partial q^*}{\partial E}\right)_{\Gamma^*}\left(\frac{\partial E}{\partial\Gamma^*}\right)_\psi \tag{A17}$$

The partial derivative $(\partial q^*/\partial\Gamma^*)_E$ in eqn. (A16) is eliminated using eqn. (A17)

$$\frac{q_\psi(2\omega)^{\frac{1}{2}}\gamma_E}{2+2u+u^2} = \left(\frac{\partial\Gamma^*}{\partial E}\right)_\psi\left[\left(\frac{\partial q^*}{\partial\Gamma^*}\right)_\psi - \left(\frac{\partial q^*}{\partial E}\right)_{\Gamma^*}\left(\frac{\partial E}{\partial\Gamma^*}\right)_\psi\right]\frac{u}{2+2u+u^2}$$

or

$$\frac{q_\psi(2\omega)^{\frac{1}{2}}\gamma_E}{2+2u+u^2} = \left[\left(\frac{\partial q^*}{\partial E}\right)_\psi - \left(\frac{\partial q^*}{\partial E}\right)_{\Gamma *}\right]\frac{u}{2+2u+u^2} \tag{A18}$$

If eqn. (A18) is introduced in eqn. (A14), it is easily seen that the resulting equation is identical with eqn. (1a).

Substitution of eqn. (A18) into eqn. (A15) yields:

$$Y_{el}'' = \frac{1}{2\sigma\omega^{-\frac{1}{2}}} - nF\frac{\sigma_R}{\sigma}\cdot\omega\gamma_E\cdot\frac{2+u}{2+2u+u^2}$$

$$-\omega\left[\left(\frac{\partial q^*}{\partial E}\right)_\psi - \left(\frac{\partial q^*}{\partial E}\right)_{\Gamma *}\right]\frac{u+u^2}{2+2u+u^2} + \omega\left(\frac{\partial q^*}{\partial E}\right)_\psi$$

or

$$Y_{el}'' = \frac{1}{2\sigma\omega^{-\frac{1}{2}}} - nF\frac{\sigma_R}{\sigma}\cdot\omega\gamma_E\cdot\frac{2+u}{2+2u+u^2}$$

$$+\omega\left[\left(\frac{\partial q^*}{\partial E}\right)_\psi - \left(\frac{\partial q^*}{\partial E}\right)_{\Gamma *}\right]\frac{2+u}{2+2u+u^2} + \omega\left(\frac{\partial q^*}{\partial E}\right)_{\Gamma *} \tag{A19}$$

Equation (A19) is identical with eqn. (1b). Thus, eqns. (1) for Y_{el} derived by REINMUTH[19] with the use of Laplace transformations, are identical with the equations derived here by an analogous method to that given by DELAHAY[18].

ACKNOWLEDGEMENT

This investigation was supported in part by the Netherlands Foundation for Chemical Research (SON) with financial aid from the Netherlands Organisation for the Advancement of Pure Research (ZWO).

SUMMARY

A critical discussion is presented of some important theories for the electrode impedance in the case that the electroactive species are specifically adsorbed at the electrode–solution interface. It is argued that the equations given by REINMUTH are the most satisfactory so far available for reversible systems. These equations are based on the idea of coupling between faradaic and double-layer charging processes, as introduced by DELAHAY. A derivation of the equations is presented in an Appendix.

Procedures are proposed for analysing impedance data according to the equations of REINMUTH. Three cases must be considered, *viz.*, no, weak, and strong reactant adsorption.

Experimental results are given for the Pb^{2+}/Pb(Hg) electrode system in *M* KNO_3–KCl mixtures. It is shown that the adsorption of lead at the interface increases with KCl concentration, as can be concluded from the increasing enhancement of the "double-layer capacitance". The proposed procedures for analysing impedance data are shown to be applicable. Some arguments are presented to show that the neutral $PbCl_2$ species is adsorbed at the interface.

REFERENCES

1 M. SLUYTERS-REHBACH, B. TIMMER AND J. H. SLUYTERS, *J. Electroanal. Chem.*, 15 (1967) 151.
2 B. TIMMER, M. SLUYTERS-REHBACH AND J. H. SLUYTERS, *J. Electroanal. Chem.*, 15 (1967) 343.
3 P. DELAHAY, *J. Phys. Chem.*, 70 (1966) 2067, 2373.
4 J. E. B. RANDLES, *Discussions Faraday Soc.*, 1 (1947) 11.
5 J. R. GALLI AND R. PARSONS, *J. Electroanal. Chem.*, 10 (1965) 245.
6 M. SLUYTERS-REHBACH, B. TIMMER AND J. H. SLUYTERS, *Rec. Trav. Chim.*, 82 (1963) 553.
7 A. M. BATICLE AND F. PERDU. *J. Electroanal. Chem.* 12 (1966) 15; 13 (1967) 364.
8 M. SLUYTERS-REHBACH, B. TIMMER AND J. H. SLUYTERS, *J. Electroanal. Chem.*, submitted.
9 G. C. BARKER, *Electrode Processes 1959*, edited by E. YEAGER, Wiley, New York, 1961, p. 325.
10 M. SENDA AND P. DELAHAY, *J. Phys. Chem.*, 65 (1961) 1580.
11 P. DELAHAY AND G. G. SUSBIELLES, *J. Phys. Chem.*, 70 (1966) 3150.
12 P. DELAHAY, K. HOLUB, G. G. SUSBIELLES AND G. TESSARI, *J. Phys. Chem.*, 71 (1967) 779.
13 K. HOLUB, G. TESSARI AND P. DELAHAY, *J. Phys. Chem.*, 71 (1967) 2612.
14 M. SLUYTERS-REHBACH, D. J. KOOIJMAN AND J. H. SLUYTERS, *Polarography, 1964*, edited by G. J. HILLS, Macmillan, London, 1966, p. 135.
15 M. SLUYTERS-REHBACH AND J. H. SLUYTERS, *Rec. Trav. Chim.*, 82 (1963) 525, 535.
16 J. H. SLUYTERS, M. SLUYTERS-REHBACH AND B. TIMMER, *J. Electroanal. Chem.*, 15 (1967) 452.
17 J. BJERRUM, G. SCHWARZENBACH AND L. G. SILLÉN, *Stability Constants of Metal-ion Complexes*, The Chemical Society, London, 1958.
18 P. DELAHAY AND K. HOLUB, *J. Electroanal. Chem.*, 16 (1968) 131.
19 W. H. REINMUTH, private communication.
20 D. J. KOOIJMAN, M. SLUYTERS-REHBACH AND J. H. SLUYTERS, *Electrochim. Acta*, 11 (1966) 1197.
21 B. TIMMER, M. SLUYTERS-REHBACH AND J. H. SLUYTERS, *J. Electroanal. Chem.*, 14 (1967) 169, 181.

ELECTROANALYTICAL CHEMISTRY AND INTERFACIAL ELECTROCHEMISTRY
Elsevier Sequoia S.A., Lausanne – Printed in The Netherlands

AN ALL-TRANSISTORIZED POTENTIAL-CONTROLLED COULOMETRIC TITRATOR FOR ANALYTICAL PURPOSES

W. WARZANSKYJ*, A. DIEZ MORENO* AND V. ALMAGRO**
Junta de Energía Nuclear, Madrid (Spain)
(Received October 24th, 1967)

INTRODUCTION

Coulometry is an electroanalytical method which has attained a high degree of development as may be seen from the literature[1-4]. Work is still in progress to find new applications of this method and, especially, to design better electronic instrumentation. A major contribution in this direction is the transistor the use of which has enabled the implementation of a more reliable and robust instrumentation.

The main problems that have to be solved in a coulometer of this kind are control of the potential difference between the cell electrodes, and the integration of the current. Several methods have been proposed and used to solve these problems[1-4], and in the work described in this paper operational amplifiers have been used to deal with both problems.

BOOMAN[5] and KELLEY *et al.*[6] first proposed a method for controlling the voltage difference, using a third electrode to sense the control voltage. The deviation or error, between this voltage and a reference voltage, externally generated, is amplified and then fed back to zero the error. These authors were also the first to use operational amplifiers in coulometry.

Transistors in coulometry were first used by JONES *et al.*[7] who proposed a method requiring three operational amplifiers. QUAYLE AND COOPER[8] proposed a partially transistorized circuit which was used as a constant current power supply.

Several other workers have introduced transistors into the design of potentiostats serving different purposes; for instance, LINDSTROM AND DAVIS[9] have designed a model which can control up to 10 V voltage difference and which delivers currents up to 5 A; WOOD[10] describes a transistorized model in which the control potential is maintained by means of a variac incorporated in a servo-mechanism loop; TACUSSEL[11] manufactures a partially transistorized potentiostat that is especially useful in pulse techniques, and another with similar characteristics, but with the additional possibility of delivering very high output currents (up to 50 A), which can be used for molten salts electrolysis.

Transistorized potentiostats have also been applied in polarography[13] and chronopotentiometry[14].

* División de Electrónica
** División de Química Analítica

CIRCUIT DESCRIPTION

The coulometer here described is based upon a similar one previously used by KELLEY and coworkers[6], although some improvements have been achieved, *i.e.*, the coulometer is fully transistorized and does not need any external power supply. It uses two operational amplifiers instead of the three used in other models[7], with a corresponding saving in cost and maintenance work.

Figure 1 gives a general schematic diagram of the coulometer for the control of a reduction reaction. A very stable 8-V power supply is obtained by means of the zener diode, D1, and the reference diode, D2. The control potential is given by the

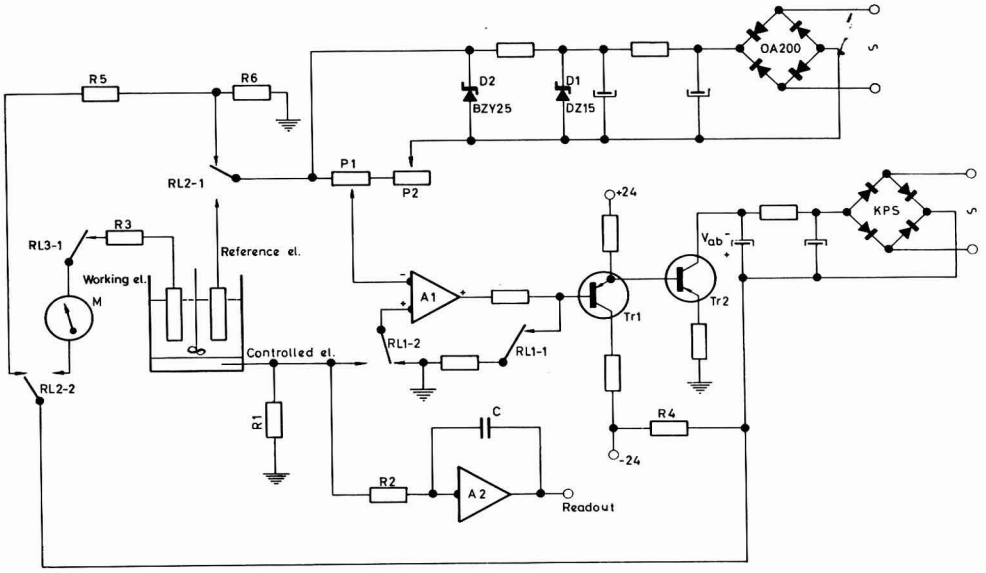

Fig. 1. Schematic diagram of the coulometer for the control of a reduction reaction.

fraction of this voltage taken up by the potentiometer, P1. The voltage drop across the solution, as measured by the reference electrode, is held equal to the control potential by means of the differential amplifier, A1. This amplifier commands a d.c. voltage power supply, V_{ab}, which delivers the instantaneous currents required by the cell. Transistors, Tr1 and Tr2, operate as an impedance match between the amplifier and the power supply. Resistor R_4 gives a path for the collector inverse saturation current of Tr2, thus preventing the passage of this current across the cell. Resistor R_3 initially limits the cell current in order to protect the electrodes. Finally, resistors R_1 and R_2 determine the fraction of the current which is integrated by the amplifier, A2. The output voltage of this amplifier is then proportional to the total charge delivered in the reaction.

Provisions have been made for controlling oxidation reactions by reversing the operation of the working and the controlled electrodes. In this case, the polarity of the two power supplies shown in Fig. 1 and the gain polarity of the amplifier A1

are reversed. Also, the operation of transistor Tr2 is switched to a common collector configuration.

An ammeter, M, reads the instantaneous current; its sensitivity can be changed from 1 mA to 1 A full-scale reading in four steps. A logarithmic scale is also provided in order to cover the complete operating range without changing scale.

Three relays have been included in order to control the operation of the coulometer. It may be seen from Fig. 1 that relay RL1 switches off the output of amplifier A1 and connects its reference input to ground. Relay RL2 switches off the cell and simultaneously connects a dummy cell composed of resistors R5 and R6 across the amplifier, A1. Special precautions have been taken to prevent transients from appearing during the switching time of the relays; when the coulometer is brought to the operating mode, a sequence takes place in which RL1 closes first, and then RL2. Once the reaction has been initiated, it can be completed either manually or automatically when the instantaneous current has decreased below a certain desired value. Relay RL3 is included for this purpose.

Description of the amplifiers

Amplifiers A1 and A2 are chopper-stabilized and are based upon the Goldberg amplifier[15]. Figure 2 gives a modification of the Goldberg amplifier used by us in order to obtain a differential response. The amplifier used has been fully described

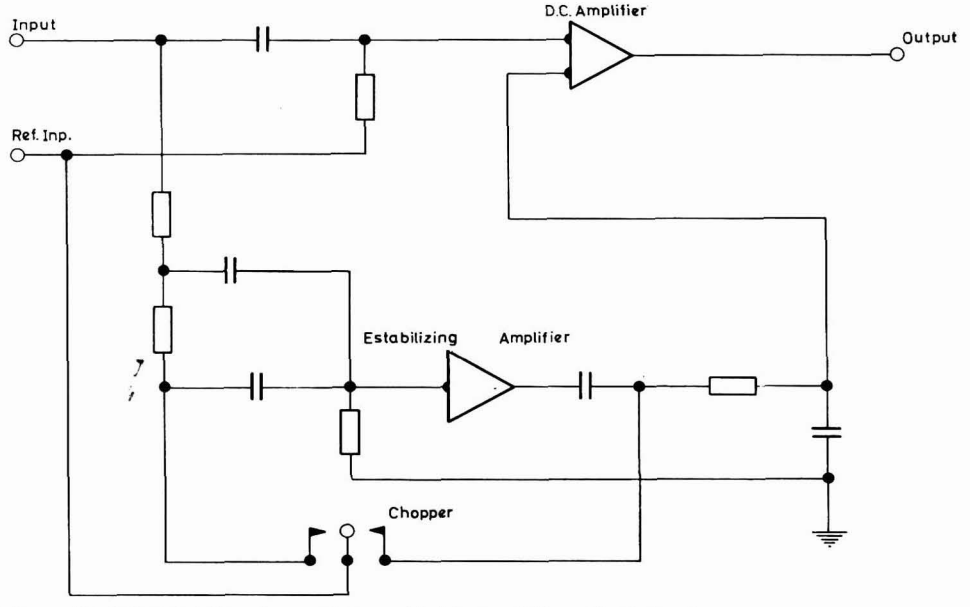

Fig. 2. Modified Goldberg's amplifier exhibiting a differential behavior.

in ref. 16 and only a brief discussion is therefore included in this paper. The input stage in both the d.c. and the correcting amplifiers, is made up of a nuvistor type vacuum tube. The use of two differential stages and one additional amplifier stage, of the "fractional" type[17], gives the d.c. amplifier an overall gain of 10^4 and keeps its

internal drift at a very low value. The "fractional" configuration is made up of two transistors and one Zener diode and is mainly characterized by providing a voltage shift which can be easily changed by proper selection of the circuit components and a non-inverting gain which depends on the ratio between the values of two of the circuit resistors. A complementary-pair emitter follower output stage enables the amplifier to deliver up to 10 mA to an external load.

The correcting amplifier has, besides the input nuvistor, two conventional amplifying stages with local feedback for both d.c. and a.c. signals. A transistor glows a Ne-2 neon lamp whenever the amplifier is not operating correctly.

The main characteristics of this amplifier are as follows:

Open loop gain	10^7
Input leakage current	10^{-11} A
Long term drift	100 μV/week
Output voltage	± 12 V
Operating temperature range	10–45°

Power supply

A very stable power supply has been designed in order to feed the operational amplifiers. It delivers 24 V at both polarities, with less than 25 mΩ output impedance and a negligible temperature coefficient in the range 15–40°. Reference 18 discusses in detail the design of a power supply to meet these requirements.

Zener diodes are used to obtain $+17$ and -12 V from $+24$ and -24 V, respectively. Other, non-stabilized tensions, required by the operational amplifiers are obtained by rectification and filtering.

EXPERIMENTAL

Coulometry

Coulometric evaluations of copper only, copper and cadmium, and copper–lead–cadmium, under various experimental conditions, were carried out in order to test the capability of the instrument described. A conventional cell was always used; a mercury pool was used as the controlled electrode, the working electrode was a platinum wire inside a Vycor 7930 tube, and the reference electrode a saturated calomel electrode, also inside a Vycor tube. Vigorous stirring was impressed through a glass bar by an electrical motor. Before every operation, purified nitrogen was bubbled through the test solution for at least 20 min.

Prior to each measurement, the "calibration factor", defined as the number of coulombs liberated in the reaction per output volt, was checked by means of a 1.345-V mercury cell and a 100 ± 0.05 Ω resistor.

The output voltage was measured by means of a Honeywell potentiometer Type 2730 which could detect 50 μV with a precision of 0.1%.

The amount of test substance in the solution is calculated by means of the expression:

$$c = kVM/nF$$

where

k = calibration factor (C/V)

V = output voltage (V)
M = atomic weight (g)
n = number of the electrons transferred to the electrode
F = Faraday's constant (C/equiv.)

Results

According to SHULTS AND THOMASON[19], copper can be determined in 1 N H_2SO_4 solution. Copper and cadmium can also be determined in the same solution, since, according to TANAKA[20], cadmium gives good results in that medium. It is possible to get the same results by means of polarographic measurements.

Copper, lead and cadmium can be successively determined in 0.5 M acid potassium tartrate medium at pH 4.5. This is deduced from TANAKA's[21] determination of cadmium, LINGANE's[22] determination of copper, and LINGANE AND JONES'[23,24] determination of lead.

The results are given in Tables 1–3. The error is always calculated by means of the expression:

$$E = \{(Y - \bar{Y})/Y\} \cdot 100$$

where Y is the total amount of the test substance and $\bar{Y}$ the average value of the data found in successive determinations.

The relative standard deviation (RSD) is calculated from a series of three successive determinations.

Copper and uranium have also been determined simultaneously in 1 N H_2SO_4 solution according to the method proposed by several authors[25,26]. First a reduction at −0.4 V is carried out; this gives the total concentration of copper and uranium. Then an oxidation at +0.1 V gives the copper concentration. The difference between these two figures gives the uranium concentration. The results are given in Table 4.

TABLE 1

COPPER DETERMINATION IN 1 N H_2SO_4; CONTROL POTENTIAL, −0.2 V

Soln. concn. (mg/ml)	*Copper amount (mg)*	*Reduction*		*Oxidation*	
		Error (%)	*RSD (%)*	*Error (%)*	*RSD (%)*
0.200	10.174	−0.1	0.24	−0.1	0.25
0.102	5.087	−0.1	0.10	+0.1	0.12
0.010	0.508	−0.5	1.50	+0.1	0.30
0.005	0.274	−0.5	1.00	+0.5	0.40
0.001	0.051	−1.0	1.10	+1.0	1.50
0.0005	0.025	−5.0	1.0	+1.0	1.20

TABLE 2

SUCCESSIVE DETERMINATION OF COPPER AND CADMIUM; CONTROL POTENTIAL, −0.10 AND −1.00 V, RESPECTIVELY

Copper amount (mg)	*Error (%)*	*RSD (%)*	*Cadmium amount (mg)*	*Error (%)*	*RSD (%)*
5.087	−0.1	0.1	6.120	−1.5	1.5
5.087	+0.1	0.5	12.300	−1.5	1.5
5.087	+0.2	0.5	24.500	−1.0	2.0
5.087	+0.5	0.5	30.600	−1.0	2.0

TABLE 3

SUCCESSIVE DETERMINATION OF COPPER, LEAD AND CADMIUM PRESENT IN 0.5 *M* ACID POTASSIUM TARTRATE SOLUTION, pH 4.5; CONTROL POTENTIALS −0.1, −0.6 AND −1.0 V, RESPECTIVELY

Copper (mg)	*Error (%)*	*RSD (%)*	*Lead (mg)*	*Error (%)*	*RSD (%)*	*Cadmium (mg)*	*Error (%)*	*RSD (%)*
5.087	+0.1	0.1	0.998	+2.0	5	6.120	−2.0	4.0
5.087	+0.1	0.5	2.000	−1.0	5	12.300	−1.0	4.5
5.087	+0.5	0.5	4.000	−1.0	5	24.500	−1.0	5.0

TABLE 4

SIMULTANEOUS DETERMINATION OF COPPER AND URANIUM IN 1 *N* H_2SO_4 SOLUTION BY REDUCTION AT −0.4 V FOLLOWED BY OXIDATION AT +0.1 V

Copper (mg)	*Error (%)*	*RSD (%)*	*Uranium (mg)*	*Error (%)*	*RSD (%)*
5.087	−0.1	0.5	7.140	+1.0	0.8
5.087	−0.1	0.5	14.140	−0.5	1.0
10.107	+0.1	1.0	14.140	−0.5	1.5

CONCLUSION

This all-transistorized coulometer which has only two operational amplifiers is useful for analytical chemistry studies. When up to three unknowns are successively determined from the same solution, the experimental errors may be as high as a 2% but usually range between 0.1 and 0.5%.

The instrument has been operated without failure for more than six months.

SUMMARY

An all-transistorized potential-controlled coulometer using two operational amplifiers is described. One of the amplifiers controls the potential difference between the electrodes; the other is used to integrate a fraction of the titration current. The coulometer is able to control titration currents ranging from 40 μA to 0.4 A; the control potential may be varied between 8 mV and 8 V. The results obtained in the estimation of copper, and copper and cadmium simultaneously, as well as in the estimation of copper, lead and cadmium, and copper and uranium, are given.

REFERENCES

1 J. J. LINGANE, *Electroanalytical Chemistry*, Interscience Publishers, New York, 1953.
2 P. DELAHAY, *New Instrumental Methods in Electrochemistry*, Interscience Publishers, 1954.
3 G. A. RECHNITZ, *Controlled-Potential Analysis*, Pergamon Press, Oxford, 1963.
4 K. ABRESCH AND I. CLAASEN, *Die Coulometrische Analyze*, Verlag Chemie, GMBH, Weinheim, 1961; English version, Chapman and Hall, 1965.
5 G. L. BOOMAN, *Anal. Chem.*, 29 (1957) 213.
6 M. T. KELLEY, H. C. JONES AND D. J. FISHER, *Anal. Chem.*, 31 (1959) 488.
7 H. C. JONES, W. D. SHULTS AND J. M. DALE, *Anal. Chem.*, 37 (1965) 680.
8 J. C. QUAYLE AND F. A. COOPER, *Analyst*, 91 (1966) 355.
9 F. LINDSTROM AND J. B. DAVIS, *Anal. Chem.*, 36 (1964) 11.
10 J. I. WOOD, *Anal. Chem.*, 37 (1965) 442.

11 J. TACUSSEL, *Electrochim. Acta*, 11 (1966) 449.
12 J. TACUSSEL, *Electrochim. Acta*, 11 (1966) 381.
13 G. L. BOOMAN AND W. B. HALBROOK, *Anal. Chem.*, 37 (1965) 795.
14 M. VOGT AND J. W. VOGT, *Anal. Chem.*, 38 (1966) 1102.
15 E. A. GOLDBERG, *RCA Rev.*, 15 (1950) 296.
16 W. WARZANSKYJ AND A. DIEZ MORENO, *Revista Telecomunicación*, 77 (1964) 2.
17 W. WARZANSKYJ, *Revista Telecomunicación*, 72 (1963) 9.
18 W. WARZANSKYJ, *Revista Telecomunicación*, 73 (1963) 2.
19 W. D. SHULTS AND P. F. THOMASON, *Anal. Chem.*, 31 (1959) 492.
20 M. TANAKA, *Bunseki Kagaku*, 6 (1957) 344; *C.A.*, 52 (1958) 15322h.
21 M. TANAKA, *Bunseki Kagaku*, 6 (1957) 477; *C.A.*, 52 (1958) 15322h.
22 J. J. LINGANE, *Anal. Chim. Acta*, 2 (1948) 584.
23 J. J. LINGANE, *Ind. Eng. Chem. Anal. Ed.*, 16 (1944) 147.
24 J. J. LINGANE AND S. L. JONES, *Anal. Chem.*, 23 (1951) 1798.
25 G. L. BOOMAN, W. B. HALBROOK AND J. E. RIEN, *Anal. Chem.*, 29 (1957) 219.
26 L. G. FARRAR, P. F. THOMASON AND M. T. KELLEY, *Anal. Chem.*, 30 (1958) 1511.

ELECTROANALYTICAL CHEMISTRY AND INTERFACIAL ELECTROCHEMISTRY
Elsevier Sequoia S.A., Lausanne – Printed in The Netherlands

OBSERVATIONS OF A BORON CARBIDE ELECTRODE

A. M. HARTLEY AND H. D. AXELROD*
Department of Chemistry and Chemical Engineering, University of Illinois, Urbana, Ill., 61801 (U.S.A.)
(Received October 3rd, 1967)

INTRODUCTION

The initial use of boron carbide as a solid electrode in electrochemical investigations had shown great promise. MUELLER AND ADAMS[1-3] have reported that the electrode exhibits low residual currents in a variety of aqueous electrolytes, and yields reproducible data for various electrochemical techniques. They have also indicated that boron carbide is chemically inert and has a large potential range overlapping the regions of both Pt and Hg electrodes. SAWYER AND SEO[4] employed the electrode for the study of the reduction of oxygen in aqueous solutions and reported a reduction mechanism similar to that found on other electrodes. MOUNTCASTLE[5] used the electrode in voltammetry and constant-current coulometry but found the results, in general, to be poor.

Because this electrode material could be of significant usefulness in electrochemistry, we decided to try to confirm the work of MUELLER AND ADAMS and to extend the investigations to other electrochemical areas. During our studies we found evidence of oxide formation on the electrode, which could lead to erroneous interpretation of data.

REAGENTS AND EQUIPMENT

All solutions were prepared with reagent-grade chemicals without further purification, and with deionized water. De-aerating nitrogen was passed through Cr(II)–H_2SO_4 wash towers and a deionized water tower prior to the purging of oxygen from solutions. Boiled linseed oil, originally produced by the Pittsburgh Plate Glass Company, Linseed Oil Division, Redwing, Minnesota, was supplied to us by DeMert and Dougherty, Inc., Chicago, Illinois.

The details of the electronic equipment used in these experiments have been previously described[6]. Voltammograms were made with a 3-electrode polarograph. Cell potentials were obtained with a high impedance follower amplifier or pH-meter placed across the cell electrodes in conjunction with a potentiometer. All potential values were measured against a Leeds and Northrup saturated calomel electrode (SCE) at room temperature, $22° \pm 3°$.

Boron carbide was obtained from the Carborundum Company, Niagara Falls,

* National Center for Atmospheric Research, Boulder, Colo.

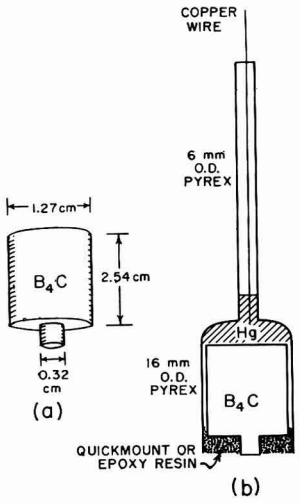

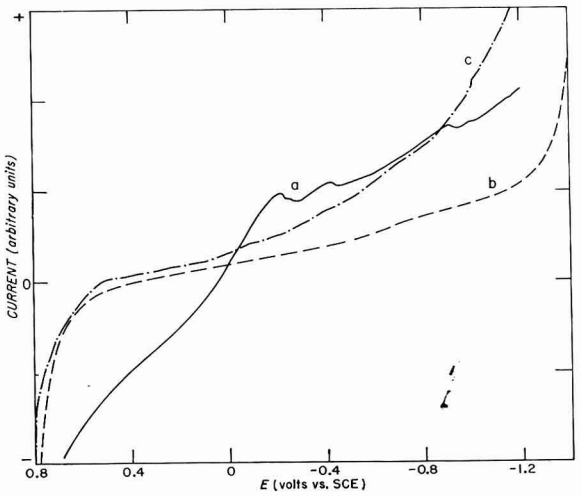

Fig. 1. Boron carbide electrode: (a), boron carbide rod; (b), boron carbide electrode mounted.

Fig. 2. Residual currents with a boron carbide electrode in de-aerated 1 *M* KCl after various electrode pretreatments: (a), 12 h in heated 7 *M* $HClO_4$ (10 μA/division); (b), followed by 24 h in boiled linseed oil (0.2 μA/division); (c), followed by 24 h in $CHCl_3$ (2.0 μA/division).

New York, in the form of rods 1.27 cm diameter × 2.54 cm length with a density of 99+% of the theoretical value (2.52 g/cm^3). Small diameter rods were not used because the company could not guarantee their high density.

Although the material is hard and brittle, one end of the cylinder was reduced in size with a diamond grinding wheel to a 0.32-cm diameter cylinder (Fig. 1a). The electrode was then sealed into 16-mm o.d. Pyrex tubing with a 6-mm o.d. Pyrex stem. The sealants used were either Cycleweld Epoxy Resin, Chrysler Corp., Trenton, Michigan, or Quickmount (self-setting resin), Fulton Metallurgical Products Corp., Pittsburgh, Pennsylvania (Fig. 1b). Both materials provided excellent seals and were generally inert. Although Quickmount is subject to attack by chloroform or benzene, its ease of preparation and short hardening time (30 min) make it preferable to the epoxy resin, which usually requires a 24-h setting time before use. With both materials, the electrode was free of leaks; removing the sealant and remaking the electrode would give a 5% deviation in the surface area. The 6-mm o.d. tubing allowed the electrode to be rotated with a Sargent 600 rev./min Synchronous Rotator.

The boron carbide was polished with either diamond paste or silicon carbide No. 600 waterproof paper to a high mirror finish. Polishing could be accomplished by hand or with the synchronous rotator.

RESIDUAL CURRENT CURVES

The residual current curves obtained with a boron carbide electrode in various de-aerated electrolytes were neither flat nor smooth. In de-aerated 1 *M* H_2SO_4, a small cathodic wave and anodic wave appeared at +0.4 V *vs.* SCE*, along with the

* All half-wave potentials are *vs.* a saturated calomel electrode (SCE).

beginning of a cathodic wave at −0.3 V. In de-aerated 1 *M* KCl, a wave was present at −0.5 V, and in 1 *M* NaOH two waves of equal height were found at −0.5 V and −0.9 V. This pair of waves occurred at the same potential as the reduction of oxygen in an oxygen-saturated NaOH solution, but was lower in magnitude. In addition, the electrode range of +0.8 V to −1.2 V in 1 *M* KCl at 0.5 μA/cm^2 was far shorter than the range reported by MUELLER[1].

The magnitude of the residual current could be influenced by electrode pretreatment. When an electrode material was placed in hot 7 *M* $HClO_4$ for 12 h, then washed with deionized water and remounted, the residual current in 1 *M* KCl was found to be 50 times higher than before pretreatment. These high currents rendered the electrode totally useless. This current can be decreased in two ways. The electrode can either be placed in a 10 m*M* Cr(II)–1 *M* H_2SO_4 solution for a period of several days, or soaked in raw or boiled linseed oil for 24 h. Our experimental results indicated that the reduction in the residual currents could be attributed neither to a change in capacitance of the electrode nor a change in surface area. In all cases, area measurements made by chronopotentiometry indicated values within 10% of the geometric area, and capacitance values were reproducible. We conclude that both the Cr(II) solution and the linseed oil act as reducing agents on the surface, with the linseed oil reaction being faster. Linseed oil has a high degree of unsaturation; probably its olefinic bonds react with the electrode to reduce the surface. Other unsaturated oils did not perform as well because their degree of unsaturation was less than that of linseed oil. The linseed oil coating could be removed by soaking the electrode in chloroform for 24 h (this also removed the Quickmount). An electrode treated with $HClO_4$, followed by soaking in linseed oil for 24 h and removing the oil with chloroform, still displayed some evidence of $HClO_4$ pretreatment. The residual currents of the electrode after various pretreatments are shown in Fig. 2. Other than lowering the residual current, the linseed oil did not appear to affect the electrode performance during the various electrochemical experiments.

VOLTAMMETRY

The oxidation and reduction of Cd(II), Cu(II), IO_3^-, $Cr_2O_7^{2-}$, $[Fe(CN)_6]^{4-}$, and $[Fe(CN)_6]^{3-}$ in 1 *M* KCl, and IO_3^-, BrO_3^- in 1 *M* H_2SO_4, was studied. These

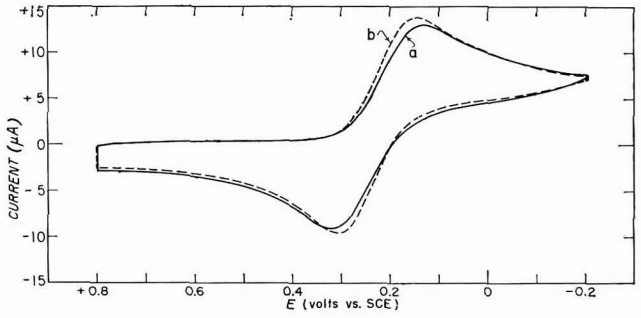

Fig. 3. Cyclic voltammogram of 0.01 *M* $K_3Fe(CN)_6$ in 1 *M* KCl at 1.0 V sec^{-1} with an oxidized and reduced boron carbide electrode: (a), reduced electrode; (b), oxidized electrode.

electroactive species were found to be irreversible on boron carbide, with the peak potential dependent upon the scan rate from very slow rates up through rates of 6 V/min. The peak currents were low and not reproducible. The peak potentials were also found to be influenced by electrode pretreatment. For example, an electrode was poised at +1.0 V or −1.0 V for 10 min prior to observing the reduction of $[Fe(CN)_6]^{3-}$ in 1 *M* KCl. The peak potential for the "prereduced" electrode was 20 mV more negative than for the "preoxidized" electrode. Furthermore, the $[Fe(CN)_6]^{3-}/[Fe(CN)_6]^{4-}$ couple was slightly more irreversible with the "prereduced" electrode than with the "preoxidized" electrode (Fig. 3).

ANODIC STRIPPING ANALYSIS

The use of the boron carbide electrode for anodic stripping analysis was investigated. Cadmium and copper were best stripped in 1 *M* KCl while Sn was oxidized in 1 *M* HCl, and Ni in 1 *M* KSCN. The anodic peaks were low in intensity with only a fraction of the reduced material being reoxidized. For example, a stirred 10^{-6} Ni(II)–1 *M* KSCN solution was electrolyzed for 100 sec at −1.0 V. The electrode was positively scanned, and a stripping peak of only 0.6 μA was observed. Furthermore, the initial stripping peaks were low, and only after several runs did the peaks reach a higher, steady-state value. The run-to-run reproducibility of current averaged 10% relative.

As in the case of the previously discussed electro-analytical techniques, pretreatment of the electrode also affected the stripping peaks. In 1 *M* KSCN, Ni(II) gave the usual stripping peak; however, if the electrode was initially prepolarized at +1.0 V in 1 *M* KCl for 30 min and then plating and stripping of Ni in KSCN attempted, a stripping peak could not be observed although a cathodic current was indicated during the deposition part of the run. The stripping peak reappeared and reached its original maximum value only after repeated cycles of attempted plating and stripping.

POTENTIOMETRY

FREEDMAN AND CORWIN'S[7] unsuccessful attempt to measure the potential of the thiol–disulfide system represents the only previous application of boron carbide to potentiometry. Since very little information in this area has been reported, a study was made of the performance of the electrode during various redox titrations.

Using the previously described boron carbide electrodes, Fe(II) was titrated with Ce(IV) in 1 *M* H_2SO_4 (Fig. 4). The electrode followed the potentials very well, the values being within 10 mV of a Pt indicator electrode and of the literature values. However, after repetitive titrations with the same electrode, the potential in excess Ce(IV) was about 40 mV more negative than for the first run. This was the only system which provided good results. The current–voltage curves for various fractions titrated showed irreversible electrode reactions for this system and the others mentioned below.

In 1 *M* H_2SO_4, Fe(III) was titrated with Cr(II). Initially, the boron carbide electrode parallelled the potential changes of the Pt electrode in solution. Just prior to the end-point, at about +0.2 V, the electrode became very sluggish and slowly

drifted toward negative potentials at a rate independent of any additional Cr(II) in the solution. If allowed to remain in a solution of excess Cr(II), the potential of the boron carbide electrode would eventually drift negatively to coincide with the potential of the Pt indicator electrode. This rate of drift was found to be dependent

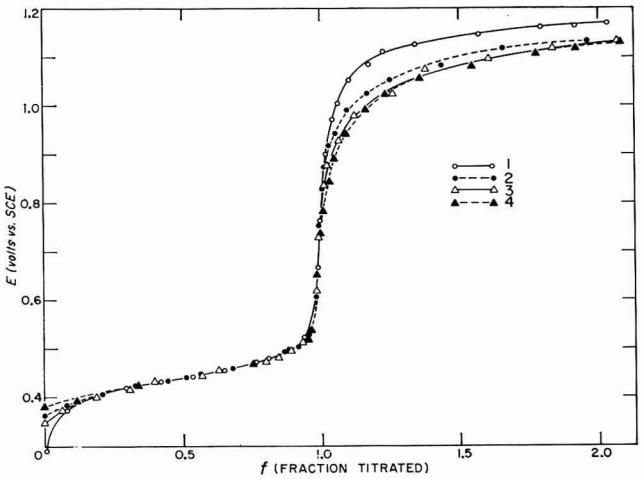

Fig. 4. Repetitive (1–4) potentiometric titrations of Fe(II) with Ce(IV) in 1 *M* H_2SO_4 with a boron carbide electrode.

upon the electrode pretreatment. An electrode was placed in a heated 7 *M* $HClO_4$ solution for 12 h, then washed and mounted; the usual high residual current in de-aerated KCl resulted. However, the rate of negative potential drift for this electrode was slower than for an electrode which had not been so treated.

The same sluggishness was apparent in other reactions, such as the titration of $[Co(NH_3)_6]^{2+}$ by $[Fe(CN)_6]^{3-}$ in 4 *M* NH_3–1 *M* ammonium citrate (pH 9.7) buffer. Here the boron carbide electrode followed the titration in the region of potential control by the $[Fe(CN)_6]^{3-}/[Fe(CN)_6]^{4-}$ couple, but near the end-point (0.0 V) and in excess $[Co(NH_3)_6]^{2+}$ solution, the electrode was very sluggish and slowly drifted negatively.

Similar electrode behavior was observed with $[Co(CN)_6]^{4-}$ titrated by $[Fe(CN)_6]^{3-}$ in 10% $(NH_4)_2CO_3$, 25% NH_3, 0.3 *M* KCN (pH 10.7) buffer. When the boron carbide and Pt electrode were placed in the initial $[Co(CN)_6]^{4-}$ solution, the boron carbide potential was 350 mV more positive than the Pt potential and continued to drift toward it. An end-point was observed, and in excess $[Fe(CN)_6]^{3-}$ the potentials of the two electrodes coincided (Fig. 5). The reverse titration again yielded large potential differences in excess $[Co(CN)_6]^{4-}$.

At the other end of the potential scale, As(III) was titrated with Br_2 in 1 *M* H_2SO_4. In this case the boron carbide electrode became sluggish around +0.7 V. Although an end-point break was observed from the shift of the potentials, the boron carbide electrode did indicate more negative potentials than the Pt electrode with excess Br_2, and failed to reach the Pt values. Electrode sluggishness was also observed for the Fe(III)–Sn(II) titration and the IO_3^-–I^- titration, both in HCl.

The potential values exhibited by boron carbide upon immersion in a solution

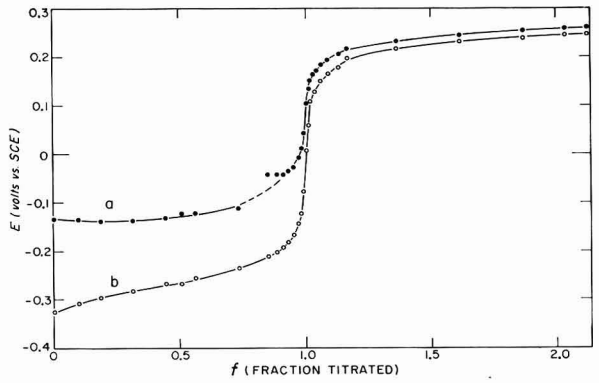

Fig. 5. Potentiometric titration of $Co(CN)_6^{4-}$ with $Fe(CN)_6^{3-}$ in 10% $(NH_4)_2CO_3$, 2.5% NH_3, and 0.3 *M* KCN (pH 10.7): (a), boron carbide electrode; (b), platinum electrode.

can be influenced by prepolarization of the electrode. If a continuously decreasing potential (+1.0 V to −1.0 V) is applied to the electrode in a de-aerated 1 *M* KCl solution and the electrode is then transferred to a Cr(II) solution, the electrode potential will be negative to Pt and slowly rise toward it. However, if a continuously increasing potential (−1.0 V to +1.0 V) is applied to the electrode in a de-aerated 1 *M* KCl solution and the electrode then placed in a Cr(II) solution, the boron carbide potential will be positive to the Pt value and slowly fall toward it. These effects were not observed upon transferring the electrode to a Fe(III)/Fe(II) solution; rather the equilibrium potential was reached almost immediately. Calculations have shown that these effects were not due to low exchange currents, and the rate of drift could not be attributed to the current drawn from the follower amplifier or pH-meter used in potential measurements.

An experiment similar to that performed on Pt, Au, and Pd by LEE, ADAMS AND BRICKER[8], was tried. A 1:1 mixture of Ce(IV)/Ce(III) in 1 *M* H_2SO_4 was used as the oxidizing solution. A cathodic current was passed through a boron carbide electrode in the cerium solution until a steady potential value (about −1.2 V) was reached. The current was stopped and the potential drift of the electrode in the oxidizing solution was followed. The electrode drifted positively to about +0.7 V when the rate slowed appreciably. The rate of return was found to be dependent upon the Ce(IV)/Ce(III) concentration. However, the irregularities in the curves observed by LEE *et al.*, due to oxidation of the metals, were not observed with the boron carbide.

CONCLUSIONS

The boron carbide electrode has little utility in electrochemical analysis. The material is expensive and difficult to machine and the general response and reproducibility in various electroanalytical applications is very poor.

Contrary to previous reports, the electrode does not appear to be inert, and suffers from surface oxidation. This idea is not startling, considering that oxide formations and corrosion of boron carbide have been previously observed[9–11].

The evidence presented shows three processes occurring at the electrode. The cathodic waves in the residual current at about -0.5 V and -0.9 V are due to the reduction of adsorbed O_2 on the electrode surface. Second, the cathodic and anodic waves at $+0.4$ V in the residual current are probably due to chemisorbed O being reduced and formed anew. Third, and most important, is the presence of an irreversible oxide system on the electrode. In this case, the oxide is reduced at around $+0.2$ V and formed at about $+0.7$ V in 1 M H_2SO_4. Thus, only the potential of couples in the middle region, *i.e.*, Fe(III)/Fe(II), $[Fe(CN)_6]^{3-}/Fe(CN)_6]^{4-}$ will be correctly indicated by the boron carbide. When the potential of the solution transverses the middle region and crosses the approximate potentials of $+0.2$ V or $+0.7$ V, the response of the electrode becomes sluggish owing to a chemical reaction between the solution and the electrode surface. Hence, a mixed potential is observed until all of the oxide is removed or formed, or the potential from the oxidized/reduced surface corresponds to the solution potential. The performance of the electrode will be influenced by pretreatment as indicated by the potentiometric and voltammetric studies. Furthermore, this oxide is so irreversibly reduced that it is not observed as a wave in the residual currents unless the electrode is previously oxidized with a reagent such as $HClO_4$.

ACKNOWLEDGEMENT

This work was supported by the National Institutes of Health, USPH GM-12009.

SUMMARY

The effectiveness of boron carbide as an electrode in electrochemical studies including voltammetry, anodic stripping, and potentiometry has been investigated. In general, the reproducibility and sensitivity of the electrode was poor. The residual current of the electrode indicated the reduction of adsorbed O_2 and chemisorbed O. Evidence also showed that an irreversible oxide was present on the electrode, which undergoes a chemical reaction with solutions. Thus, pretreatment and present condition of the electrode is an important consideration, since the oxide formation can influence data.

REFERENCES

1 T. R. Mueller, Ph.D. Thesis, University of Kansas, 1963.
2 T. R. Mueller and R. N. Adams, *Anal. Chim. Acta*, 23 (1960) 467.
3 *Ibid.*, 25 (1961) 482.
4 D. T. Sawyer and E. T. Seo, *J. Electroanal. Chem.*, 3 (1962) 410.
5 W. R. Mountcastle, Jr., *Anal. Chim. Acta*, 32 (1965) 332.
6 H. D. Axelrod, Ph.D. Thesis, University of Illinois, 1967.
7 L. D. Freedman and A. H. Corwin, *J. Biol. Chem.*, 181 (1949) 601.
8 J. K. Lee, R. N. Adams and C. E. Bricker, *Anal. Chim. Acta*, 17 (1957) 321.
9 L. M. Litz and R. A. Mercuri, *J. Electrochem. Soc.*, 110 (1963) 921.
10 L. Ya. Markovskii and G. V. Kaputovskaya, *J. Appl. Chem. USSR, English Transl.*, 33 (1960) 574.
11 T. N. Nazarchuk, *Russ. J. Inorg. Chem., English Transl.*, 4 (1959) 1233.

ELECTROANALYTICAL CHEMISTRY AND INTERFACIAL ELECTROCHEMISTRY
Elsevier Sequoia S.A., Lausanne – Printed in The Netherlands

THE ELECTROREDUCTION OF NIOBIUM(V) IN HYDROCHLORIC ACID SOLUTIONS AT MERCURY ELECTRODES

I. POLAROGRAPHY AND CHRONOPOTENTIOMETRY

JOHN G. McCULLOUGH*† AND LOUIS MEITES‡
Department of Chemistry, Polytechnic Institute of Brooklyn, Brooklyn, N.Y. (U.S.A.)
(Received November 17th, 1967)

INTRODUCTION

The analytical chemistry of niobium in aqueous solutions is complicated by the tendency of niobium(V) to hydrolyze and by the instability of the lower oxidation states of the element[1–3]. The reduction of niobium(V) to niobium(III) by zinc in sulfuric acid solutions is usually incomplete, owing to hydrolysis of part of the niobium(V)[4]; it can be made stoichiometric in acidic fluoride media, but there niobium(III) is oxidized fairly rapidly by protons[5]. Attempts to reduce niobium(V) to niobium(IV) yield some niobium(III) as well, either by disproportionation or by further reduction of niobium(IV). Partial reduction to niobium(II) has also been reported[6–8].

VIVARELLI *et al.* studied the electroreduction of niobium(V) in hydrochloric acid solutions, at least some of which contained traces of fluoride[6–8]. Since ion-exchange studies have shown that niobium(V) is strongly complexed by fluoride in such solutions[9], it seems likely that their results represent the behavior, not of chloroniobium species, but of chlorofluoroniobium species. This is the first of two papers describing the electroreduction of niobium(V) at mercury electrodes in aqueous solutions of hydrochloric acid from which other complexing agents were carefully excluded.

EXPERIMENTAL

Niobium pentoxide, supplied by the Fansteel Metallurgical Corporation (North Chicago, Ill.) or by Johnson–Matthey Ltd. (London, England), was dissolved in 3–5 times its weight of fused potassium hydroxide in a nickel crucible. The melt was cooled and leached with water, and the solution was diluted to about 0.1 *F* in niobium and filtered.

The resulting alkaline niobate solutions were standardized by the procedure of HEADRIDGE AND TAYLOR[5] with the following modifications. A Pyrex reductor

* This paper is based on a thesis submitted by John G. McCullough to the Faculty of the Polytechnic Institute of Brooklyn in partial fulfillment of the requirements for the Ph.D. degree in June, 1967.
† Present address: Union Carbide Chemicals Division, P. O. Box 65, Tarrytown, N. Y., U.S.A.
‡ To whom correspondence and requests for reprints should be addressed. Present address: Department of Chemistry, Clarkson College of Technology, Potsdam, N.Y. 13676, U.S.A.

column and receiving vessel were used instead of plastic. The ferrous ion produced in the receiving vessel was titrated potentiometrically with standard potassium dichromate, using a platinum indicator electrode. Solutions were not de-aerated before passage through the reductor because oxygen is reduced by zinc under these conditions, but the receiving vessel was de-aerated throughout the determination, both to protect niobium(III) from oxygen and to expel hydrogen, which interfered with the measurements of potential. Recoveries of niobium pentoxide, dissolved quantitatively in hydrofluoric acid, were $99.8 \pm 0.1\%$. The assays of the alkaline niobate solutions did not change perceptibly in a year.

Acidic solutions of niobium(V) were prepared volumetrically from alkaline solutions, concentrated hydrochloric acid, and distilled water.

Polarograms were obtained with damping, using a locally constructed conventional polarograph. The H-cell was of the type described by MEITES AND MEITES[10] and was always thermostatted at $25.00 \pm 0.05°$. Solutions were de-aerated with prepurified nitrogen that had been scrubbed with chromous chloride solution and equilibrated with the supporting electrolyte in the manner previously described[11]. Mercury was purified by the procedure of MEITES AND MOROS[12].

A silver–silver chloride–1 F potassium chloride reference electrode of the type described by MEITES AND MOROS[12], together with a 1 F potassium chloride bridge, was used in all the work reported here (saturated potassium chloride solutions could not be used because of the precipitation that occurs when they are brought into contact with concentrated hydrochloric acid). The potential of this electrode was -4 ± 1 mV *vs.* SCE, and all potentials have been corrected to refer to the SCE. The constancy and reproducibility of the polarographic half-wave potentials indicate that the liquid-junction potentials across the KCl–HCl interfaces, though undoubtedly large, did not change over long periods.

Chronopotentiograms were obtained at room temperature with a mercury-pool indicator electrode having a diameter of 1.85 cm in a cylindrical plastic cell, using commercial constant-current sources and pen-and-ink recorders.

RESULTS AND DISCUSSION

The effect of acid concentration on the solubility of niobium(V)

When a solution containing 10.75 F hydrochloric acid and 10 mF, or less, niobium(V) is prepared by mixing the concentrated acid and an alkaline niobate solution, a fluffy white precipitate of niobic acid forms and quickly redissolves. Stepwise dilution of the resulting solution with water causes niobic acid to precipitate gradually as the concentration of acid falls below 9 F. A dense white suspension is eventually formed at lower acidities, but the precipitate redissolves abruptly at the composition, 4.8 F acid–4.4 mF niobium(V). If the acidic solution is first boiled, no precipitate ever appears as it is diluted to 2.9 F acid–2.7 mF niobium(V). Most of these phenomena have been previously reported[1], but the redissolution of the precipitate at low acidities has not.

Polarograms of such solutions show that the heights of the niobium waves decrease gradually as the concentration of acid decreases; the waves disappear at acidities below 5 F, whether precipitation occurs or not, but can be regenerated by reacidifying the solution with concentrated acid. These facts show that the niobium

species soluble at low acidity are not reducible, and that the hydrolytic reactions are reversible.

A boiled solution containing 9.5 mF niobium(V) and 10.1 F acid, and an unboiled solution containing 1.90 mF niobium(V) in 11.8 F acid, were diluted stepwise with water, and the diffusion current, i_1, of the first polarographic wave was measured after each stage of dilution. Two ranges of behavior were found. If the stoichiometric concentration, C_{Nb}, of niobium(V) was low enough, and if the mean ionic activity, $a_{\pm}$, of the acid was high enough, it was found that i_1/C_{Nb} was equal to 3.2 μA mmole^{-1} l for both solutions. Lower values of i_1/C_{Nb} were obtained at lower values of $a_{\pm}/C_{Nb}$,

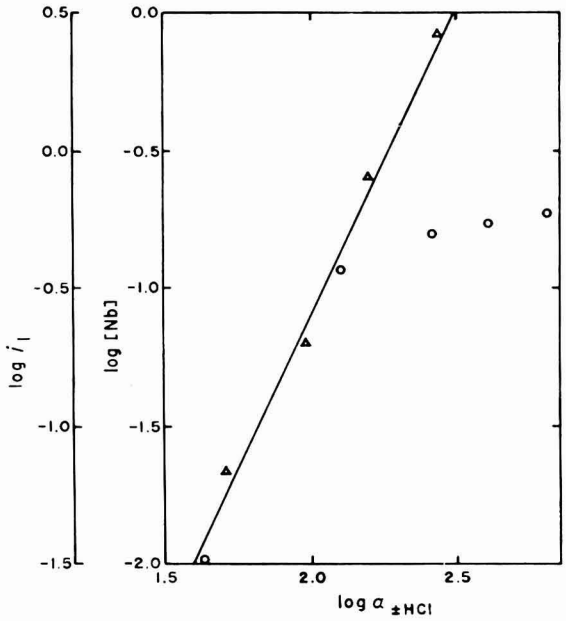

Fig. 1. Effects of acid activity on the height of the first polarographic wave and the concn. of reducible Nb(V) computed therefrom by eqn. (1). (○), data obtained with unboiled solns., $C_{HCl}/C_{Nb} = 6.84 \cdot 10^3$; (△), data obtained with boiled solns., $C_{HCl}/C_{Nb} = 1.06 \cdot 10^3$.

as shown in Fig. 1. Assuming that the niobium is entirely in the reducible form when $a_{\pm}/C_{Nb}$ is high, and letting [Nb] denote the concentration of this form, it follows that

$$i_1 = 3.2[\mathrm{Nb}] \tag{1}$$

in all cases. The second ordinate scale of Fig. 1 was calculated from this relation. The straight line in Fig. 1 obeys the equation

$$[\mathrm{Nb}] = c a_{\pm}^{2.2} \tag{2}$$

at the lower values of $a_{\pm}/C_{Nb}$, c being a numerical constant whose value is the same for boiled as for unboiled solutions. Thus the concentration of the reducible species is proportional to the square of the mean ionic activity of the acid.

NABIVANETS[13] showed by electrodialysis that niobium(V) is anionic in hydrochloric acid solutions more concentrated than 5 F, but is cationic at lower acidities.

The simplest assumption that can account for all these observations is that niobium(V) can exist as an anion A, an uncharged species B, or a cation C, among which the relations are

$$A^{-i+j} \overset{-i\,Cl^- - j\,H^+}{\rightleftharpoons} B^0 \overset{-i\,Cl^- - j\,H^+}{\rightleftharpoons} C^{+i-j} \tag{3}$$

$$i > j \tag{4}$$

$$K_1 = a_\pm^{i+j}(B)/(A) \tag{5}$$

$$K_2 = (B)/(C)a_\pm^{i+j} \tag{6}$$

where it is assumed that

$$a_{H^+} = a_{Cl^-} = a_\pm \tag{7}$$

and where parentheses are used to denote the concentrations or activities of the individual species. The total solubility of niobium will be given by:

$$S = (A) + (B) + (C) \tag{8}$$

If species B is slightly soluble, so that

$$K_s = (B), \tag{9}$$

these equations can be combined to yield

$$S = K_s(1 + K_1^{-1}a_\pm^{i+j} + K_2^{-1}a_\pm^{-i-j}) \tag{10}$$

If the precipitate is AC rather than B, writing

$$K_s' = (A)(C) = K_s^2/K_1K_2 \tag{11}$$

again leads to eqn. (10); if AC precipitates and species B does not exist, the constant term disappears from within the parentheses in eqn. (10). In any event, eqn. (10) shows that the solubility passes through a minimum at some intermediate value of $a_\pm$, and at high acidities is given by:

$$S = (K_s/K_1)a_\pm^{i+j} \tag{12}$$

Together with the slope of the line in Fig. 1, eqn. (2) signifies that

$$i + j = 2 \tag{13}$$

The only integral solution of eqns. (4) and (13) is $i = 2$, $j = 0$, whence eqn. (3) becomes

$$A^{2-} \overset{-2Cl^-}{\rightleftharpoons} B^0 \overset{-2Cl^-}{\rightleftharpoons} C^{2+} \tag{14}$$

If species B does not exist, the half-integral values, $i = \frac{3}{2}$, $j = \frac{1}{2}$, are admitted, and eqn. (3) then becomes

$$A^- = C^+ + 3\,Cl^- + H^+ \tag{15}$$

If niobium(V) is hexacoordinate and monomeric, it cannot have a charge more negative than -1 in this medium, for none of the possible ligands carries more than a single negative charge. Consequently, the species A^{2-} would have to be polymeric, and eqn. (14) might take the form:

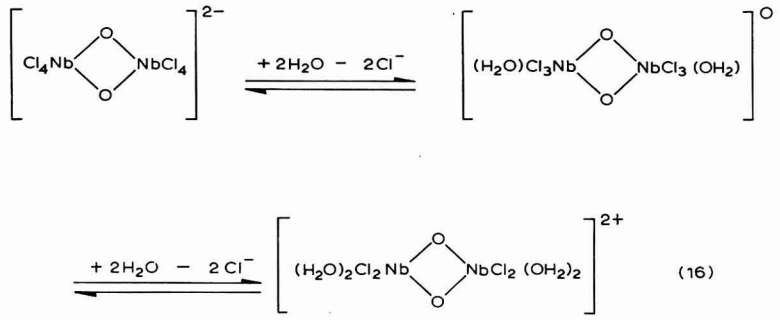

(16)

whereas eqn. (15) could be realized both by polymeric species

(17)

and by mononuclear species

$$NbCl_6^- + 3\,H_2O = 3\,Cl^- + H^+ + NbCl_3(OH)(OH_2)_2^+ \qquad (18)$$

However, both the polarographic evidence described below and the controlled-potential electrolytic results to be set forth in a subsequent paper, show that dimeric species must be involved, and therefore eqns. (16) or (17) seem most likely to be correct. Dimers bridged by a single oxygen atom, rather than the doubly-bridged species shown, can also be made to fit the hydrolytic scheme, but intramolecular electron-transfer processes are found to be important and would seem more likely if the coordination octahedra share an edge (double bridging) than if they share only a corner (single bridging). Furthermore, the structures proposed in eqns. (16) and (17) are more plausible because they resemble those of niobium(V) alkoxides in alcoholic solutions and of solid $NbOCl_3$ and NbI_4[14].

The hydrolytic reactions shown in eqns. (16) and (17) can thus explain the precipitation and redissolution of niobium(V) on lowering the acid concentration. Boiled solutions, however, do not yield precipitates when diluted. It is possible that boiling and cooling could produce a cationic species by the reactions:

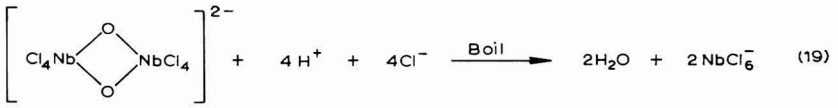

(19)

and

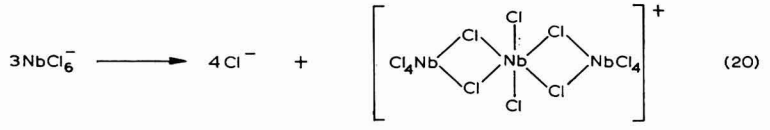

(20)

or

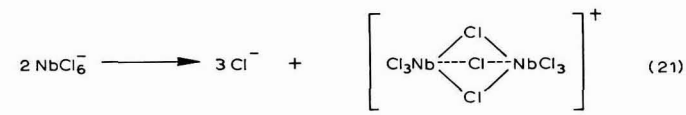

(21)

As the niobium–oxygen bond is stronger than the niobium–chlorine bond, higher temperatures should favor chloride ion over water in the competition for niobium. If the chloride bridges were slow to hydrolyze, the products of reactions (20) and (21) could not lose their charges by hydrolysis and would not precipitate.

TABLE 1

POLAROGRAPHIC DATA FOR NIOBIUM(V)

$C_{Nb}(mF)$	I_{1+2}	n_1	$(E_{\frac{1}{4}})_1$ (V vs. SCE)	$-dE/d\log[i_1/(i_{d1}-i_1)]$ (mV)	$(E_{\frac{1}{4}})_2$ (V vs. SCE)
A. Unboiled solutions					
0.0359		1.078	−0.497	60±2	
0.0691		1.074			
0.1423		1.096	−0.500	60	
0.2955		1.134	−0.500		
0.587		1.196	−0.505	61–68	
1.239	2.430	1.232	−0.504		−0.749
2.29	2.413	1.286	−0.514	≥69	−0.747
4.06	2.436	1.312	−0.508		−0.740
6.22	2.407	1.362	−0.514	79–92	−0.746
9.33	2.440	1.392	−0.515		−0.751
Av.:	2.425±0.012				−0.747±0.003
B. Boiled solutions					
0.0366		1.061			
0.0704		1.054			
0.1451		1.076	−0.492	≥60	
0.301		1.135	−0.495		
0.598	2.620	1.170	−0.498	63–73	
1.265	2.500	1.246	−0.504		−0.746
2.335	2.560	1.262	−0.506	*ca.* 72	−0.745
4.07	2.455	1.327	−0.509	≤82	−0.741
6.34	2.390	1.370	−0.516		−0.747
9.51	2.380	1.372	−0.519	62–88	−0.749
Max.:	2.62				Av.: −0.746±0.002

Polarography

Niobium(V) yields two waves at concentrations between 0.03 and 10 mF in 10.75 F hydrochloric acid, and their characteristics are summarized in Table 1. As the concentration of niobium(V) increases, the half-wave potential of the first wave becomes more negative and its diffusion current constant increases. Because the waves overlap somewhat, the height of the first wave was arbitrarily measured at the point of inflection between the two waves. Such values cannot be very accurate, but the typical polarogram shown in Fig. 2 portrays the obvious inequality of the wave heights*. At niobium(V) concentrations below 1 mF, the second wave is obscured

* The height of the first wave is nearly proportional to the 1.06 power of the concentration. The use of eqn. (1) is justified by the fact that the deviation of this relationship from linearity is far smaller than the effect of acid concentration shown in Fig. 1.

by hydrogen-ion discharge, but in more concentrated unboiled solutions its half-wave potential is -0.747 ± 0.003 V *vs.* SCE and the diffusion current constant of the combined waves is 2.425 ± 0.012.

Seven polarographic waves of arsenic(III) and (V) and tungsten(V) and (VI) in 10–12 *F* hydrochloric acid are reported in the literature to have diffusion current

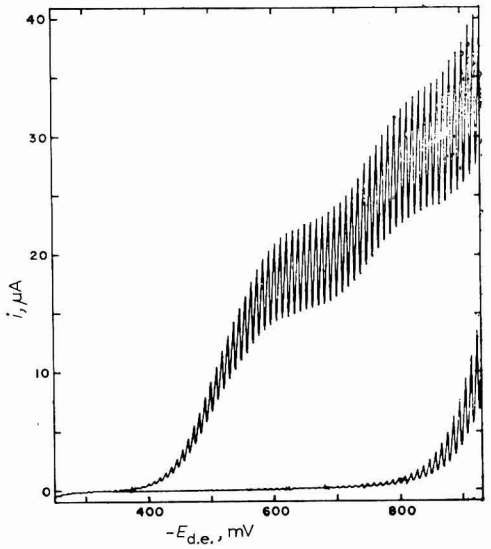

Fig. 2. Residual-current curve of 10.75 *F* hydrochloric acid and polarogram of 6.22 m*F* Nb(V) in the same medium.

constants given by $I = (1.34 \pm 0.06)n$[15,16]. Comparison with the above value suggests that the combined waves of niobium(V) in this medium correspond to a two-electron reduction. The effect of the polymerization considered above can be estimated by JANDER's rule[17], which predicts that a spherical k-mer will have a diffusion coefficient D_k given by

$$D_k/D_1 = k^{-\frac{1}{3}} \tag{22}$$

where D_1 is the diffusion coefficient of the monomer. If each reducible atom accepts n electrons regardless of the degree of polymerization, combining eqn. (22) with the Ilkovič equation yields:

$$I_k/I_1 = k^{-\frac{1}{6}} \tag{23}$$

Table 2 shows the values of the hypothetical diffusion current constant of monomeric niobium(V) obtained by assuming different values of k, together with the values of n obtained from these and the relation $n_1 = I_1/1.34$, which involves the assumption that the monomeric species of arsenic(III) and (V), tungsten(V) and (VI), and niobium(V) are of similar size. These show that the overall n-value for niobium must be 2, and suggest that the niobium species is dimeric.

The two wave heights became more nearly equal when ethylene glycol was added, and 0.99 electron/atom of niobium was consumed when a solution containing

5.45 mF niobium(V), 10.88 F hydrochloric acid, and 1.06 F ethylene glycol was subjected to controlled-potential electrolysis at a potential on the plateau of the first wave. These facts tend to confirm the n-values deduced for glycol-free solutions. The effects of ethylene glycol have been described by VIVARELLI *et al.* and were not investigated further; all other data reported here were obtained from glycol-free solutions.

TABLE 2

POLAROGRAPHIC n-VALUES AND DEGREES OF POLYMERIZATION OF NIOBIUM(V)

k	$k^{\frac{1}{3}}$	I_1 ($=2.425\,k^{\frac{1}{3}}$)	n_1
1	1	2.425	1.81
2	1.122	2.72	2.03
3	1.201	2.91	2.17
4	1.260	3.06	2.28
6	1.348	3.27	2.44
8	1.414	3.43	2.56

On this basis, n was taken as 2 for the combined waves of niobium(V). In Table 2, values of n_1 for the unboiled solutions were calculated from the equation:

$$n_1 = 2I_1/I_{1+2} \tag{24}$$

by taking I_{1+2}, the overall diffusion current constant of the combined waves, equal to the average value obtained at high concentrations. The value of n_1 increases with increasing concentration of niobium(V) from about 1.07 below 0.1 mF niobium to 1.39 with 9.3 mF niobium.

The data for boiled solutions in Table 1 were obtained by diluting a solution containing 9 mF niobium(V) and 10.1 F hydrochloric acid with 10.75 F acid. As Fig. 1 indicates, the solubility of reducible niobium was slightly exceeded in the more concentrated of these solutions, and this is responsible for the apparent decrease of I_{1+2} at high concentrations. Values of n_1 for boiled solutions less concentrated than

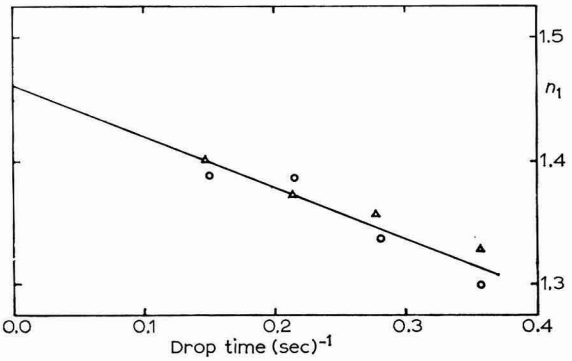

Fig. 3. Effect of drop time on the polarographic values of n_1. (○), data obtained with unboiled solns. containing 6.74 mF Nb(V); (△), data obtained with boiled solns. containing 6.34 mF Nb(V).

1 mF were calculated by using the highest measured value (2.62) of I_{1+2} in eqn. (24); allowance was made for the fact that not all of the niobium was in its reducible form in more concentrated solutions, by using the total measured diffusion current constant for each solution to compute the corresponding value of n_1. The diffusion coefficient of niobium(V) is slightly increased by boiling and cooling, which is not unreasonable in view of eqns. (16), (17), and (21), but the values of n_1 are identical within experimental error for the boiled and unboiled solutions. When the concentration of niobium was high, the values of n_1 increased slightly with increasing drop time and approached a limit close to 1.46 at infinite drop time, as shown in Fig. 3.

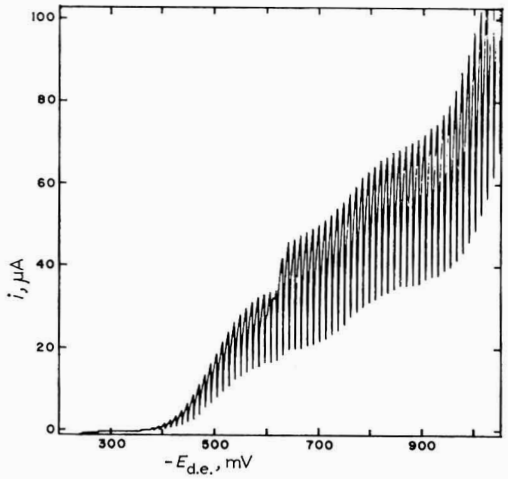

Fig. 4. Polarogram of 12.68 mF Nb(V) in 10.75 F hydrochloric acid, recorded without damping.

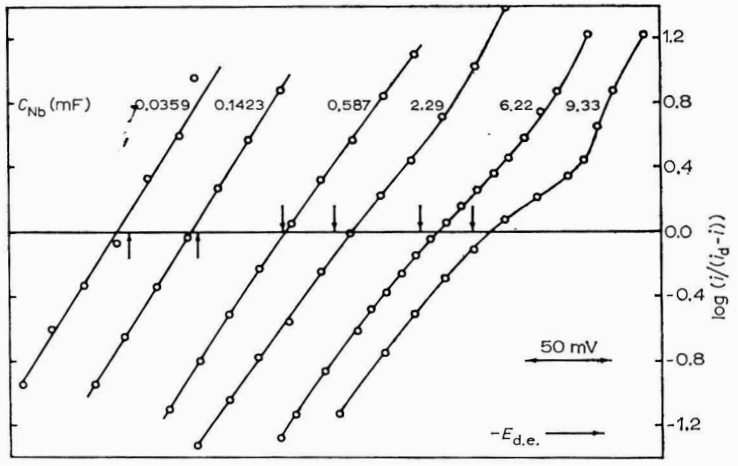

Fig. 5. Plots of log $[i/(i_d-i)]$ *vs.* $-E_{d.e.}$ for the first waves on polarograms of unboiled solns. containing 10.75 F hydrochloric acid and various concns. of Nb(V). The arrow near each plot marks the potential, −0.500 V *vs.* SCE, for that curve.

Polarograms of unboiled niobium solutions more concentrated than 8 mF are distorted by an indentation near the top of the first wave. This is most clearly visible on an undamped polarogram like the one in Fig. 4. LAVIRON AND DEGRAND[18] have shown that such behavior arises from the adsorption of an intermediate product of the electrode reaction on to the electrode surface, and its desorption at the potential where the current suddenly rises. Here the desorption occurs abruptly at -0.61 V *vs.* SCE; just before it begins, eqn. (24) and Fig. 4 indicate that the current corresponds to $n=1.1$.

Figure 5 shows plots of $E_{d.e.}$ *vs.* $\log[i/(i_d-i)]$ for the first wave obtained with unboiled solutions of niobium(V). At the lowest concentrations the plots are linear and have slopes close to -60 mV: the reduction appears to involve one electron and to be reversible, in agreement with the conclusion of VIVARELLI *et al.* In more concentrated solutions, however, the plots are curved and have higher average slopes. The plot for an unboiled 9.3 mF solution is markedly distorted by the adsorption mentioned above, whereas that for an equally concentrated boiled solution is a smooth curve having the shape that characterizes a wave consisting of two closely overlapping components whose heights are at least approximately equal.

The second wave, a totally irreversible one for which $\alpha n_a=0.76$, is unaffected by boiling or by changing the concentration of niobium.

TABLE 3

CHRONOPOTENTIOMETRIC DATA FOR 8.09 mF NIOBIUM(V) IN 10.75 F HYDROCHLORIC ACID

i/A (mA cm^{-2})	$i\tau_1^{\frac{1}{2}}/A$ (mA sec$^{\frac{1}{2}}$ cm^{-2})	$[\tau_1/(\tau_1+\tau_2)]^{\frac{1}{2}}$	$(E_{\tau/4})_1$ (V vs. SCE)	$(E_{\tau/4})_2$ (V vs. SCE)
0.758	1.84		-0.494	
	1.96	0.45	-0.494	
1.26	2.00	0.50	-0.494	-0.684
	1.89	0.45	-0.494	
	1.71		-0.501	
1.89	1.85	0.47	-0.499	-0.699
2.70	1.94		-0.501	
	1.74	0.49	-0.504	-0.707
	Av.: 1.87 ± 0.08	0.47 ± 0.02	-0.498 ± 0.004	

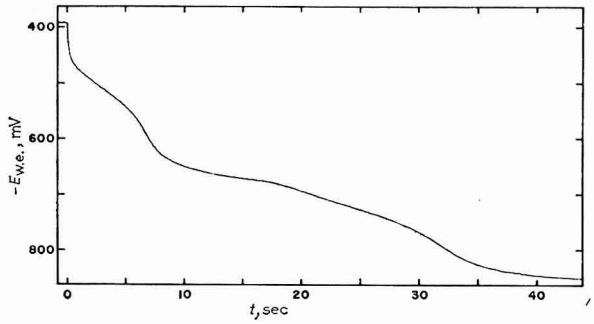

Fig. 6. Chronopotentiogram of 8.09 mF Nb(V) in 10.75 F hydrochloric acid, obtained with a current density of 0.76 mA/cm^2.

Chronopotentiometry

Chronopotentiograms of unboiled solutions containing 8.09 mF niobium(V) in 10.75 F hydrochloric acid have the characteristics summarized in Table 3. If the first transition time is less than about 2 sec, two waves of regular form are obtained. The first is reversible and can be identified with the first polarographic wave; it has $E_{\tau/4} = -0.500$ V *vs.* SCE, independent of current density. The second corresponds to the second, irreversible, polarographic wave; it has $E_{\tau/4}$ = *ca.* -0.7 V *vs.* SCE, becoming more negative as the current density increases. The values of $[\tau_1/(\tau_1+\tau_2)]^{\frac{1}{4}}$ show that $n_1 = n_2 = 1$.

An intermediate transition, for which $E_{\tau/4}$ is about -0.63 V, is also observed when τ_1 exceeds about 2 sec, as shown in Fig. 6. It is so ill-defined that its total transition time $(\tau_1+\tau_1')$ cannot be measured precisely; the average of the experimental values, $[(\tau_1+\tau_1')/(\tau_1+\tau_1'+\tau_2)]^{\frac{1}{4}} = 0.80$, is rather uncertain. In the light of the last sentence of the preceding paragraph, this must mean that each niobium atom has consumed a total of 1.6 electrons at the end of the intermediate transition. This is not far from the n-value obtained polarographically at long drop-times (Fig. 3).

CONCLUSIONS

Although VIVARELLI *et al.*[6-8] attributed the effect of the concentration of niobium(V) on the diffusion current constant of the first polarographic wave to a second-order disproportionation of niobium(IV), their explanation is untenable for several reasons. It does not account for the behavior shown in Fig. 3. At the temperature and acid activity used in this work, their data would correspond to a value of only 0.56 l mole^{-1} sec^{-1} for the rate constant of this disproportionation. If this were correct, only about 2.5% of the niobium(IV) formed during the life of a mercury drop at a potential on the plateau of the first wave in a 9 mF solution of niobium(V) would disproportionate during a 5-sec drop-time, which is far too little to account for an apparent n-value of 1.4. Their interpretation also does not account for the chronopotentiometric observations reported above. Moreover, as will be shown in a subsequent paper, the controlled-potential electrolysis of such a solution at a potential on the plateau of the first wave gave clear evidence that the reduction proceeds stepwise, with 0.5 electron/atom of niobium being consumed in the first step, and confirmed the existence of dimeric niobium species.

The following scheme accounts for all our observations. Here, we shall discuss only its relation to the polarographic and chronopotentiometric data; its behavior in controlled-potential electrolysis will be discussed in a subsequent paper. It is assumed that dimeric species of niobium(V) predominate in a 9 mF solution in 10.75 F hydrochloric acid, and that the following reactions occur:

$$[\mathrm{Nb(V)}]_2 + e \overset{-0.494\ \mathrm{V}}{\rightleftharpoons} [\mathrm{Nb(V)\cdot Nb(IV)}] \tag{25}$$

$$[\mathrm{Nb(V)\cdot Nb(IV)}] + e \overset{-0.52\ \mathrm{V}}{\rightleftharpoons} [\mathrm{Nb(IV)}]_2\ \text{(adsorbed)} \tag{26}$$

$$[\mathrm{Nb(IV)}]_2 \overset{k}{\rightarrow} [\mathrm{Nb(V)\cdot Nb(III)}]; \quad k < 0.5\ \mathrm{sec}^{-1} \tag{27}$$

$$[\mathrm{Nb(V)\cdot Nb(III)}]+e \overset{-0.63\ \mathrm{V}}{\rightleftharpoons} [\mathrm{Nb(IV)\cdot Nb(III)}] \tag{28}$$

$$[\mathrm{Nb(IV)}]_2+2e \xrightarrow{-0.747\ \mathrm{V}} [\mathrm{Nb(IV)\cdot Nb(II)}] \tag{29}$$

$$[\mathrm{Nb(IV)\cdot Nb(II)}] \xrightarrow{\text{fast}} 2\ \mathrm{Nb(III)} \tag{30}$$

The niobium(V) dimers are in equilibrium with monomers, which predominate at lower concentrations and undergo the following reactions:

$$\mathrm{Nb(V)}+e \overset{-0.494\ \mathrm{V}}{\rightleftharpoons} \mathrm{Nb(IV)} \tag{31}$$

$$\mathrm{Nb(IV)}+2e \xrightarrow{-0.747\ \mathrm{V}} \mathrm{Nb(II)} \tag{32}$$

$$\mathrm{Nb(IV)}+\mathrm{Nb(II)} \rightarrow 2\ \mathrm{Nb(III)} \tag{33}$$

At low niobium concentrations, the first wave is due simply to reaction (31), and the polarographic n-value is 1. At high concentrations it is due to reactions (25)–(28). The two overlapping waves composing the first wave are due to reactions (25) and (26), which have nearly equal half-wave potentials, and reaction (28). The niobium(IV) dimer is adsorbed on the electrode surface and does not undergo reaction (28) until it is desorbed. As the drop-time increases without limit, reaction (27) becomes more and more nearly complete and n_1 approaches 1.5, but at any finite drop-time this reaction is incomplete and n_1 has a somewhat smaller value. In chronopotentiometry, reaction (27) is unimportant if the first transition time is less than about 2 sec, and the first wave is then due to reactions (25) and (26). At lower current densities, however, the extent of reaction (27) becomes appreciable and reaction (28) gives rise to the intermediate transition, whose product represents the consumption of 1.5 electron/atom of niobium if reaction (27) is complete. In the presence of ethylene glycol, niobium(V) is present as a monomeric complex, and reaction (31) alone accounts for the first wave at all concentrations.

The value αn_a for the second polarographic wave admits the value $n_a=2$, in accord with eqns. (29) and (32). Controlled-potential coulometry gave evidence that niobium(II) is formed by the half-reactions responsible for this wave. At negative potentials and high concentrations of niobium, reactions (29) and (30) follow reactions (25) and (26) so rapidly that reaction (27) is bypassed, and the combined waves represent the consumption of 2 electrons/atom of niobium. Reaction (33) can be detected in controlled-potential coulometry because it gives rise to n-values above 2, but it is fast enough to make niobium(III) the only product that can be detected polarographically when the concentration of niobium is high enough to permit precise correction for the residual current in measuring the height of the second wave. In eqns. (30) and (33), niobium(III) is written as monomeric because its behavior in both polarography and controlled-potential electrolysis is too straightforward to require a more exotic assumption.

SUMMARY

The electroreduction and hydrolysis of niobium(V) in concentrated solutions

of hydrochloric acid were studied by polarography and chronopotentiometry and a detailed mechanism is presented to account for the data obtained. In dilute solutions, niobium(V) is monomeric and undergoes stepwise reduction to niobium(IV) and niobium(II), which react rapidly to yield niobium(III). In more concentrated (10 mF) solutions, niobium(V) is dimeric and is reduced first to a niobium(IV) dimer that disproportionates intramolecularly to [Nb(V)·Nb(III)], whose further reduction to [Nb(IV)·Nb(III)] yields an ill-defined intermediate transition in chronopotentiometry but merges with the first wave on a polarogram. At more negative potentials, the niobium(IV) dimer is reduced to [Nb(IV)·Nb(II)], which disproportionates rapidly to yield niobium(III). The niobium(V) dimer is probably anionic and its niobium atoms are probably joined by two oxygen bridges. Upon dilution of the acid, the dimer first loses its charge by hydrolysis and precipitates, and then on further hydrolysis redissolves as a non-reducible cation. If the solution is boiled before being diluted, a cationic chloride-bridged polymer is formed; this becomes non-reducible on hydrolysis but does not precipitate.

REFERENCES

1 H. REMY, *Treatise on Inorganic Chemistry*, Vol. 2, Elsevier Publishing Co., Amsterdam, 1956, pp. 104–110.
2 S. KALLMANN, *Niobium and Tantalum*, in *Treatise on Analytical Chemistry*, edited by I. M. KOLTHOFF AND P. J. ELVING, Part II, Vol. 6, Interscience Publishers, New York, 1964.
3 R. W. MOSHIER, *The Analytical Chemistry of Niobium and Tantalum*, Pergamon Press, New York, 1964.
4 W. F. HILLEBRAND, G. E. LUNDELL, H. A. BRIGHT AND J. I. HOFFMAN, *Applied Inorganic Analysis*, John Wiley & Sons, New York, 2nd ed., 1953, pp. 588 *ff*.
5 J. B. HEADRIDGE AND M. S. TAYLOR, *Analyst*, 87 (1962) 43.
6 D. COZZI AND S. VIVARELLI, *Ric. Sci.*, 23 (1953) 2244.
7 *Idem*, *Z. Elektrochem.*, 58 (1954) 177.
8 D. COZZI, S. VIVARELLI AND M. DISTEFANO, *ibid.*, 61 (1957) 849.
9 K. A. KRAUS AND G. E. MOORE, *J. Am. Chem. Soc.*, 73 (1951) 9.
10 L. MEITES AND T. MEITES, *Anal. Chem.*, 23 (1951) 1194.
11 Y. ISRAEL AND L. MEITES, *J. Electroanal. Chem.*, 8 (1964) 99.
12 L. MEITES AND S. A. MOROS, *Anal. Chem.*, 31 (1959) 23.
13 B. I. NABIVANETS, *Zh. Neorgan. Khim.*, 9 (1964) 1079.
14 D. C. BRADLEY, in *Inorganic Polymers*, edited by F. G. A. STONE AND W. A. G. GRAHAM, Academic Press, New York, 1962, pp. 413–416.
15 L. MEITES, *Polarographic Characteristics of Inorganic Substances*, in *Handbook of Analytical Chemistry*, edited by L. MEITES, McGraw-Hill Book Co., New York, 1963, pp. 5–50 *ff*.
16 L. MEITES, *Polarographic Techniques*, Interscience Publishers, New York, 1955.
17 G. JANDER AND H. SPANDAU, *Z. Physik. Chem.*, A185 (1939) 325.
18 E. LAVIRON AND C. DEGRAND, in *Polarography 1964*, edited by G. J. HILLS, Interscience Publishers, New York, 1966, p. 337.

ELECTROANALYTICAL CHEMISTRY AND INTERFACIAL ELECTROCHEMISTRY
Elsevier Sequoia S.A., Lausanne – Printed in The Netherlands

DISPROPORTIONATION OF ELECTROCHEMICALLY-GENERATED URANIUM(V) IN MOLTEN LiF–BeF_2–ZrF_4 AT 500°*

D. L. MANNING
Analytical Chemistry Division, Oak Ridge National Laboratory, Oak Ridge, Tennessee (U.S.A.)
GLEB MAMANTOV
Department of Chemistry, University of Tennessee, Knoxville, Tennessee (U.S.A.)
(Received November 22nd, 1967)

In a previous communication[1] it was pointed out that voltammetric studies in molten fluorides in the potential region anodic to the platinum quasi-reference electrode are complicated by the presence of traces of impurities such as H_2, OH^- and O^{2-}. It is in this light that we now believe that an earlier assignment[2] of an anodic wave to the oxidation of U(IV) to U(V) in molten LiF–NaF–KF (46.5–11.5–42 mole %) and LiF–BeF_2 (66–34 mole %) is in error. Voltammetric and chronopotentiometric studies of the reduction of U(IV) to U(III) in molten LiF–BeF_2–ZrF_4 at fast rates of voltage scan, and high current densities (short transition times) are described elsewhere[3]. The results of our study on the U(IV) oxidation by the same techniques are summarized here.

EXPERIMENTAL

The experimental set-ups employed in this study have been described previously[1]. The solvent used was LiF–BeF_2–ZrF_4 (65.6–29.4–5.0 mole %). Uranium was added as UF_4 or LiF–UF_4 (27 mole %). Pyrolytic graphite, platinum, and platinum–rhodium (10 and 40% Rh) working electrodes were employed. The experimental temperature was 500°.

Pyrolytic graphite electrodes were prepared by machining spectrographic-grade graphite rods into substrates with a 3/16 in. diam. × 1/2 in. long shoulder joined to a 1 mm diam. × 10 mm long tip. The substrates were coated with pyrolytic graphite to a thickness of approximately 2–3 mils. We are indebted to the Metals and Ceramics Division at ORNL for this service. After coating, the shoulder of the electrode is tapped with a 3/32 in. hole and the electrode is joined to a 1/8 in. nickel rod tapped with 3/32 in. threads. The electrodes are extremely fragile and utmost care is utilized in handling.

The controlled potential-controlled current cyclic voltammeter is described elsewhere[4]. With this instrument, scan rates from 0.05 to 500 V/sec are available and cell currents to 100 mA can be measured. In the controlled current mode, currents from a few microamperes to 100 mA can be passed through the cell. The built-in time base allows transition times from 400 sec to 4 msec to be measured.

* Research sponsored by the U. S. Atomic Energy Commission under contract with the Union Carbide Corporation.

A Tektronix Type 549 storage oscilloscope with a Type 1A7 pre-amplifier was used for read-out of the curves. Photographs were made with a Tektronix Type C-12 camera attachment and Type 42 Polaroid film.

RESULTS

Typical voltammograms for the oxidation of U(IV) at the unsheathed pyrolytic graphite (PG) working electrode are shown in Fig. 1. The oxidation of U(IV) occurs at $\sim +1.2$ V *versus* a platinum quasi-reference electrode. It should be noted that at scan rates much smaller than 1 V/sec, the re-reduction of the product is not observed.

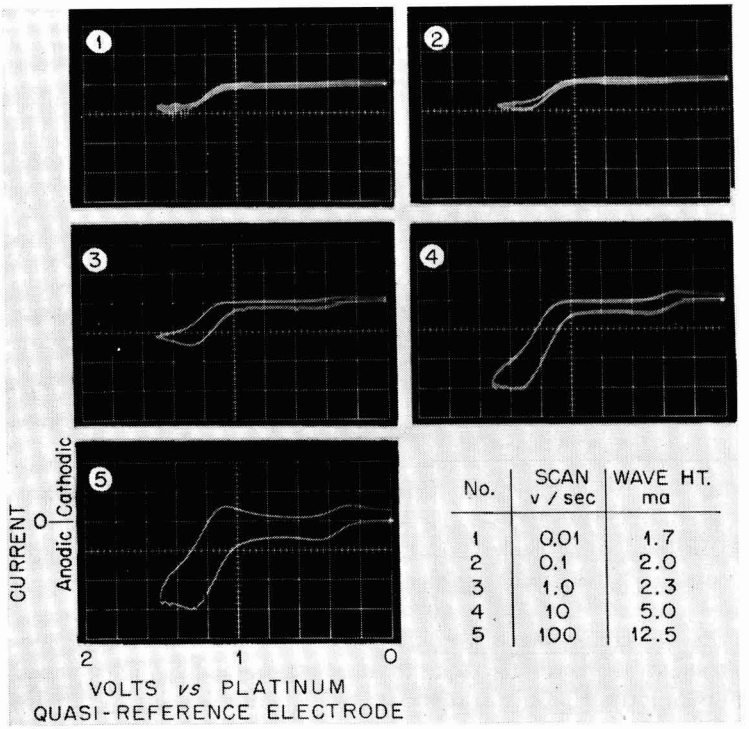

Fig. 1. Voltammograms for the oxidation of U(IV) at the pyrolytic graphite electrode. Formality of U(IV): $6.3 \cdot 10^{-2}$ *F*. Current scale in 5 is increased by a factor of 2.5.

At large scan rates (>10 V/sec), the peak currents for the oxidation of U(IV) and the re-reduction of the product (measured to the extension of the anodic curve[5]) are approximately equal. The small prewave at approximately +0.4 V (Fig. 1) is believed to be due to adsorbed H_2 (produced electrochemically from traces of H_2O or HF at 0 to +0.2 V) on the electrode. The dependence of $i_p/v^{\frac{1}{2}}$ on the scan rate at the PG electrode is shown in Fig. 2. At the Pt–10% Rh electrode, the function $i_p/v^{\frac{1}{2}}$ increases with v at scan rates greater than 2 V/sec. At scan rates <1 V/sec the behavior is similar to that at the PG electrode (Fig. 2). At scan rates <1 V/sec, the peak currents for the oxidation of U(IV) are considerably larger than the peak currents for the

reduction of U(IV) to U(III) at electrodes of comparable area; the peak currents for the oxidation and reduction of U(IV) at higher scan rates (>1–2 V/sec) are about the same.

The chronopotentiometric $i_0\tau^{\frac{1}{2}}$ for the oxidation of U(IV) at the PG electrode is shown in Fig. 3, as a function of $i_0^{\frac{2}{3}}$ (see below). $i_0\tau^{\frac{1}{2}}$ increases with i_0 (for large i_0) when the oxidation of U(IV) is carried out at the Pt–10% Rh electrode; the increase in $i_0\tau^{\frac{1}{2}}$ at small i_0 is less pronounced than at the PG electrode.

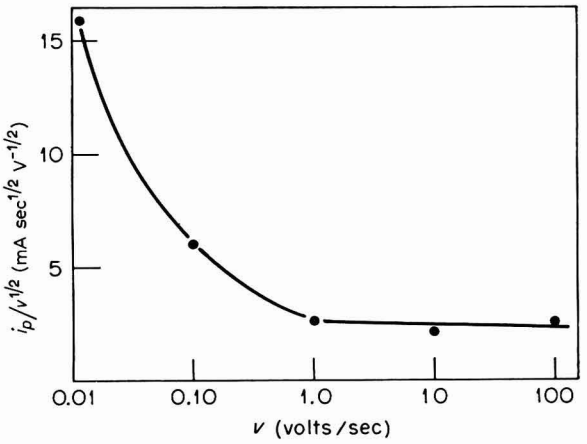

Fig. 2. Effect of scan rate on the voltammetric oxidation of U(IV).

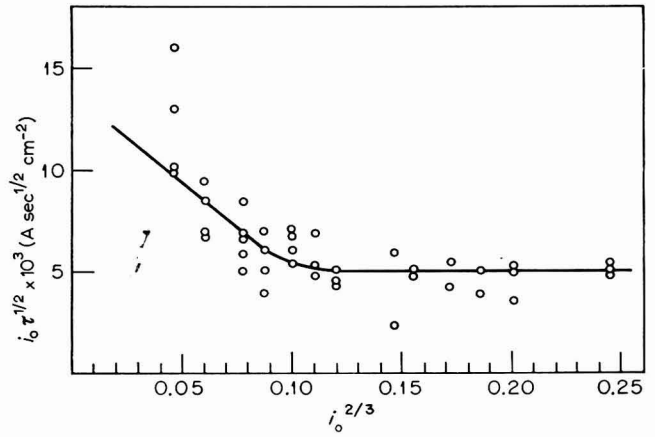

Fig. 3. Plot of chronopotentiometric data for U(IV) oxidation in $LiF–BeF_2–ZrF_4$ at 500°. Formality of U(IV): $6.3 \cdot 10^{-2}$ *F*.

Application of a potential step that corresponds to the peak potential of the U(IV) oxidation results in a steady current (measured on an X–Y recorder); a similar chronoamperometric experiment for the reduction of U(IV) results in the expected decrease of current with time.

DISCUSSION

The results for the oxidation of U(IV) at PG and Pt–10% Rh electrodes differ in that for the latter electrode the voltammetric $i_p/v^{\frac{1}{2}}$ increases with v (at large scan rates) and the chronopotentiometric $i_0\tau^{\frac{1}{2}}$ increases with i_0. This behavior points to the adsorption of the reactant U(IV) at the Pt–10% Rh electrode[6,7]. Additional evidence for the adsorption of U(IV), studied *via* the less complex reduction of U(IV) to U(III), is reported elsewhere[3]. The results obtained at the PG and Pt–10% Rh (at small scan rates) electrodes, such as: (a) much larger currents at small scan rates for oxidation of U(IV) than for the reduction of the same species, the currents being equal at large scan rates; (b) no current owing to re-reduction at small scan rates; and (c) steady current in chronoamperometry owing to the oxidation of U(IV), clearly point to a catalytic regeneration of U(IV) from U(V), the likely reactions being:

$$U(IV) \rightarrow U(V) + e$$

$$2\,U(V) \rightarrow U(IV) + U(VI).$$

The theory of linear sweep voltammetry for an electrochemical reaction followed by a second-order chemical reaction has not been worked out, but similarity with Case VII of NICHOLSON AND SHAIN[5] is to be expected. The variation of $i_p/v^{\frac{1}{2}}$ with v, observed for the oxidation of U(IV) at the PG electrode, is similar to that predicted for Case VII. It may be estimated[1] that the cylindrical diffusion effects may be neglected at scan rates >0.01 V/sec for the experimental conditions employed.

The disproportionation of U(V) in aqueous solutions, produced electrochemically under chronopotentiometric conditions, has been treated by FISCHER AND DRACKA[8] and by FELDBERG AND AUERBACH[9]. According to FISCHER AND DRACKA[8], the rate constant for the disproportionation is given by

$$k = 3\pi B/8CS^3 \qquad (1)$$

where C is the concentration (moles/cm^3), S is the slope for the plot of $i_0\tau^{\frac{1}{2}}$ *vs.* $i_0^{\frac{3}{2}}$ (in the region where the slope is negative) and B is the value of $i_0\tau^{\frac{1}{2}}$ at large current densities ($i_0\tau^{\frac{1}{2}}$ is then constant). This equation assumes that the diffusion coefficients for the oxidized and reduced forms are equal.

The results obtained in this work (Fig. 3) are in agreement with the predicted[8] variation of $i_0\tau^{\frac{1}{2}}$ with $i_0^{\frac{3}{2}}$. Because of poor reproducibility, particularly at the longer transition times, the rate constant may only be given as $\sim 1.6 \cdot 10^5$ cm^3/mole sec (at 500°). Again, effects of cylindrical diffusion were found to be negligible at the longer transition times, according to the criteria of PETERS AND LINGANE[10]. It is believed that the poor reproducibility is caused by the attack of UF_6, probably produced in the disproportionation reaction, on the electrode material. Better reproducibility, presumably due to increased resistance to UF_6, was noted in going from Pt, to Pt–10% Rh, and Pt–40% Rh as the electrode materials for the study of oxidation of U(IV).

It is interesting to note that although the crystalline fluoride complexes of U(V) are stable at 350°–400°[11], an increase in temperature to 500°, accompanied by a change to a liquid phase and medium of relatively low free fluoride ion activity (primary anions are believed to be BeF_4^{2-} and ZrF_6^{2-}), results in rapid decomposition of U(V).

SUMMARY

Electrochemical oxidation of U(IV) has been studied in molten LiF–BeF_2–ZrF_4 (65.6–29.4–5.0 mole %) at 500° by means of voltammetry (scan rate, v, 0.01–100 V/sec), chronopotentiometry, and chronoamperometry at unsheathed pyrolytic graphite and Pt–10% Rh electrodes. The following results point to the disproportionation of the electrochemically-produced U(V): (a) no voltammetric currents owing to the re-reduction of the product at $v \ll 1$ V/sec, the peak currents (i_p) for the oxidation of U(IV) and re-reduction of the product being approximately equal at $v \gg 1$ V/sec; (b) peak currents for the reduction of U(IV) to U(III) and the oxidation of U(IV) are the same at large scan rates; (c) the observed increase in $i_p/v^{\frac{1}{2}}$ *vs.* v at $v < 1$ V/sec; (d) the observed variation of $i_0\tau^{\frac{1}{2}}$ with $i_0^{\frac{3}{2}}$ is in agreement with theoretical predictions of FISCHER AND DRACKA[8]. At Pt–10% Rh electrodes, evidence for the adsorption of U(IV) has been obtained. The reproducibility of voltammograms and chronopotentiograms for the oxidation process is poor, presumably owing to attack of the working electrode by U(VI) produced in the disproportionation.

REFERENCES

1 G. MAMANTOV AND D. L. MANNING, *Anal. Chem.*, 38 (1966) 1494.
2 D. L. MANNING AND G. MAMANTOV, *J. Electroanal. Chem.*, 6 (1963) 328.
3 G. MAMANTOV AND D. L. MANNING, *J. Electroanal. Chem.*, 18 (1968) 309.
4 T. R. MUELLER AND H. C. JONES, *Ann. Progr. Rept., Anal. Chem. Div., ORNL-4039*, Jan. 1967, p. 1.
5 R. S. NICHOLSON AND I. SHAIN, *Anal. Chem.*, 36 (1964) 706.
6 R. H. WOPSCHALL AND I. SHAIN, *Anal. Chem.*, 39 (1967) 1514.
7 S. V. TATWAWADI AND A. J. BARD, *Anal. Chem.*, 36 (1964) 2.
8 O. FISCHER AND O. DRACKA, *Collection Czech. Chem. Commun.*, 24 (1959) 3046.
9 S. W. FELDBERG AND C. AUERBACH, *Anal. Chem.*, 36 (1964) 505.
10 D. G. PETERS AND J. J. LINGANE, *J. Electroanal. Chem.*, 2 (1961) 1.
11 R. A. PENNEMAN, L. B. ASPREY AND G. STURGEON, *J. Am. Chem. Soc.*, 84 (1962) 4608.

ELECTROANALYTICAL CHEMISTRY AND INTERFACIAL ELECTROCHEMISTRY
Elsevier Sequoia S.A., Lausanne – Printed in The Netherlands

DIE ELEKTRISCHE LEITFÄHIGKEIT DER SYSTEME $BiCl_3$–Sn, $BiCl_3$–In UND $BiCl_3$–Cd IM SCHMELZFLUSS

TEIL I. UNTERSUCHUNGSMETHODE UND MESSERGEBNISSE

P. LAMBRECHT UND R. BERTRAM

Institut für Physikalische Chemie, Abt. Elektrochemie, Technische Hochschule, Braunschweig (Deutschland)

(Eingegangen am 12. Oktober 1967)

EINLEITUNG

Von den Metall–Metallsalzmischungen im flüssigen Zustand wurden bisher ausschliesslich solche Schmelzen konduktometrisch untersucht, die aus dem Salz und dem korrespondierenden Metall bestehen[1]. Über Art und Ladungsverteilung der bei der Zugabe des Metalles entstehenden Spezies und der damit verbundenen Umstrukturierung der Ausgangsschmelze liegen nur wenige gesicherte Daten vor. Durch die Aufnahme von Fremdmetallen, werden in der Schmelze andersartige Ionen und Ionenassoziate gebildet, die den Transportmechanismus, also auch die Leitfähigkeit in charakteristischer Weise verändern. Für diese Untersuchung wurde als "Lösungsmittel" $BiCl_3$ gewählt, weil der Schmelzpunkt niedrig liegt, und weil eine bemerkens-

TABELLE 1

CHEMISCHE UND PHYSIKALISCHE EIGENSCHAFTEN VON WISMUTTRICHLORID

Molekulargewicht	315.371 g Mol^{-1}
Schmelzpunkt	232° (760 mm Hg)[2]
Siedepunkt	447° (760 mm Hg)[2]
Dichte (300°)	3.79 g cm^{-3} [3]
	Messwerte zwischen 260 und 340°
	weitere Literatur[4–7]
Viskosität (300°)	0.230 abs. Einheiten[3]
	Messwerte zwischen 260 und 340°
Dampfdruck (300°)	30.4 mm Hg[10]
	Messwerte zwischen 235 und 410°
Oberflächenspannung (331°)	58.1 erg cm^{-2} [5]
	Messwerte zwischen 271 und 382°
Leitfähigkeit (300°)	0.497 Ω^{-1} cm^{-1} [6]
	Messwerte zwischen 226 und 600°
	weitere Literatur[3,8,9,11]
magn. Suszeptibilität (330°)	$-0.277 \cdot 10^{-6}$ [4]
	Messwerte zwischen 280 und 430°
gasförmige $BiCl_3$-Molekel (220–230°)	
Winkel Cl–Bi–Cl	100 ± 6°
Bindungsabstände Bi–Cl	2.48 ± 0.02 Å [12]
Angaben zur Darstellung von $BiCl_3$	[6,13]

werte Aufnahmefähigkeit für eine Reihe von Metallen beobachtet wird. Die chemischen und physikalischen Eigenschaften des Wismuttrichlorids sind weitgehend bekannt (Tab. 1). Die elektrische Leitfähigkeit von reinem geschmolzenen $BiCl_3$ zeigt insofern eine Besonderheit, als oberhalb der Schmelztemperatur bei etwa 450° ein Leitfähigkeitsmaximum[8] auftritt.

Das korrespondierende System $BiCl_3$–Bi ist mehrfach auf thermodynamischer[7,10,14–16], optischer[17,18], magnetischer[4] und elektrochemischer[19–21] Grundlage untersucht worden. Von ATEN[3], VOIGT UND BILTZ[6], GRANTHAM[9] sowie ICHIKAWA UND SHIMOJI[11] wurde die elektrische Leitfähigkeit der flüssigen $BiCl_3$–Bi-Mischungen gemessen. Die Folgerungen aus diesen Untersuchungen besitzen noch sehr hypothetischen Charakter, so dass für eine endgültige Aufklärung zusätzliche Untersuchungen erforderlich sind. Es ist die Aufgabe der vorliegenden Arbeit, durch Vergleich mit den am System $BiCl_3$–Bi gewonnenen Erkenntnissen zum besseren Verständnis metalldotierter homogener $BiCl_3$-Schmelzen beizutragen.

EXPERIMENTELLES

Leitfähigkeitsmessungen von geschmolzenen Elektrolyten wurden bisher überwiegend mit Wechselstrombrücken niedriger Frequenz ausgeführt. Die Elektroden aus Metall oder Kohle stehen dabei in direktem Kontakt mit dem Messgut. Die Nachteile dieser Methoden liegen in den schwer kontrollierbaren Einflüssen der Phasengrenzimpedanz, in einer Veränderung der Elektrodenoberfläche und in einer Verunreinigung der Schmelze, hervorgerufen durch eine gewisse Löslichkeit des Elektrodenmaterials. Bei den vorliegenden Untersuchungen wird ein oscillometrisches Verfahren benutzt[22], das unter Verwendung geeigneter "elektrodenloser" Zellen[23] die Leitfähigkeit mit geringerem Zeitaufwand zu messen gestattet. Es besteht im wesentlichen aus einem Messwert-Frequenz-Wandler, in dessen frequenzbestimmendes Netzwerk die Messzelle geschaltet ist. Eine auf den Leitwert des Messgutes ansprechende Differenzfrequenz von Wandler und zusätzlichem Messender wird über einen Frequenzmesser auf den Eingang eines Kompensationsschreibers übertragen, so dass eine verzögerungsfreie und kontinuierliche Registrierung gewährleistet wird.

Die ungefüllte Zelle (Abb. 1) besteht im wesentlichen aus zwei Zylindern, die über eine Kapillare miteinander verbunden sind. Um die Füllmenge klein zu halten und um eine hinreichend grosse Wandkapazität zu erhalten, sind beide Zylinder konzentrisch eingestülpt. Die Zelle ist so bemessen, dass sie im temperaturkonstanten Bereich des Ofens liegt. Die Abmessung der beiden Hohlzylinder werden von den Erfordernissen der sog. *elektrodenlosen* Leitfähigkeitsmessungen bestimmt[23]. Die als Kontakte dienenden Metallbeläge werden aussen auf die doppelwandigen Hohlzylinder aufgebracht. Die elektrische Wirkungsweise der Messzellen ist aus Abb. 2 zu ersehen. Der innerhalb der gestrichelten Umrandung liegende Teil gibt das vollständige Ersatzschaltbild der Zelle im Ofen an. R stellt dabei den ohmschen Widerstand des Messgutes dar. Die an der Grenzfläche zwischen Quarzwand und Zellinhalt auftretenden Grenzschichten sind nicht berücksichtigt worden, da diese gegenüber dem Einfluss der Quarzwand vernachlässigt werden können. Mit den Werten für den spezifischen Widerstand und für die DK der Quarzglaswand lässt sich abschätzen, dass der Einfluss der Elemente $R_{w,1}$ und $R_{w,2}$ gegenüber $1/\omega C_{w1}$, bezw. $1/\omega C_{w,2}$ (Abb. 2) nicht ins Gewicht fällt, da die beiden ohmschen Widerstände je nach Temperatur bis zu 6 Grös-

senordnungen kleiner sind als die konstanten kapazitiven Widerstände, so dass im verwendeten Frequenzbereich Widerstandsänderungen der Quarzglaswand erst oberhalb 400° zu berücksichtigen sind. Bei gewöhnlichen Gläsern mit höheren Leitfähigkeiten sind je nach Glassorte schon oberhalb 100–200° Korrekturen erforderlich. Der Einfluss der Dielektrizitätskonstanten der Schmelze, der im Symbol K (Abb. 2) Berücksichtigung findet, wird unwirksam, da R um mehrere Grössenordnungen kleiner ist als $1/\omega K$[22–24]. In den Messwert gehen daher neben R nur die konstanten Blindwiderstände der Quarzglaswand $1/\omega C_{w,1}$ und $1/\omega C_{w,2}$ ein.

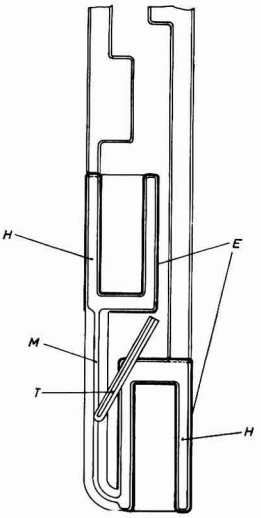

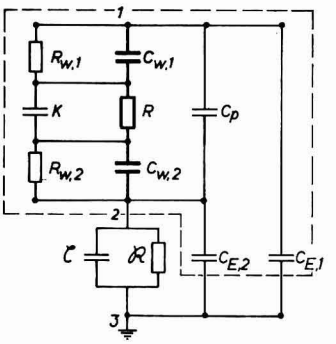

Abb. 1. Bauweise der Messzellen. (E) Metallbeläge; (H), Hohlzylinder; (M), Messkapillare; (T), Thermoelementkapillare.

Abb. 2. Ersatzschaltbild der Zellen im Ofen (umrandeter Teil). (R), ohmscher Kapillarwiderstand; (K), Kapazität des Inhaltes der Messkapillare; ($C_{w,1}$, $C_{w,2}$), Kapazitäten der Quarzwände; ($R_{w,1}$, $R_{w,2}$), ohmsche Widerstände der Quarzwände; (C_p), Streukapazitäten; ($C_{E,1}$, $C_{E,2}$), Streukapazitäten zwischen Hohlzylindern und Erde.

Das elektrische Verhalten der Zelle wird durch eine entsprechende Phantomschaltung simuliert. Dazu sind die Streukapazitäten zwischen den Zuleitungen und den äusseren Flächen der beiden Hohlzylinder C_p (Abb. 2), die Kapazitäten der Hohlzylinder gegen die Heizspirale des Ofens, $C_{E,1}$ und $C_{E,2}$ sowie die Kapazitäten der Quarzwände mit ausreichender Genauigkeit bestimmt worden. Mit einer so angepassten Schaltung, die auf ± 0.1 abs. Ω genau vermessene Widerstände zwischen 100 und 1000 Ω enthält, wird die erforderliche Zuordnung zwischen Widerständen und Differenzfrequenzen vorgenommen. Zur Bestimmung der Zellkonstante wird 3 *N* KCl-Lösung in die Zelle gefüllt, deren Leitfähigkeit bekannt ist zu $\varkappa_{25°} = 0.2984\,\Omega^{-1}\mathrm{cm}^{-1}$ [25]. Die bei den vorliegenden Untersuchungen verwendeten Zellen ergaben Formfaktoren zwischen 100–200 cm^{-1}.

Die thermische Ausdehnung der Quarzkapillare bei einer Temperaturerhöhung von 0 auf 400° ($\alpha = 0.54 \cdot 10^{-6}\ \mathrm{grad}^{-1}$) ist vernachlässigbar gering[26], so dass die Werte für die Formfaktoren ohne Korrektur bei 400° verwendet werden können.

Das die Messkapillare berührende Thermoelement aus Chromel- und Alumellegierung wird an einen Kompensationsschreiber angeschlossen. Die Schreiberskala wird mit Hilfe der Schmelzpunkte von Zinn, Cadmium und Zink in °C geeicht. Die Temperaturangaben können bei 300° Fehler von etwa $\pm 0.5°$ aufweisen.

Zur Temperierung der Zelle wird ein elektrisch beheizter Rohrofen verwendet. Die beheizte Länge des Rohres beträgt 500 mm, die lichte Weite des Arbeitsrohres 50 mm, die temperaturkonstante Zone ist 150 mm lang.

Das verwendete Zinnmetall ist von p.a. Qualität, die Reinheit des Cadmium beträgt 99.95% (beide Fa. Riedel de Haen), die des Indiums 99.99% (Unterharzer Berg- und Hüttenwerke).

Als Ausgangssalz wird Wismuttrichlorid, krist. (Riedel de Haen) verwendet. Die Feuchtigkeit und ein grosser Teil des Oxidchlorids im $BiCl_3$ wird durch Erwärmen bzw. durch Einleiten von HCl-Gas bei *ca.* 300° entfernt. Andere Verunreinigungen und Reste an Oxidchlorid werden durch Destillation des Salzes beseitigt. Wegen der Empfindlichkeit des gereinigten Salzes gegenüber Feuchtigkeit wird die Schmelze während der Messung durch sauerstoffreies, trockenes Argon abgedeckt.

Von jedem der drei Systeme $BiCl_3$–Sn, $BiCl_3$–In und $BiCl_3$–Cd werden zwei Versuchsreihen ausgewertet. Es werden nur die Messungen in der homogenen Schmelzphase berücksichtigt, also ausserhalb der auftretenden Mischungslücke. Nach entsprechender Eichung sind die registrierten Messwerte auf 0.005 $\Omega^{-1}\,cm^{-1}$ genau ablesbar.

MESSERGEBNISSE

Abbildung 3 stellt die Temperaturabhängigkeit der elektrischen Leitfähigkeit für reines $BiCl_3$ dar. Aufgeführt sind alle Werte, die zu Beginn jeder Messreihe mit reinem $BiCl_3$ ohne Metallzusatz gemessen werden. Lediglich die erste Wertefolge stammt aus einer einzelnen Messung. Es handelt sich in allen Fällen um getrennt voneinander getrocknetes und destilliertes Wismutchlorid, das zu verschiedenen

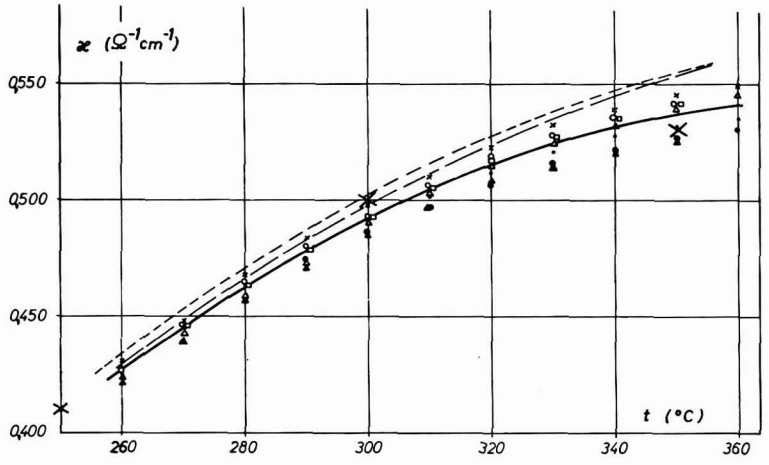

Abb. 3. Spezifische Leitfähigkeiten der reinen $BiCl_3$-Schmelze. Eigene Werte: (·), Einzelmessung; (○), 1; (×), 2; (△), 3; (□), 4; (●), 5; (▲), 6; Messreihe. (——), Mittelwertskurve; Werte nach: (— —), ATEN[3]; (– – –), GRANTHAM[9]; (×), ICHIKAWA UND SHIMOJI[11].

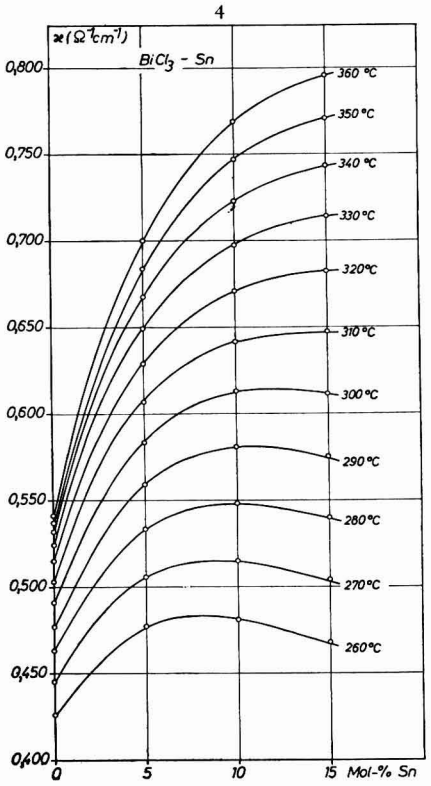

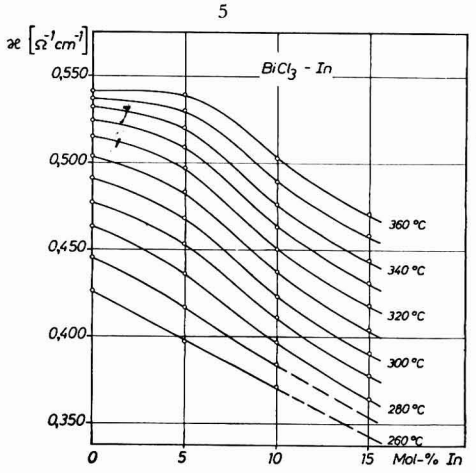

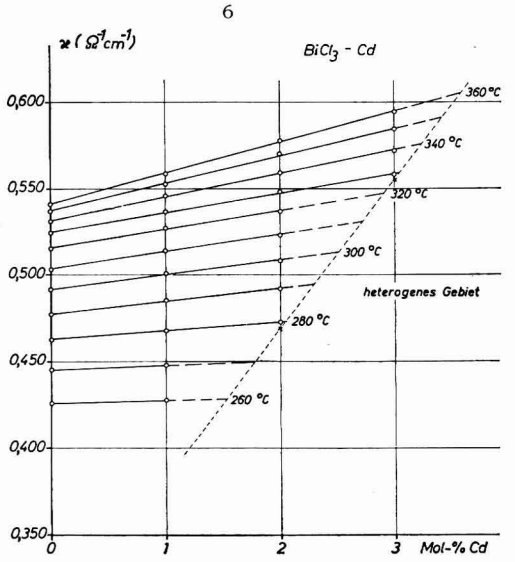

Abb. 4–6. Spezifische Leitfähigkeiten (4) zinnhaltiger $BiCl_3$-Schmelzen; (5) indiumhaltiger $BiCl_3$-Schmelzen; (6), cadmiumhaltiger $BiCl_3$-Schmelzen.

Zeitpunkten bezogen worden ist. Die Werte streuen etwa $\pm 1.8\%$ um die dick ausgezogene Mittelwertskurve.

Die Abweichungen unserer Ergebnisse für reines Salz von den entsprechenden Werten anderer Autoren[3,9,11] sind einmal in den unterschiedlichen Ausgangssubstanzen und Reinigungsmethoden zu suchen; zum anderen sind die Vergleichsmessungen mit direktem Elektrodenkontakt und niedrigfrequentem Wechselstrom ausgeführt worden. Der Einfluss der Phasengrenzimpedanz auf die Messwerte ist dabei nicht hinreichend berücksichtigt worden.

In Abb. 4 sind die Leitfähigkeiten der zinnhaltigen Schmelzen mit der Temperatur als Parameter gegen die Metallzugabe aufgetragen. Es handelt sich um Mittelwertskurven aus je zwei Messungen an Schmelzen mit 0, 5, 10 und 15 Mol.-% Fremdmetall. Die Streuung beträgt für diese Kurven etwa $\pm 1.8\%$.

Die Mittelwertskurven für die Konzentrationsabhängigkeit der Leitfähigkeiten des Systems $BiCl_3$–In (Abb. 5) ergeben ein ganz anderes Bild als die Werte des Systems $BiCl_3$–Sn. Es sind gleichfalls zwei Messreihen ausgeführt worden, die die gleichen prozentualen Abweichungen von den Mittelwerten aufweisen wie die Messwerte des $BiCl_3$–Sn-Systems. Es ergeben sich im Vergleich zu den entsprechenden Schmelzen des vorangegangenen Systems wesentlich geringere Leitfähigkeiten.

Im Unterschied zu den Systemen $BiCl_3$–Sn und $BiCl_3$–In sind die $BiCl_3$–Cd-Schmelzen nur bis zu 4 Mol.-% Metall untersucht worden. Mischungen mit 4 Mol.-% Metall und darüber im Temperaturbereich zwischen 260 und 360° liegen in einem zweiphasigen Gebiet, so dass Messungen bei 4 Mol.-% Metall nicht ausgewertet werden. Die Leitfähigkeiten der reinen Salzschmelze und der Schmelzen mit 1 Mol.-% Cadmium verlaufen kontinuierlich (Abb. 6). Die Zugabe an Cadmium bewirkt eine Leitfähigkeitserhöhung, die mit abnehmender Temperatur jedoch bis auf einen minimalen Rest abnimmt. An den Punkten ($t=278°$; $\varkappa=469\ \Omega^{-1}\ cm^{-1}$; 2 Mol.-%) und ($t=328°$; $\varkappa=0.556\ \Omega^{-1}\ cm^{-1}$; 3 Mol.-%) wird die Grenze des heterogenen Gebietes erreicht. Der Beginn des heterogenen Gebietes wird in Abb. 6 mit einer durch die bezeichneten Punkte gelegten Geraden angedeutet.

Die Diskussion der Messergebnisse wird in einem 2. Teil in Zusammenhang mit einer Strukturbesprechung der reinen $BiCl_3$-Schmelze gegeben.

An dieser Stelle sei der Deutschen Forschungsgemeinschaft und dem Verband der Chemischen Industrie gedankt, die durch grosszügige Unterstützung die Durchführung dieser Arbeit ermöglicht haben.

ZUSAMMENFASSUNG

Mit Hilfe einer oszillometrischen Methode wurden die Temperatur- und Konzentrationsverläufe der elektrischen Leitfähigkeit von zinn-, indium- und cadmium-haltigen $BiCl_3$-Schmelzen unter beträchtlicher Verkürzung der bisher im Hochtemperaturbereich üblichen Messzeiten bestimt. Bei allen untersuchten Mischungen nimmt mit zunehmender Temperatur die elektrische Leitfähigkeit zu, der Temperaturkoeffizient nimmt ab. Mit Fremdmetallzugabe erfolgt in den Systemen $BiCl_3$–Sn und $BiCl_3$–Cd eine Zunahme, im System $BiCl_3$–In eine Abnahme der Leitfähigkeit. Bei Temperaturen unter 310° treten in $BiCl_3$–Sn-Schmelzen Maxima in den Leitfähigkeitsisothermen auf.

SUMMARY

The temperature- and concentration-dependence of the electrical conductivity of tin-, indium- and cadmium-containing $BiCl_3$ melts was determined by an oscilloscopic method permitting a considerable shortening of the usual period in the high temperature region. With all the mixtures investigated, the electrical conductivity increased with increasing temperature, while the temperature coefficient decreased. Addition of the foreign metal caused an increase in the conductivity of $BiCl_3$–Sn and $BiCl_3$–Cd systems and a decrease in the $BiCl_3$–In system. At temperatures below 310°, a maximum in the conductivity isotherm occurs in $BiCl_3$–Sn melts.

LITERATUR

1 R. BERTRAM, *Z. Physik. Chem. N.F.*, 51 (1966) 183.
2 H. REMY, *Lehrbuch d. anorg. Chemie*, Bd. I, 10. Aufl., Leipzig, 1960.
3 A. H. W. ATEN, *Z. Physik. Chem.*, 66 (1909) 641.
4 N. H. NACHTRIEB, *J. Phys. Chem.*, 66 (1962) 1163.
5 F. M. JAEGER, *Z. Anorg. Allgem. Chem.*, 101 (1917) 1.
6 A. VOIGT UND W. BILTZ, *Z. Anorg. Allgem. Chem.*, 133 (1924) 277.
7 F. J. KENESHEA UND D. CUBICCIOTTI, *J. Phys. Chem.*, 62 (1958) 843.
8 L. F. GRANTHAM UND S. J. YOSIM, *J. Phys. Chem.*, 67 (1963) 2506.
9 L. F. GRANTHAM, *J. Chem. Phys.*, 43 (1965) 1415.
10 D. CUBICCIOTTI, F. J. KENESHEA UND C. M. KELLY, *J. Phys. Chem.*, 62 (1958) 463.
11 K. ICHIKAWA UND M. SHIMOJI, *Trans. Faraday Soc.*, 62 (1966) 3543.
12 H. A. SKINNER UND L. E. SUTTON, *Trans. Faraday Soc.*, 36 (1940) 681.
13 O. HÖNIGSCHMID UND L. BIRKENBACH, *Z. Elektrochem.*, 26 (1920) 403; *Chem. Ber.*, 54 (1921) 1889.
14 B. G. EGGINK, *Z. Physik. Chem.*, 64 (1908) 449.
15 S. Y. YOSIM, A. J. DARNELL, W. G. GEHMAN UND S. W. MAYER, *J. Phys. Chem.*, 63 (1959) 230.
16 S. W. MAYER, S. J. YOSIM UND L. E. TOPOL, *J. Phys. Chem.*, 64 (1960) 238.
17 H. A. LEVY, M. A. BREDIG, M. D. DANFORD UND P. A. AGRON, *J. Phys. Chem.*, 64 (1960) 1959.
18 C. R. BOSTON UND G. P. SMITH, *J. Phys. Chem.*, 66 (1962) 1178; 67 (1963) 1849.
19 L. E. TOPOL UND R. A. OSTERYOUNG, *J. Electrochem. Soc.*, 108 (1961) 573.
20 L. E. TOPOL, S. J. YOSIM UND R. A. OSTERYOUNG, *J. Phys. Chem.*, 65 (1961) 1511.
21 Y. K. DELIMARSKII UND Y. G. ROMS, *Ukr. Khim. Zh.*, 31, 9 (1965) 998.
22 R. BERTRAM, *Z. Anal. Chem.*, 222 (1966) 189.
23 R. BERTRAM UND K. CRUSE, *Ber. Bunsenges. Phys. Chem.*, 69 (1965) 215.
24 K. CRUSE UND R. HUBER, *Die Hochfrequenztitration*, Verlag Chemie GmbH Weinheim/Bergstr., 1967.
25 LANDOLT-BÖRNSTEIN, 6. Aufl., Bd. II, 7. Teil, 1960.
26 L. HOLBORN UND F. HENNING, *Ann. Physik*, 4, 10 (1903) 446.

ELECTROANALYTICAL CHEMISTRY AND INTERFACIAL ELECTROCHEMISTRY
Elsevier Sequoia S.A., Lausanne – Printed in The Netherlands

POLAROGRAPHY OF COPPER(II)–CYCLOHEXANE-1,2-DIAMINE-N,N,N',N'-TETRAACETIC ACID

A. M. GIULIANI, D. GATTEGNO AND A. FURLANI
Centro per lo studio dei composti di coordinazione del C.N.R., Istituto di Chimica generale e inorganica, Università di Roma (Italy)
(Received August 9th, 1967; in revised form January 16th, 1968)

INTRODUCTION

In a previous study[1] of the polarographic behaviour of Cu(II) in complexing solutions of 1,4-cyclohexanediaminetetraacetic acid, a positive shift of the half-wave potential with ligand concentration was observed when excess metal was present in solution.

With the same ligand, the Zn(II) ion shows an analogous behaviour[2].

A systematic investigation of the polarographic behaviour of Cu(II) complexones in the presence of excess metal has been undertaken to support the conclusions of the preceding papers.

In the present work, the results concerning the Cu(II)–1,2-cyclohexanediaminetetraacetic acid system are reported.

EXPERIMENTAL

Chemicals and apparatus

Cyclohexane-1,2-diamine-N,N,N',N'-tetraacetic acid (1,2-CyDTA) was a certified Merck reagent and was used without purification.

All other chemicals were reagent-grade.

Experimental conditions were the same as in the previous work[1] on 1,4-CyDTA, except for the gelatine concentration. A concentration of 0.003% was sufficient to suppress the polarographic maxima with the present ligand.

Reference should be made to the same paper[1] for details of instruments, cells and electrodes.

The capillary constant was 1.756 $mg^{\frac{2}{3}}\ sec^{-\frac{1}{2}}$ and the drop-time 7.76 sec in water at open circuit.

The wave height was always determined at the maximum of the oscillations.

RESULTS

The effect of both pH and ligand concentration has been studied; the pH was varied from 3 to 7 and the ligand: metal ratio from 1:20 to 100:1. Preliminary experiments at constant pH and metal: ligand ratio indicated that the half-wave potential is strongly influenced by the ionic strength. Thus, while a concentration of $1.0 \cdot 10^{-3}\ M$

of Cu(II) could be used in the presence of excess metal, it was necessary to decrease the copper concentration to $5.0 \cdot 10^{-4}$ M for measurements with excess ligand in order to keep the ionic strength constant also at the highest ligand:metal ratio (100:1). On the other hand, $E_{\frac{1}{2}}$ for the complex wave shifts to more negative potentials as the metal ion concentration increases and potential data in the presence of excess metal are therefore not directly comparable with data in the presence of excess ligand.

Effect of ligand concentration

In the absence of 1,2-CyDTA, a single well-defined wave is present at all pH-values. On the addition of the ligand, a second wave appears at more negative potentials. The limiting current of the first wave due to the reduction of the "free" copper ions decreases linearly with the concentration of the ligand and disappears for a metal:ligand ratio, 1:1. The height of the second wave increases linearly with the concentration of the complexing agent up to a ligand:metal ratio 1:1, and then remains constant. This behaviour is found for the whole pH-range examined. As an example, the limiting current of the two waves is plotted against the ligand:metal ratio, at pH = 4.96 in Fig. 1.

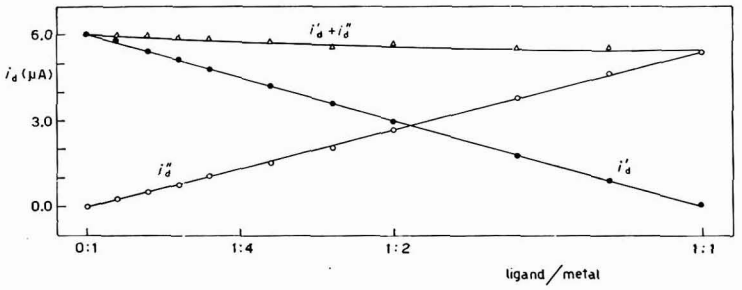

Fig. 1. Diffusion currents of the first and second wave as a function of ligand:metal ratio. pH = 4.96, t = 25.0±0.1°, μ = 0.5 with $NaClO_4$; $[Cu^{2+}] = 1.0 \cdot 10^{-3}$ M.

TABLE 1

HALF-WAVE POTENTIAL (V *vs.* SCE) FOR THE COMPLEX WAVE AT DIFFERENT LIGAND:METAL RATIOS AND pH-VALUES

($[Cu^{2+}] = 1.0 \cdot 10^{-3}$ M, t = 25.0±0.1°; μ=0.5 with $NaClO_4$, acetate buffers)

pH	*Ligand:metal*								
	1:10	*1:6.6*	*1:5*	*1:3.33*	*1:2.5*	*1:2*	*1:1.44*	*1:1.19*	*1:1*
3.65		−0.410	−0.404	−0.392	−0.383	−0.371	−0.356	−0.352	−0.345
4.10	−0.458	−0.441	−0.433	−0.419	−0.413	−0.401	−0.389	−0.382	−0.371
4.20		−0.452	−0.442	−0.434	−0.425	−0.410	−0.399	−0.392	−0.379
4.40		−0.466	−0.452	−0.448	−0.433	−0.425	−0.411	−0.404	−0.393
4.58	−0.483	−0.475	−0.465	−0.455	−0.446	−0.432	−0.422	−0.411	−0.403
4.73		−0.481	−0.472	−0.460	−0.449	−0.438	−0.426	−0.419	−0.410
4.96		−0.498	−0.487	−0.476	−0.465	−0.450	−0.435	−0.427	−0.420
5.25		−0.518	−0.509	−0.495	−0.482	−0.471	−0.464	−0.454	−0.442
5.56		−0.524	−0.515	−0.501	−0.494	−0.484	−0.471	−0.463	−0.456
7.12		−0.558	−0.547	−0.534	−0.528	−0.523	−0.513	−0.506	−0.498

The diffusion constants, I, are 3.4 and 3.1 for the "free" copper and complex wave, respectively. The limiting current of the complex wave, at every ligand:metal ratio is proportional to the square root of the mercury head (*i.e.*, diffusion controlled). However, according to LAITINEN *et al.*[3], a diffusion-control at the plateau does not imply the same at the foot of the wave, if the wave is irreversible. Therefore, the rising portion of the complex wave was examined with this in mind and the wave was found to be irreversible (current independent of the reservoir height at the foot of the wave).

The half-wave potential of the first wave is constant at constant pH and corresponds to $E_{\frac{1}{2}}$ for uncomplexed Cu(II) in acetate buffers. The logarithmic analysis of this wave indicates a slightly irreversible two-electron reduction of Cu(II) to amalgam.

The half-wave potential of the second wave (Table 1) is shifted towards more positive values as the ligand:metal ratio is increased from 1:20 to 1:1 (Fig. 2).

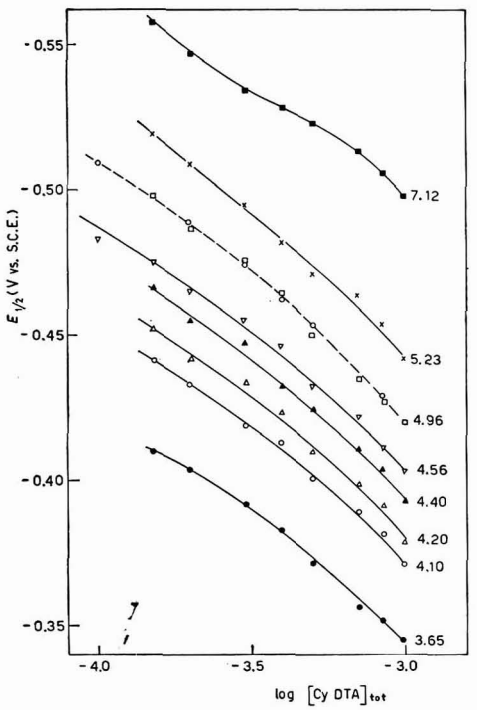

Fig. 2. Variation of $E_{\frac{1}{2}}$ with log of total ligand concn. at different pH-values in presence of excess metal. Numbers of curves are pH-values; $[Cu^{2+}] = 1.0 \cdot 10^{-3}$ M, $t = 25.0 \pm 0.1°$, $\mu = 0.5$ with $NaClO_4$.

For higher ligand:copper ratios, $E_{\frac{1}{2}}$ shifts to more negative values; the slope of the plot of $E_{\frac{1}{2}}$ against the logarithm of ligand concentration (Fig. 3) is not constant and increases with ligand excess.

The reversibility of the complex wave in the presence of excess chelating agent was tested by plotting $\log i/(i_d - i)$ *vs.* the applied potential. Straight lines are obtained with a slope of -65 mV, indicating an irreversible reduction of the complex to amalgam. When excess metal is present, the plots of $\log (i_d'' - i'')/(i'' + i_d')$ *vs.* E (see below,

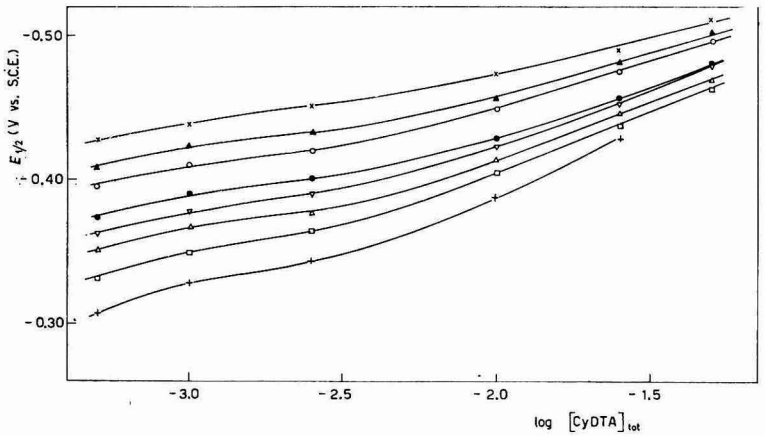

Fig. 3. Variation of $E_{\frac{1}{2}}$ with ligand concn. at different pH-values in presence of excess ligand. $[Cu^{2+}] = 5.0 \cdot 10^{-4}$ M, $t = 25.0 \pm 0.1°$, $\mu = 0.5$ with $NaClO_4$. (×), pH 5.53; (▲) 5.23; (○) 4.95; (●) 4.57; (▽) 4.40; (△) 4.22; (□) 3.79; (+) 3.65.

eqn. (4)) for the complex wave at all pH-values are almost linear with a slope of +60/ +67 mV/ log unit.

Data obtained in the presence of excess 1,2-CyDTA have been used to calculate the kinetic parameters of the irreversible electrode reaction.

The wave equation for such a process is[4]:

$$E = E_{\frac{1}{4}} - (0.054/\alpha n) \log i/(i_d - i) \qquad (1)$$

where α is the transfer coefficient and the other symbols have their usual meaning. Fom the slope of the plots, E *vs.* $\log i/(i_d - i)$, an α-value of 0.44 ± 0.03 has been obtained in the pH-range 3–6 and at all ligand concentrations. Almost the same value for α was obtained by plotting the logarithm of the maximal current against the applied potential. Such a plot should obey the following equation:

$$\log i = \log nFAC_c k_{f,h}^0 - (nF\alpha/2.3\,RT)\,(E + 0.241) \qquad (2)$$

where C_c is the concentration of reacting species at the electrode, A the electrode surface area, $k_{f,h}°$ the heterogeneous rate constant at 0 V *vs.* NHE and the other symbols have their usual meaning.

In the present case we have obtained an α-value of 0.46. From the same plot, by extrapolation of the linear portion to $E = -0.241$ V *vs.* SCE (0 V *vs.* NHE), the value of $k_{f,h}°$ can be calculated[5]: $k_{f,h}° = 3 \cdot 10^{-8}$ cm sec^{-1}, using $n = 2$, $A = 1.63 \cdot 10^{-3}$ cm^2, $C_c = 5.0 \cdot 10^{-4}$moles/l.

A Koutecký analysis[6] of the polarographic waves has also been performed, and from the plot of $\log \chi$ *vs.* E a value of $8 \cdot 10^{-8}$cm sec^{-1} was estimated for the heterogeneous rate constant, $k_{f,h}°$, which is in acceptable agreement with the other value obtained.

An α-value of 0.44 will be used in all our calculations, even in the absence of an excess ligand. This assumption seems justified because the same value was obtained at a metal:ligand ratio as low as 1:1.

Effect of pH

When excess metal is present, two waves appear in the pH-range examined.

$E_{\frac{1}{2}}$ for the wave at more negative potentials is plotted in Fig. 4. These plots exhibit, at all ligand:metal ratios, a linear portion with a slope of −62 mV/pH unit between

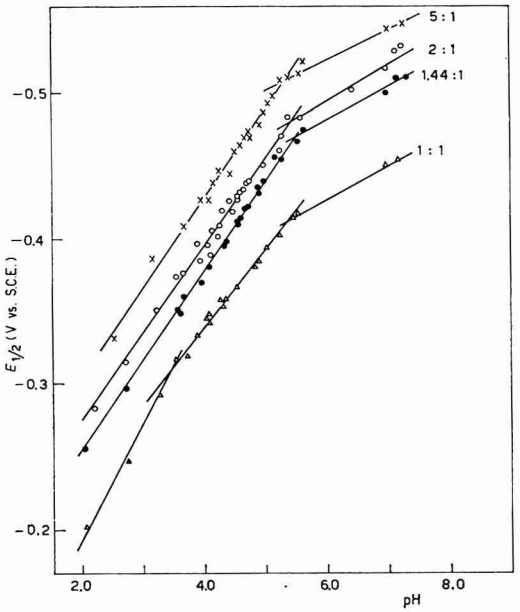

Fig. 4. Variation of $E_{\frac{1}{2}}$ with pH at various metal:ligand ratios for the second wave. Numbers on curves indicate metal:ligand ratios; $[Cu^{2+}] = 1.0 \cdot 10^{-3}$ M, $t = 25.0 \pm 0.1°$, $\mu = 0.5$ with $NaClO_4$.

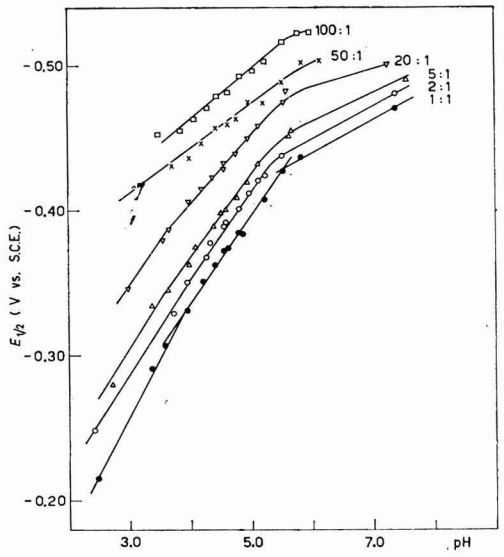

Fig. 5. Variation of $E_{\frac{1}{2}}$ with pH in presence of different excesses of ligand. Numbers on curves are ligand:metal ratios; $[Cu^{2+}] = 5.0 \cdot 10^{-4}$ M, $t = 25.0 \pm 0.1°$, $\mu = 0.5$ with $NaClO_4$.

pH ~3 and ~5.5. At higher pH-values, the slope decreases indicating that a smaller number of hydrogen ions is consumed in the electrode process.

For ligand:metal ratios higher than 1:1, $E_{\frac{1}{2}}$ shifts to more negative values with increasing pH. The plots of $E_{\frac{1}{2}}$ *vs.* pH (Fig. 5) at different metal:ligand ratios exhibit a variable slope, which decreases with increasing pH. This demonstrates that the higher the pH, the lower is the number of hydrogen ions consumed in the electrode process.

DISCUSSION AND CONCLUSIONS

In complexing solutions of 1,2-CyDTA, Cu(II) forms two chelates, one protonated and one unprotonated[7].

The stability constant for the protonation equilibrium is:

$$K_1 = [CuHY^-]/[CuY^{2-}]\,[H^+] = 10^{6.50}$$

(Y^{4-} = ligand anion). Therefore at pH < 6.5, the protonated form predominates in solution.

From the behaviour of the limiting currents with respect to the ligand concentration, it is evident that a very stable 1:1 complex is formed quantitatively. This species is reduced in a single well-defined step. The pronounced displacement of the half-wave potential of the second wave towards more positive values at increasing ligand concentration cannot be justified on a consideration of the changes in the amalgam concentration due to the metal excess[1] alone; it is necessary to assume that $E_{\frac{1}{2}}$ is independent of the concentration of complexing agent.

The electrode reaction, at pH < 6, may be written in a general way as follows:

$$CuHY^- + H^+ \underset{k_{-1}}{\overset{k_1}{\rightleftarrows}} CuH_2Y \underset{k_{-2}}{\overset{k_2}{\rightleftarrows}} Cu^{2+} + H_2Y^{2-}$$
$$\qquad\qquad\qquad\qquad\qquad\qquad\qquad\qquad\qquad\qquad k_f \downarrow {\scriptstyle +2e+Hg}$$
$$\qquad\qquad\qquad\qquad\qquad\qquad\qquad\qquad\qquad\qquad Cu(Hg) \qquad\qquad (a)$$

where k_1, k_{-1}, k_2, k_{-2} are homogeneous rate constants and k_f is the rate constant of the electrode reaction proper.

To justify the large positive shift of $E_{\frac{1}{2}}$ with increasing ligand concentration, it is necessary to assume that the second step is irreversible (*i.e.*, $k_{-2} \ll k_2$). We may then write:

$$\frac{d[CuH_2Y]}{dt} = k_1\,[CuHY^-]\,[H^+] - k_2\,[CuH_2Y] - k_{-1}\,[CuH_2Y]$$

No accumulation of CuH_2Y is detectable, therefore a steady state is established, in which:

$$\frac{d[CuH_2Y]}{dt} = 0 \quad \text{and} \quad [CuH_2Y] = \frac{k_1}{k_2 + k_{-1}}\,[CuHY^-]\,[H^+]$$

From the height of the complex wave, we know that the concentration of CuH_2Y in the steady state must be very small. Therefore, k_2 or k_{-1}, or both, are much larger than k_1. Let us suppose the first step to be irreversible (*i.e.*, $k_{-1} \ll k_1$) then $k_2 \gg k_1$.

For the second step we have:

$$\frac{d[Cu^{2+}]}{dt} = k_2[CuH_2Y] - k_f[Cu^{2+}] = \frac{k_2 k_1}{k_2 + k_{-1}}\,[CuHY^-][H^+] - k_f[Cu^{2+}]$$

Because Cu(II) ions do not accumulate:

$$k_f[Cu^{2+}] = \{k_2k_1/(k_2+k_{-1})\}[CuHY^-]\,[H^+] = \{k_1/(1+k_{-1}/k_2)\}\,[CuHY^-]\,[H^+]$$

As $k_2 \gg k_1$, we may write:

$$[Cu^{2+}] = (k_1/k_f)\,[CuHY^-]\,[H^+] \tag{3}$$

The wave equation is then:

$$E'' = E^\circ + (0.054/\alpha n)\log(k_1/k_f)\,[CuHY^-]\,[H^+]/C_a^{tot} \tag{4}$$

(the symbols here and in the following equations are the same as in the preceding paper[1]).

Since:

$$i_d'' - i'' = k_c C_c,\ i'' = k_a C_a'',\ C_a^{tot} = C_a' + C_a'' = (i_d' + i'')/k_a$$

eqn. (4) becomes:

$$E'' = \varepsilon_0'' + \frac{0.054}{2\alpha}\log\frac{i_d''-i''}{i_d'+i''} + \frac{0.054}{2\alpha}\log[H^+] \tag{5}$$

For $i'' = i_d''/2$

$$E_{\frac{1}{2}}'' = \varepsilon_0'' + \frac{0.054}{2\alpha}\log\frac{i_d''/2}{i_d'+i_d''/2} + \frac{0.054}{2\alpha}\log[H^+] \tag{6}$$

Equation (6) was used to calculate the shift of $E_{\frac{1}{2}}$ with ligand concentration at constant pH, and $E_{\frac{1}{2}}$ at a ligand:metal ratio of 1:1 was used to "fit" the theoretical curve to the experimental curve. In Fig. 2, the circles on the dotted line represent calculated values and the squares are experimental points: the agreement is satisfactory. The slope of the plot, $E_{\frac{1}{2}}$ *vs.* pH, predicted by eqn. (6) is −62 mV/pH unit (with $\alpha = 0.44$), in excellent agreement with the experimental values.

At high ligand concentrations, the rate of recombination of the ligand is no longer negligible and the concentration of CuH_2Y increases. This in turn influences the rate of the first step, *viz.*, the rate of deprotonation becomes larger. Two equilibria might then be considered, one for the first step with constant $K_2 = [CuH_2Y]/[CuHY^-]\,[H^+]$, and one for the second step with constant $K_3 = [CuH_2Y]/[Cu^{2+}]\,[H_2Y^{2-}]$. The Cu(II) concentration is then given by:

$$[Cu^{2+}] = K_2[CuHY^-]\,[H^+]/K_3[H_2Y^{2-}]$$

$E_{\frac{1}{2}}$ should now become dependent on the 1,2-CyDTA concentration; this effect should be more pronounced as the ligand concentration increases, as, indeed, is the case (Fig. 3).

Equation (3) must be obeyed at each potential along the wave, *i.e.*, a steady state has to be attained by the system instantaneously as the potential changes. The rate of the faradaic reaction changes with the applied potential because k_f is an exponential function of E; consequently, the rate of the chemical reactions preceding the electron transfer must also change with potential. This means that the preceding chemical reactions take place in a thin layer of solution near the electrode and proceed under the direct influence of the electrode field. This influence may be twofold: the concentration of the reacting particle at the electrode surface is different from that in the bulk of the solution or the rate constants change under the influence of the field.

At pH-values above ~6, another process (b), should take place simultaneously

with (a), because the ligand-form predominating in solution is no longer H_2Y^{2-}, but HY^{3-} (for the equilibrium $H_2Y^{2-} \rightleftarrows HY^{3-} + H^+$, $pK = 6.12$ at $\mu = 0.1$ and $t = 20°$)[8]

$$CuHY^- \xrightarrow{k_3} Cu^{2+} + HY^{3-} \xrightarrow{+2e+Hg} Cu(Hg) \qquad (b)$$

This assumption is supported by the fact that the dependence of $E_{\frac{1}{2}}$ on the 1,2-CyDTA concentration is the same throughout the pH-range considered, but the dependence on pH varies. On decreasing the acidity, $E_{\frac{1}{2}}$ tends to be pH-independent (Fig. 4).

At high ligand concentration the back-reaction, with rate constant k_3, also becomes important and the following equilibrium has to be considered:

$$CuHY^- \rightleftarrows Cu^{2+} + HY^{3-} \quad K_4 = [CuHY^-]/[Cu^{2+}]\,[HY^{3-}]$$

Therefore, we can conclude that, at pH < 6, the electrochemical process is preceded by a fast irreversible protonation and a fast irreversible dissociation of ligand; at higher pH-values the dissociation takes place without assumption of protons.

The process is essentially the same at all ligand concentrations, but, at high ligand concentration equilibria have to be considered for both the proceding steps, because the rate of the back-reactions are no longer negligible; $E_{\frac{1}{2}}$ becomes dependent on CyDTA concentration.

A fast ligand dissociation before the electrode reduction, has been found also for the very similar Cu(II)–EDTA system in acetate buffers, by means of chronopotentiometry[9].

SUMMARY

The polarographic behaviour of the Cu(II)–1,2-CyDTA system has been examined in acetate buffers. The effect of ligand concentration has been studied both in the presence and absence of excess metal. The effect of pH and mercury reservoir height has been investigated.

Kinetic parameters of the irreversible reduction of the complex have been evaluated and a wave equation which explains the experimental results is given.

REFERENCES

1 A. FURLANI, D. GATTEGNO AND A. M. GIULIANI, *J. Electroanal. Chem.*, 15 (1967) 381.
2 A. M. GIULIANI, D. GATTEGNO AND A. FURLANI, *Gazz. Chim. Ital.*, 97 (1967) 1076.
3 P. KIVALO, K. B. OLDHAM AND H. A. LAITINEN, *J. Am. Chem. Soc.*, 75 (1953) 4148.
4 R. TAMAMUSHI AND N. TANAKA, *Bull. Chem. Soc. Japan*, 22 (1949) 227.
5 L. MEITES, *Polarographic Techniques*, Interscience Publishers Inc., New York, 1st ed., p. 238.
6 J. KOUTECKÝ, *Collection Czech. Chem. Commun.*, 18 (1953) 597.
7 G. SCHWARZENBACH, R. GUT AND G. ANDEREGG, *Helv. Chim. Acta*, 37 (1954) 937.
8 G. SCHWARZENBACH AND H. ACKERMANN, *Helv. Chim. Acta*, 32 (1949) 1682.
9 C. FURLANI AND A. FURLANI, *Ric. Sci.*, 32 (II-A) (1962) 439.

ELECTROANALYTICAL CHEMISTRY AND INTERFACIAL ELECTROCHEMISTRY
Elsevier Sequoia S.A., Lausanne – Printed in The Netherlands

POLAROGRAPHY OF POLYCYCLIC AROMATIC HYDROCARBONS

III. THE ENHANCING EFFECT OF VARIOUS HYDROCARBONS ON THE POLAROGRAPHIC MAXIMUM OF METHYL-*p*-BENZOQUINONE

KIYOKO TAKAMURA
Tokyo College of Pharmacy, Uenosakuragi, Taito-ku, Tokyo (Japan)
TSUTOMU TAKAMURA
Central Research Laboratory, Tokyo Shibaura (TOSHIBA) Electric Co., Ltd., Komukai, Kawasaki (Japan)
(Received December 28th, 1967)

INTRODUCTION

It has previously been reported[1] that anthracene enhances the polarographic maximum of methyl-*p*-benzoquinone (I) in 2-methoxyethanol solution. This is contrary to the generally accepted view that polycyclic aromatic hydrocarbons behave as maximum suppressors[2]. The enhancing effect of anthracene was explained on the basis of VON STACKELBERG's theory[3] by assuming the charge-transfer complex between (I) and anthracene to be adsorbed strongly on the electrode surface.

Such an enhancement was also found for other polycyclic aromatic hydrocarbons and was particularly marked on the addition of compounds of higher ring number. Polycyclic aromatic hydrocarbons, especially those having higher ring number, adsorb strongly on the surface of the mercury electrode in the positive region of the electrocapillary curve[4]. Adsorption of such compounds on the electrode surface lowers the surface tension of the mercury–solution interface. In the present paper, the problem of whether or not the adsorption of hydrocarbons on the mercury surface is an important step in the maximum-enhancing phenomenon, is discussed polarographically in an attempt to support the theories put forward in the previous paper.

EXPERIMENTAL

The polarographic measurements were carried out at 25° with the apparatus previously described[1].

(I) and 2-methoxyethanol were purified as described earlier[1]. 0.25 *M* lithium chloride was usually used as a supporting electrolyte. Aromatic hydrocarbons of guaranteed reagent-grade were further purified according to the following procedures.

Benzene: distilled at atmospheric pressure, and the distillate (80.0 ~ 80.2°) collected.

Naphthalene: purified by repeated sublimation.

Phenanthrene and pyrene: recrystallized repeatedly from ethanol.

Perylene and 1,2-benzanthracene were used without further purification and anthracene was the same reagent as in the previous experiment[1].

RESULTS AND DISCUSSION

The polarogram obtained with a freshly-prepared solution of (I) showed a single reduction wave having a typical maximum[1]. The half-wave potential was about −0.17 V *vs.* the mercury pool electrode. Most aromatic hydrocarbons used in the present experiment did not give the reduction waves in the potential range investigated because of their highly negative reduction potentials.

The enhancing effect on the maximum height of (I) was examined for benzene, naphthalene, anthracene, phenanthrene, pyrene, perylene and 1,2-benzanthracene and all showed an enhancing effect. The effect was more marked for the compounds of higher ring number. Gradual increase of hydrocarbon concentration caused the maximum to become higher and wider up to a limiting value. The addition of hydrocarbon scarcely affected the diffusion current of (I). These results were similar to those obtained in the (I)–anthracene system[1].

In order to compare the enhancement produced by the various hydrocarbons, the heights of maxima at a fixed concentration of (I) were measured for solutions containing the same amounts of hydrocarbons. The results are shown in Fig. 1. The addition of 6.8 mM benzene to the solution barely enhanced the maximum of (I), but in the presence of the same concentration of naphthalene, pyrene etc., a distinct enhancement was observed as seen in Fig. 1. In the case of perylene, although the concentration was lower than that of other additives because of its low solubility in the solvent, the enhancing effect was clearly apparent.

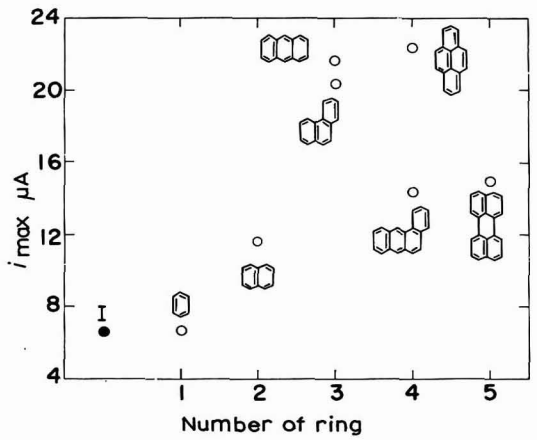

Fig. 1. Comparison of the enhancement of the maximum of (I) reduction wave by various hydrocarbons at 25°. Max. heights (i_{max}) were obtained in the solns. containing $1.2 \cdot 10^{-3}$ M (I) and $6.8 \cdot 10^{-3}$ M hydrocarbon (perylene, $3.4 \cdot 10^{-3}$ M, nearly satd. soln). (●), in the absence of hydrocarbon.

As described in the previous report[1], the enhancing effect of hydrocarbons can also be explained on the basis of VON STACKELBERG's theory. The maximum of the first kind in the positive branch of the electrocapillary curve is caused by the increased rate of supply of electro-reducible substances to the electrode, as a result of the streaming brought about by the difference in the interfacial tension between the neck and the base of the mercury drop. The streaming of the solution around the mercury drop could

be detected by observing the flow of talc powder suspended in the solution. The addition of hydrocarbons to the solution caused the positive branch of the electrocapillary curve to become steeper than that of base electrolyte solution. The steeper the electrocapillary curve, the larger the streaming induced and, consequently, the higher the maximum obtained.

The relation between the maximum height and the amount of adsorption will be treated in some detail. At present, for simplicity, it is assumed that only the hydrocarbon adsorbs strongly on the mercury surface. In the presence of specific adsorption of anion, the hydrocarbon adsorbs through a competitive process, but the following conclusion is not altered seriously if the adsorptive force of the anion is weaker than that of the hydrocarbon and if we consider only the effective maximum height brought about solely by the hydrocarbon.

If the rate of charge transfer is very fast, the maximum current, i_{max}, is proportional to the rate of supply of electro-reducible substance to the electrode. The rate of supply is proportional to the streaming velocity[3], v, which is brought about by the difference in the interfacial tension, $\Delta\gamma$, between the neck and the base of the mercury drop. At constant quinone concentration, the maximum height can then be expressed by the equation,

$$i_{max} = k_1 v, \tag{1}$$

where k_1 is a constant defined by the concentration, diffusion coefficient, etc. The streaming velocity is given by:

$$v = k_2 \Delta\gamma, \tag{2}$$

where k_2 is a constant which includes hydrodynamic properties. At a constant applied potential E, owing to the potential difference, ΔE, between the neck and the base of the mercury drop, $\Delta\gamma$ is given by eqn. (3), since ΔE is a very small change in E,

$$\Delta\gamma = (\partial\gamma/\partial E)_\mu \Delta E. \tag{3}$$

It can readily be shown by eqn. (3) that $\Delta\gamma$ is proportional to the slope of the electrocapillary curve at fixed ΔE. Since it can be assumed that ΔE is constant for any given capillary and electrolytic conditions, eqn. (3) can be rewritten

$$\Delta\gamma = k_3 \Gamma \tag{4}$$

where k_3 is a constant and Γ is the amount of adsorption of hydrocarbon. In the derivation of eqn. (4) from eqn. (3), we assume that Γ is proportional to the effective charge of the dipole which is caused by the aromatic π-electron system through adsorption. This assumption is verified qualitatively by the increasing slope of the electrocapillary curve with increase of concentration of aromatic hydrocarbon; this is seen clearly in Fig. 2.

The maximum height at constant potential will then be given by the following expression:

$$i_{max} = K\Gamma \tag{5}$$

where K is a constant. The deduction holds for the effective height of the maximum brought about by the addition of aromatic hydrocarbon. If Γ obeys the Langmuir isotherm, we can rewrite eqn. (5) as a function of concentration (activity a) by eqn. (6),

$$i_{max} = K\beta a \Gamma_s/(1+\beta a) \tag{6}$$

where β represents the constant part of the free energy and Γ_s, the saturated amount of adsorption.

From eqn. (6) we have

$$1/i_{max} = (1/K\Gamma_s\beta)(1/a) + 1/K\Gamma_s$$

The plot of $1/i_{max}$ at constant potential against the reciprocal of the hydrocarbon concentration was almost a straight line. Two examples of this plot, obtained for the (I)–naphthalene and (I)–pyrene systems, are given in Fig. 3. Similar results were also obtained in other cases.

Although the value of β for hydrocarbons could be expected to be obtained from the plot using the relative concentration, C/C_s,(C_s: saturated concentration)

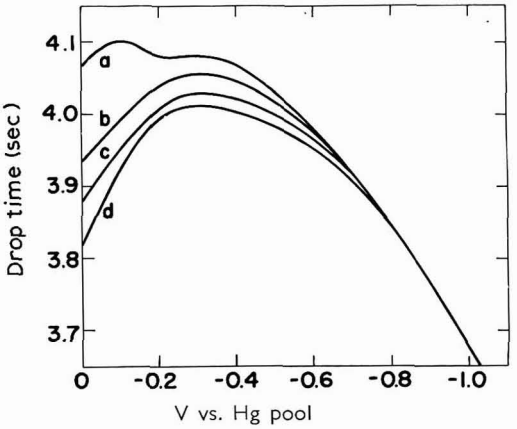

Fig. 2. Drop time curves of base electrolyte solns. containing: (a), 0; (b), $0.94 \cdot 10^{-2}$; (c) $4.13 \cdot 10^{-2}$; (d), $11.0 \cdot 10^{-2}$ M pyrene, at 25°.

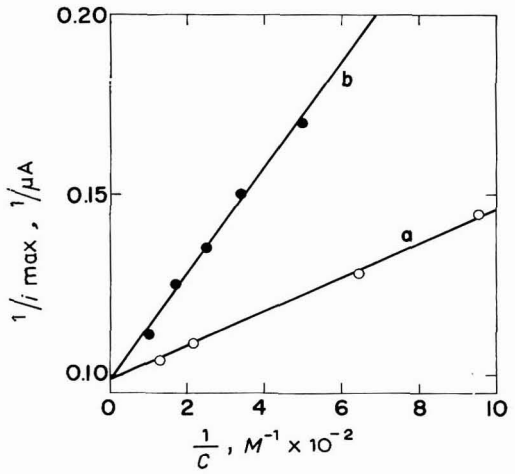

Fig. 3. Plots of $1/i_{max}$ against the reciprocal concn. of added hydrocarbon. i_{max} were observed at −0.2 V *vs.* mercury pool electrode in $1.1 \cdot 10^{-3}$ M (I) soln. containing various concns. of (a), naphthalene; (b), pyrene.

instead of concentration C, the lack of solubility data (or solvation energy data, crystal energy data, etc.) of hydrocarbons in 2-methoxyethanol solution precludes any discussion of the adsorption energy of hydrocarbons on the mercury electrode.

The results obtained for all the hydrocarbons investigated can be explained from the same standpoint as above. The experimental results show that the addition to the solution of aromatic compounds of higher ring number causes greater streaming around the mercury drop. According to FRUMKIN[4], the adsorptive power of aromatic hydrocarbons on a mercury electrode increases with increase of ring number. These compounds adsorb strongly in the positive region of the electrocapillary curve because the adsorption is due to the mutual attraction between the π-electron system of the hydrocarbons and the electrode surface. This fact was confirmed under the present experimental condition as follows: The drop-time, *i.e.*, the interfacial tension of the mercury–solution interface, obtained in a solution containing hydrocarbons but no (I) decreased in the positive region with increasing concentration of added hydrocarbons. The results are shown in Fig. 4, in which the drop-time at 0 V (*vs.* Hg pool) are plotted against the hydrocarbon concentration. In Fig. 4, the lowering of the drop-time by the addition of hydrocarbons is intensified in the order: naphthalene, phenanthrene, pyrene.

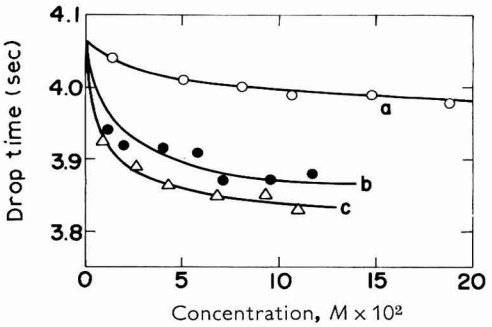

Fig. 4. The relation between drop-time (measured at 0 V *vs.* mercury pool electrode) and hydrocarbon concn. in the supporting electrolyte soln. in the presence of: (a), naphthalene; (b), phenanthrene; (c), pyrene.

Although there is a rational explanation for the effect of the aromatic hydrocarbon on the maximum of the quinone wave, the hydrocarbon did not increase the maximum of the reduction wave of Cu^{2+} in the same solution. In fact, the original maximum of the Cu^{2+} reduction wave was rather suppressed by the addition of the aromatic hydrocarbon and this effect cannot be explained on the basis of the above considerations alone.

In the above explanation we assumed that the rate of electron transfer is much faster than the rate of supply of electro-reducible substances. This would be true for the quinone–hydrocarbon system because of the considerable affinity between them.

We cannot expect such an affinity between the hydrocarbon and Cu^{2+} because of the very low solubility of the copper salt in the hydrocarbon. When the adsorbed species repel the electro-reducible substances and the rate of electron transfer is hindered

by the adsorbed film, insufficient current can flow although the amount of electroreducible substance at the electrode surface is adequate. This causes a decrease in the rate of streaming, and, consequently, the maximum height will be decreased. The depression of the maximum of the Cu^{2+} reduction wave by the hydrocarbon is considered to correspond to such a case. On the contrary, molecular interaction is expected between quinones and hydrocarbons, for example, the formation of charge-transfer complexes[5-7]. Such complexes have a high adsorptive power because of their large dipole moment. In fact, the solution containing both (I) and hydrocarbon gave a lower and steeper interfacial tension curve than that obtained in the solution containing either (I) or hydrocarbon, as already shown in the previous paper.

SUMMARY

The effect of polycyclic aromatic hydrocarbons on the polarographic maximum of methyl-*p*-benzoquinone (I) has been investigated in 2-methoxyethanol solution containing 0.25 *M* lithium chloride. (I) gave a single reduction wave having a typical maximum which was enhanced by the addition of hydrocarbons. Increasing the concentration of hydrocarbons caused the maximum to become higher and wider. The enhancing effect was more marked for compounds of higher ring number. This phenomenon was explained on the basis of VON STACKELBERG's theory by assuming the Langmuir adsorption of hydrocarbons on the electrode surface.

REFERENCES

1 K. TAKAMURA AND T. TAKAMURA, *Trans. Faraday Soc.*, 61 (1965) 1270.
2 C. E. SEARLE, *Nature*, 184 (1959) 1716.
3 M. VON STACKELBERG AND R. DOPPELFELD, *Advances in Polarography*, Vol. 1, Pergamon Press, Oxford, 1960, pp. 68–104.
4 A. N. FRUMKIN, *Proc Intern. Congr. Surface Activity, 2nd London, 1957*, Vol. III, Butterworths, London, 1957, pp. 58–66.
5 M. CHOWDHURY, *Trans. Faraday Soc.*, 57 (1961) 1482.
6 S. K. CHAKRABARTI AND S. BASU, *Trans. Faraday Soc.*, 60 (1964) 16.
7 M. E. PEOVER, *Trans. Faraday Soc.*, 60 (1964) 417.

ELECTROANALYTICAL CHEMISTRY AND INTERFACIAL ELECTROCHEMISTRY
Elsevier Sequoia S.A., Lausanne – Printed in The Netherlands

ELECTROOXIDATION MECHANISMS OF HEXAMETHYLBENZENE AND 1,5-DICHLOROANTHRACENE

ARTHUR E. COLEMAN, H. H. RICHTOL AND D. A. AIKENS
Department of Chemistry, Rensselaer Polytechnic Institute, Troy, New York, 12181 (U.S.A.)
(Received November 15th, 1967)

Electrooxidation reactions of aromatic hydrocarbons are characterized by rapid, irreversible chemical reactions following electron transfer. The products often accumulate on the electrode and suppress the current and thus interfere with determinations by conventional anodic polarography. Rapid sweep voltammetry is a promising alternative to conventional polarography for such determinations because much less material is electrolyzed and interference by products is minimized. In rapid sweep voltammetry, however, the time required to scan the potential range in which a species is electroactive becomes comparable to the chemical lifetime of the species. The sweep rate therefore interacts in a complex manner with the rates of coupled chemical reactions to determine the morphology of the current–potential curve. Hence, effective selection of optimum sweep rates and interpretation of results requires knowledge of the overall mechanism.

Mechanisms have been inferred from knowledge of the final products for electrooxidation of polymethylbenzenes[1–3] and of anthracene[3–5] but these studies do not reveal the lifetimes of electroactive intermediates and are therefore of limited use in interpreting the results of rapid sweep voltammetry. Studies of electrooxidation of polycyclic aromatic hydrocarbons by PEOVER and co-workers[6,7] using cyclic voltammetry, clearly established the importance of coupled chemical reactions, but the primary objective of the work was evaluation of reversible oxidation potentials and the coupled chemical reactions were not studied in detail.

These examples indicate that establishment of mechanisms for electrooxidation of aromatic hydrocarbons requires both chemical and electrochemical studies. This paper presents the results of a detailed study of the mechanisms for electrooxidation of hexamethylbenzene (HMB) and of 1,5-dichloroanthracene (DCA). Hexamethylbenzene was selected as representative of monocyclic aromatics and 1,5-dichloroanthracene was selected because electrooxidation of anthracene yields bianthronyl and 1,5-dichloroanthracene permits the study of the effect of steric hindrance on the mechanism.

EXPERIMENTAL

A conventional three-electrode potentiostatic polarograph based on operational amplifiers was used. Sweep voltage for cyclic voltammetry was supplied by a Hewlett-Packard 202 A function generator with added offset, voltage divider and synchronizing circuits. Voltammetric curves at sweep rates below 0.4 V/sec were recorded with a

Houston Omnigraphic X–Y recorder, and above this sweep rate a Tektronix 535 oscilloscope and camera were used. Charging currents at high sweep rates were compensated automatically using dual cells and the residual non-Faradaic ohmic drop was compensated by the positive feedback method[8].

The isolated silver reference electrode in 0.1 *M* $AgClO_4$, 0.5 *M* $NaClO_4$ in acetonitrile is similar to that described by LUND[4]. The working electrode in all voltammetry experiments was a platinum disc 2.3 mm in diameter mounted in Teflon and pretreated by cycling between 0.0 V and 2.0 V at 0.1 Hz in the supporting electrolyte until the current–potential curve became reproducible. For steady-state polarograms, the electrode was rotated at 600 rev./min and the potential was scanned at 100 mV/min. The working electrode for coulometric determination of *n*-values and preparative electrolysis was a platinum gauze 5 cm by 3 cm. All measurements were made at 25.0±0.1°.

The supporting electrolyte was 0.5 *M* $NaClO_4$ in acetonitrile de-aerated with high purity nitrogen. Acetonitrile was purified by the method of O'DONNELL, AYRES AND MANN[9] and anhydrous $NaClO_4$ was dried at 140° under vacuum for 24 h. Eastman White Label grade HMB was recrystallized thrice from benzene, and DCA was prepared by the method of BERGMANN AND WEIZMANN[10]. The identity of each reaction product was established by comparison with an authentic sample by infrared and a mixed melting point except for the previously unreported 1,5-dichloro-9-acetamido-10-anthrone which was identified by infrared and elemental analysis.

ASSIGNMENT OF MECHANISMS

The steady-state polarograms at the rotated platinum electrode together with the *n*-value of each wave and the identities of the final products define the overall electrode reactions clearly, but give little insight into the mechanisms. Establishment of the mechanisms requires analysis of the single sweep and cyclic stationary electrode polarograms. This analysis is based on interpretation of the effect of sweep rate on the morphology of the polarograms through application of the diagnostic criteria of NICHOLSON AND SHAIN[11,12]. In this analysis two limitations are significant. First, in considering the complex mechanisms of interest here, NICHOLSON AND SHAIN found it necessary to consider electron transfer either as reversible or as totally irreversible. Hence, the term reversible will include quasi-reversible electron transfers as well as Nernstian steps. Second, the uncertainty in potential measurement in oscillographic polarograms is of the order of 0.02 V which precludes quantitative interpretation of peak potentials. For this reason, assignment of mechanisms is based primarily on the number and magnitude of peaks in rapid sweep polarograms, and potential shifts are considered only qualitatively.

OXIDATION OF HMB

Steady-state polarography and electrolysis

Polarograms of HMB at the rotated platinum electrode exhibit two well-defined anodic waves of approximately equal height between 0.0 V and +1.5 V. A third anodic wave at approximately +1.6 V is poorly defined and will not be considered in any detail. The half-wave potential of the first wave is 1.124 V at the

1-mM level and shifts slightly to less anodic potentials with increasing concentration, reaching a value of +1.113 V at the 5-mM level. These potentials are consistent with the value of +1.16 V reported by NEIKAM, DIMELER AND DESMOND[13] using an internal silver reference electrode. The small positive shift in their value is attributed to stabilization of HMB through formation of the silver–HMB complex[14]. The value of βn is 1.0 and the value of n, measured at +1.15 V, is 2.0. The half-wave potential of the second wave is +1.42 V and the value of βn is 1.1. These results indicate that both polarographic waves correspond to loss of 2 electrons and that the overall electrode processes are irreversible.

Controlled-potential oxidation of HMB at +1.5 V yields a deep red solution which on addition of water yields pentamethylbenzylacetamide as reported by EBERSON AND NYBERG[2]. Electrolysis at +1.50 V yields an orange solution but attempts to isolate products were unsuccessful.

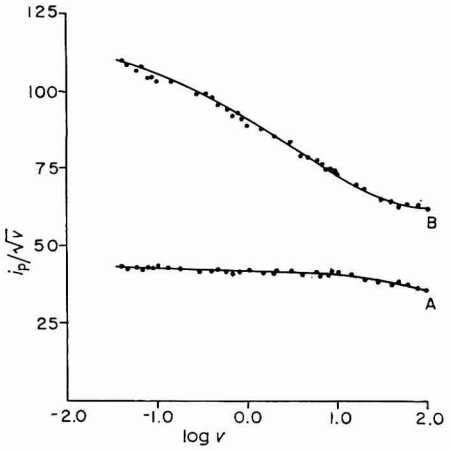

Fig. 1. Peak current functions for electrooxidation of HMB and DCA. (A), First peak of HMB; (B), first peak of DCA.

Single sweep voltammetry

Single sweep stationary electrode polarograms over the potential range 0.0 V to +1.5 V at sweep rates from 0.04 V/sec to 100 V/sec show two anodic peaks corresponding to the two anodic waves in the steady-state polarograms. The current function for the first peak, $i_p/v^{\frac{1}{2}}$, is plotted *vs.* v in Curve A of Fig. 1 where i_p is the peak current in μA and v is the sweep rate in V/sec. The current function is essentially independent of sweep rate at sweep rates below 10 V/sec and above this sweep rate the current function decreases slightly with increasing sweep rate. The current function for the second peak is not plotted because the tail of the first peak must be extrapolated to estimate the peak current, and the accuracy is poor. Qualitatively, however, the current function for the second peak decreases markedly with increasing sweep rate. As an example, the current function drops from approximately 40 units at a sweep rate of 0.1 V/sec to approximately 20 units at a sweep rate of 100 V/sec.

The current functions for the two peaks indicate that the two-electron transfer steps are reversible and are coupled by an irreversible chemical step to form an ECE mechanism as outlined in eqn. (1).

$$A \underset{E_1}{\overset{-2e}{\rightleftharpoons}} B \overset{k_f}{\rightarrow} C \underset{E_2}{\overset{-2e}{\rightleftharpoons}} D \qquad E_2 > E_1 \qquad (1)$$

This conclusion is based primarily on the behavior of the current function for the first peak which is well characterized experimentally and corresponds very well with the theoretical current function for the ECE mechanism with reversible electron transfer given by NICHOLSON AND SHAIN[12]. The theoretical current function is independent of sweep rate at low sweep rates and passes through a broad transition range at intermediate sweep rates in which the current function decreases by 10% to a limiting value at high sweep rates. The experimental current function in Curve A of Fig. 1, which decreases from a value of 43 ± 3 units at the lowest sweep rate to a value of 37 ± 2 units at the highest sweep rate, agrees very well with the theoretical curve. The experimental curve has been fitted approximately to the data points without attempting to match the theoretical current function because the theoretical curve is not strongly sensitive to the kinetic parameters and the scatter in the data precludes more quantitative interpretation.

The existence of the irreversible chemical reaction between the two-electron transfer steps is verified by the sharp drop in the current function of the peak at +1.4 V as the sweep rate is increased. This fact indicates that B is not oxidized directly but first must be transformed to C. At low sweep rates, the time required for the potential to become sufficiently positive to oxidize C is longer than the chemical lifetime of B and sufficient C is formed to give a large anodic peak at +1.4 V. As the sweep rate is increased, however, less time is available for formation of C and the peak at +1.4 V is depressed.

Both peaks show a slight but consistent shift toward more positive potentials as the sweep rate is increased, as illustrated by the half-peak potential of the first peak which shifts from +1.09 V at a sweep rate of 0.1 V/sec to +1.18 V at a sweep rate of 100 V/sec. The potential-dependence of the first peak arises because the chemical step removes B more effectively at low sweep rates than at high sweep rates and the concentration of B at the electrode surface influences the peak potential directly through the Nernst equation. The fact that both the first and second peaks show a similar potential-dependence indicates that the second electron transfer step is also reversible and followed by an irreversible chemical step. Thus both electron transfer steps are reversible and are followed by irreversible chemical steps and the mechanism corresponds to the ECEC type. Hence, both electrode reactions are reversible as observed over short times but irreversible as observed over long times. The dependence of reversibility on the time scale of observation explains why the steady-state polarograms at the rotated platinum electrode are irreversible, but the rapid sweep polarograms are reversible.

Cyclic voltammetry

The cyclic stationary electrode polarograms in Fig. 2 summarize the effects of sweep rate and switching potential. Figures 2a and 2b represent a fixed switching potential of +2.00 V and demonstrate the effect of sweep rate. At a sweep rate of

0.01 V/sec in Fig. 2a, no cathodic peaks appear on the reverse sweeps while at a sweep rate of 100 V/sec in Fig. 2b, two cathodic peaks appear on the reverse sweeps, each corresponding to reduction of an oxidation product formed in the two anodic peaks on the forward sweep. This identification of the two cathodic peaks is confirmed in Figs. 2b and 2c which demonstrate switching potentials of +2.00 V and +1.40 V, respectively. Reducing the switching potential from +2.00 V to +1.40 V eliminates both the more positive anodic peak on the forward sweep and the more positive cathodic peak on the reverse sweep. Simultaneously, the magnitude of the less positive cathodic peak on the reverse sweep increases, indicating that it corresponds to the less positive anodic peak.

The cyclic polarograms confirm the reversibility of the two-electron transfer steps and the coupling of both electron transfer steps with following chemical reactions. The appearance of the two cathodic peaks on the reverse sweep at high sweep rates verifies that both electron transfer steps are reversible if the following chemical steps do not proceed significantly. The disappearance of both cathodic peaks at lower sweep rates confirms that both electron transfer steps are followed by

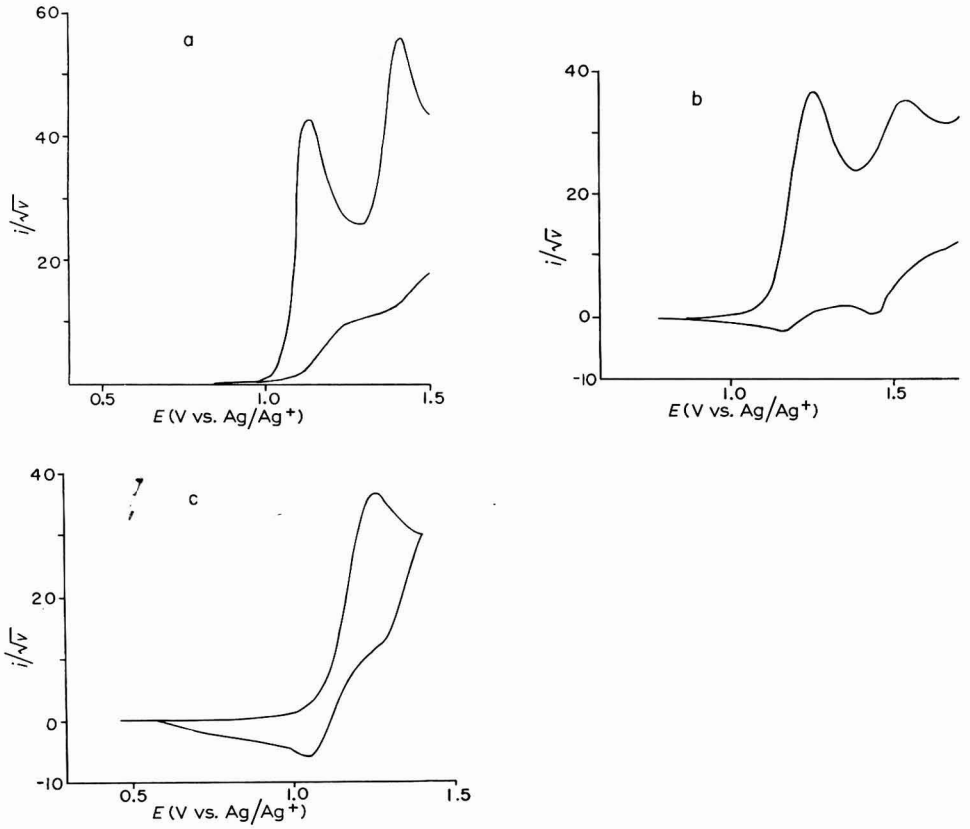

Fig. 2. Effect of sweep rate and switching potential on cyclic polarograms of HMB. (a), Sweep rate 0.01 V/sec, switching potential 2.00 V; (b), sweep rate 100 V/sec, switching potential 2.00 V; (c), sweep rate 100 V/sec, switching potential 1.40 V.

irreversible chemical steps. At the lower sweep rates, the product of the anodic peak on the forward sweep is removed by the chemical step before the potential becomes sufficiently negative to give the corresponding cathodic peak on the reverse sweep.

The value of k_f, the rate constant for conversion of B to C, is estimated to be approximately 300 sec^{-1} using the method of NICHOLSON AND SHAIN[11] based on the ratio of the peak current for oxidation of C to the peak current for reduction of B in the cyclic polarograms. The necessary ratio of peak currents was not determined directly from the polarogram because the baseline for the peaks is not well known, but was estimated using the semi-empirical method of NICHOLSON[15].

Detailed mechanism

The kinetic information deduced from the steady-state and rapid sweep polarograms and the identity of the final product of the first electron transfer step, lead to the mechanism in eqn. (2), which is a more comprehensive version of that proposed by EBERSON AND NYBERG[2] for the first electrode reaction on the basis of product analysis.

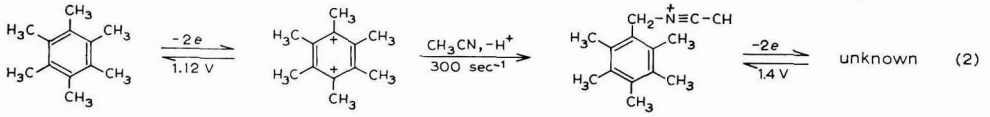

(2)

Deprotonation of B undoubtedly precedes attack by acetonitrile but it is not possible to separate these two first-order steps experimentally and they are combined in the mechanism. Formation of the nitrilium ion, C, was first proposed by EBERSON AND NYBERG[2] and is consistent with isolation of the observed product, pentamethyl-N-benzylacetamide, after hydrolysis. The product of the second oxidation step at +1.4V was not isolated and comments on this part of the mechanism must therefore be more speculative. The electrochemical evidence indicates that the mechanism for this step in general corresponds to that for the first step. Hence, it is likely that the product of electron transfer reacts with the solvent to form a dinitrilium ion analogous to C.

OXIDATION OF DCA

Steady-state polarograms and preparative electrolysis

Polarograms of DCA at the rotated platinum electrode between 0.0 V and +2.0 V show a single well-defined anodic wave. At the 0.5-mM level, the half-wave potential is +1.040 V, but as with HMB the half-wave potential shifts slightly to less anodic values with increasing concentration, reaching a value of +1.003 V at the 2-mM level. The value of βn is 1.1 and the value of n at 1.10 V is 2.0. Polarograms recorded in acetonitrile containing 5% ethanol exhibit a high but reproducible background current. The half-wave potential is +0.97 V and the wave height is 0.55 times that observed in the absence of ethanol, indicating a one-electron oxidation.

Controlled-potential oxidation of DCA at +1.10 V gives a red solution which upon addition of water yields a brown solid. Chromatography on alumina and recrystallization yield two fractions identified as 1,5-dichloroanthraquinone in 38%

yield and 1,5-dichloro-9-acetamido-10-anthrone in 29% yield. The latter compound has not been reported previously and its identity is based on the infrared spectrum and elemental analysis. The results of elemental analysis are: calcd. for $C_{16}H_{11}Cl_2NO_2$: C, 60.02, H 3.46, Cl 22.15, N 4.38; found: C, 60.32, H 3.41, Cl 21.89, N 4.28%. The infrared spectrum in KBr shows an N–H band at 3300 cm^{-1}, an aromatic carbonyl band at 1670 cm^{-1}, and amide bands at 1640 cm^{-1} and 1530 cm^{-1}. Electrolysis in acetonitrile containing 5% ethanol at +1.05 V gives a white solid which after recrystallization from xylene was identified as 1,1,5,5-tetrachlorobianthronyl with an overall yield of 75%.

Single sweep voltammetry

Single sweep stationary electrode polarograms at sweep rates from 0.04 V/sec to 100 V/sec between 0.0 V and 2.0 V display two anodic peaks. The first peak exhibits a half-peak potential at approximately +1.05 V and hence this peak corresponds to the steady-state polarographic wave at +1.04 V. The second peak, with a half-peak potential of approximately +1.4 V, is not reflected in the steady-state polarogram. The current function for the first peak is plotted *vs.* sweep rate in Curve B of Fig. 1. The current function decreases continuously with increasing sweep rate from the maximum value of 112 ± 3 at a sweep rate of 0.04 V/sec to a limiting value of 62 ± 2 at sweep rates between 40 V/sec and 100 V/sec. The electrode reaction thus undergoes a transition from loss of two electrons at low sweep rates, to loss of only one electron at high sweep rates. The current function for the second peak is not plotted because accurate estimation of the peak current is difficult, but it is clear that the current function for this peak increases with increasing sweep rate. The second peak is barely discernible at the lowest sweep rates, but increases in magnitude rapidly with increasing sweep rate and at a sweep rate of 100 V/sec the second peak is approximately one-half the magnitude of the first peak.

The steady-state and single sweep polarograms indicate that the electrode reaction basically conforms to the ECE mechanism with reversible electron transfer steps and an irreversible chemical step, but with two complexities. First, the mechanism branches after removal of the first electron and the side branch leads to direct removal of a second electron at more positive potentials without the intervening chemical step. Second, in the ECE sequence, the second electron is removed at least as readily as the first. The general mechanism is summarized in eqn. (3).

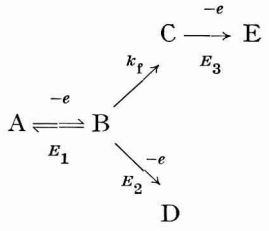

$$E_2 > E_1 \qquad E_3 < E_1 \qquad (3)$$

The most direct evidence for the proposed mechanism is the manner in which the current functions for the two peaks in the single sweep polarograms, depend on the sweep rate. The transition of the first peak from a two-electron process at low sweep rates to a one-electron process at high sweep rates is attributed to a correspond-

ing transition in the mechanism for this peak as the sweep rate is increased. At low sweep rates sufficient time is available for essentially complete conversion of B to C and this chemical step is followed immediately by removal of the second electron to give E. The net result is the two-electron oxidation of A to E. At high sweep rates there is insufficient time for formation of a significant amount of C and removal of a second electron from B is possible only at more positive potentials. The net result is the one-electron oxidation of A to B. The electrode reaction for the first peak thus undergoes a transition from the two-electron ECE mechanism at low sweep rates to simple removal of one electron at high sweep rates. This transition is confirmed by the strong increase in the current function for the second peak with increasing sweep rates. The second peak corresponds to oxidation of B to D and the current function increases with increasing sweep rate because the fraction of B that escapes conversion to C and can be oxidized directly to D increases with the sweep rate.

The reversibility of the first electron transfer step and the presence of the following irreversible chemical reaction are demonstrated by the continuous anodic shift of the first peak with increasing sweep rate. The peak potential shifts from +1.07 V at a sweep rate of 0.1 V/sec to +1.14 V at a sweep rate of 100 V/sec and this shift reflects the influence of the following chemical step on the surface concentration of B. At low sweep rates, B is scavenged effectively by the chemical step, but at high sweep rates relatively little B is transformed to C in the short time required to sweep the peak. The effective concentration of B at the electrode surface thus increases with increasing sweep rate. Hence, oxidation of A requires a more anodic potential at high sweep rates than at low sweep rates.

Cyclic voltammetry

Cyclic stationary electrode polarograms are given in Figs. 3a and 3b for scan rates of 0.1 V/sec and 100 V/sec, respectively. The polarogram at 0.1 V/sec sweep rate shows no cathodic peaks on the reverse sweeps, but on the second forward sweep a small new anodic peak appears at +1.0 V near the foot of the major anodic peak at +1.09 V. The polarogram at 100 V/sec sweep rate shows a cathodic peak at +1.1 V on the reverse sweep, but the new anodic peak at +1.0 V observed at a sweep rate of 0.1 V/sec is absent at a sweep rate of 100 V/sec.

The characteristics of the new anodic peak at +1.0 V indicate that it represents oxidation of C to E. The peak is only observed after completion of the first

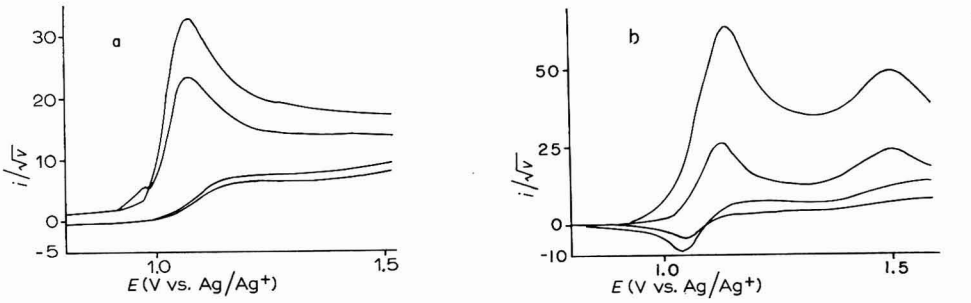

Fig. 3. Effect of sweep rate on cyclic polarograms of DCA. Sweep rate: (a), 0.1; (b), 100 V/sec. Switching potential 2.00 V for all traces.

anodic sweep and therefore it represents oxidation of the product of a prior anodic step. The disappearance of the peak as the sweep rate is increased means the electrode reaction follows a chemical step. Thus, the new anodic peak in the cyclic polarogram represents the last step of the overall ECE sequence which comprises the first peak on the single sweep polarograms. The fact that oxidation of C to E proceeds more readily (+1.0 V) than does oxidation of A to B (+1.1 V) also explains the failure to isolate this step of the ECE mechanism by single sweep polarography. At potentials sufficiently positive for oxidation of A to B, oxidation of C to E goes to completion and the extent of conversion of A to E is limited by the rate of conversion of B to C.

The cathodic peak at +1.1 V which appears on the reverse sweep at high sweep rates represents reduction of B to A and confirms that removal of the first electron from A is reversible. The identity of the peak is established by its disappearance at low sweep rates. At high sweep rates, significant amounts of B survive until the potential becomes sufficiently negative for reduction of B to A, but at low sweep rates B is converted to C before the potential becomes sufficiently negative and reduction of B is not observed.

The value of k_f, the rate constant for conversion of B to C estimated from the cyclic polarogram as described earlier for oxidation of HMB, is 200 sec^{-1}.

Detailed mechanism

The results of the electrolysis experiments and the general mechanism outlined in eqn. (3) give the mechanism for electrooxidation of DCA outlined in eqn. (4).

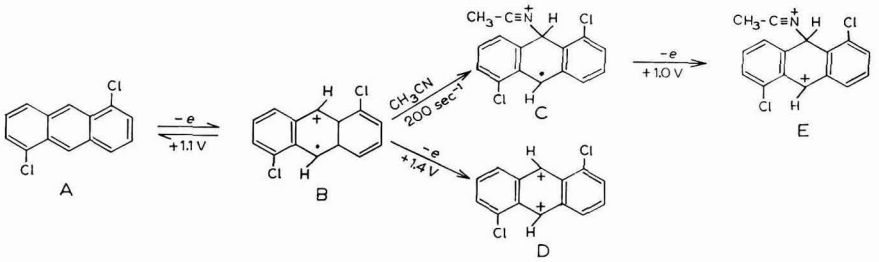

(4)

The reversibility of the oxidation of C could not be established because the much larger peak for oxidation of A prevents accurate characterization of the peak for oxidation of C. Oxidation of C to E is irreversible at all sweep rates studied, as evidenced by failure to observe the cathodic peak on the reverse sweep. It is not known, however, whether the irreversibility results from a slow electron transfer or from chemical reaction of E. The nitrililium ion, E, is consistent with the observed products of hydrolysis in the presence of air. The initial product of hydrolysis, 1,5-dichloro-9,10-dihydro-9-acetamido-10-anthranol would be readily oxidized to the observed 1,5-dichloro-9-acetamido-10-anthrone, and hydrolysis of the acetamido group would yield the second product, 1,5-dichloroanthraquinone.

On the basis of the identities of the electrolysis products and the mechanistic information for oxidation of anthracene, electrooxidation of DCA appears to be generally similar to electrooxidation of anthracene. Electrooxidation of anthracene in acetonitrile was studied by PEOVER AND WHITE[7] using cyclic voltammetry and their conclusions, although qualitative and limited to the initial steps, agree well

with this mechanism. They estimated the lifetime of the radical cation as a few milliseconds, but they did not study in detail the oxidation of the product of the chemical step nor did they observe the direct oxidation of the radical cation. The general similarity of the two electrooxidation mechanisms is confirmed by the fact that in the presence of ethanol both anthracene[5] and DCA yield the respective bianthronyl. This observation is consistent with the fact that the polarographic wave height indicates loss of only one electron from DCA in the presence of ethanol. Apparently, ethanol stabilizes the positive charge of the radical cation sufficiently to prevent attack by acetonitrile and subsequent loss of the second electron and thus permits coupling of the radical to give the bianthronyl. Isolation of 1,1,5,5-tetrachlorobianthronyl as the oxidation product of DCA indicates that the chloro-substituents do not cause sufficient steric interference to prevent coupling and modify the mechanism.

ACKNOWLEDGEMENT

Taken in part from the thesis submitted by ARTHUR E. COLEMAN to Rensselaer Polytechnic Institute, May, 1967, in partial fulfilment of the requirements for the Ph.D. degree. A.E.C. acknowledges support from the National Institute of General Medical Sciences in the form of a Public Health Service Fellowship No. 1-F1-GM-30, 831-01.

SUMMARY

Electrooxidation of hexamethylbenzene in acetonitrile involves the reversible loss of two electrons to form the pentamethylbenzyl cation, which reacts rapidly ($k_f \simeq 300$ sec^{-1}) with the solvent to form the easily hydrolyzed pentamethylbenzyl nitrilium ion. This nitrilium ion undergoes a further two-electron oxidation at a more anodic potential. Electrooxidation of 1,5-dichloroanthracene involves reversible loss of one electron to form the radical cation, which reacts rapidly ($k_f \simeq 200$ sec^{-1}) with the solvent. This product then loses a second electron at a less anodic potential. If the radical cation escapes the chemical reaction, a more anodic potential is required to remove the second electron. In the presence of ethanol, the radical cation couples, and the final stable product is 1,1′,5,5′-tetrachlorobianthronyl.

REFERENCES

1 L. EBERSON AND K. NYBERG, *Acta Chem. Scand.*, 18 (1964) 1568.
2 L. EBERSON AND K. NYBERG, *Tetrahedron Letters*, (1966) 2389.
3 S. D. ROSS, M. FINKELSTEIN AND R. C. PETERSEN, *J. Am. Chem. Soc.*, 86 (1964) 4139.
4 H. LUND, *Aata Chem. Scand.*, 11 (1957) 491.
5 K. E. FRIEND AND W. E. OHNESORGE, *J. Org. Chem.*, 28 (1963) 2435.
6 T. A. GOUGH AND M. E. PEOVER, *Proc. 3rd International Polarography Congress, Southampton, 1965*, Macmillan, London, 1966, p. 1017.
7 M. E. PEOVER AND B. S. WHITE, *J. Electroanal. Chem.*, 13 (1967) 93.
8 G. L. BOOMAN AND W. B. HOLBROOK, *Anal. Chem.*, 35 (1963) 1793.
9 J. F. O'DONNELL, J. T. AYRES AND C. K. MANN, *Anal. Chem.*, 37 (1965) 1161.
10 E. BERGMANN AND A. WEIZMANN, *J. Am. Chem. Soc.*, 60 (1938) 1801.
11 R. S. NICHOLSON AND I. SHAIN, *Anal. Chem.*, 36 (1964) 706.
12 R. S. NICHOLSON AND I. SHAIN, *Anal. Chem.*, 37 (1965) 178.
13 W. C. NEIKAM, G. R. DIMELER AND M. M. DESMOND, *J. Electrochem. Soc.*, 111 (1964) 1190.
14 N. OGEMACHI, L. J. ANDREWS AND R. M. KEEFER, *J. Am. Chem. Soc.*, 78 (1956) 2210.
15 R. S. NICHOLSON, *Anal. Chem.*, 38 (1966) 1406.

ELECTROANALYTICAL CHEMISTRY AND INTERFACIAL ELECTROCHEMISTRY
Elsevier Sequoia S.A., Lausanne – Printed in The Netherlands

THE ELECTROCHEMICAL OXIDATION OF *p*-DIMETHYLAMINOPHENOL IN AQUEOUS SOLUTION

MARK F. MARCUS AND M. D. HAWLEY
Department of Chemistry, Kansas State University, Manhattan, Kan., 66502 (U.S.A.)
(Received November 27th, 1967)

Previous workers have shown that simple aromatic amines often exhibit relatively complex electrode behavior[1–5]. The major difficulties that are encountered in the interpretation of their electrode mechanisms arise from a series of chemical reactions accompanying charge transfer. Whether or not a particular reaction will occur is determined by the pH of the solution and the acid–base behavior of the starting amine and its oxidation product. Frequently, the product of the follow-up chemical reaction is also reactive and its electrochemical and chemical reactions complicate the interpretation further.

Despite these apparent complexities, a fuller understanding of these systems is necessary before more complex amines of chemical and biochemical significance can be studied effectively. In this paper we summarize the results of our investigation for the electrochemical oxidation of *p*-dimethylaminophenol. The behavior of this tertiary amine is shown to differ significantly from that reported previously for the unsubstituted *p*-aminophenol[2,4].

EXPERIMENTAL

Instrumentation

Chronoamperometric and chronopotentiometric measurements were made on a combination potentiostat–galvanostat constructed in this laboratory. The circuits for this instrument have been described previously by UNDERKOFLER AND SHAIN[6] and were modified only slightly to allow the incorporation of transistorized amplifiers. The electronic scanner employed a Philbrick P25AU operational amplifier in a standard integrator configuration. Switching of the voltage scan at the anodic and cathodic limits was effected by a comparator[7] driving a multipole mercury-wetted relay (Type HG6F-1028, C. P. Clare and Co.). Current–potential and potential–time curves from this instrument were recorded on a Moseley X–Y recorder, Model 7030A.

A second potentiostat, which employed the circuit of Fig. 15a, ref. 8, was used for coulometry and oscilloscope work. The control amplifier in this unit consisted of a P45ALU operational amplifier in a non-inverting configuration driving a Harrison Model 6824A amplifier[9]. The current and integrator circuits employed Philbrick P35AU and P25AU amplifiers, respectively, in standard configurations. A Hewlett-Packard Model 3300 function generator and Model 3302A trigger served as the signal generator for oscilloscope work; a manually-controlled potentiometer was used for this function in coulometry. The detector was a Tektronix 564 oscilloscope equipped

with Type 2A63 and 2B67 plug-ins for short-term chronoamperometric experiments. Either a potentiometer or a strip-chart recorder was used in the voltage readout for coulometry.

Visible and ultraviolet spectra were recorded on a Cary Model 14 spectrophotometer. The pK_a of PDAP was determined spectrophotometrically by standard techniques. The ESR experiments were carried out in the cavity of a Varian 4500 Spectrometer equipped with a 12-in. magnet.

Cells and electrodes

A carbon paste electrode, having a geometric area of 0.16 cm^2, served as the working electrode for most chronoamperometric and chronopotentiometric experiments. The auxiliary electrode for these studies was a small platinum foil. A large platinum gauze was used as the working electrode for controlled-potential electrolysis; a mercury pool isolated from the working electrode compartment by means of a salt bridge served as the auxiliary electrode for the exhaustive electrolysis work. A saturated calomel electrode was used exclusively as the reference electrode. The cell was thermostated at 25.0° ± 0.1.

Chemicals

With the exception of *p*-dimethylaminophenol, all organic and inorganic chemicals were reagent-grade and were used without further purification. PDAP was prepared by the method of ZANDSTRA AND EVLETH[10]. Because of the susceptibility of the free base to air oxidation, PDAP was converted to its corresponding HCl salt. All solutions of this compound were prepared by adding an accurately weighed amount of sample to the de-aerated buffer just prior to the experimental run. McIlvaine buffers (citrate–phosphate) were used in the pH range 3–8, while carbonate buffers were employed at pH 9–10.

OBSERVATIONS AND DISCUSSION

The electrochemical behavior of PDAP was studied as a function of increasing

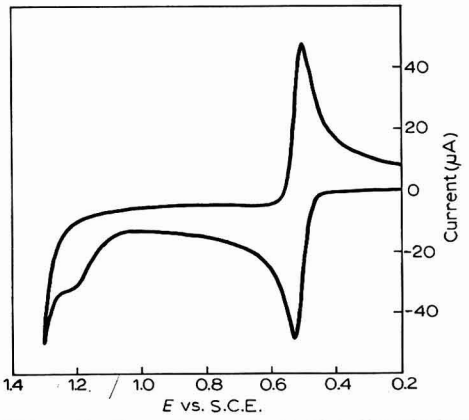

Fig. 1. Cyclic voltammogram of *p*-dimethylaminophenol (PDAP) in 2 *M* H_2SO_4. Concn., 2 m*M*; scan rate, 33.3 mV/sec.

pH. A cyclic voltammogram of PDAP in 2 M H_2SO_4 (Fig. 1) shows two anodic waves, the first occurring at 0.53 V and the second occurring just prior to background at 1.2 V. Upon reversal of the potential scan at 1.3 V, a single reduction wave at 0.50 V is noted on the cathodic sweep. In order to determine the processes responsible for the three waves, both the scan rate and the switching potential were varied. By reversing the direction of the potential scan between the first and second anodic waves, the ratio of the peak cathodic to the peak anodic current was found to exceed one, at all scan rates. This suggests that a chemical reaction precedes electron transfer. By increasing the rate of the anodic potential sweep, $i_p/v^{\frac{1}{2}}$ for the first peak decreased while $i_p/v^{\frac{1}{2}}$ for the second wave increased. This result indicates that both oxidations are kinetically-controlled and that the two electroactive species are in equilibrium with one another. The chemical and electrochemical processes consistent with these results are shown in eqns. (1)–(3):

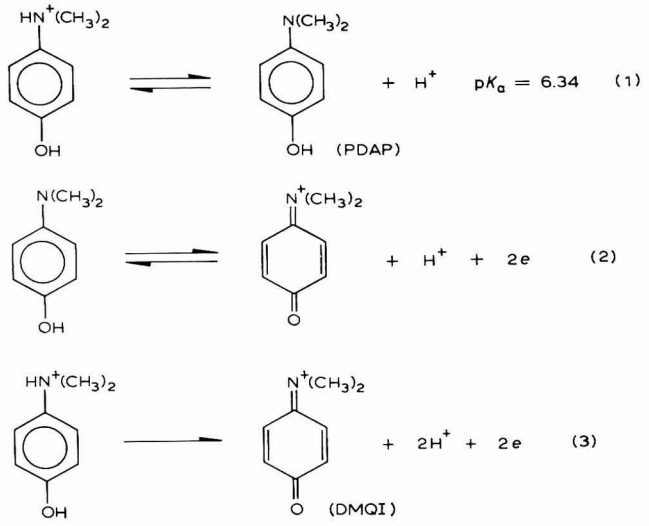

The protonated PDAP is the more difficult of the two species to oxidize.

The cyclic voltammetric behavior of PDAP at pH 3 appears to be free of complication (Fig. 2). On the first anodic sweep, the two-electron oxidation of PDAP to give *p*-N,N-dimethylbenzoquinoneimine (DMQI) occurs at 0.4 V. Upon reversal of the potential scan at 0.7 V, only the reduction of DMQI back to PDAP is seen on the cathodic sweep. On subsequent cycles, only this one system is observed.

Controlled-potential electrolysis of PDAP at 0.6 V confirms the $n=2$ interpretation for the oxidation of PDAP. However, if one studies a solution of PDAP by cyclic voltammetry shortly after exhaustive electrolysis, a second reduction wave emerges cathodic of the DMQI wave (Fig. 2). The magnitude of this second wave increases with time while the peak current for the DMQI wave decreases. The new process arises from the reduction of benzoquinone and was identified by the comparison of a cyclic voltammogram and u.v. spectrum of this system with those of an authentic sample of benzoquinone. Benzoquinone would be the expected product

from the electrolysis if the initial product of electron transfer, DMQI, undergoes hydrolysis:

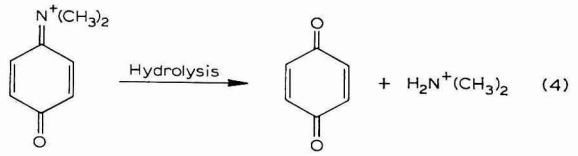

Coulometric oxidation of PDAP and subsequent examination of the electrolyzed solution by cyclic voltammetry revealed that the hydrolysis of DMQI also occurs in strong acid solution. The rate of this hydrolysis, however, is considerably slower in acidic media than is the corresponding hydrolysis rate for either *p*-benzoquinoneimine or *p*-N-methylbenzoquinoneimine[4]. This is consistent with the results of KOEHLER, SANDSTROM AND CORDES who also observed a marked decrease in the rate of imine hydrolysis in acidic media with increasing substitution on the nitrogen atom[11].

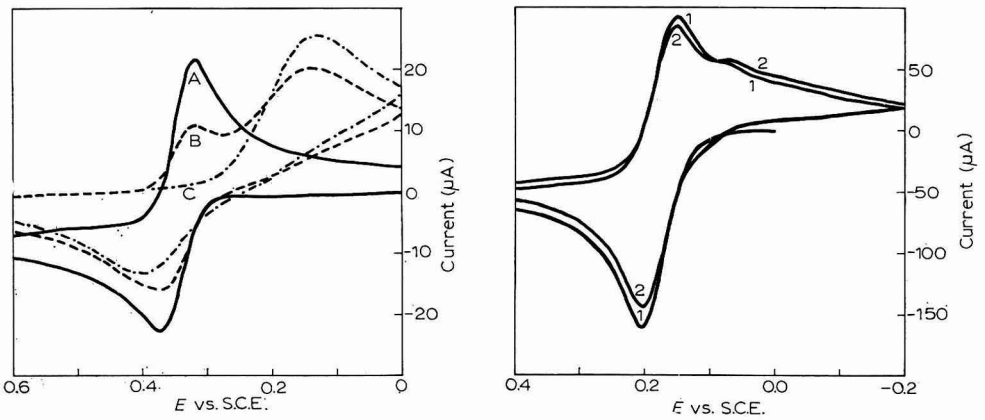

Fig. 2. Cyclic voltammograms of PDAP and its oxidation products at pH 3. Scan rate, 83.3 mV/sec; the original soln. was 0.33 m*M* in PDAP. (A), before electrolysis; (B), shortly after exhaustive electrolysis; (C), after 1 h.

Fig. 3. Cyclic voltammetry of PDAP at pH 6. Concn., 2 m*M*; scan rate, 83.3 mV/sec; (1 and 2), first and second cycles, respectively.

The electrochemical behavior of PDAP becomes increasingly more complicated at higher pH. The cyclic voltammetry of PDAP at pH 6 (Fig. 3) shows three cathodic waves. The most positive of the three peaks arises from the reduction of the unhydrolyzed DMQI back to PDAP, while the more negative of the remaining two peaks results from the reduction of benzoquinone, one of the hydrolysis products of DMQI. On the second, and all subsequent anodic sweeps, there is an additional anodic process occurring just slightly cathodic of the main oxidation wave for PDAP. Since hydroquinone is oxidized at nearly the same potential as PDAP, the cathodic wave interposed between the peaks corresponding to the reductions of DMQI and benzoquinone and this newly formed anodic wave, represent a third redox couple. The identity of this couple and its behavior will be discussed in a later section. On the second cathodic sweep, the peak current for the DMQI wave decreases, while

the peak currents for the other two waves increase. This indicates that the latter two processes arise as a result of follow-up reactions involving DMQI.

The cyclic voltammetry of PDAP at pH 7 is qualitatively similar to that at pH 6, although the rate of the initial follow-up reaction is significantly larger at the higher pH. The increase in rate is predicted if hydrolysis results from the nucleophilic attack of hydroxide ion upon the positively charged quinoneimine[11,12]. The value of the rate constant cannot be determined by the usual applications of chronoamperometric and chronopotentiometric methods, however. Whereas $it^{\frac{1}{2}}$ and $i\tau^{\frac{1}{2}}$ for the oxidation process at pH 4 are independent of time and current, respectively, the corresponding values at higher pH are kinetically-controlled. The variation in these values is essentially what one might expect if n were to change effectively during the experimental run from two at short times, to three at long times. This behavior suggests an ECE process in which a chemical reaction is interposed between charge-transfer steps[13,14]. A chemical process consistent with this interpretation is the Michael 1,4-addition of a hydrolysis product, dimethylamine, to DMQI:

$$H_2N^+(CH_3)_2 \rightleftharpoons HN(CH_3)_2 + H^+ \qquad (5)$$

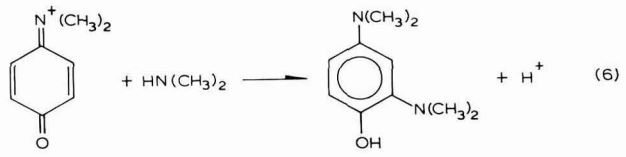

(6)

As a consequence of amine substitution, 2,4-bis(dimethylamino)phenol is more easily oxidized than the starting aminophenol and can be oxidized by the unhydrolyzed DMQI to 3-dimethylamino-*p*-N,N-dimethylbenzoquinoneimine (DDQI):

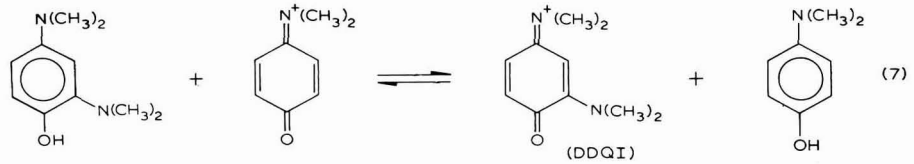

(7)

The PDAP generated in solution by the chemical redox reaction is then oxidized electrochemically according to eqn. (2). The 2,4-bis(dimethylamino)phenol formed by the process described in eqn. (6) gives rise to the small anodic wave in Fig. 3 which precedes the main oxidation wave of PDAP on the second anodic sweep. The effect of DMQI hydrolysis and the subsequent 1,4-addition of dimethylamine to DMQI is to cause a change in the apparent n-value from a limit of $n=2$ when no hydrolysis occurs, to a limit of $n=3$ when all chemical reactions are extremely fast.

A Michael 1,4-addition reaction involving the two hydrolysis products, benzoquinone and dimethylamine, can also occur (eqn. (8))[15]:

(8)

However, since nucleophilic attack of unprotonated dimethylamine should occur much more rapidly on the positively charged DMQI than on the uncharged benzoquinone, this latter reaction probably does not need to be considered as long as DMQI is present. Separate chronoamperometric experiments in which benzoquinone was generated *in situ* in the presence of excess dimethylamine support the conclusion that dimethylamine addition to benzoquinone is relatively slow at pH 7.

The results of controlled-potential electrolysis of PDAP at pH 7 and of the subsequent examination of the solution at various times during the electrolysis are consistent with the reaction scheme presented above. Whereas controlled-potential electrolysis of PDAP in solutions of pH 4 or less gave $n=2$, the required coulombs for $n=3$ were passed quickly at pH 7. Electrolysis continued beyond this point, although much more slowly, and finally ceased when n was equal to four. This suggests that DDQI is also undergoing hydrolysis, but at a rate much slower than DMQI (eqn. (9)).

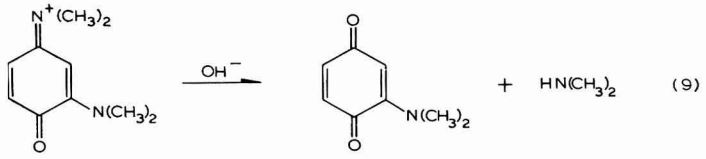

(9)

The effect of dimethylamine substitution is not only to stabilize the positively charged DDQI towards hydrolysis, but also to deactivate dimethyl-*p*-benzoquinone towards nucleophilic attack by dimethylamine. Hence, the dimethylamine formed from this hydrolysis (eqn. (9)) adds to benzoquinone obtained during the initial hydrolysis and not to dimethyl-*p*-benzoquinone (eqn. (10)).

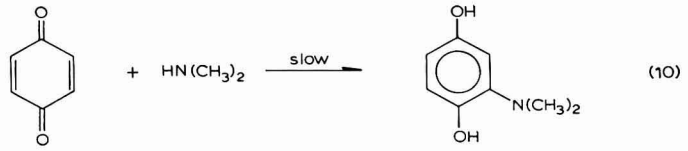

(10)

Dimethylaminohydroquinone is then oxidized to the corresponding quinone, accounting for the observed $n=4$ by coulometry (eqn. (11)).

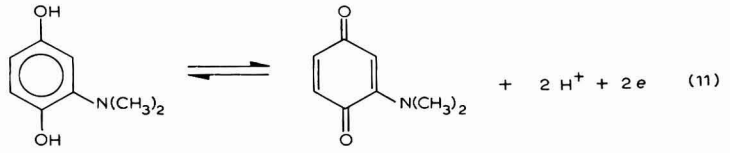

(11)

Two anodic and two cathodic waves are seen in the cyclic voltammogram (Fig. 4) of a PDAP solution electrolyzed to the point, $n=2$. At this stage in the oxidation, the system should contain benzoquinone, an equal molar amount of DDQI, and unelectrolyzed PDAP (0.33 of the amount originally present). Since the anodic sweep is initiated cathodic of the two reduction processes, the first anodic wave near 0.05 V is the reoxidation of 2,4-bis(dimethylamino)phenol to DDQI, while the second process is a composite wave for the oxidation of benzoquinone and PDAP. Upon reversal of the potential scan at 0.50 V, sufficient time has elapsed

for almost complete hydrolysis of DMQI; consequently, no cathodic wave can be clearly discerned in the voltammogram for the reduction of DMQI back to PDAP. The reductions of DDQI and benzoquinone occur near 0.0 V and −0.05 V, respectively, and are partially merged.

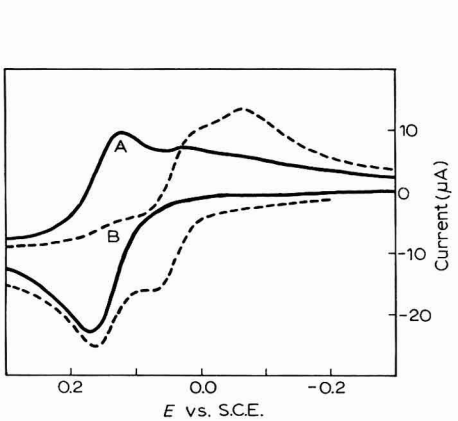

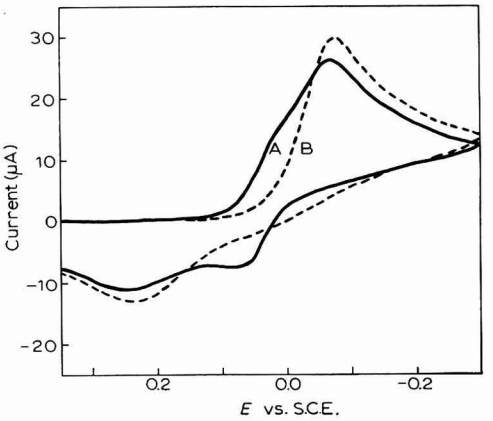

Fig. 4. Cyclic voltammograms of PDAP at pH 7. Concn. 0.33 mM; scan rate, 83.3 mV/sec. (A), before electrolysis; (B), at the point $n = 2$.

Fig. 5. Cyclic voltammetry of the PDAP oxidation products at pH 7. Concn., 0.33 mM in PDAP prior to electrolysis; scan rate, 83.3 mV/sec. (A), at the point $n = 3$; (B), after exhaustive electrolysis ($n = 4$).

According to the sequence of reactions described above, when electrolysis has proceeded to the point $n=3$, the two predominant products should be DDQI and benzoquinone. The cyclic voltammogram of this solution (Fig. 5) again shows two anodic and two cathodic waves. The major difference between this voltammogram and Fig. 4 is the absence of any significant amount of anodic current upon application of the cathodic-going sweep at 0.6 V. This would occur if either or both of the reactions described in eqns. (9) and (10) were slow. The partially merged cathodic waves are due again to the reduction of DDQI and benzoquinone; the anodic waves result from reoxidation of the products formed on the cathodic sweep. Because of the electrochemically irreversible behavior of the benzoquinone–hydroquinone system, hydroquinone is oxidized at the more positive of the two potentials.

A cyclic voltammogram of the completely electrolyzed solution (Fig. 5) shows a single oxidation wave near 0.25 V and a cathodic peak near −0.08 V. On the subsequent cycles, no other processes are observed. As would be expected, the cyclic voltammetric behavior of 2-dimethylamino-*p*-benzoquinone, the final product, is very similar to benzoquinone and differs only slightly in the location of the peak potentials.

The completely electrolyzed solution of PDAP was red in color. Examination of this solution in the visible and ultraviolet regions showed peaks at 500 and 232 mμ, and a shoulder at 265 mμ. This spectrum is identical with the one recorded by TUBER AND HASSELBACH for an authentic sample of 2-dimethylamino-*p*-benzoquinone[16].

Two different radicals were observed by ESR before and during the controlled-

potential electrolysis at pH 7. Initially, the solution had a faint tinge of red and orange and gave a spectrum identical with the one reported by ZANDSTRA AND ELVETH for the phenoxy radical of PDAP[10]. Even though all solutions were deaerated, traces of oxygen remaining in the solution could cause some oxidation and the concomitant formation of the radical. A solution electrolyzed to the point of $n=3$ was intensely purple in color. Examination of a portion of this solution in the ESR cavity revealed the five-line spectrum of *p*-benzosemiquinone free radical. Since small amounts of the radical are normally present in benzoquinone solutions at pH 7, this lends further support to the conclusion that dimethylamine addition is to DMQI and not to benzoquinone. The purple color, which is probably due to DDQI, was absent in the completely electrolyzed solution. No ESR signal could be detected at this point ($n=4$).

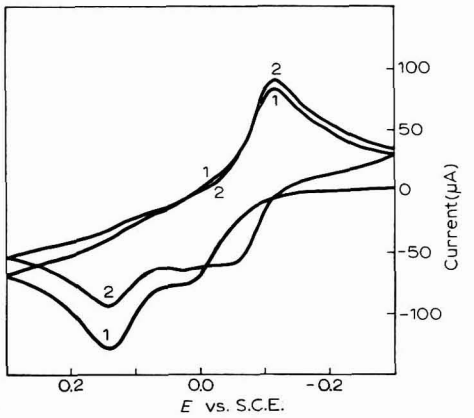

Fig. 6. Cyclic voltammetry of PDAP at pH 9. Concn., 2 m*M*; scan rate, 83.3 mV/sec; (1 and 2), first and second cycles, respectively.

At pH 8, an inflection in the PDAP oxidation was noted. At slightly higher pH (Fig. 6), the main oxidation wave is split into two. The first of these two waves is observed to shift cathodically with increasing pH, while the second wave is independent of pH. Since variation of the scan rate does not affect the relative heights of the two waves, we ascribe this result to successive one-electron oxidations, the first one-electron oxidation giving the phenoxy radical, the second oxidation the quinoneimine:

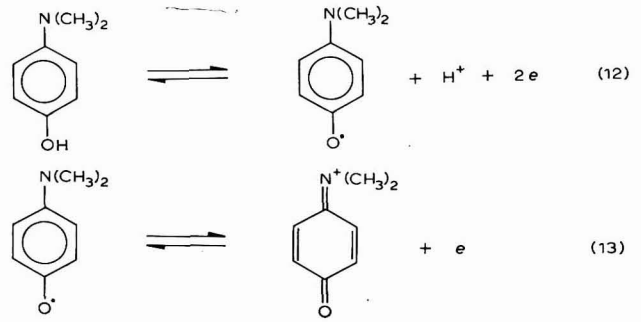

The small cathodic wave near 0.0 V arises from the reduction of the phenoxy radical back to PDAP. Since the quinoneimine which is formed by the one-electron oxidation of the radical undergoes rapid hydrolysis at this pH, no cathodic wave for its reduction can be observed at these scan rates. The anodic wave which appears near −0.05 V on the second cycle arises from the oxidation of 2,4-bis(dimethylamino)phenol. Although cyclic voltammetry is not in itself definitive at this pH, the cathodic processes merged near −0.10 V and −0.18 V probably arise from the reduction of DMQI, benzoquinone, and dimethyl-*p*-benzoquinone. The reoxidation waves for the two hydroquinones that are formed on the cathodic sweep are buried beneath the PDAP oxidation waves.

SUMMARY

The electrochemical oxidation of *p*-dimethylaminophenol (PDAP) has been studied over its stable pH-range. In acidic media, a chemical transformation of the protonated *p*-dimethylaminophenol to the free base precedes electron transfer. The product of this two-electron oxidation, *p*-N,N-dimethylbenzoquinoneimine, then undergoes hydrolysis to give benzoquinone and dimethylamine. The oxidation of PDAP in the pH-range 6–9 is a four-electron process which yields 2-dimethylamino-*p*-benzoquinone as the product. The intermediates and reactions which lead to this product have been identified by electrochemical and spectroscopic methods. In basic media, oxidation proceeds in two one-electron steps, giving first the phenoxy radical, and then the quinoneimine.

REFERENCES

1 H. B. Mark and F. C. Anson, *Anal. Chem.*, 35 (1963) 722.
2 A. C. Testa and W. R. Reinmuth, *ibid.*, 32 (1960) 1512.
3 T. Mizoguchi and R. N. Adams, *J. Am. Chem. Soc.*, 84 (1962) 2058.
4 M. D. Hawley and R. N. Adams, *J. Electroanal. Chem.*, 10 (1965) 376.
5 Z. Galus, H. Y. Lee and R. N. Adams, *J. Electroanal. Chem.*, 5 (1963) 17.
6 W. L. Underkofler and I. Shain, *Anal. Chem.*, 35 (1963) 1778.
7 R. P. Buck and R. W. Eldridge, *ibid.*, p. 1829.
8 W. M. Schwarz and I. Shain, *ibid.*, p. 1770.
9 Hewlett-Packard, Harrison Division, *Power Supply-Amplifier: Concepts and Modes of Operation*, Application Note 82, 1966, p. 6.
10 P. J. Zandstra and E. M. Elveth, *J. Am. Chem. Soc.*, 86 (1964) 2664.
11 K. Koehler, W. Sandstrom and E. H. Cordes, *J. Am. Chem. Soc.*, 86 (1964) 2413.
12 L. K. J. Tong, *J. Phys. Chem.*, 58 (1954) 1090.
13 G. S. Alberts and I. Shain, *Anal. Chem.*, 35 (1963) 1859.
14 A. C. Testa and W. H. Reinmuth, *ibid.*, 33 (1961) 1320.
15 R. Baltzly and E. Lorz, *J. Am. Chem. Soc.*, 70 (1948) 861.
16 H.-J. Tuber and M. Hasselbach, *Chem. Ber.*, 92 (1959) 674.

Elsevier Sequoia S.A., Lausanne – Printed in The Netherlands

SHORT COMMUNICATIONS

Simultaneous anion and cation specific adsorption at an ideal polarized electrode. A thermodynamic analysis for thallium(I) nitrate

The structure of the electrical double layer with specific adsorption (SA) of a single ionic species is well understood, but it is only recently that an attempt was made[1], in the particular case of $TlNO_3$, to separate anion and cation SA when both species undergo strong simultaneous SA. A non-thermodynamic approach was followed and, in addition to the usual application of the Gouy–Chapman theory, it was necessary to postulate a simple distribution of potential in the compact double layer and to introduce assumed distances between the electrode and the inner and outer Helmholtz planes. These assumptions were not made without misgivings but they were in line with current thinking on the double-layer structure, and moreover there was some internal checking of the calculated amounts of specifically adsorbed Tl^+ and NO_3^-. It was concluded that there is strong enhancement in SA of each ionic species because of SA of the species of opposite ionic valence.

It was pointed out by PARSONS[2] that separation of anion and cation SA was feasible by double-layer measurements (interfacial tension and/or differential capacity) at constant ionic strength. This method was worked out previously for single ionic SA by HURWITZ[3] and DUTKIEWICZ AND PARSONS[4]. The principle is as follows:

We consider two series of solutions having the following compositions:

$$(y-x)M\ TlF + xM\ TlNO_3 \qquad (A)$$

$$(y-x)M\ KNO_3 + xM\ TlNO_3 \qquad (B)$$

where y is a constant and x is varied. Thermodynamic analysis then yields for series A

$$-d\gamma = q\,dE_+ + (RT/F)q_-^1\,d\ln x \qquad (1)$$

and for series B

$$-d\gamma = q\,dE_- + (RT/F)q_+^1\,d\ln x \qquad (2)$$

where γ is the interfacial tension, q the charge density on the electrode, E the potential with respect to a reference electrode that is reversible to Tl^+ (E_+) or NO_3^- (E_-), q_-^1 and q_+^1 the amounts of specifically adsorbed NO_3^- and Tl^+, respectively and R, T and F have their usual significance. There are some reasonable assumptions made in the derivation of eqns. (1) and (2) which are the same as those introduced for single ionic SA[3,4]. It follows from eqns. (1) and (2) that q_-^1 and q_+^1 are directly obtained from plots of γ *vs.* $\ln x$ at constant E_+ or E_-. This approach is applied here, and results are compared with those of the previous non-thermodynamic study.

Experimental

Solutions were prepared from Baker "Analyzed Reagent" $TlNO_3$ and KNO_3,

the former salt having been recrystallized twice. TlF was obtained from A. D. Mackay, New York and was used directly. All solutions were treated with purified activated charcoal ("Barker technique").

The following cell was used:

$$\mathrm{Hg} \,||\, \underset{(y=0.2)}{\text{soln. A or B}} \,|\, \underset{(y=0.2)}{\text{soln. A or B}} \,|\, 0.2\ M\ \mathrm{KNO_3} \,|\, 0.1\ M\ \mathrm{KCl} \,||\, 0.1\ \mathrm{NCE}$$

where the second compartment on the left-hand side containing solutions A or B was introduced in the design of the cell to prevent contamination due to transfer between compartments. This precaution may have been superfluous. The junction potential between solution A or B and 0.2 M KNO_3 did not vary by more than 2 mV in this work and was supposed to be constant. The precision in interfacial tension measurements was ± 0.05 and ± 0.03 dyn cm^{-1} for solutions A and B, respectively. All electrocapillary curve measurements of solution B were repeated 3 times until results that were judged satisfactory were obtained. Differential capacity measurements were of the conventional type. Temperature: $25 \pm 2°$.

Results

Electrocapillary curves were obtained for $x = 0.1$ and 0.14 for solution A, and $x = 0.1$, 0.15 and 0.2 for solution B. The curves for solution B were obtained directly whereas those for solution A were determined by integration of the differential capacities using γ-data (with the same solutions) for the computation of the two integration constants. This procedure was adopted for the fluoride solutions because γ-measurements appear somewhat more difficult than with other anions (etching of glass?). It was hoped that such calculated electrocapillary curves were a little more reliable than directly measured curves*.

Interfacial tensions for 0.2 M $TlNO_3$ were 0.6–0.8 dyn cm^{-1} higher than those previously reported[1] from $+0.1$ to -0.1 V *vs.* 0.1 NCE. The discrepancy increased to 1.2 dyn cm^{-1} at -0.2 V *vs.* 0.1 NCE. This difference alone is not large enough to account for major differences in results deduced from the two sets of data.

The charge density on the electrode for 0.2 M $TlNO_3$, as obtained by graphical differentiation and by a 3-point numerical differentiation, was nearly the same as previously reported[1]. Present values were higher by 0.1–0.2 μC cm^{-2} for $E > 0$ V *vs.* 0.1 NCE, and were practically the same at more negative potentials.

Values of $q_-{}^1$ and $q_+{}^1$ deduced by application of eqns. (1) and (2) are plotted against q in Fig. 1 together with previously reported values[1]. Two significant conclusions can be drawn from Fig. 1:

(a) Amounts of specifically adsorbed ions obtained by this method are higher than those computed by the non-thermodynamic method based on a simple electrostatic model for distribution of potential in the compact double layer. Such a method, therefore, is even less satisfactory than was suspected.

(b) There is strong enhancement of Tl^+ SA because of NO_3^- SA and *vice-versa*, NO_3^- SA is enhanced by Tl^+ SA. This conclusion, which was already drawn from the

* This is open to question since electrocapillary data are needed anyway to integrate the differential capacity. Unfortunately, it was not possible to apply the usual procedure of determining the point of zero charge (Tl^+ reduction!).

previous results[1], is evident if one compares $q_{-}{}^{1}$ of Fig. 1* with values of $q_{-}{}^{1}$ reported by PAYNE[5] in the absence of cation SA. Likewise, $q_{+}{}^{1}$ in Fig. 1 is higher than the values of $q_{+}{}^{1}$ for pure TlF previously reported[6] (only minor anion SA).

The potential, ϕ_2, in the outer Helmholtz plane was calculated from $q + q_{-}{}^{1} + q_{+}{}^{1}$ by application of the Gouy–Chapman theory. Results are compared in Fig. 2 with those previously reported[1]. Tl^+ SA brings ϕ_2 into the positive range. Conversely,

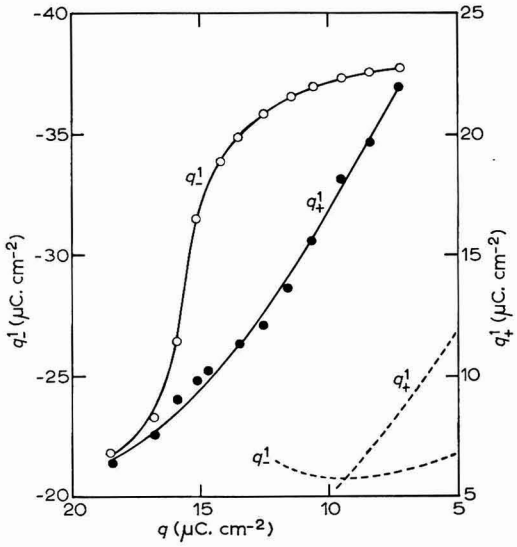

Fig. 1. Amount of specifically adsorbed Tl^+ (●) and NO_3^- (○) for 0.2 *M* $TlNO_3$ *vs.* charge density on electrode. Dashed curves according to ref. 1.

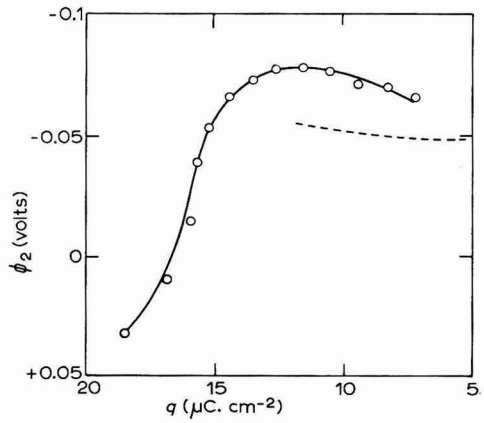

Fig. 2. Potential in outer Helmholtz plane *vs.* charge density on the electrode. Dashed curve according to ref. 1.

* Values of $q_{-}{}^{1}$ decrease as q becomes more positive but one would expect ultimately $q_{-}{}^{1}$ to increase with q. This probably occurs outside the experimentally feasible range of potentials because of Hg-oxidation.

NO_3^- SA results in negative values of ϕ_2 for $q>0$. Only negative ϕ_2's are computed for NO_3^- SA without cation SA for the q-values covered here[5]. Conversely, only positive ϕ_2's were computed for TlF for $q>0$.

The measurements could be extended to other values of y in solutions A and B, and an attempt could be made to assign an isotherm for mixed SA, as was done previously[1]. This work, however, was beyond the scope of this investigation.

Acknowledgement

This work was supported by the National Science Foundation. One of the authors (B.B.) is also indebted to the Electrochemical Society for a Summer Fellowship in 1967.

Department of Chemistry,
New York University,
New York, N.Y. 10003 (U.S.A.)

B. BARON
P. DELAHAY
D. J. KELSH*

1 G. G. SUSBIELLES, P. DELAHAY AND E. SOLON, *J. Phys. Chem.*, 70 (1966) 2601.
2 R. PARSONS, *J. Electrochem. Soc.*, 113 (1966) 971.
3 H. D. HURWITZ, *J. Electroanal. Chem.*, 10 (1965) 35.
4 E. DUTKIEWICZ AND R. PARSONS, *ibid.*, 11 (1966) 100.
5 R. PAYNE, *J. Phys. Chem.*, 69 (1965) 4113.
6 P. DELAHAY AND G. G. SUSBIELLES, *ibid.*, 70 (1966) 647.

Received November 23rd, 1967

* Present address: Department of Chemistry, Gonzaga University, Spokane, Washington 99202.

Potentiometric estimation of tripotassium aquo-trihydroxotetracyanomolybdate(IV) and determination of standard potential

No mention is made in the existing chemical literature of the redox processes involved in an aqueous solution of tripotassium aquo-trihydroxotetracyanomolybdate(IV), or of its quantitative estimation. The redox potential for the reaction, $[Mo(CN)_8]^{3-}+e=[Mo(CN)_8]^{4-}$, has been given as +0.82 V. When four CN^- groups are replaced by four OH^- groups, $E_{Mo(V)/Mo(IV)}=+0.10$ V and the potential of hydroxotetracyanomolybdate at pH 13.5 is, $E_{Mo(V)/Mo(IV)}=-0.76$ V[1].

During the hydrolytic transformation of hydroxocyanomolybdates—

$$\left[\begin{matrix} & (OH)_4 & \\ Mo & & \\ & (CN)_4 & \end{matrix}\right]^{4-} \xrightarrow{aq.} \left[\begin{matrix} & (OH)_3 & \\ Mo & (OH_2) & \\ & (CN)_4 & \end{matrix}\right]^{3-} \xrightarrow{aq.} \left[\begin{matrix} & (OH)_2 & \\ Mo & (OH_2)_2 & \\ & (CN)_4 & \end{matrix}\right]^{2-},$$

there is a significant change in the basicity of the solution as well as in the redox potential characteristic of this system.

This communication deals with the estimation of tripotassium aquo-tri-

hydroxotetracyanomolybdate(IV) using $K_3[Fe(CN)_6]$ and $KMnO_4$ as oxidants, and the determination of E^0 of the redox couple in aqueous alkaline medium.

Experimental

Preparation and purity of complex salts

Tripotassium aquo-trihydroxotetracyanomolybdate(IV) dihydrate[2,3]. The crystalline red-violet complex, $K_4[Mo(CN)_4(OH)_4]$, was prepared by the modified method of JAKOB AND TURKIEWICZ[4]. It was then hydrolyzed with water to give the soluble blue compound, $K_3[Mo(CN)_4(OH)_3(H_2O)]$[5], which was isolated in the solid state by fractional precipitation with ethanol. It was kept over $CaCl_2$ in a vacuum desiccator.

Potassium hexacyanoferrate(III). The A.R.-grade product was recrystallised from water and air-dried. The iron content of the complex was determined iodometrically as Fe(III)[6].

All other reagents used were either of A.R.-grade (B.D.H) or Merck reagent-grade. The complex salt solutions were stored in coloured bottles wrapped in black paper.

Apparatus. A Pye Precision Vernier Potentiometer (Cat. No. 7568) in conjunction with a ballistic galvanometer and lamp and scale arrangement was used for potential measurements. A bright platinum electrode was used as an indicator and a saturated calomel electrode as the reference electrode. Pure nitrogen was used to maintain an inert atmosphere.

All measurements were made in a darkened room. The temperature was maintained constant within $\pm 0.1°$ in a Townson and Mercer thermostat.

Results and discussion

Estimation with alkaline $K_3[Fe(CN)_6]$. Tripotassium aquo-trihydroxotetracyanomolybdate(IV) was determined potentiometrically by titration in alkaline solution with potassium hexacyanoferrate(III). The galvanic circuit was as follows:

$$\overline{Pt} \;\Big|\; K_3[Mo(CN)_4(OH)_3(H_2O)] \;\Big\|\; KCl \;\Big\|\; \begin{matrix} KOH \\ 1\ M \end{matrix} \;\; \begin{matrix} Hg_2Cl_2 \\ (satd.) \end{matrix} \;\Big|\; Hg^+$$

The titrations were carried out in 1 *M* KOH at 30° with 0.1 *M* $K_3[Fe(CN)_6]$. A typical curve is shown in Fig. 1a.

The intensity of blue colour of the solution decreases as the titration proceeds. At the equivalence point, the solution turns colourless and excess of titrant then gives a permanent yellow colour. A break of 0.52 V/0.1 ml was observed at the equivalence point.

The redox reaction may be represented as:

$$[Mo(CN)_4(OH)_3(H_2O)]^{3-} + 2[Fe(CN)_6]^{3-} \rightleftharpoons [Mo(CN)_4(OH)_3(H_2O)]^{-} + 2[Fe(CN)_6]^{4-} \quad (1)$$

for which the equilibrium constant has been calculated using $E^0[Fe(CN)_6]^{3-}/[Fe(CN)_6]^{4-} = +0.36$ V[7] and $E^0[Mo(CN)_4(OH)_3(H_2O)]^{-}/[Mo(CN)_4(OH)_3(H_2O)]^{3-} = -0.6827$ V (as described below). The value of $K = 5.71 \cdot 10^{10}$ indicates that at equilibrium, almost all the $[Mo(CN)_4(OH)_3(H_2O)]^{3-}$ is oxidized to $[Mo(CN)_4(OH)_3(H_2O)]^{-}$ by ferricyanide ions.

The method is accurate to $\pm 0.01\%$.

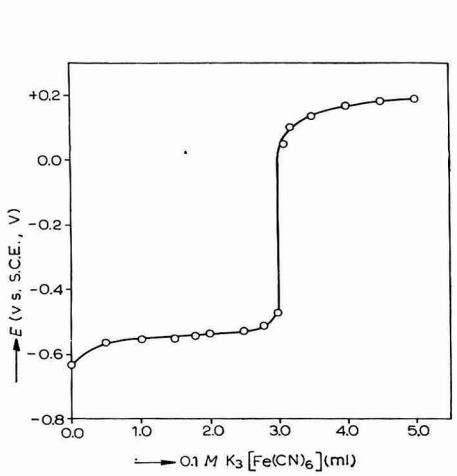

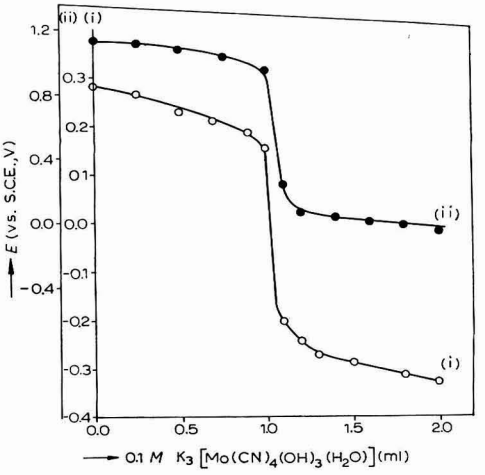

Fig. 1a. Potentiometric titration of $K_3[Mo(CN)_4(OH)_3(H_2O)]$ with $K_3[Fe(CN)_6]$.
Fig. 1b. Potentiometric titration with $K_3[Mo(CN)_4(OH)_3(H_2O)]$ of: (i), $K_3Fe(CN)_6$ in alkaline medium; (ii), $KMnO_4$ in acid medium.

The estimation was also carried out with $K_3Fe(CN)_6$ in the cell and titrating with hydroxocyanomolybdate. The yellow colour of potassium hexacyanoferrate(III) disappears and excess of hydroxocyanide gives a blue colour to the solution. Results of potentiometric titrations at 30° in 1 *M* KOH are given in Fig. 1b (curve i). A potential jump of 0.37 V/0.1 ml was observed at the equivalence point.

Estimation with acid $KMnO_4$. Only reverse titrations ($KMnO_4$ in the cell) are possible. The $KMnO_4$ solution in 4 *N* H_2SO_4 was titrated with 0.1 *M* hydroxocyanide and was gradually decolourized on reduction. Any hydroxocyanide added after the equivalence point is decomposed by the acidity of the reaction mixture. A potential break of 0.705 V/0.1 ml was observed. The results are shown in Fig. 1b (curve ii).

Determination of E^0. E^0 was determined by the potential mediator method. 10 ml of hydroxocyanide (0.014 *M*) was titrated with 0.1 *M* $K_3[Fe(CN)_6]$. After each addition, sufficient time was allowed for the system to come to equilibrium; the potential was then measured at the bright platinum electrode. Titrations were continued until a sudden change in potential was observed. Experiments were carried out with varying concentrations of KOH (0.1–5.0 *M*).

The value of E^0 was determined using the relation:

$$E = E^0 - [RT/nF] \ln [t/t_c - t]$$

where E is the electrode potential, t the amount of oxidant added at any point during the titration, t_c the amount of oxidant added at the equivalence point and R, T, F and n have their usual significance. The mean values of E^0, determined graphically by plotting $\log [t/t_c - t]$ *vs.* electrode potential (Fig. 2), in the presence of varying KOH concentrations are recorded in Table 1.

It can be seen from Fig. 2 that the slope of the various straight lines is −0.03, so that n, the number of electrons taking part in the equilibrium process, is equal to 2.

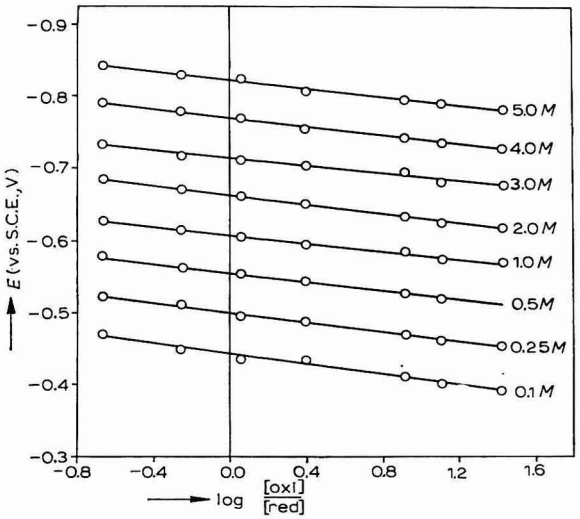

Fig. 2. Plot of electrode potential *vs.* log [ox]/[red] at varying KOH concn.

TABLE 1

VALUES OF E^0 IN THE PRESENCE OF VARYING CONCENTRATIONS OF KOH

KOH concn. (M)	*E^0 (from plot) (V)*	*KOH concn. (M)*	*E^0 (from plot) (V)*
0.10	−0.683	2.0	−0.702
0.25	−0.698	3.0	−0.703
0.50	−0.693	4.0	−0.708
1.0	−0.696	5.0	−0.710

The oxidation–reduction reaction may be represented as:

$$[Mo(IV)(CN)_4(OH)_3(H_2O)]^{3-} \rightleftharpoons [Mo(V)(CN)_4(OH)_3(H_2O)]^{2-} + e \rightleftharpoons$$
$$[Mo(VI)(CN)_4(OH)_3(H_2O)]^{-} + e \qquad (2)$$

The effect of KOH concentration on the E^0-value of the system may be interpreted in a similar manner to that proposed by KOLTHOFF[8] for the effect of HCl concentration on the ferro–ferricyanide system. On the basis of these considerations the equation

$$E(\text{ox/red}) = E^0 - [RT/nF] \ln [\text{ox}]/[\text{red}][\text{KOH}]^{\alpha} \qquad (3)$$

holds instead of the usual equation:

$$E = E^0 - [RT/nF] \ln [\text{ox}]/[\text{red}].$$

The plot of E *vs.* log [KOH] at a fixed value of [ox]/[red] is a straight line the slope of which gives a value of $\alpha = 0.5$. Thus, the equation representing the effect of KOH on the redox couple is:

$$E(\text{ox/red}) = E^0 - [RT/nF] \ln [\text{ox}]/[\text{red}][\text{KOH}]^{0.5} \qquad (4)$$

Effect of ionic strength and calculation of thermodynamic quantities. The ionic strength was adjusted with KNO_3 solution. Experiments carried out at different ionic strengths show that the oxidation potential increases with increase in ionic strength.

TABLE 2

VALUES OF E^0 AT DIFFERENT TEMPERATURES ($\mu = 0.1750$)

Temp. (°K)	E^0 (V)	*Temp.* (°K)	E^0 (V)
303	−0.683	323	−0.713
308	−0.693	328	−0.721
313	−0.702	333	−0.730
318	−0.705	—	—

E^0 was measured at different temperatures (Table 2) in the range 303–333°K at intervals of 5°. These values were used to calculate ΔF^0, ΔH^0 and ΔS^0 for the system at various temperatures; the values at 303°K are 31.491, 52.440 and 0.069 kcals, respectively.

Acknowledgement

We thank Professor A. R. KIDWAI and Dr. S. M. F. RAHMAN for providing the facilities for this work and the Council of Scientific and Industrial Research, New Delhi, for the award of a Junior Fellowship to one of us (K.U.).

Department of Chemistry,
Aligarh Muslim University,
Aligarh (India)

M. AIJAZ BEG
A. A. KHAN
KABIR-UD-DIN

1 K. N. MIKHALEVICH, *Nauch. Zapiski L'vov. Politekh. Inst., Ser. Khim.-Tekhnol.*, 29 (1955) 51; *C.A.*, 51 (1957) 10285.
2 N. V. SIDGWICK, *Chemical Elements and Their Compounds*, Vol. II, Oxford University Press, 1950, p. 1056.
3 A. W. ADAMSON AND J. R. PERUMAREDDI, *Inorg. Chem.*, 4 (1965) 247.
4 W. F. JAKOB AND E. TURKIEWICZ, *Roczniki Chem.*, 11 (1931) 569; Z. JAKOB AND W. JAKOB, *Zeszyty Nauk. Uniw. Jagiel., Ser. Nauk. Mat.-Przyrod., Mat., Fiz., Chem.*, No. 2 (1956) 49; *C.A.*, 52 (1958) 17981.
5 W. R. BUCKNALL AND W. WARDLAW, *J. Chem. Soc.*, (1927) 2981.
6 A. I. VOGEL, *Quantitative Inorganic Analysis*, Longmans, Green and Co., New York, 1951, p. 356.
7 I. M. KOLTHOFF AND W. J. TOMSICEK, *J. Phys. Chem.*, 39 (1935) 945.
8 I. M. KOLTHOFF, *Chem. Weekblad*, 16 (1919) 1406.

Received October 31st, 1967; in revised form, December 28th, 1967

Dissolution of the anodic oxide film on aluminium in a sulphuric acid solution. Comment on the paper by Nagayama and Tamura

Introduction

A discussion of the paper by NAGAYAMA AND TAMURA is presented. Several inadequate conclusions are examined and a refined treatment is proposed. This treatment will explain all the experimental phenomena observed during anodizing—whether at high or low operating temperatures. This refined model is considered to lead naturally to the truncated cone-shaped pores presented by PAOLINI, MASOERO, SACCHI AND PAGANELLI.

A recent paper by NAGAYAMA AND TAMURA[1], reported the results of an examination of the rate of dissolution, in 10% sulphuric acid, of anodically-formed oxide on aluminium, during and after anodisation. The authors have shown that, while the film was forming, approximately two-thirds of the aluminium consumed during anodising remained as oxide, and the remaining one-third passed into solution.

NAGAYAMA AND TAMURA gave the following expression for the total amount of aluminium present as oxide during anodising (W_a^0) as:

$$W_a^0 = kh_i d(1 - \pi r_i^2 N) \quad (1)$$

where k is the weight of aluminium in alumina, assuming 13% sulphate ion incorporation, h_i is the porous film thickness the density of which is d, r_i is the initial pore radius and N is the number of pores/cm^2. This equation could equally well be written as:

$$W_a^0 = W_T^a(1 - V) \quad (2)$$

where $W_T^a = kh_i d$, the total amount of aluminium present in the oxide when the oxide is pore-free, and where V is the fractional pore volume. From these and other equations and the experimental results, NAGAYAMA AND TAMURA concluded that the degree of dissolution of the porous film at its outer surface was negligible. It is clear from the expression relating W_a^0, W_T^a and V, that, if outer surface porous film dissolution is negligible, this is tantamount to assuming a pore volume for the forming conditions used, of 33%. From the results of pore volume determinations, both theoretical[2] and experimental[3], a value of 15–20% for the pore volume has been shown under equivalent experimental conditions to those used by NAGAYAMA AND TAMURA.

It can be shown that the results of NAGAYAMA AND TAMURA[1] can be adequately accounted for by assuming the pore volume to be 15%, and considering the remaining aluminium in solution as due to a 20–30% outer surface dissolution resulting in oxide films that are thinner than theoretically expected. WOOD, MARRON AND LAMBERT[4] have shown that, at 30°, porous films on an aluminium–magnesium alloy are only 66% of the theoretical thickness. Similar results have been found by the present authors[5], where the outer surface dissolution has been effectively determined and it is therefore suggested that eqns. (1) and (2) be modified to include a term which describes this outer surface dissolution process. For example,

$$W_0{}^a = W_T{}^a(1-V) - W_T{}^a(1-V)ct \quad (3)$$

where t is the anodising time, and c is a temperature-dependent dissolution rate constant. From the results of NAGAYAMA AND TAMURA and assuming $V=0.15$, it can be shown that the second term in eqn. (3), *i.e.*, the aluminium lost to solution due to oxide dissolution, contributes approximately 65% of the total $W_0{}^a$.

Further consideration of eqn. (3) can also explain the low coating ratios that have been observed for the porous film formation on aluminium[6,7], without recourse to abnormal valency states for aluminium or to low aluminium dissolution current efficiencies. Theoretical values for the coating ratio, *i.e.*, 2.2, are not observed because although aluminium is consumed with a 100% current efficiency[8], it does not all remain as oxide owing simply to outer surface dissolution. It can also be seen how this coating ratio decreases rapidly with increasing temperature, decreases with increasing electrolyte concentration and increases with increasing formation current density. At low anodising temperatures, the theoretical value of 2.20 is approached, but not attained, since even at these temperatures (0–5°) outer surface dissolution may still be operative.

An outer surface dissolution process, which might be expected to penetrate some distance down the pores of the film, would lead naturally to the slanting pore wall model of these porous films proposed by PAOLINI *et al.*[9]. The slanting pore wall model would also account for the decrease, after a certain time, in the ratio, $W_0{}^a/W_T{}^a$, since this would be due to a slightly increased pore volume term, V.

The present authors[5] have also observed the electrode potential shifts reported by NAGAYAMA AND TAMURA for the dissolution of these oxide films upon "open circuit" but have, however, placed a different significance upon these results, particularly upon the term, t_R, as used by NAGAYAMA AND TAMURA[1].

Electrochemistry Laboratory, J. W. DIGGLE
The University of Pennsylvania,
Philadelphia, Pa. 19104 (U.S.A.)
Rutherford College of Technology, T. C. DOWNIE
Newcastle-upon-Tyne (England)
Sunderland Technical College, C. W. GOULDING
Sunderland (England)

1 M. NAGAYAMA AND K. TAMURA, *Electrochim. Acta*, 12 (1967) 1097.
2 F. KELLER, M. S. HUNTER AND D. L. ROBINSON, *J. Electrochem. Soc.*, 100 (1953) 411.
3 R. B. MASON, *Metal Finishing*, 8 (1957) 55.
4 G. C. WOOD, V. J. J. MARRON AND B. W. LAMBERT, *Nature*, 199 (1963) 239.
5 J. W. DIGGLE, T. C. DOWNIE AND C. W. GOULDING, to be published.
6 R. B. MASON AND P. E. FOWLE, *J. Electrochem. Soc.*, 101 (1954) 53.
7 R. B. MASON AND C. J. SLUNDER, *Ind. Eng. Chem.*, 39 (1947) 1602.
8 M. TOSTERUD AND R. B. MASON, *J. Electrochem. Soc.*, 90 (1946) 221.
9 G. PAOLINI, M. MASOERO, F. SACCHI AND M. PAGANELLI, *J. Electrochem. Soc.*, 112 (1965) 32.

Received December 18th, 1967

Calculation of the amount of specifically adsorbed ions. Application to potassium iodide in the 10^{-2}–10^{-3} M range

GRAHAME[1,2] developed a method for calculating the amount of specifically adsorbed ion at an ideal polarized electrode on the assumption that only one ionic species undergoes specific adsorption. An alternative but similar calculation, involving the same assumptions as those made by GRAHAME, is reported here. The method is applied to potassium iodide in the range, 10^{-2}–10^{-3} M using differential capacities measured by the coulostatic method developed in this laboratory[3].

Method of calculation

We consider the case of a 1:1 electrolyte, to simplify matters, and assume that only the anion is specifically adsorbed. We start with the thermodynamic relationship:

$$\left(\frac{\partial q}{\partial \mu}\right)_{E_+} = \left(\frac{\partial \Gamma_-}{\partial E_+}\right)_{\mu} \tag{1}$$

where q is the charge density on the electrode, Γ_- the relative surface excess of anion, μ the chemical potential of the electrolyte, and E_+ the potential of the electrode against a reference electrode which is reversible to the cation.

One has

$$\Gamma_- = (1/F)\,(q + q_+^{2-s}) \tag{2}$$

where F is the faraday and q_+^{2-s} is the charge density of cations in the diffuse double layer. By combining eqns. (1) and (2) one obtains, after noting that $C = (\partial q/\partial E_+)$ is the differential capacity,

$$\left(\frac{\partial q_+^{2-s}}{\partial q}\right)_{\mu} = F\,\frac{1}{C}\left(\frac{\partial q}{\partial \mu}\right)_{E_+} - 1 \tag{3}$$

All quantities on the right-hand side of eqn. (3) can be deduced from measurements of C at different values of μ and E_+; q is obtained by integration of C, and, consequently, the point of zero charge must be measured for each μ. If it is assumed that the Gouy–Chapman theory is valid*, as GRAHAME did[1,2], one has[4]

$$q_+^{2-s} = A\{\exp(-\tfrac{1}{2}f\phi_2) - 1\} \tag{4}$$

with

$$A = (RT\varepsilon c^s/2\pi)^{\frac{1}{2}} \tag{5}$$

$$f = RT/F \tag{6}$$

Notations are the usual ones and c^s represents the bulk concentration of the electrolyte. It follows that the quantity, λ, defined by eqn. (7a) below can be computed from experimental data. Thus:

* It was pointed out by Dr. PARSONS[10] that computation *via* ϕ_2 can be avoided by integration of eqn. (3) with q_+^{2-s} at very negative potential as integration constant. This constant is easily obtained from the charge in the diffuse double layer. This procedure is more direct than the one we followed.

$$\lambda = -\frac{2}{Af}\left(\frac{\partial q_+^{2-s}}{\partial q}\right)_\mu \tag{7a}$$

$$= \left(\frac{\partial \phi_2}{\partial q}\right)_\mu \exp(-\tfrac{1}{2} f\phi_2) \tag{7b}$$

Hence, integration of λ from a given charge density, q', to q at constant μ yields:

$$\int_{q'}^{q} \lambda \, dq = -\frac{2}{f}\left[\exp(-\tfrac{1}{2} f\phi_2)\right]_{\phi_2 \text{ at } q'}^{\phi_2 \text{ at } q} \tag{8}$$

If q' is sufficiently negative, one can safely assume that anions are not specifically adsorbed, and thereby calculate ϕ_2 at q' from the Gouy–Chapman theory[4]. The potential, ϕ_2, can now be computed from eqn. (8) for all values of q, and Γ_- can then be obtained from eqns. (2) and (4). The separation of $F\Gamma_-$ into the specifically adsorbed charge, q_-^1, and the anion charge density, q_-^{2-s}, in the diffuse double layer is immediate since the latter is given by the Gouy–Chapman theory (*Cf.* eqn. (4) with a minus sign in front of the right-hand side and a plus sign in front of the argument of the exponential).

We now compare the above procedure with GRAHAME's method. Both methods required the computation of q by integration of C with respect to potential.

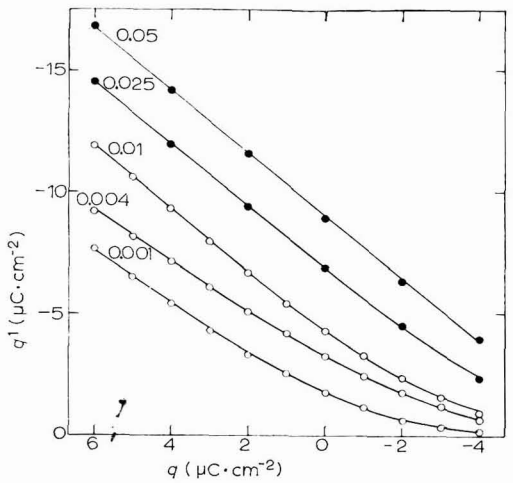

Fig. 1. Amount of specifically adsorbed iodide *vs.* charge density on the electrode for different KI concns. (*M*). (○), this work; (●), GRAHAME's data[7,8].

Our method requires the evaluation of $(\partial q/\partial \mu)_{E_+}$ by differentiation of q *vs.* μ curves at constant E_+ whereas GRAHAME's method involves the computation of $(\partial C/\partial \mu)_{E_+}$. This is followed by one integration in our method and two consecutive integrations in GRAHAME's method. By basing our computation on q rather than C, we have a total of two integrations whereas GRAHAME's procedure involves two consecutive integrations and a separate computation of q by integration. The two procedures are analogous, but ours seems more direct and perhaps a little less sensitive to experimental errors.

Application to potassium iodide in the range 10^{-2}–10^{-3} M

Differential capacities were measured by the previously reported[3] coulostatic method. The potential at the point of zero charge was measured with a streaming mercury electrode (method V in GRAHAME's paper[5]), special attention being paid to removing oxygen from solution and thus avoiding the resulting shift in the measured potential at open circuit[6]. The capacity and point of zero charge were measured for the following concentrations: 0.01, 0.04, 0.1, 0.4, 1, 4 and 10 mM. Data were interpreted by the above method, but only results in the 1–10 mM range were retained since values of q_-^{-1} for lower concentrations did not appear to be sufficiently reliable. Experimental errors on differential capacities, as obtained by the coulostatic method, are greater (perhaps 3–5%) than for capacities measured with a bridge at higher concentrations. Moreover, we took only 3 concentrations/decade whereas GRAHAME took 7.

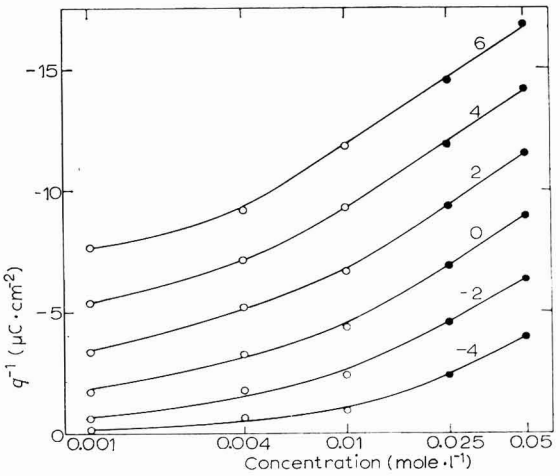

Fig. 2. Amount of specifically adsorbed iodide *vs.* log KI concn. for different charge densities on electrode (μC cm^{-2}). (○), this work; (●), GRAHAME's data[7,8].

Results are shown in Figs. 1 and 2 together with GRAHAME's data[7,8] for 25 and 50* mM. Continuity between his data and ours is good. Moreover, the near linearity in GRAHAME's plot[7] corresponding to Fig. 2 disappears at lower concentrations as one would expect. Figure 2 is similar to the same plot for chloride ion at higher concentrations[9].

Acknowledgement

This work was supported by the National Science Foundation.

Department of Chemistry,
New York University,
New York, N.Y. 10003 (U.S.A.)

P. DELAHAY
D. J. KELSH**

* Data for 50 mM are given in ref. 8.
** Present address: Department of Chemistry, Gonzaga University, Spokane, Washington 99202.

1 D. C. GRAHAME, *Chem. Rev.*, 41 (1947) 441.
2 D. C. GRAHAME AND B. A. SODERBERG, *J. Chem. Phys.*, 22 (1954) 449.
3 P. DELAHAY AND D. J. KELSH, *J. Electroanal. Chem.*, 40 (1968) 116.
4 P. DELAHAY, *Double Layer and Electrode Kinetics*, Interscience-Wiley, New York, 1965, p. 47.
5 D. C. GRAHAME, R. P. LARSEN AND M. A. POTH, *J. Am. Chem. Soc.*, 71 (1949) 2978.
6 P. DELAHAY AND G. TESSARI, *J. Electroanal. Chem.*, 40 (1968) 273.
7 D. C. GRAHAME, *J. Am. Chem. Soc.*, 80 (1958) 4201.
8 D. C. GRAHAME, Technical Report to the Office of Naval Research, No. 5, 2nd series, contract N-onr-2309(01), August 1, 1957.
9 D. C. GRAHAME AND R. PARSONS, *J. Am. Chem. Soc.*, 83 (1961) 1291.
10 R. PARSONS, private communication.

Received November 13th, 1967

Evidence for an azide-catalyzed polarographic reduction of Ga(III)

In an earlier paper[1] we showed that acidified concentrated ($>7.0\ M$) thiocyanate is an effective medium for promoting reversible charge transfer to Ga(III) at the dropping mercury electrode (DME), a fact which was later confirmed by MOORHEAD AND FURMAN[2] and SAGADIEVA[3]. Experimental difficulties which arose from the aforementioned need for such concentrated base electrolytes were considerably simplified as a result of a recent communication[4] which demonstrated that charge transfer is controlled by both SCN^- *and* ionic strength, and that it is possible to obtain reversible Ga(III) reduction from mineral acid at a half-wave potential ($E_{\frac{1}{2}}$) of -0.781 V *vs.* SCE (the estimated[5,8] reversible $E_{Ga}{}^0$ in non-complexing media is approximately -0.8 V *vs.* SCE) using 5–6 M $NaClO_4$ containing as little as 0.1 M SCN^-, a potential 320 V more positive (less reducing) than the $E_{\frac{1}{2}}$ recorded for Ga(III) reduction from non-complexing media[1,4,5]. The question of the actual mechanism underlying the Ga(III)–SCN^- interaction became considerably more intriguing from a theoretical viewpoint when it was verified[1,2,4,9] that acidified halides up to 5.0 M are totally ineffective in accelerating the charge transfer rate. As a group characteristic, the rate-enhancing effect of halides on other irreversibly reduced *aquo* metal cations is well established, and was recently discussed by ENGLE *et al.*[6], and LAWSON AND AIKENS[7].

It was decided to capitalize on the rate-sensitizing effect of ionic strength to ascertain whether Ga(III) reduction is catalyzed by anions isoelectronic to SCN^-.

We wish to report here what we believe to be the first conclusive evidence for the azide-catalyzed polarographic reduction of Ga(III) from acid media.

Experimental

The a.c. and d.c. polarographic instrumentation was of conventional operational amplifier design and utilized a 3-electrode cell which was thoroughly degassed with N_2 and equilibrated to $30.0 \pm 0.05°$ prior to each run. This and ancillary instrumentation necessary for the a.c. studies are described elsewhere[4,9]. A.c. results reported here refer to an applied 50 Hz, 10 mV r.m.s. signal. Reported potentials are *vs.* saturated calomel electrode (SCE) whose potential was corrected *only* for the junction potential existent in the reduction of Tl(I) from 0.1 M $NaNO_3$ solution, the $E_{\frac{1}{2}}$ of which was assumed

equal to -0.461 ± 0.003 V *vs.* SCE[10]. Hopkin and Williams ("low chlorate") or B.D.H. ("low chloride") $NaClO_4$ was used. Eastman NaN_3 was used after one recrystallization from hot water–ethanol. Standardized Ga solutions were prepared from Johnson-Matthey "Specpure" salts, and distilled or triple-distilled water was used as required.

Results and discussion

Cyanate (OCN^-) and selenocyanate ($SeCN^-$). As cyanate and selenocyanate decomposed more or less rapidly (for example, appearance of reddish colloidal Se in the case of $SeCN^-$) on adjustment of the Ga(III) test solutions to the required acid pH (2–3), experiments involving these anions proved fruitless. Though unavailable for evaluation, tellurocyanate probably resembles $SeCN^-$ in its acid instability.

Azide (N_3^-). Because it was necessary to carry out polarographic measurements at acidities below pH 2.5 (to avoid precipitation of the hydrous metal oxide), the slight dissociation of dissolved HN_3 (reported $pK = 4.39$ at 1.0 *M* $NaClO_4$[11]) presented a serious obstacle to the attainment of sufficient free N_3^- in solution. In an attempt to overcome this problem, base electrolyte solutions were adjusted to contain a high formal concentration of NaN_3.

Initial polarographic examination of oxygen-free solutions comprising 2.84 m*M* Ga(III), 1.0 *F* NaN_3 and 5.0 *M* $NaClO_4$ carefully adjusted to pH 2.3, produced a well-defined (21.6 μA) d.c. Ga(III) step at $E_{\frac{1}{2}} = -0.802$ V *vs.* SCE, located in advance of proton reduction and only 21 mV more negative than the Ga(III) a.c. peak observed previously in 0.1 *M* NaSCN, 5.0 *M* $NaClO_4$[4,9]. A plot[12] of $\log [i/(i_d - i)]$ *vs.* $E_{d.m.e.}$ for this polarogram proved linear over the log range -1.3 to $+2.4$, but careful measurement of the slope of this and similar plots gave $n = 2.5$ electrons, a somewhat unexpectedly low value which is attributed in this case to probable error in the blank correction for the background current, as the foot of the hydrogen reduction wave is superposed on the Ga(III) step beyond -0.8 V. The corresponding first harmonic a.c. polarographic peak, which was sharp and visibly symmetrical, verified that the reduction was d.c.-reversible.

Judging from previous thiocyanate studies[1,2,4,9], there seemed little doubt that the reversible reduction resulted from the presence of azide.

The above conclusions were substantiated by the following facts obtained from a separate series of experiments: (a) polarograms obtained on a degassed 20-ml solution containing only 1.95 m*M* Ga(III) and 6.0 *M* in $NaClO_4$ resulted in a flat residual baseline current out to -0.95 V *vs.* SCE with no evidence of a Ga reduction wave; (b) addition to solution (a) of 5.0 ml each of degassed 6.0 *M* $HClO_4$ (which was also 9.77 m*M* in Ga(III) to yield 2.9 m*M* for the resulting Ga(III) concentration) and 6.0 *M* NaN_3 gave virtually the same residual current curve except for the expected earlier onset of the hydrogen wave which began its rise at about -0.8 V *vs.* SCE. This solution would not be expected to harbor much, if any, free N_3^- at this low pH (approximately zero); (c) rapid adjustment of solution (b) to a final pH of 2.3 (to increase the free N_3^- concentration), by careful drop-wise addition with stirring, of 1.0 ml concentrated NaOH then produced a d.c. step (corresponding to 2.8 m*M* final concentration of Ga-(III)) with virtually the same shape and location as that described above. A slow time-decay of the diffusion current at fixed applied potential was attributed either to re-adjustment of solution N_3^- owing to some loss of gaseous HN_3, or to hydrous metal oxide formation, though precipitation in the solution was not in evidence. Identical

measurements carried out in the absence of N_3^- did not produce a Ga step, which verified that the reduction is not OH^--catalyzed[6,7,9].

The absence of any Ga(III) current from the more acidic azide solutions in (b) above, together with the fact that the d.c. step in (c) exhibited reversible morphology, are strong evidence for azide catalysis and fairly good proof that the d.c. step did not arise from a thiocyanate trace impurity. A SCN^--catalyzed wave would have been readily discernible in the strong acid media[3,4,9]; moreover, the occurrence of such a wave requires more than trace concentrations of SCN^- [9].

That N_3^-, like isoelectronic SCN^-, brings about reversible reduction of Ga(III) at high ionic strength, while other types of anions do not, seems odd. This coincident effect of the two ions could be viewed as an implication that the charge transfer mechanism is governed by a more specific type of cation–anion interaction involving something in addition to simple coulombic influences. An interesting, but as yet incompletely assessed possibility, is whether under certain circumstances the pseudohalides, by virtue of their linear 3-atom configuration and dual bonding ability, may promote heterogeneous electron transfer *via* a bridging mechanism somewhat analogous to that already identified for homogeneous electron transfer by, *e.g.*, BALL AND KING[13] and HAIM AND SUTIN[14]. Further experimental comparison of the pseudohalides is currently underway in this laboratory.

Acknowledgement

The authors thank the Alfred P. Sloan Foundation, The Research Corporation and the Research Council of Rutgers University for grants-in-aid in support of this research. One of us (G.M.F. II) gratefully acknowledges the receipt of a National Aeronautics and Space Administration Pre-doctoral Traineeship.

School of Chemistry,
Rutgers-The State University,
New Brunswick, N.J. 08903 (U.S.A.)

E. D. MOORHEAD
G. M. FRAME II

1 W. M. MACNEVIN AND E. D. MOORHEAD, *J. Am. Chem. Soc.*, 81 (1959) 6382.
2 E. D. MOORHEAD AND N. H. FURMAN, *Anal. Chem.*, 32 (1960) 1507.
3 K. SAGADIEVA, *Zh. Analit. Khim.*, 19 (1964) 677.
4 E. MOORHEAD, *J. Am. Chem. Soc.*, 87 (1965) 2503.
5 G. CHALLENGER, Ph.D. thesis, Harvard Univ., 1945.
6 A. ENGLE, J. LAWSON AND D. AIKENS, *Anal. Chem.*, 37 (1965) 203.
7 J. LAWSON AND D. AIKENS, *J. Electroanal. Chem.*, 15 (1967) 193.
8 W. SALTMAN AND N. NACHTRIEB, *J. Electrochem. Soc.*, 100 (1953) 126.
9 E. D. MOORHEAD AND G. M. FRAME, II, *Anal. Chem.*, 40 (280) 1968.
10 I. M. KOLTHOFF AND J. J. LINGANE, *Polarography*, Vol. 2. Interscience Publishers, New York, 1952.
11 E. A. BURNS AND F. D. CHANG, *J. Phys. Chem.*, 63 (1959) 1314.
12 J. HEYROVSKÝ AND D. ILKOVIČ, *Collection Czech. Chem. Commun.*, 7 (1935) 198.
13 D. L. BALL AND E. L. KING, *J. Am. Chem. Soc.*, 80 (1958) 1091.
14 A. HAIM AND N. SUTIN, *ibid.*, 88 (1966) 434.

Received November 10th, 1967

Formal oxidation–reduction potentials of copper(II)–copper(I) systems in acetonitrile

The oxidation capacities of cupric salts in acetonitrile have been found to depend on the nature of the anion[1-3] and in the order: perchlorate > nitrate > chloride. The measurement of the formal redox potentials of Cu(II)–Cu(I) systems confirms this observation.

Standard solutions of copper(II) chloride, nitrate and perchlorate were prepared by dissolving the appropriate quantities of anhydrous (or dehydrated) salts in acetonitrile; the exact strength was checked by EDTA titrations[1-3]. Solutions of copper(I) nitrate were prepared by the interaction of metallic copper and silver nitrate in acetonitrile[4]. Copper(I) chloride, prepared by the reduction of the cupric salt with metallic copper, was used to prepare solutions of copper(I) chloride in acetonitrile[5]. Various Cu(II)–Cu(I) systems were prepared by either mixing cupric and cuprous solutions, or by partially reducing the cupric solution.

Potentials were measured at $25 \pm 0.2°$ using Pleskov's electrode and an aqueous saturated calomel electrode, as reference electrodes.

Mixtures of copper(II) and copper(I) salts in various proportions were put in the potentiometric cell fitted with a bright platinum electrode. The potential measurements were made of the following two cells:

Ag	$AgNO_3$ (0.01 M in acetonitrile)	Cu(II) Cu(I) $c_1 + c_2$ in acetonitrile	Pt

(i)

and

Hg,Hg_2Cl_2(s) satd KCl	KCl–agar agar bridge	Cu(II) Cu(I) $c_1 + c_2$ in acetonitrile	Pt

(ii)

The formal redox potentials of Cu(II)–Cu(I) systems were determined using the Nernst equation, from the straight lines obtained (Fig. 1) by plotting the measured potentials against the logarithmic ratio Cu(II):Cu(I). The potentials thus obtained are presented in Table 1.

It is clear from these results that the formal redox potential of the Cu(II)–Cu(I) system in acetonitrile is higher for perchlorate than for nitrate and chloride. The polarographic $E_{\frac{1}{2}}$-values for the copper(II) species in acetonitrile reported by KOLTHOFF and others[6-7] are in good agreement with the measured formal potential of the Cu(II)–Cu(I) perchlorate system.

Perchlorate ions have the least tendency to form complexes with metal ions and therefore the perchlorate system has a higher potential; the other ligands, nitrate and chloride, have a pronounced tendency to complex with metal ions and these systems therefore have considerably lower potentials. Conductometric measurements and molecular weight determinations of copper(II) perchlorate and nitrate in acetonitrile show that perchlorate is extensively dissociated compared to the nitrate[8]. Solutions of copper(II) chloride in acetonitrile are only partially dissociated[9]. These

facts support gradation in oxidation capacity and formal potentials exhibited by different cupric salts. Similar differences in redox potentials have been observed with the ceric–cerous couple associated with different anions[10].

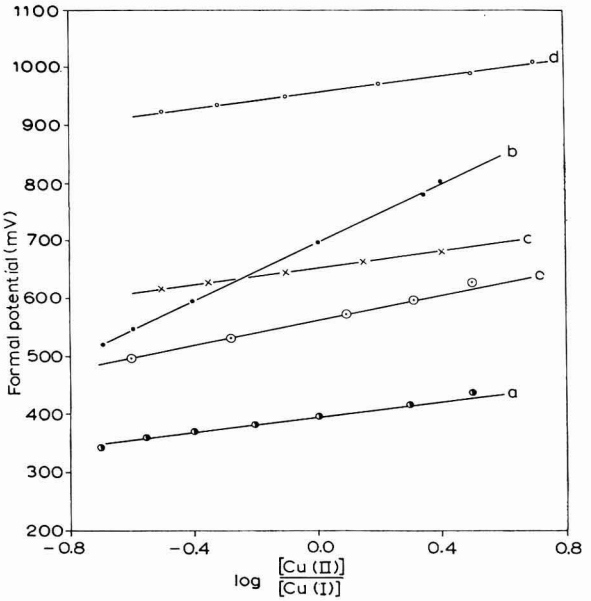

Fig. 1. Variation of formal oxidation–reduction potentials with $\log([Cu^{2+}]/[Cu^{+}])$ of copper salts in acetonitrile *vs.* (i) $Ag/AgNO_3$ (0.01 *M*) and (ii) SCE reference electrodes. (a), Nitrate salt *vs.* (i); (b), nitrate salt *vs.* (ii); (c), perchlorate salt *vs.* (i); (d), perchlorate salt *vs.* (ii); (e), chloride salt *vs.* (ii).

TABLE 1

FORMAL REDOX POTENTIALS OF Cu(II)–Cu(I) COUPLES IN ACETONITRILE

Cu(II)–Cu(I) system	*Redox potential vs. SCE (mV)*	*Redox potential vs. Pleskov's electrode (mV)*	*Redox potential on the standard hydrogen scale (V)*
Perchlorate	950	650	1.194
Nitrate	695	395	0.939
Chloride	560	—	0.804

Effect of perchlorate on the redox potentials of the copper(II)–copper(I) nitrate and chloride systems

The formal redox potentials of the Cu(II)–Cu(I) nitrate and chloride systems increase considerably in the presence of sodium perchlorate. The increase in potential was found to depend on the concentration of perchlorate present in the solution. Maximum values of 860 mV (*vs.* SCE) and 840 mV (*vs.* SCE) were observed with

solutions of copper nitrate and copper chloride, respectively, when saturated with sodium perchlorate (Table 2).

Perchlorate ions can replace the nitrate group in copper(II) nitrate to form mixed molecular species of the type: $[Cu(ClO_4)_{2-x}(NO_3)_x]$, the value of x being determined by the experimental conditions. For example, nitrosyl perchlorate may be used to replace one equivalent of nitrate in $Cu(NO_3)_2$ to produce the compound, $[Cu(ClO_4)(NO_3)]$[11]. On the other hand, if anhydrous perchloric acid is used, 89% of nitrate can easily be replaced by perchlorate to give a compound of formula: $[Cu(ClO_4)_{1.78}\ (NO_3)_{0.22}]$[12].

TABLE 2

EFFECT OF PERCHLORATE IONS ON THE FORMAL REDOX POTENTIALS OF COPPER(II)–COPPER(I) NITRATE AND CHLORIDE SYSTEMS IN ACETONITRILE

Redox system	*Concn. of anhydrous sodium perchlorate (M)*	*Formal redox potential vs. Pleskov's electrode (mV)*	*Formal redox potential vs. SCE (mV)*
Copper(II)–copper(I) nitrate	0	395	693
	0.010	445	750
	0.025	525	820
	0.050	545	845
	0.100	545	845
	Satd. (~2 *M*)	555	860
Copper(II)–copper(I) chloride	0	—	560
	Satd. (~2 *M*)	—	840

The addition of a soluble perchlorate to a solution of copper(II) nitrate could give rise to similar molecular species. Such mixed molecular species are likely to be more ionic in character and might therefore dissociate further into the component ionic species than pure copper(II) nitrate and perhaps enhance the cupric ion activities in the system. The replacement of the nitrate group in the cuprous nitrate molecule by perchlorate ions, is also possible. The anion does not appear, however, to have any effect on the cuprous species since these ions are so strongly coordinated with acetonitrile molecules that they are shielded by the solvent molecules against the effect of anions. Even cuprous nitrate, which is extremely unstable in water, is quite stable in acetonitrile. The addition of a soluble perchlorate is, therefore, unlikely to change the cuprous ion activity in the system. These two factors could be responsible for the observed increase in the formal potentials of the system in the presence of added perchlorate ions. A similar explanation can be extended to the behaviour of the chloride system.

The increase in potential of the Cu(II)–Cu(I) nitrate and chloride systems attains a limiting value when the solutions are saturated with perchlorate. This enhanced limiting potential is, however, lower by nearly 100 mV than the potential observed with the perchlorate system. As already mentioned, the addition of perchlorate to the copper(II) nitrate and chloride systems brings about the formation of

mixed molecular species which may attain an equilibrium condition. It may not, therefore, be possible for the system to reach the potential of pure perchlorate.

This difference in the formal potential of the systems is reflected in their capabilities to oxidize iodide ion. When a solution of iodide is titrated with copper(II) perchlorate in acetonitrile, two well-defined potential jumps are observed, corresponding to the formation of triiodide ion, I_3^-, and its dissociation into iodine. In the case of copper(II) nitrate, only one jump is registered at the addition of two-thirds of an equivalent of oxidant, corresponding to the formation of triiodide ion. If the

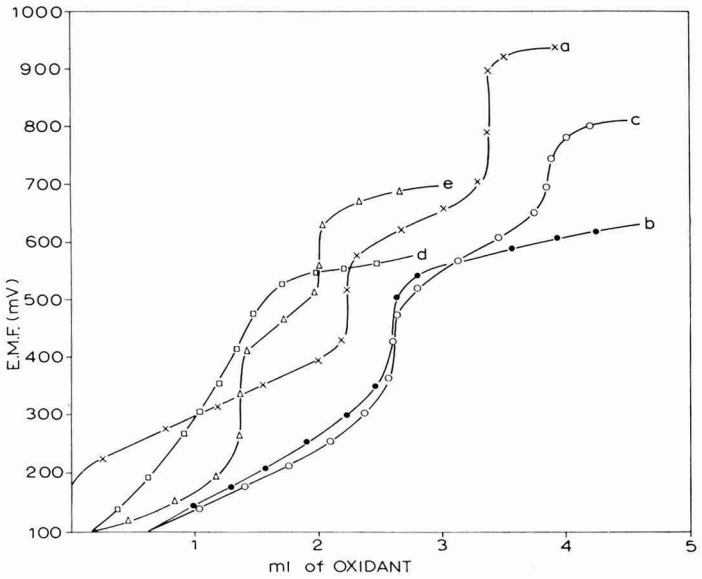

Fig. 2. Potentiometric titration curves for the oxidation of iodide by Cu(II) salts in acetonitrile using glass electrode–platinum electrode couple. (a), Cu(II) perchlorate; (b), Cu(II) nitrate; (c), Cu(II) nitrate and $NaClO_4$ (0.1 *M*); (d), Cu(II) chloride; (e), Cu(II) chloride and $NaClO_4$ (0.1 *M*).

same reaction is carried out in the presence of sodium perchlorate (0.1 *M*) two jumps are observed (Fig. 2) as in the case of cupric perchlorate, corresponding to the complete liberation of iodine. The addition of perchlorate is found to have a similar effect on the oxidation capacity of copper(II) chloride. These results show that the addition of perchlorate ion enhances the oxidation capabilities of the copper(II) nitrate and chloride systems.

Department of Inorganic and Physical Chemistry,
Indian Institute of Science,
Bangalore-12 (India)

H. C. MRUTHYUNJAYA
A. R. VASUDEVA MURTHY

1 H. C. MRUTHYUNJAYA AND A. R. VASUDEVA MURTHY, in press.
2 H. C. MRUTHYUNJAYA AND A. R. VASUDEVA MURTHY, in press.
3 B. KRATOCHVIL, D. A. ZATKO AND R. MARKUSZEWSKI, *Anal. Chem.*, 38 (1966) 770.
4 H. H. MORGAN, *J. Chem. Soc.*, 123 (1923) 2901.
5 CHARLES B. DEWITT, *Chemist-Analyst*, 24 (4) (1935) 15.

6 I. M. KOLTHOFF AND J. F. COETZEE, *J. Am. Chem. Soc.*, 79 (1957) 1852.
7 F. FARHA AND R. T. IWAMOTO, *J. Electroanal. Chem.*, 8 (1964) 55.
8 B. J. HATHAWAY AND A. E. UNDERHILL, *J. Chem. Soc.*, (1960) 3705.
9 M. BAAZ, V. GUTMANN, G. HAMPEL AND J. R. MASAGUER, *Monatsh.*, 93 (1962) 1416.
10 G. F. SMITH AND C. A. GETZ, *Ind. Eng. Chem. Anal. Ed.*, 10 (1938) 191.
11 B. J. HATHAWAY, *Proc. Chem. Soc.*, (1958) 344.
12 B. J. HATHAWAY AND A. E. UNDERHILL, *J. Chem. Soc.*, (1960) 648.

Received April 24th, 1967; in revised form, January 18th, 1968

J. Electroanal. Chem., 18 (1968) 200–204

A new carbon paste electrode holder and a simple method for preparing reproducible electrode surfaces.

It is difficult to find a method for the pretreatment of solid electrodes that will give reproducible results. Practically every investigator using platinum electrodes has developed an individual method of pretreatment. Nevertheless, it is still very difficult to obtain reproducible results.

Wax-impregnated graphite rods can give fairly reproducible results if the tips are cut off or sandpapered before each analysis. MORRIS AND SCHEMPF[1] reported peak currents and half-peak potentials at a single graphite rod with mean deviations of only $\pm 1.4\%$ and ± 2 mV, respectively. However, this order of reproducibility is uncommon.

ADAMS and coworkers[2–5] have developed a very useful type of electrode, the carbon paste electrode. A new electrode, *e.g.*, a fresh paste, can be prepared in a few minutes before each run, simply by using a spatula. This method gives a variation coefficient of about 6% for the measurements of peak currents[3]. With some experience and very careful preparation an operator can obtain a variation coefficient of 2–3%[6].

In this paper, a new carbon paste electrode holder is described, together with a method for the preparation of reproducible electrode surfaces with the aid of 0.2-mm piano wire.

Experimental

To 8 g of graphite (Merck 4207) in a glass dish is added a solution of 6 ml of bromonaphthalene (Fluka AG P 51456) in 6 ml of *n*-pentane. The mixture is stirred with a glass rod for 5–10 min until most of the pentane is evaporated.

The construction details of the paste holder are shown in Fig. 1. Note that the inner diameter of the Teflon tip should be about 0.2 mm smaller than that of the metal tube. The paste is tamped into the tube with a glass rod. When the threaded piston rod is turned, the paste is pressed out (0.1–0.3 mm seems to suffice). Instead of removing the excess paste by smoothing with a spatula[3], the electrode is put into a chuck of a lathe or similar device and rotated (about 600–700 rev./min) while the excess paste is cut off with a stretched length of 0.2-mm piano wire. The cutting procedure is repeated with clean portions of the wire until all excess paste is removed. The preparation of a new surface takes about 1 min.

Polarograms were run by the conventional electroanalytical method with a

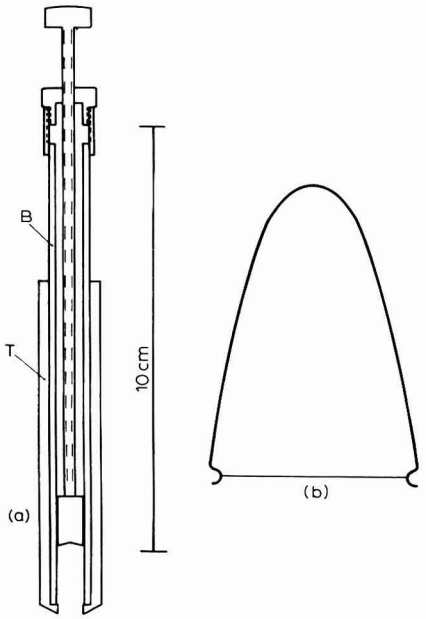

Fig. 1. (a) Carbon paste electrode holder: (T), Teflon; (B), nickel-plated brass. (b) Cutting device: a length of 0.2-mm piano wire stretched with a bow-shaped piece of 1.2-mm piano wire.

stationary electrode configuration in a quiet solution. The scan rate of 0.18 V/min was delivered by an operational amplifier circuit. The combined supporting and buffer solution was a 0.4 *M* acetate buffer, pH 4.6. The reference electrode was a saturated calomel electrode and the temperature was kept constant at 23 $\pm$0.1° using a thermostat.

The reproducibility of the electrode surfaces was examined by running eleven polarograms for the oxidation of $5 \cdot 10^{-4}$ *M* hydroquinone. Before each run, a fresh surface was prepared using the wire method. The peak current (i_p) was reproduced to 0.27% (coefficient of variation) and the half-peak potential to better than $\pm$1 mV.

Department of Analytical Chemistry, JÖRGEN LINDQUIST
University of Uppsala,
Uppsala (Sweden)

1 J. B. MORRIS AND J. M. SCHEMPF, *Anal. Chem.*, 31 (1959) 286.
2 R. N. ADAMS, *Anal. Chem.*, 30 (1958) 1576.
3 C. OLSON AND R. N. ADAMS, *Anal. Chim. Acta*, 22 (1960) 582.
4 C. OLSON AND R. N. ADAMS, *Anal. Chim. Acta*, 29 (1963) 358.
5 L. S. MARCOUX, K. B. PRATER, B. G. PRATER AND R. N. ADAMS, *Anal. Chem.*, 37 (1965) 1446.
6 E. S. JACOBS, *Anal. Chem.*, 35 (1963) 2113.

Received January 16th, 1968

Elsevier Sequoia S.A., Lausanne – Printed in The Netherlands

BOOK REVIEWS

Modern Aspects of Electrochemistry No. 4, edited by J. O'M. BOCKRIS, Plenum Press, New York, 1966, 316 pages, £4.6.0.

The fourth volume of *Modern Aspects of Electrochemistry* comprises four reviews. In the first paper, VAN RYSSELBERGHE deals with electrochemical equilibria and kinetics from the standpoint of classical and, in part, also irreversible thermodynamics. This second approach is new in the review. The method used by the author is that of MARCELLIN AND DE DONDER. The original paper by MARCELLIN (*Ann. Phys.*, 3 (1915) 158) is concerned with formalization of kinetic equations using affinities. This treatment does not deal with activation energies of reaction which is essential for the discussion of reacting systems in electrochemical kinetics. No attempt is made in this paper to arrive at results based solidly on theory and proved by experiment (*e.g.* the equations of exchange current). The author's final equations are in considerable disagreement with those generally accepted and I fear that they may present a distorted picture of electrochemical kinetics to the beginner. The reader is sometimes taken aback by unusual terms originating in the nomenclature proposed by the author and his coworkers (*Electrochim. Acta*, 9 (1964) 1343.) Apart from "tensions" there are barely acceptable terms for different parts of the electrical double-layer, the term "tensiometric cell", etc.

The subject of the second paper by PIERSMA AND GILEADI is the electrocatalytic process of oxidation of organic substances that may be used as fuels in fuel cells. The methodology of measurement, adsorption and mechanism of oxidation has been dealt with in great detail which makes (together with the clear presentation of the subject-matter) this review very useful as a reference source. Unfortunately, only literature up to 1964 is referred to, apart from the papers by BOCKRIS, CONWAY and their co-workers. The latest papers published in Russian date from 1963. This is of course a disadvantage in view of the rapid development of this field.

There are some controversial statements in the review. The aim of organic polarography is doubtless not only analysis (see *e.g.* STREITWIESER, *Molecular Orbital Theory for Organic Chemists*, p. 173–185). The authors' objections to the voltammetric method do not seem fully justified. The diffusion-controlled adsorption cannot extend to 15 min at the conditions stated on p. 96. The proportionality of adsorbed quantity to $\sqrt{t}$ is limited to time intervals for which

$$t < \frac{\pi}{4} \cdot \frac{\Gamma_m}{Dc_0}$$

where Γ_m is maximum surface concentration in moles cm^{-2} and c_0 the concentration in moles cm^{-3}. Again, on p. 157, the Delahay–Trachtenberg theory is used for high coverages of the electrode although it was deduced for the validity range of linear adsorption isotherm. Sometimes the rate equations based on too many adjustable parameters (even on the choice of isotherms, *cf.* p. 111) are not very persuasive.

The excellent review by GORUK, YOUNG AND ZOBEL on ionic and electronic currents at high fields in anodic oxide films is restricted to very thin films of glassy oxide, mostly of tantalum, with mention of silicon, germanium, aluminum and niobium. After a brief discussion of the model of ionic transport in the electric field

in the oxide layer, the experimental results with ionic currents (in dilute aqueous solutions) are reviewed in some detail. The final sections of this review deal with the electronic currents measured in the system, Ta|oxide film|metal counter-electrode.

The present economic trends in the electrochemical industry of the U.S.A. are discussed by WENGLOWSKI in the fourth review of the present volume.

The book is well produced although an alphabetical order in the references might be preferable. Electrochemists should read this book, as should solid state physicists and those interested in microelectronic devices.

J. KORYTA, J. Heyrovský Polarographic Institute

J. Electroanal. Chem., 15 (1967) 206–207

Fundamental Aspects of Electrocrystallization, by J. O'M. BOCKRIS AND G. A. RAZUMNEY, Plenum Press, New York, 1967, xii+155 pages, $7.50.

The appearance of a monograph on *Fundamental Aspects of Electrocrystallization* is welcome.

The authors have attempted to present those aspects of electrolytic growth of crystals considered to be of basic mechanistic significance. The book is directed mainly towards three groups of readers: (i) technologists familiar with the many technological aspects of the deposition of metals; (ii) scientists with a general background in physical chemistry; (iii) electrochemists who wish to deepen their general knowledge in the area of electrocrystallization.

The monograph is divided into 14 chapters. Atomic movements—of ions and molecules in solution, of adsorbed substances on the surface of metals, of steps on a growing crystal have been of primary consideration. In the first two chapters (*Retrospect* and *Perspective*) the authors have tried to outline the most valuable contributions in the field of electrocrystallization. Apart from some incompleteness and inaccuracies of the facts presented, the chapters are interesting and useful.

The methods of investigation are discussed briefly in Chapter 3. Pulse potentiostatic methods for studying nucleation processes and the new X-ray methods for investigating twinning processes in electrodeposited metals are not discussed. Also not enough attention is paid to electron diffraction methods. There are few references in this chapter.

In Chapters 4, 5 and 6 (giving the basic models of atomic movements, transients and some basic questions concerning path and rate-determining step) the authors have been mainly concerned with the work of BOCKRIS and co-workers. In many cases, insufficient attention is paid to the results of other authors. Nucleation phenomena are not considered in a concise manner. In this respect, VETTER's *Elektrochemische Kinetik* (Springer-Verlag, 1961) and FLEISCHMANN AND THIRSK's paper *Metal deposition and Electrocrystallization* (*Advances in Electrochemistry*, Vol. 3; edited by DELAHAY, Interscience Publishers Inc., New York, 1963, chapter 3) give the reader more information.

In chapter 9, *Mechanistic Aspect of Morphology*, the interesting results of Russian scientists (GORBUNOVA, VAGRAMYAN, etc.), and the investigations of Professor PIONTELLI's school, etc., are omitted. Too much attention is again given to the results of BOCKRIS and co-workers.

It could be said for almost all chapters of the monograph, (as a general criticism) that insufficient experimental data were used for adequate conclusions. In many cases, this can mislead the readers for whom the book is intended.

In the last Chapter 14, (*Prospects*) the research goals for the future are dealt with competently. Questions relating to nucleation and the effect of various factors upon the process, the problems of simultaneous deposition of two ions and the structure of the deposited alloys, are not included. The same applies to the fine structure of electrodeposited metals (twinning processes, deformation defects, etc.). Researches in this field could also throw light on the mechanism of electrocrystallization processes.

This monograph is easy to read. It is an introductory book dealing with some problems of electrocrystallization, but the reader should question critically some of the inferences raised by discussion in this book.

N. PANGAROV, Bulgarian Academy of Sciences

J. Electroanal. Chem., 18 (1968) 207–208

ANNOUNCEMENT

TWELFTH CONFERENCE ON ANALYTICAL CHEMISTRY IN NUCLEAR TECHNOLOGY. GATLINBURG, TENN., OCTOBER 1968

The Twelfth Conference on Analytical Chemistry in Nuclear Technology will be held in Gatlinburg, Tenn., on October 8, 9 and 10, 1968, under the sponsorship of the Analytical Chemistry Division, Oak Ridge National Laboratory. All sessions of the Conference will be held in the Mountain View Hotel. Registration will begin on October 7 at 4 p.m. in the hotel lobby and continue each day for the duration of the Conference. Sessions will begin at 9 a.m. each day.

Technical program

The theme of the Conference this year is *The role of the analytical chemist: (1) in research on the production and chemical properties of the actinide elements, and (2) in the elucidation and solution of problems in the field of environmental pollution and related areas.* Papers, up to 25 minutes in length, that describe original, unpublished work on the following topics are solicited by the Program Committee:

Analytical chemistry of the actinide elements. 1. Ionic methods of analysis; *2.* Radiochemical methods of analysis; *3.* New methods or techniques potentially useful to the analytical chemist—improved nuclear measurements, methods of separation, and other useful processes; *4.* Special facilities and equipment that have been developed and tested in actual operations.

Environmental pollution and related areas. Participation in the sessions on Environmental Pollution will be on an invited paper basis. However, a limited number of papers are solicited on the following topics: *1.* Identification of environmental hazards in water; *2.* Identification of environmental hazards in the atmosphere; *3.* Criteria and standards for environmental quality and control.

General information

Abstracts. Those who wish to make contributions should submit an abstract of 200–500 words not later than 1 July, 1968. The title, name of the author, an estimate of the time that will be required for the presentation, and, in case of multiple authorship, an indication of the name of the speaker should accompany the abstract.

Abstracts of papers and any inquiries concerning the Conference, including requests for programs, should be directed to the Oak Ridge National Laboratory, P. O. Box X, Oak Ridge, Tenn. 37830, Attention: L. J. BRADY, Chairman.

Registration fee. The registration fee, except for full-time students, is $5.00 per person.

Tape recordings. In lieu of published proceedings, tape recordings will be made of all papers and copies will be available on a loan basis after the Conference. Speakers who do not wish recordings made of their papers should so inform the committee.

Reservations. Reservations for lodging should be made by direct communication with: The Mountain View Hotel and Motor Lodge, Gatlinburg, Tenn. 37738.

Vol. 18 No. 1/2 JOURNAL OF ELECTROANALYTICAL CHEMISTRY AND INTERFACIAL ELECTROCHEMISTRY JULY 1968

CONTENTS

(Continued on the next page)

(Continued from previous page)